Remodelling of the immune landscape and its effect on tumour immunity in a model of IFNγ-insensitive murine melanoma

Vivian W. C. Lau
Linacre College
University of Oxford

Supervised by Professor Audrey Gerard
Kennedy Institute of Rheumatology
Hilary 2023

This thesis is submitted to the Medical Science Division, University of Oxford, in partial fulfilment of the requirements for the degree of DPhil in Infection, Immunology and Translational Medicine

Table of Contents

List of Figures

List of Tables

Abstract

Loss of IFNγ-sensitivity by tumour cells appears to enable evasion against T cell-dependent cytotoxicity, as some cancers lacking IFNγ-signalling demonstrate clinical resistance to checkpoint immunotherapy. However, recent studies have demonstrated that IFNγ-resistant tumours can sensitize the immune system for improved anti-tumour immunity. As a pleiotropic cytokine, the functions of IFNγ appears to have disparate modalities depending on context and magnitude of signalling in the tumour microenvironment.

In this thesis, we adopted a B16F10 murine melanoma model deficient in IFNGR1 and hypothesized that IFNGR1KO tumours would outgrow WT tumours due to impaired antigen presentation to $CD8^+$ T cells. Unexpectedly, IFNGR1KO tumours implanted into independent mice grew at equivalent rates despite minimal MHC-I/II expression on KO tumours. However, when WT and KO cells were admixed prior to implantation, the expected clinical phenotype was restored, as KO cells outgrew WT and preferential recruitment of $CD8^+$ T cells in 'WT zones' is observed. To explain this paradox, we measured the levels of intratumoural IFNγ via ELISA and found an accumulation within KO tumours compared to WT. We hypothesized that this level of IFNγ is capable of triggering active re-modelling of the tumour microenvironment which in turn preserves anti-tumour immunity. Analysis of single-cell RNAseq data from tumour-infiltrating $CD45^+$ cells found that transcriptional changes within the myeloid compartment to promote less pro-tumourigenic macrophages may be key to modulating tumour control. Consequently, future experiments will attempt to elucidate whether macrophages are the key to enabling $CD8^+$ T cell-dependent anti-tumour responses in KO tumours. This work highlights MHC-independent pathways within the immune microenvironment which are absent or enhanced following loss of IFNγ sensitivity, to better understand the paradoxical effects of IFNγ on tumour control over time.

Acknowledgments

My PhD journey has been a difficult one, and although there were times I wasn't sure I would make it, I was sure that I was very lucky for the amount of support and friendship I found along the way.

Thank you to my supervisor, Audrey, for your guidance, mentoring, compassion, and taking me into your lab under the most unconventional circumstances. After we had first met, Enzo said, "I really like her. Shall we ask her to be your co-supervisor?" and I'm very glad we did.

Thank you to my lab mates, Julie and Lion, for welcoming me when I arrived at the Kennedy, and all of your help and support over the years. I am so proud of you guys, and everything we've achieved individually and together.

Thank you, Gennaro and Uzi, for teaching me and supporting me when I was on Level 7 – I am thankful for the lab space, conversations, and coffee that we got to share. Thank you to Athena and James, my good friends from the beginning without whom the journey through COVID would have been unbearable.

Thank you to Becky, my constant friend and partner in crime from the very beginning, for all our adventures up North and down South, and always giving me something to look forward to even if it means sharing a prison cell. Thank you to Libby, India, and Alina, for past and future bingo trips we are sure to never remember. Thank you to Gabi and Fabi, our lab neighbours and enablers of shenanigans both inside and outside the lab.

Thank you to all the people I've met at Linacre powerlifting, especially Carrie and Shez, who taught me that failure is, indeed, an option.

Thank you to my friends back home in Canada, Laura, Arya, Anne-Laure, Danielle, Catherine, who gave me so much support over the years, provided me with a home, literally and figuratively, when I needed it most. The lessons you've taught me carried me through and I am grateful for our friendship despite the distance I decided to put between us!

Thank you to all my mentors along the way of my academic career who taught me that the beauty of immunology is in the things we struggle to make sense of, rather than what we know.

Abbreviations

AF	Alexa Fluor™
ANOVA	analysis of variance
APC	antigen presenting cell
BTLA	B- and T-lymphocyte attenuator
BV	Brilliant Violet™
BUV	Brilliant Ultraviolet™
B2m	beta-2-microglobulin
CAR	chimeric antigen receptor
CCL	chemokine (C-C motif) ligand
CCR	C-C chemokine receptor
CD	cluster of differentiation
CIITA	class II transactivator
CO2	carbon dioxide
CRISPR	Clustered Regularly Interspaced Short Palindromic Repeats
CSF	colony-stimulating factor
CSF1R	colony-stimulating factor receptor
CTL	cytotoxic lymphocyte
CTLA4	cytotoxic T-lymphocyte-associated protein 4
CXCL	chemokine (C-X-C motif) ligand
DAPI	4′,6-diamidino-2-phenylindole
DC	dendritic cell
DEG	differentially expressed genes
DN	double-negative
DP	double-positive
DNA	deoxyribonucleic acid
DTR	diphtheria toxin receptor

EC50	median effective concentration
EDTA	ethylenediaminetetraacetic acid
ELISA	enzyme-linked immunosorbent assay
EYFP	enhanced yellow fluorescent protein
FACS	fluorescence-activated cell sorting
FCS	foetal calf serum
FGF	fibroblast growth factor
GAS	gamma activating site
GFP	green fluorescent protein
GSEA	gene set enrichment analysis
HGF	hepatocyte growth factor
HIV	human immunodeficiency virus
HLA	human leukocyte antigen
HPV	human papillomavirus
ICAM	intercellular adhesion molecule 1
ICB	immune checkpoint blockade
IDO	indoleamine 2,3-dioxygenase
IFN	interferon
IFNGR	interferon gamma receptor
IL	interleukin
IRF	interferon regulatory factor 1
ISG	interferon-stimulated gene
ISRE	interferon-sensitive response element
IV	intravenous
JAK	Janus kinase 1
KO	knockout
LAG3	lymphocyte-activation gene 3

LN	lymph node
LPS	lipopolysaccharide
MDSC	myeloid-derived suppressor cell
MFI	mean/median fluorescence intensity
MHC	major histocompatibility complex
MMP	matrix metallopeptidase 9
MPEC	memory precursor effector cell
NIR	near infrared
NK	natural killer
NY-ESO1	New York esophageal squamous cell carcinoma 1
OVA	ovalbumin
PD-1	programmed cell death protein 1
PD-L1	programmed cell death ligand 1
PDGF	platelet-derived growth factor
PE	phycoerythrin
PFA	para-formaldehyde
PMA	phorbol 12-myristate 13-acetate
RIG-I	retinoic acid-inducible gene I
RNA	ribonucleic acid
ROS	reactive oxygen species
scRNAseq	single-cell RNA sequencing
SHP	Src homology region 2 domain-containing phosphatase-1
SOCS	suppressor of cytokine signalling
SOM	self-organizing maps
STAT	signal transducer and activator of transcription
TAM	tumour-associated macrophage
TAP	transporter associated with antigen processing

TCR	T cell receptor
tdLN	tumour-draining lymph node
TGF	transforming growth factor
TIGIT	T cell immunoreceptor with immunoglobulin and ITIM domain
TIL	tumour-infiltrating lymphocyte
TIM-3	T cell immunoglobulin and mucin-domain containing-3
TME	tumour microenvironment
tSNE	t-distributed stochastic neighbour embedding
UMAP	uniform manifold approximation and projection
VEGF	vascular endothelial growth factor
WT	wild-type
XCL1	chemokine (C motif) ligand 1

General Introduction

1.1 Defining cancer: A cell biologist versus immunologists' view

Cancer represents a group of heterogeneous diseases which share the feature of uncontrolled cell division in a malignant manner. From a cell biologists' standpoint, cells which become progressively more neoplastic will acquire specific survival mechanisms in succession. A guiding principle of these mechanisms was coined in 2000 as the hallmarks of cancer, which describes the different methods by which pathogenesis is achieved.[1] However, defining cancer using these hallmarks is challenging; benign and malignant tumours share five of the six original hallmarks, and not all are found in all tumour types universally.[2] The original hallmarks did not recognize extracellular factors, such as the immune response, which are key in impeding cancer progression. A revision of these hallmarks in 2011 included additional mechanisms which were further reaching, such as tumour-promoting inflammation, or evasion of immune destruction, and began to recognize processes external to the cancer cells which affects growth and metastasis (**Figure 1**).[3]

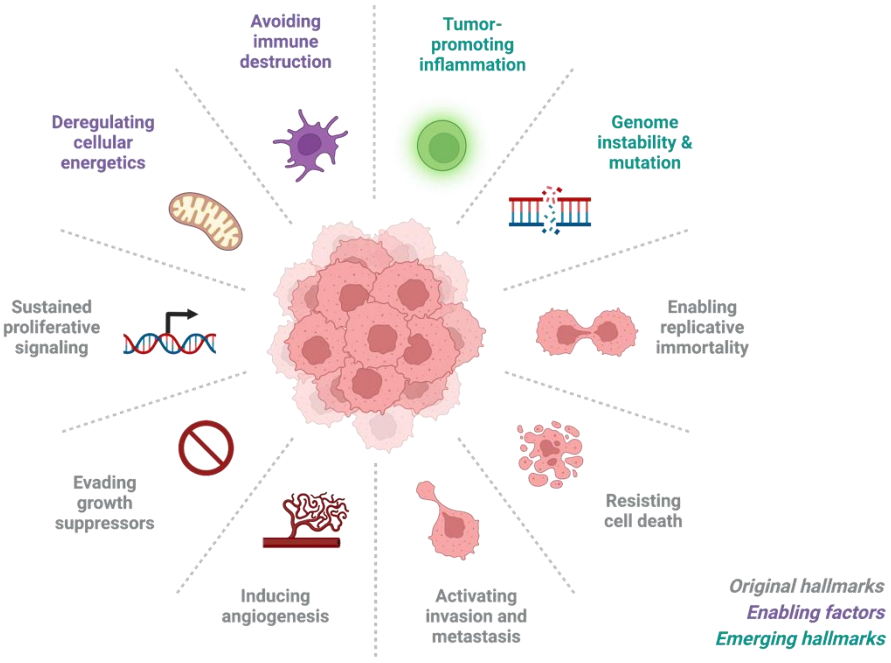

Figure 1. Hallmarks of cancer. The original hallmarks of cancer, shown in grey, are characteristics acquired by cancer cells which allow them to persist and eventually develop clinical disease. Enabling factors and emerging hallmarks recognized cell extrinsic factors, such as adaptations in metabolism, or interaction with the immune system, which result in further survival advantages conferred to the cancer cells. Created with BioRender.com, adapted from Hanahan, D (2022).[3]

To an immunologist, cancer can be viewed as a disease of the immune system, whereby an individual's immune cells have failed to detect and reject transformed cells which eventually lead to clinical disease. More importantly, it can be theorized that mutations cannot arise in cancer cells without selective pressure applied by the immune system. The remainder of the introduction for this thesis aims to outline the immunological processes which promote and inhibit cancer pathogenesis, and how our understanding of the role of the immune system in cancer has led to a new generation of therapies which subvert anti-tumour mechanisms which have failed. In particular, we are interested in the role that cytokines, such as interferon gamma (IFNγ), play in orchestrating the anti-tumour response. Inadvertently, some of these mechanisms have been exploited by cancer cells for pro-tumourigenic functions.

1.2 Introduction to cancer and immunity

1.2.1 Theories of tumour progression and immunity

The immunosurveillance theory postulates that cancer cells in the body arise continuously at a rate similar to pathogens, but are routinely cleared by the immune system due to tumour-specific antigens.[4] Early experiments supported this theory as tumours implanted into syngeneic hosts were rejected whereas healthy tissues were not, indicating that tumours can acquire mutations which render them more immunogenic and distinguishable.[5] Furthermore, the discovery of tumour-reactive T cells showed that tumours are capable of eliciting a specific immune response to self-tissues, which allowed for tumour eradication.[6] Mutant murine models such as *Rag1* knockout mice deficient in T, B and NKT cells[7], IFNγ knockout[8] and IFNγ-receptor knockout mice[9] all showed significant deficiencies in their cancer immunosurveillance capabilities. However, these observations were made

primarily in murine models of cancer where tumours were chemically induced or genetically predisposed to occur.

Evidence for cancer immunosurveillance in humans is driven primarily by the observation that patients under strong immunosuppression following organ transplantation had much higher incidence of cancers.[10] Immunodeficient individuals due to chronic infection such as HIV showed similar patterns of increased cancer risk.[11] These observational studies were largely superseded by technologies which could definitively identify tumour-specific T cells and antibodies in humans thus demonstrating that the tumour is capable of eliciting a specific immune response.[12,13]

Since then, a new and improved theory of cancer immunosurveillance, termed 'cancer immunoediting', has been introduced to further explain how immune involvement shapes tumour development over time (**Figure 2**).[14] The first of three phases in tumour immunoediting is the elimination phase, which encompasses the theory of immunosurveillance as tumour cells are successfully identified, targeted, and cleared by an active immune response. The second phase, equilibrium, describes the process by which selection of tumour variants occurs due to immune pressure, and mechanisms of tumour clearance by immune cells which become increasingly ineffective. Clinically apparent disease occurs during the final phase of escape, where tumour cells successfully evade immune clearance, and have acquired resistance against immune detection. Although immune escape is often thought to be driven by genetic mutations by tumour cells, many pro-tumourigenic mechanisms also contribute to escape such as recruitment of immune cells which have immunosuppressive functions.

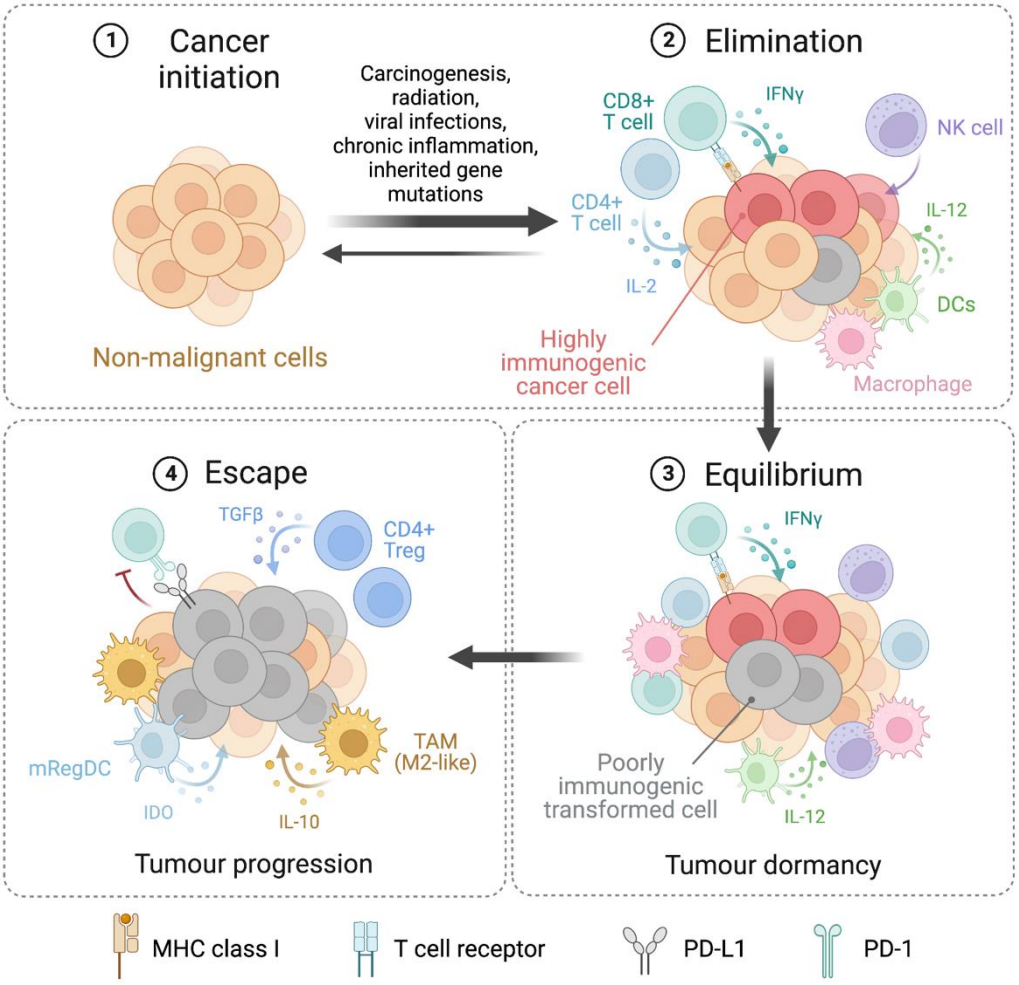

Figure 2. The three phases of cancer immunoediting and immune responses associated with each phase. Tumourigenesis is initiated by various factors which cause mutagenesis, or by genetically inherited cancer genes. During the first stage of cancer immunoediting, innate and adaptive immune responses actively recognize transformed cells carrying mutations which are highly immunogenic. Immune cells exert effector functions and secrete pro-inflammatory cytokines, which results in elimination of transformed cells before they become clinically apparent. In the next stage, equilibrium, tumour cells become less immunogenic through acquisition of mutations as a result of immune selective pressure. Outgrowth of these tumours is actively controlled by an active immune response which keeps the tumour growth in a state of dormancy. Continued immunoediting leads to the escape phase, whereby mutations acquired by the tumour now result in variants which cannot be targeted by immune cells, such as loss of MHC class I expression. Additional immunosuppressive mechanisms such as functions conferred by M2-like macrophages and $CD4^+$ Treg infiltration prevent anti-tumour functions of effector cells. At this stage, clinically apparent disease develops, and outgrowth is no longer prevented by an active and effective immune response. Created with BioRender.com.

In this thesis, we explore the concepts of immunoediting as we observe that loss of IFNγ-signalling in one tumour cell population effectively allows for immune escape over time. In our animal model however, the initial phase of elimination does not apply as the cell lines originate from a single host in which tumour immunosurveillance has already failed. In this way, we can explore and manipulate the other phases of immunoediting which are most applicable to human clinical disease.

1.2.2 CD8$^+$ T cell-dependent anti-tumour immunity

One of the most important cell types in orchestrating the anti-tumour response are T cells. In cancer, naïve CD8$^+$ T cells are cross-primed by a subset of dendritic cells (DCs) called cDC1 in the tumour-draining lymph node which promotes T cell maturation and trafficking to the tumour (**Figure 3**).[15] Tumour-specific T cells infiltrate the tumour and produce the pro-inflammatory response required to stimulate other immune cells present. When CD8$^+$ T cells recognize a tumour target, it can elicit apoptosis through production of cytotoxic granules (e.g. granzyme B and perforin), cytokine secretion (such as IFNγ and TNFα), or Fas-mediated cell death.[16–18]

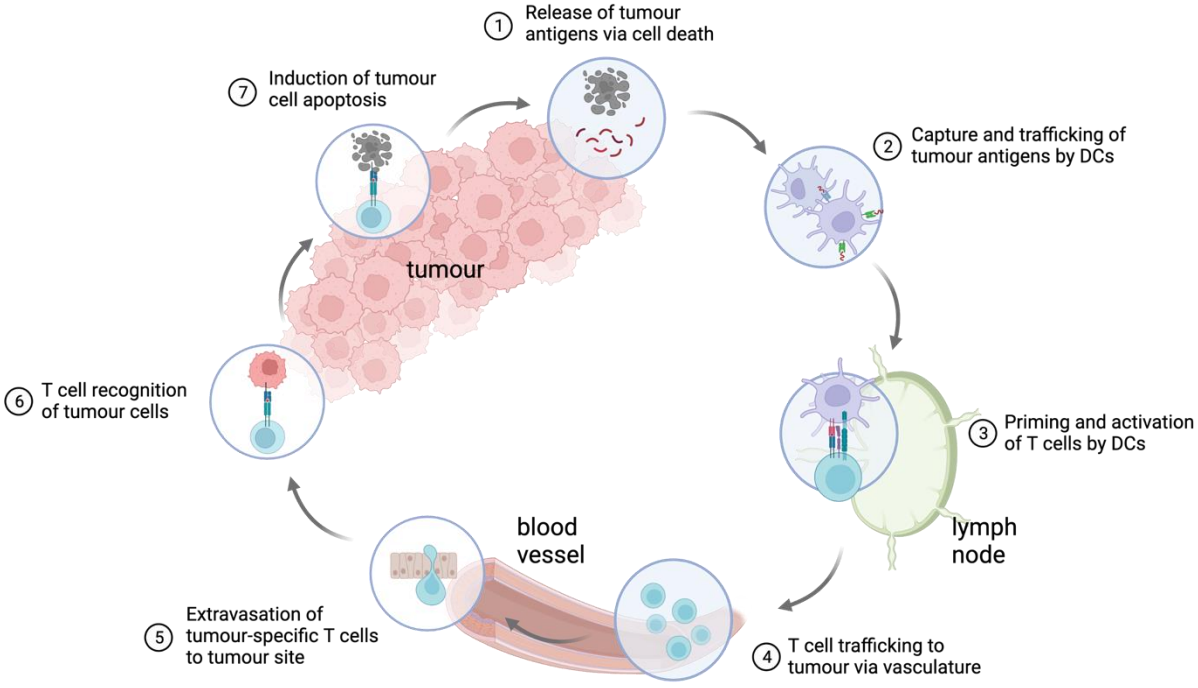

Figure 3. The cancer-immunity cycle describes the priming, circulation, and functions of T cells and tumour cells. Passive or active release of cancer cell antigens from apoptosis allows antigens to be picked up by migratory dendritic cells and APCs, which traffic between the tumour site and secondary lymph organs such as tumour-draining lymph nodes. Tumour antigen presented by APCs in the lymph nodes prime naïve T cells, which become activated and differentiate into cytotoxic T cells (CTLs) which enter into circulation and traffic to the tumour through vasculature. At the tumour site, CTLs extravasate into the tumour microenvironment to encounter its cognate antigen presented by the cancer cells, which leads to cytotoxic killing and elimination of cancer cells. This in turn completes the cycle by releasing more cancer cell antigen to continue the process of T cell immunity. Created with BioRender.com, adapted from Chen, D.S. and Mellman, I. (2013).[19]

T cell receptors (TCRs) on $CD8^+$ T cells interact with major histocompatibility complex class 1 (MHC-I) molecules on the surface of antigen presenting cells (APCs) and target cells such as tumour cells, which display peptides produced by cytoplasmic proteasomal digestion.[20] More importantly, secondary signals from costimulatory molecules such as CD28, and tertiary signals in the form of pro-inflammatory cytokines, are required to be present for $CD8^+$ T cell activation, differentiation, and proliferation.[21,22] In cancer, resident DCs in the LNs[23], migratory DCs which transfer antigen[24], tumour-infiltrating DCs[25], or antigen presentation by the tumour cells themselves[26], all play a significant role in stimulating $CD8^+$ T cells *in situ*. Mutations due to genome instability during carcinogenesis result in production of abnormal proteins which can be processed and presented as novel, non-self epitopes on MHC-I.[27,28] These epitopes, termed neoantigens, are key in maintaining effective tumour recognition by cytotoxic T cells during anti-tumour immunity. Higher tumour mutational burden (i.e., the number of mutations found in tumours), in theory, dictates the greater chance that tumour neoantigens will be immunogenic.[29]

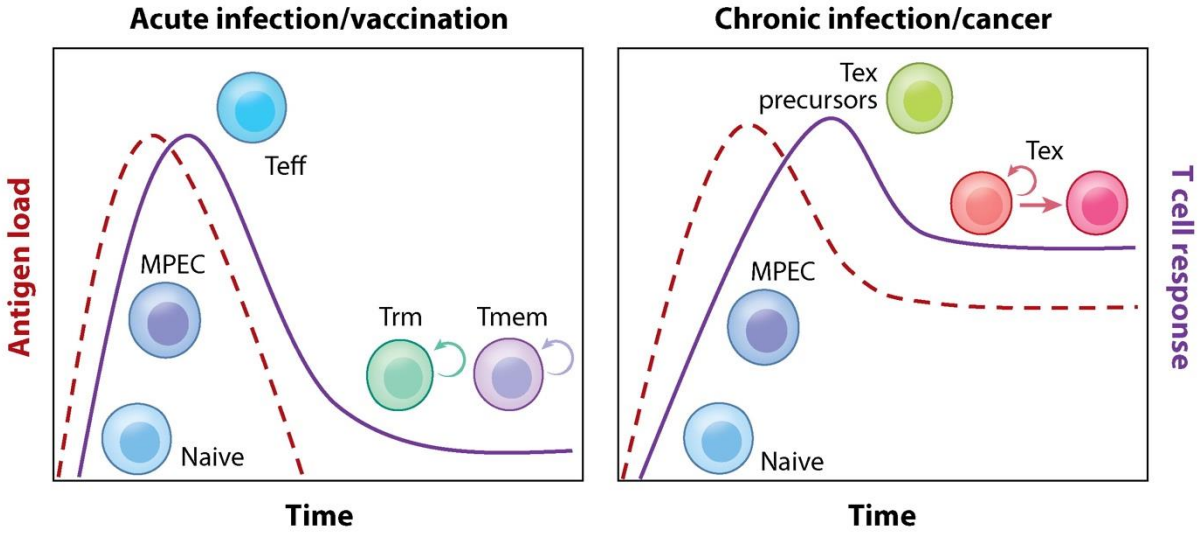

Figure 4. Formation of T cell differentiation states during acute infection and vaccination versus chronic infection and cancer. During acute states of infection and vaccination (left), naïve T cells respond to antigen and differentiate into memory precursor effector cells (MPECs). As peak antigen load increases, MPECs fully differentiate into effector T cells and clonally expand into large cell numbers. As antigen decreases and infection is controlled, a majority of effector T cells die off and remaining long-lived memory T cells persist. Memory T cells (Tmem) reside long-term in secondary lymphoid organs, or remain in tissues as resident memory T cells (Trm) for reactivation if antigen re-exposure occurs. During chronic infection and cancer, naïve T cells respond to antigen in a similar manner to acute infection. After the peak of the antigen load occurs, the source of antigen is not fully cleared, and persists as a chronic infection or tumour growth. Precursor exhausted T cells are unable to clear the infection or clear the tumour, and develop into exhausted T cells (Tex). The terminally exhausted Tex

state express high levels of checkpoint receptors, and may persist as a self-renewing population, or lead to apoptosis. Figure retrieved from [30].

An important feature of T cell-mediated immunity is their ability to form long-term memory against specific antigens. Upon antigen encounter during acute infection, effector T cells rapidly divide and exert cytotoxic functions to clear the pathogen (**Figure 4**).[31] Once eliminated, most effector cells die, leaving behind a small pool of long-lived memory cells which re-activate rapidly if the same pathogen is encountered again.[32,33] However, when the pathogen is not cleared and antigen remains, as is the case during the process of tumourigenesis, chronic stimulation of antigen-specific T cells can result in a dysfunctional state also known as T cell exhaustion.[34,35]

1.2.3 T cell exhaustion and rescuing anti-tumour immunity

T cell exhaustion is characterized by progressive loss of effector functions, including decreased proliferation, cytokine production, and impaired cytotoxicity.[36] Tumourigenesis is different from chronic infection in that cancer in humans are usually derived from single mutants, resulting in a co-evolutionary process between T cell dysfunction and disease progression.[37] T cell exhaustion in cancer has been divided into two categories, early exhaustion, and late exhaustion, which are differentiated by observation that late exhaustion is marked by irreversible cellular and epigenetic changes.[35] Despite the terms ‘dysfunction’ and ‘exhaustion’ used to describe these populations, recent studies demonstrate that dysfunctional T cells are a major compartment of intratumoural cells, and that ‘exhausted’ T cells are in fact highly proliferating, clonal, and continuously differentiating populations.[38] Thus, TIL dysfunctional represents a distinct T cell state compared to T cell exhaustion as classically described in chronic infection models.[39,40]

In tumour immunology, the terms ‘cold tumours’ versus ‘hot tumours’ have been used to describe the immunophenotypic response present in a given tumour microenvironment.[41] Whereas ‘hot tumours’ have been characterized by T cell infiltration and accumulation of pro-inflammatory cytokines in the TME, ‘cold tumours’ feature exclusion of T cells towards

tumour margins, and absence of T cell infiltration into the tumour altogether.[42] However, it would appear that defining tumours simply by T cell infiltration would be misleading, as the determinants of 'hot' versus 'cold' status are heavily influenced by other factors in the TME.

1.2.4 The many components of tumour microenvironment

Broadly speaking, the immune response to cancer involves both myeloid and lymphoid components (reviewed in detail in [43]). Myeloid components include primarily monocytes, macrophages, dendritic cells, neutrophils, and myeloid-derived suppressor cells at significant frequencies, as well as mast cells and eosinophils. Lymphoid components are composed of T cells, B cells, and NK cells, with several subsets of each which have both pro- and anti-tumour functions. Examples of these cells and their functions are summarized in **Table 1**. It is worth noting that these are brief, and generalized descriptions as most cellular functions are contextual and/or cancer-specific.

Table 1. Overview of tumour-infiltrating immune populations and their functions.

Myeloid compartment			
Cell Type	**Pro-tumour Functions**	**Anti-tumour Functions**	**References**
Neutrophils (tumour-associated neutrophils)	Release of ROS for oxidative DNA damage Release of DNA traps (aka NETs) to promote tumour cell proliferation	Direct cytotoxicity towards tumour cells via nitric oxide production 'Trogoptosis', or ingestion of cancer cell membranes	[44–48]
Monocytes (tumour-infiltrating monocytes)	Promoting angiogenesis through paracrine signalling with angiopoietin-producing endothelial cells Secretion of cytokines (e.g., IL-1β, IL-8) to support cancer-related inflammation	Phagocytosis of tumour-derived exosomes and fragments via antibody-mediated binding Differentiation into monocyte-derived DCs which augment T cell function	[49–52]
Macrophages (tumour-associated macrophages)	**TAMs**: Promotion of epithelial-mesenchymal transition of tumour and stromal cells	**M1 macrophages**: Activation of lymphoid-dependent cytotoxicity via IL-6, IL-12 and TNF production	[53–56]

	TAMs: Release of tumour-promoting growth factors (e.g., PDGF, TGFβ1, HGF, bFGF) **TAMs**: PD-L1-mediated suppression of cytotoxic T cells		
Dendritic cells (DCs)	**mRegDCs**: Immunoregulatory phenotype (*Cd274*, *Cd200*, *Pdcd1lg2*) upon tumour antigen uptake associated with reduced immunostimulatory function **cDCs**: Expression of IDO to drive differentiation of $CD4^+$ T cells into Tregs	**cDC1s** and **cDC2s**: Capture and delivery of tumour antigen for cross-presentation to cytotoxic $CD8^+$ and $CD4^+$ T cells **cDC1s**: Production of T cell chemoattractants (CXCL9/10) and cytokines for activation (IL-12)	[57–61]
Myeloid-derived suppressor cells (MDSCs)	Recruitment of Tregs via production of CCR5 ligands CCL3, CCL4 and CCL5 and induction of Tregs via IFNγ and IL-10 Direct suppression of effector T cells via secretion of TGFβ and IL-10 Production of IFNγ-derived nitric oxide for suppression of T cell proliferation		[62–65]
Other Granulocytes (mast cells, basophils, eosinophils)	**Mast cells**: Release of proteases such as tryptase and chymase which degrade the extracellular matrix and allow for tumour expansion **Basophils**: Production of IL-4/IL-13 for M2 macrophage and Th2 response induction	**Mast cells**: Production of CXCL10, CCL3 and CCL5 that recruit CD8 and CD4 T cells **Basophils**: Production of TNF and granzyme B for direct tumour cell lysis/apoptosis **Eosinophils**: Production of CCL5, CCL9 and CXCL10 for recruitment of $CD8^+$ T cells and IFNγ/TNF for skewing towards Th1 responses	[66–68]
Lymphoid compartment			
Cell Type	**Pro-tumour Functions**	**Anti-tumour Functions**	**References**
NK cells		Recruitment of cDC1s via CCL5 and XCL1/2 Direct lysis of tumour cells through activating receptors, or 'missing self' on tumour cells Indirect recognition of tumour cells via antibody-dependent cell cytotoxicity	[69–71]

$CD4^+$ T cells	**Tregs**: CTLA4-mediated suppression of APCs which inhibits activation/priming of cytotoxic T cells **Tregs**: Depletion of available IL-2 for cytotoxic T cells via competitive consumption	**Th1**: Licensing of cDC1s for efficient cytotoxic T cell priming **Th1/Tfh**: Recruitment of tumour-infiltrating lymphocytes for induction/formation of tertiary lymphoid structures **Th1**: Activation of NK and cytotoxic T cells via IL-2 production	[72–76]
$CD8^+$ T cells		Direct lysis of tumour cells via granzyme B and perforin release Primary producer of IFNγ, IL2, TNFα for stimulation and upregulation of antigen presentation by other immune cells Formation of anti-tumour memory responses and stem-like niche in secondary lymphoid organs	[77–79]
B cells	**Regulatory B cells**: Secretion of IL-10, IL-35 and TGFβ to inhibit $CD8^+$ T cell responses and conversion of $CD4^+$ T cells into Tregs in a TGFβ-dependent pathway	Antigen presentation of tumour-specific antigens for T cell activation in the tumour Formation of tertiary lymphoid structures which prolong anti-tumour responses Production of tumour-specific antibodies to enable antibody-dependent cellular cytotoxicity	[80–83]

1.2.5 Origins, recruitment, and functions of tumour-associated macrophages

Tumour-associated macrophages are one of the most abundant immune cell types in the tumour microenvironment, and harbour both tumour promoting and suppressing functions.[84] Although tissue macrophages were originally believed to originate from blood monocytes which emerge from bone marrow hematopoietic stem cells at a constant rate, fate mapping studies have shown that circulating monocytes only differentiate into macrophages in specific tissues such as dermis, intestine, and heart.[85,86] In other tissues such as skin, liver, or lung, macrophages are derived from embryonic precursors from the yolk sac and fetal liver.[87] As such, tumours in different locations may very well recruit

macrophages of specialized function which contribute to the overall TME. Experimental evidence showed that up to 50% of the TAMs found in murine brain, lung and pancreatic tumour models were derived from tissue-resident macrophages, and were associated with higher expression of immunosuppressive genes.[88–90]

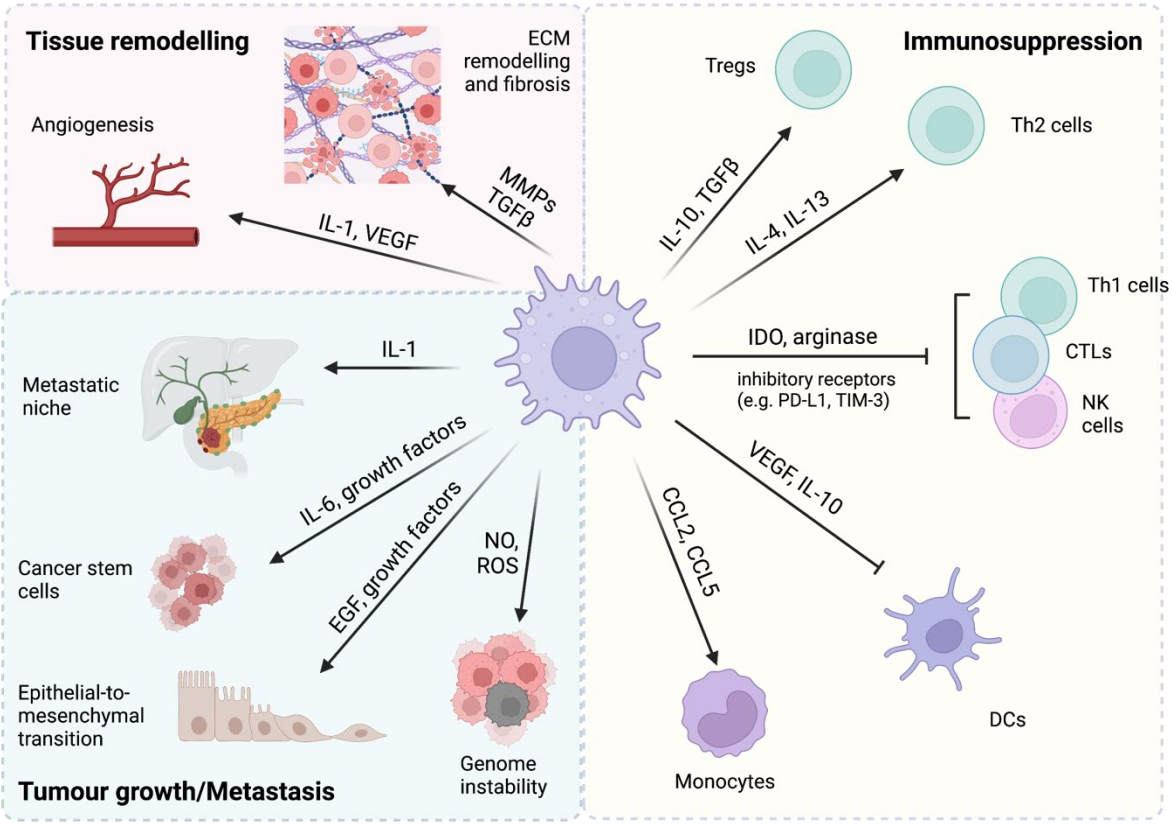

Figure 5. Pro-tumourigenic functions of tumour-associated macrophages. TAMs have universal functions in the tumour microenvironment by secreting cytokines, chemokines, proteases, and growth factors which act on a large number of different targets. (Top left) TAMs remodel the local tissue structure by degrading the extracellular matrix (ECM) with matrix metalloproteinases (MMPs), and promoting angiogenesis via IL-1 and VEGF secretion. (Bottom left) TAMs promote tumour growth and metastasis through production of reactive oxygen species such as nitric oxide, which induces genome instability cancer cells. Growth factors such as epidermal growth factor stimulate epithelial-to-mesenchymal transition of structural cells and promotes cancer stem cell survival. (Right) Major functions of immunosuppression is through skewing and differentiation of lymphocytes towards Th2, and suppression of effector functions by cytotoxic T cells (CTLs) and NK cells via metabolic modulation or inactivation via inhibitory receptors. TAMs also recruit additional monocytes from the periphery, and suppress effector activity indirectly by inhibiting DC function in the tumour. Created with BioRender.com.

While macrophages have the potential to kill tumour targets, damage vasculature, phagocytose tumour antigens and mediate antibody-dependent cytotoxicity, TAMs often contribute to tumour progression by promoting angiogenesis, cancer cell proliferation, and suppression of effector T cell responses (**Figure 5**). As such, presence of significant macrophage infiltration in human tumours is associated with poor prognosis.[91] TAMs are

primarily recruited as monocytes in circulation primarily rely on M-CSF, CCL2, CX3CL1, CCL3 and CCL5 as chemoattractants into the tumour microenvironment.[92] M-CSF, encoded by the gene *Csf1*, functions to recruit monocytes and polarize them toward M2 phenotypes, but also plays a role in self-renewal of tissue-resident macrophages.[93,94] CCL2 acts as the strongest chemoattractant for $CCR2^{+}$ monocytes, and a clear clinical correlation between high CCL2 expression and TAM infiltration has been implicated.[92,95,96]

TAMs express high levels of PD-L1, which has significant implications on the efficacy of anti-PD-1 and anti-PD-L1 ICB. Although PD-L1 expression by immunohistochemistry is a diagnostic tool which stratifies patients who are eligible for therapy, it is not a robust biomarker for successful clinical outcomes. Indeed, studies have shown that PD-L1 on tumour cells was not predictive of ICB responsiveness; rather, PD-L1 expression by host myeloid cells in the tumour were indispensable for therapy success.[97] Apart from checkpoint blockade, other strategies to target TAMs include depletion using anti-CSF1R/CCL2/CCR2 antibodies, or antagonists of CCR2 and CCR5 to modulate their recruitment to the TME.[84,98] These are currently being tested in the clinic, often in combination with anti-PD-1/PD-L1/CTLA4 therapy or traditional chemotherapy.[99]

1.2.6 The role of inflammation in tumour progression

Inflammation is a biological response triggered by infection, tissue damage and other harmful stimuli, and is necessary in the control of pathogens or repair of tissues.[100] Uncontrolled inflammation which continues to disrupt tissue homeostasis is the underlying cause of many diseases, including several cancer types.[101] Up to 20% of cancers are caused by chronic inflammation, such as in sustained *Helicobacter pylori* infection in gastric cancer.[102] At the same time, cancer also causes inflammation as cancer cell elimination is an inherently inflammatory process which requires T cell cytotoxic functions and recruitment of innate immune cells such as NK cells. As tumour growth progresses, the immune cell subtypes infiltrating the tumour become increasingly tolerogenic, and the tumour microenvironment becomes chronically inflamed.[103] Although inflammatory cytokines are

crucial for the initial anti-tumour response, chronic, persistent and dysregulated production of these molecules instead support cancer progression.[6]

Many of the cytokines in chronic inflammation of cancer have dual roles (**Figure 6**). Our group has recently focused on the role of interferon gamma (IFNγ) during tumourigenesis as it is responsible for a plethora of both anti- and pro-tumour responses across many types of cancer. Furthermore, recent studies have shown that immunotherapy-resistant tumours acquire mutations within the IFNγ signalling pathway which render them IFNγ-insensitive.[105] The upcoming sections aim to detail the function, role and biological relevance of IFNγ in cancer immunology.

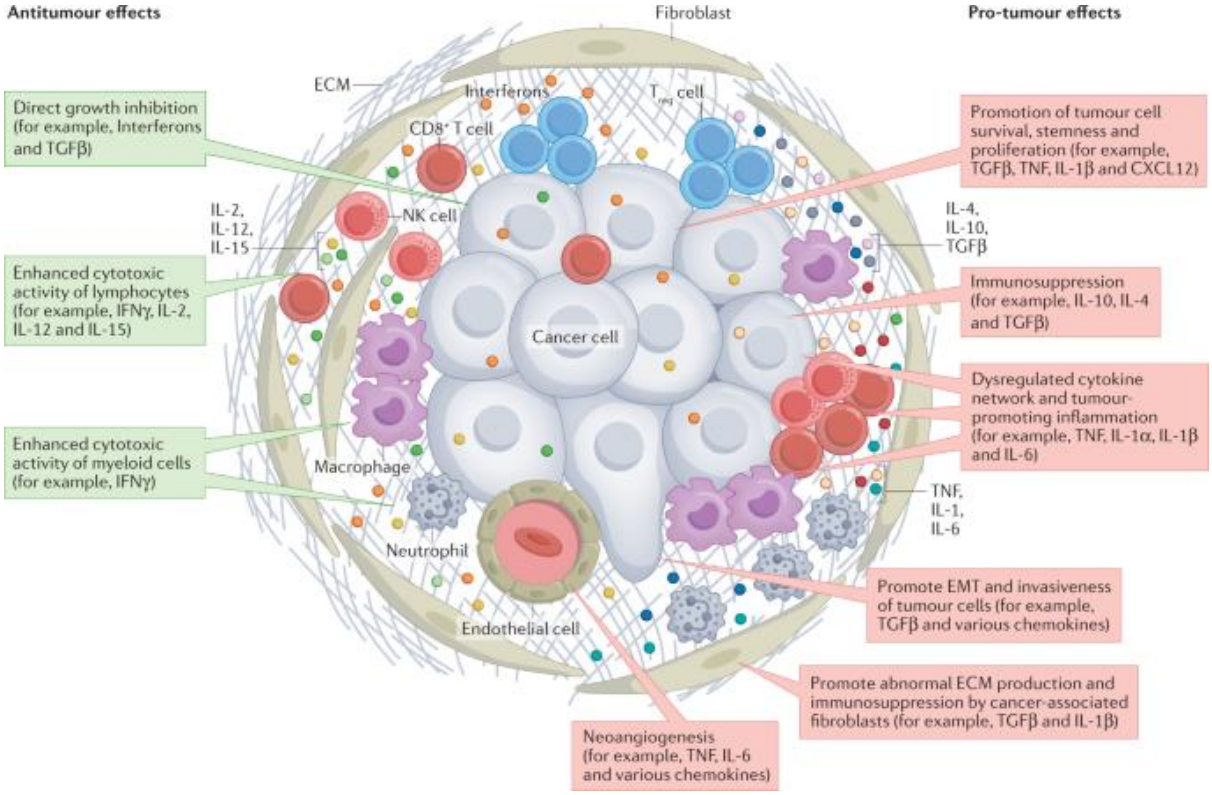

Figure 6. Cytokine networks in the tumour microenvironment. Diagram which shows the immune and non-immune components of the microenvironment. Anti-tumour effects of cytokine signalling are shown on the left, and pro-tumour effects on the right. Figure retrieved from [106].

1.3 Introduction to IFNγ and signal transduction

1.3.1 IFNγ structure and its cognate receptor

Interferon gamma, also referred to as type II interferon, is key cytokine essential for nearly all adaptive immune responses.[107] IFNγ is structurally dissimilar from type I

interferons (IFNα and IFNβ) as it adopts a homodimer structure, whereas IFNα/β are monomeric.[108] The cognate receptor for IFNγ is composed of IFNGR1 and IFNGR2 chains, which are independently expressed in humans by two genes located on chromosome 6 and 21, respectively (**Figure 7**).[109,110] Furthermore, the two chains have independent functions which are both required for signal transduction; IFNGR1 binds IFNγ dimers with high affinity, and the intracellular tail of IFNGR2 contains docking sites for Janus kinase 1 (JAK1) binding. Functionally, IFNGR1 and IFNGR2 are not tightly associated prior to interaction with IFNγ, and do not possess intrinsic tyrosine phosphorylation activity.

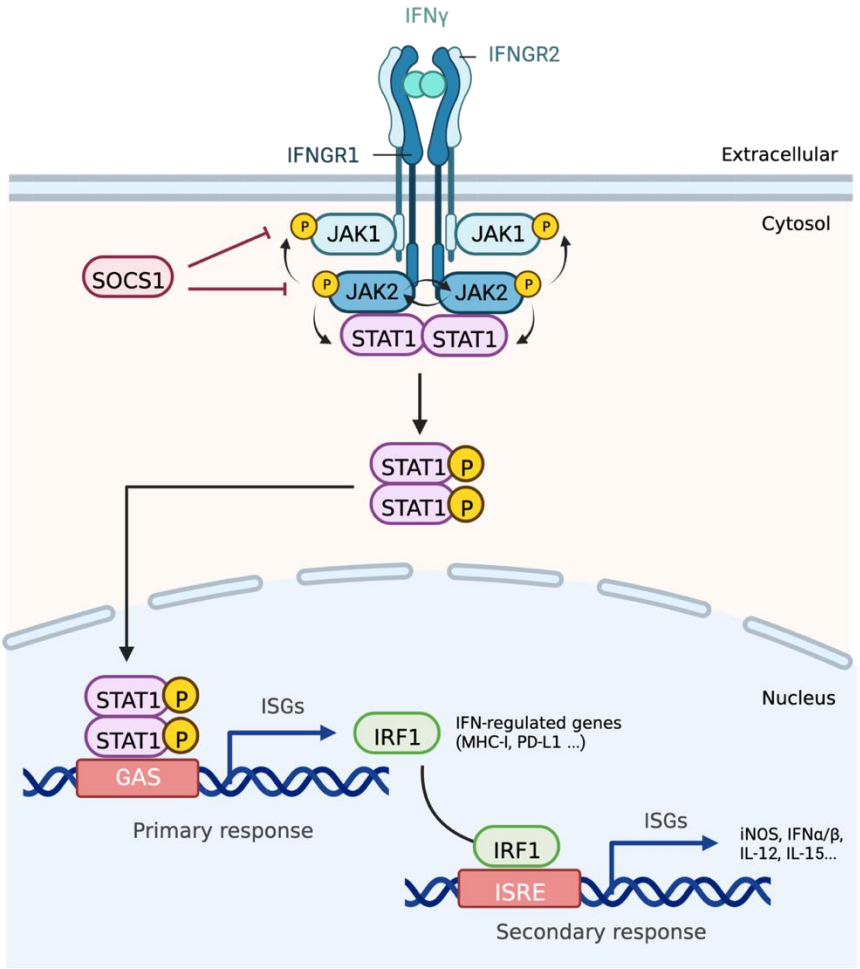

Figure 7. The IFNγ signalling pathway. Signal transduction begins when a IFNγ homodimer binds to the high affinity receptor subunit IFNGR1, which induces rapid dimerization to create a binding site recognized by the extracellular domain of IFNGR2. The heterodimeric complex consists of two IFNGR1 chains and two IFNGR2 chains, bringing together Jak1 and Jak2 kinases which are constitutively associated with each intracellular domain of the receptor subunits, respectively. Once in close proximity, Jak2 autophosphorylates and transphosphorylates Jak1, which enables phosphorylation of an intracellular IFNGR1 tyrosine and acts as STAT1 docking sites on the ligated receptor. Two STAT1 molecules are brought together in close proximity of the activated JAKs, which lead to STAT1 phosphorylation. The phosphorylated STAT1 homodimers translocate to the nucleus, acting as transcription factors which bind to gamma interferon activation sites (GAS) for induction of

the primary interferon-stimulated genes (ISGs) such as MHC class I molecule subunits and PD-L1. Most notably, the primary response results in transcription and translation of interferon response factor 1 (IRF1), which can recognize IFN-stimulated response elements (ISREs) for transcription of secondary response genes for production of type I IFNs, pro-inflammatoy cytokines, etc. Created with BioRender.com.

Downstream signalling of IFNγ is dependent on JAK1 and JAK2, which bind to IFNGR1 and IFNGR2, respectively, but are not enzymatically active until brought into close proximity by IFNγ ligation.[111,112] IFNγ binding induces autophosphorylation of JAK2, and further transphosphorylation of JAK1.[113] A conformational change in the phosphorylation of IFNGR1 allows for docking of transcription factor STAT1, which is then phosphorylated by JAK2.[114] Phosphorylation of STAT1 dimers facilitate its translocation to the nucleus, where it can bind to conserved IFNγ activation sites (GAS) which activate transcription of interferon stimulated genes (ISGs).[115]

ISGs are any genes which are induced by IFN stimulation. Many ISGs following IFNγ stimulation are transcription factors themselves, such as interferon regulatory factor 1 and 9 (IRF1 and IRF9) which drive the next wave of transcription.[116] ISGs include many proteins which have immune modulatory functions, including chemokines, pattern recognition receptors (PRRs) and key antiviral or antibacterial cytokines.[117]

1.3.2 Molecular regulation of IFNγ signalling

IFNGR1 and IFNGR2 are differentially regulated in expression, which provides a mechanism for controlling IFNγ signalling. While IFNGR1 is ubiquitously expressed by all nucleated cells in the body, many studies have shown the several different cell types modulate IFNGR2 expression as a way to regulate IFNγ signal transduction**.**[118,119] For example, naïve T cells retain expression of IFNGR2 and remain IFNγ-sensitive, whereas neither IFNGR2 protein nor mRNA transcript was detected in polyclonally activated T cells.[120] Furthermore, high levels of IFNGR2 surface expression can induce rapid activation of STAT1 and interferon regulatory factor-1 (IRF-1), which then triggers apoptosis**.**[121] In macrophages, high IFNGR2 expression following bacterial infection facilitates apoptosis of infected macrophages.[122] Conversely, low surface expression was correlated with

proliferation, which demonstrates how IFNγ is able to produce both population expansion and contraction of T cells, as well as other immune populations during immune responses.[121]

Negative regulation of JAK/STAT signalling following IFNγ stimulation is also facilitated by the suppressor of cytokine signalling (SOCS) family of proteins.[123] SOCS1 expression is induced following IFNγ stimulation and directly inhibits JAK1 and JAK2 catalytic activity to suppresses phosphorylation and further signal transduction.[124] Furthermore, JAK proteins may be dephosphorylated by protein tyrosine phosphatases (PTPs) SHP-1 and SHP-2 and have been shown to limit the inhibitory effects on proliferation elicited by IFNγ.[125] Lastly, phosphorylated STAT1 homodimers bound to DNA are dephosphorylated by PTPs which then enables nuclear protein export and termination of signaling.[126,127]

1.4 IFNγ in the context of cancer

1.4.1 Animals tumour models deficient in IFNγ-signalling

Genetically modified animal models have been instrumental in understanding how IFNγ influences host anti-tumour responses. In early studies using chemically-induced fibrosarcoma, knockout of IFNGR or STAT1 in mice resulted in larger, and more frequent tumour formation than in WT mice.[8] This supported the hypothesis that cancer immunosurveillance was dependent on IFNγ-signalling in the host. Furthermore, tumours grown in the absence of IFNγ (i.e., IFNγ-deficient mice) were rejected more readily when transplanted into WT hosts compared to tumours grown in WT hosts. This indicates that selective pressure is dependent on IFNγ, and tumours grown in the absence of IFNγ are able to retain their immunogenicity. Tumours engineered to be IFNγ-insensitive also resulted in more frequent and larger tumour formation compared to controls.[9] Control tumours, but not IFNγ-insensitive tumours, were also responsive to LPS-induced tumour regression which is an IFNγ-dependent mechanism. This study was one of the first to show that the tumour

itself is a key target for IFNγ, and IFNγ plays an indispensable role in development of lymphocyte-dependent anti-tumour immunity.

Although these early studies led us to believe that the role of IFNγ in cancer is primarily anti-tumourigenic, there is now significant evidence that these effects are only true during the elimination phase of immunoediting. During immune escape, the pro-tumour effects of IFNγ become much more apparent, as IFNγ-driven upregulation of checkpoint receptors successfully subvert T cell cytotoxicity in the tumour.

1.4.2 The anti-tumour effects of IFNγ

In the tumour microenvironment, IFNγ is secreted by activated $CD4^+$ (Th1) T cells, $CD8^+$ T cells, γδ T cells, NK cells, and NKT cells. The anti-tumour effects of IFNγ are well-supported by clinical observations where higher expression of IFNγ pathway genes are associated with better responses to immune checkpoint blockade therapy.[128,129]

IFNγ has opposing effects on T cell subsets depending on the subtype; in Th1 cells, IFNγ stimulation maintains T-bet expression and re-enforces Th1 differentiation and genetic stability.[130] Conversely, IFNγ induces Treg fragility resulting in loss of suppressive activity and tumour tolerance.[131] In DCs, monocytes, and macrophages, IFNγ is the primary inducer of CXCR3 ligands CXCL9, CXCL10 and CXCL11.[132] These chemokines are key in recruiting effector T cells and NK cells to the tumour and has been shown to be a critical component of effective immunotherapy regimens.[133,134] IFNγ also supports tumouricidal activity of macrophages by stimulating the production of nitric oxides, and upregulates production of additional pro-inflammatory cytokines such as IL-1β, TNFα, and IL-12.[135,136] In turn, IL-12 induces additional IFNγ production by intratumoural Th1 cells, enabling a multicellular positive feedback loop which sustains anti-tumour immunity.[137]

Aside from immune cells, IFNγ can directly inhibit tumour cell proliferation via suppression of cyclin-dependent kinase activity and *c-myc* expression, which is a transcription factor important for regulation of cellular proliferation.[138–140] IFNγ also sensitizes tumour cells to caspase-dependent programmed cell death through upregulation of caspase-

1 and 8.[141,142]Apoptosis can also be indirectly induced through Fas and Fas ligand upregulation following IFNγ exposure, however, this is not limited to tumour cells and has also been shown cause apoptosis of other cells including tumour stroma.[143] By the same mechanisms, T cell-derived IFNγ is also a potent inhibitor of angiogenesis through suppression of endothelial cell survival and proliferation.[144–146] Indirectly, IFNγ can skew macrophages toward an M1-like phenotype which suppresses vascular endothelial growth factor (VEGF) secretion which reduces intratumoural angiogenesis.[147]

A final key function of IFNγ relevant for anti-tumour immunity is the upregulation of MHC-I and MHC-II on nearly all cells in the tumour microenvironment. IFNγ upregulates enzymatic components of the immunoproteasome LMP2, LMP7 and MECL-1, which replace the constitutive expressed subunits β1, β5, and β2 during inflammation.[148,149] The immunoproteasome is important for priming tumour-specific $CD8^+$ T cell responses as it alters the quantity and diversity of peptides presented by APCs on MHC-I.[150] Similarly, constituents of the MHC-II complex, MHC-II transactivator (CIITA), and invariant chain (Ii) which enables peptide binding to the MHC-II molecule are also upregulated in response to IFNγ.[151,152] The effects of IFNγ are non-specific, and causes upregulation of MHC-I and II on virtually all cells in the tumour microenvironment. This allows tumour cells to be targeted by $CD8^+$ T cells and NK cells through presence or absence of MHC-I, respectively.[17,153] As expected, evasion of MHC-I-dependent killing is a primary mechanism of immune resistance, which will be discussed in the following sections.

1.4.3 The pro-tumour functions of IFNγ

The pro-tumourigenic effects of IFNγ are primarily indirect, such as suppression of cytotoxic immune functions rather than direct promotion of tumour cell growth. IFNγ upregulates indoleamine 2,3-dioxygenase (IDO) which is widely expressed by DCs, macrophages, endothelial cells, and tumour cells themselves.[154] IDO is a negative prognostic marker in many human solid tumours, and has been shown to promote Treg

differentiation and recruitment in animal models.[155–157] Furthermore, Tregs can also condition DCs to express IDO, which further amplifies its effects in a positive feedback loop.[158]

Low doses of IFNγ present in the tumour microenvironment is associated with poorer patient survival, indicating that the functions of IFNγ may be concentration dependent. This was attributed to inducing tumour stemness rather than apoptosis by upregulation of ICAM-1 and CD133 on tumour cells.[159] IFNγ-dependent ICAM-1 expression on tumour cells confers an especially aggressive phenotype and eventual metastasis as its adhesion properties can enable transendothelial tumour cell migration into circulation.[160,161]

IFNγ can also drive cytokine-induced senescence of cancer cells, which contributes to the success of some therapies[162], but also contributes to relapse and metastasis as senescent cells retain cellular longevity.[163] Recent studies have shown that cancer cell senescence may render the tumour more sensitive to local IFNγ, which boosts MHC-I-dependent tumour rejection.[164] However, this may be occurring only in treatment-naïve animal tumour models, as therapy-induced senescence has been observed in patients following chemotherapy or radiotherapy treatments.[165] While it is beneficial that the cancer cells are under growth arrest, they acquire a secretory phenotype for immunosuppressive cytokines such as IL-6 and IL-8, which increases neighbouring cell invasiveness and stemness.[166,167] Whether IFNγ can cause immune cell senescence through prolonged exposure in the context of cancer remains to be explored.

Lastly, a major function of IFNγ is the induction of programmed death-ligand 1 (PD-L1) upregulation on tumour, stromal, and myeloid cells, which inhibits activated T cells via its receptor, PD-1.[168] PD-1/PD-L1 interactions are important for limiting excessive T cell activation which prevents autoimmunity during tissue homeostasis and wound healing. However, engagement of PD-L1 on tumour cells and APCs causes T cells dysfunction and suppresses anti-tumour activity.[169,170] As a result, the PD-1/PD-L1 pathway has significant clinical relevance due to the clinical benefit of antibodies which can interrupt this pathway and restore anti-tumour immunity in several types of solid tumours.[168] The target of PD-1 signalling was recently reported to be CD28, which provides co-stimulatory signals in

addition to T cell receptor-(TCR) based for efficient T cell activation.[171] In addition to PD-L1, CTLA4 was also found to be upregulated by IFNγ on human melanoma cell lines, indicating the possibility that multiple immune checkpoint pathways can be triggered simultaneously by IFNγ.[172]

1.5 The role of IFNγ in immune checkpoint blockade

1.5.1 Immune correlates of checkpoint blockade therapy

In 2013, the Science 'breakthrough of the year' revolved around significant discoveries in the field of cancer immunotherapy, one of which was the use of antibodies in the blocking of immune checkpoint receptors.[173] These receptors include, but are not limited to, PD-1, CTLA-4, LAG3, TIM3, TIGIT, and BTLA, which function as inhibitory receptors on multiple immune cell subsets to limit their activation.[174] As a result, immune checkpoint blockade (ICB) has shown magnificent success in the treatment of some cancer types as they block the inhibitory ligand-receptor interaction, thereby restoring anti-tumour responses which were formerly inhibited by these pathways.[175]

Response rates for single agent ICB such as anti-CTLA4 and anti-PD-1 in melanoma were reported to be 19% and 43.7%, respectively, while combination therapy increased to 57.6%.[176] Although ICB has significantly improved overall survival of patients and can achieve complete responses in some patients, many patients do not respond to therapy, or experience ICB-resistant relapse.[177] In anti-PD-1 ICB for example, patients are screened for intratumoural PD-L1 expression prior to treatment, yet only a third of treated patients with PD-L1^{+} tumours showed objective response. More confoundingly, up to 15% of patients with PD-L1^{-} tumours also showed response to therapy, indicating that there must be underlying mechanisms which are not fully understood.[178]

Immune biomarkers are used in the predicting and understanding of ICB responsiveness and resistance. Early reports showed that pre-treatment CD8^{+} TIL infiltration, and high infiltration of T cells overall, were significant biomarkers for positive anti-

PD-1 treatment response in melanoma.[179,180] Responding patients have higher tumour mutational burden and presence of neoantigens, which are tumour-specific mutations which harbour greater immunogenicity due to its aberrant nature compare to normal tissues.[181] Studies comparing transcriptomes of tumours from non-responding patients show an upregulation of genes involved in epithelial-to-mesenchymal transition, cell adhesion, extracellular matrix remodelling, angiogenesis, and wound healing.[182] Similarly, transcriptional analysis of tumours from anti-PD-1 responders contained IFNγ-responsive genes including antigen presentation, chemokine expression, and T cell cytotoxicity.[183,184] These transcriptional pathways overlap with the anti- and pro-tumour functions of IFNγ, which shows the likely role this cytokine has in determining treatment success and failure.

1.5.2 Primary and acquired resistance against ICB

Primary resistance occurs when patients do not respond to therapy upon treatment, whereas acquired resistance occurs following initial response to therapy followed by therapy resistance and disease progression (**Figure 8**).[185,186] Generally speaking, primary and acquired resistance is established when tumour cells evade T cell-dependent cytotoxicity, and this occurs primarily through loss of antigen presentation mechanisms, or becoming resistant to IFNγ.

Downregulation of MHC-I is correlated with poor prognosis and primary resistance to ICB, and has been described in 40-90% of human tumours.[187,188] Reduction of MHC expression can be achieved through genetic mutations in the components of antigen presentation, but also dysregulation of protein expression at the epigenetic or post-translational level.[189] Mutations in the antigen presentation machinery components such as beta-2-microglobulin (β2m) and peptide processing proteins impair the presentation of peptides on MHC class I and II.[190–192] Mutations in the transporter associated with antigen processing (TAP) complex or tapasin, which are essential for peptide-loading onto MHC-I, are also frequently found in many cancer types.[193] Downregulation of MHC-I may also be driven by downregulation of upstream NF-κB-dependent signalling[194], or microRNAs which

suppress mRNA translation post-transcriptionally.[195,196] Although T cell-derived IFNγ counteracts some mechanisms of MHC-I downregulation, MHC-I low or mutated tumours often lack T cell infiltration[197,198], or gain resistance to IFNγ in response to selective pressure.

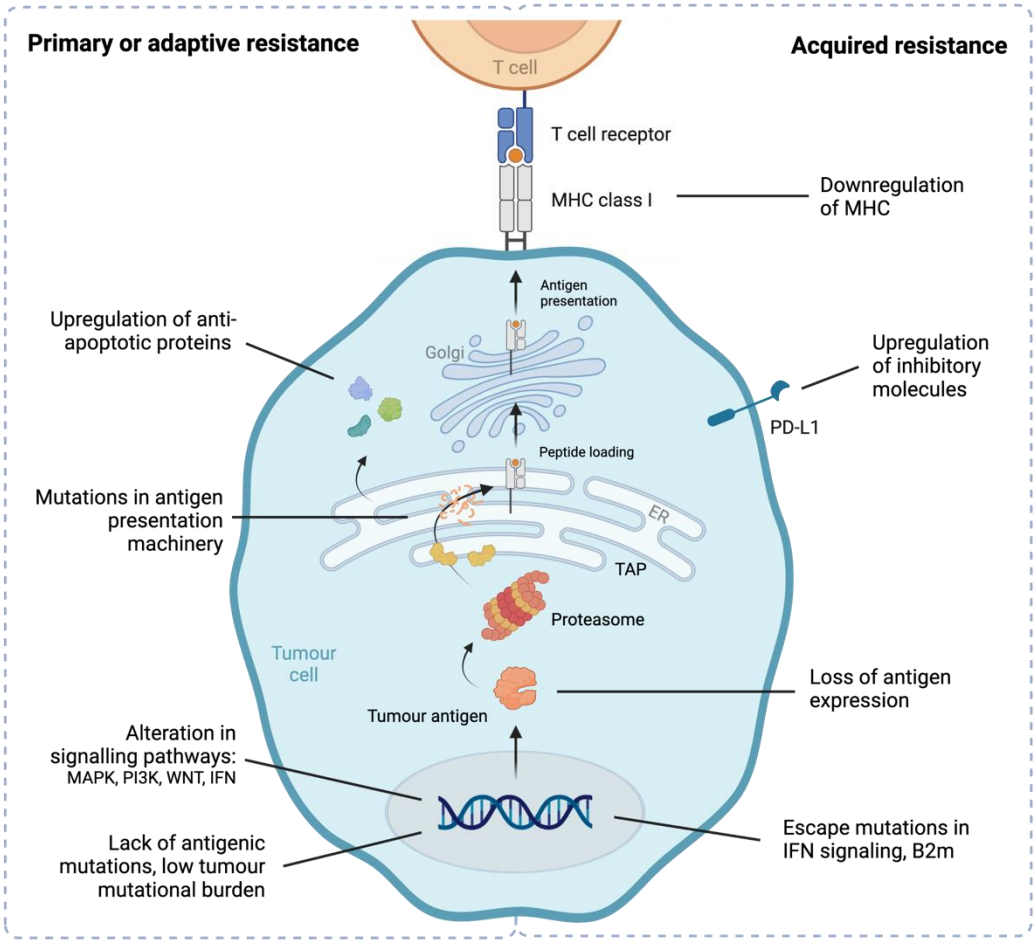

Figure 8. Tumour-intrinsic primary, adaptive, and acquired resistance pathways to immune checkpoint therapy. Factors which lead to primary or adaptive resistance (left) and acquired resistance (right) which are intrinsic to the tumour itself. Primary resistance is a result of the natural immune response against the tumour in the absence of immunotherapy, whereas acquired resistance are traits gained following immunotherapy. Both are the result of immune selective pressure, and pathways are not restricted to one type of immune resistance. Created with BioRender.com, adapted from Sharma, P., *et al.* (2017).[185]

Mutations for all components of the IFNGR1 pathway (e.g. IFNGR2, JAK1/2, STAT1 and IRF1) have also been found in human tumours during both primary or acquired resistance to ICB.[105,182,199–202] Lack of IFNγ response by tumour cells also mitigates the anti-proliferative or apoptotic effects exerted by the cytokine. Although PD-L1 upregulation is reduced in these tumours, the MHC-I-low and PD-L1-low phenotype is likely not conducive to ICB treatment efficacy.[201] Human cancer cell lines have also demonstrated elevated

expression of multiple SOCS family proteins, which inhibits JAK-STAT-dependent signalling and confers resistance against IFN-dependent signalling.[203]

1.5.3 Strategies to overcome primary and acquired ICB resistance

As ICB resistance is primarily dependent on MHC-mediated, T cell-dependent mechanisms, strategies to overcome escape may include restoring MHC expression, or harnessing non-MHC-dependent pathways of anti-tumour immunity. Studies have shown that loss of tumour IFNγ sensitivity does not necessarily abolish recognition by T cells.[202,204] Patient-derived melanoma cell lines carrying JAK1 or JAK2 knockouts retained basal MHC-I expression and the capacity to activate tumour-specific T cells *in vitro*. Recent studies have also shown that loss of MHC-I upregulation due to IFNγ-signalling deficiencies can be rescued using TLR agonist mimetics which induces MHC-I expression in an IFNγ-independent manner.[205,206] Similarly, activation of innate immunoreceptors such as retinoic acid-inducible gene I (RIG-I) has been shown to induce antigen presentation by tumour cells, thereby restoring T cell activity.[207]

For strategies which circumvent MHC expression, $CD8^+$ T cell-derived IFNγ was capable of maintaining Fas/FasL-dependent apoptosis of antigen-negative cells.[208] Recent studies which use $\beta2m^-$/ $\beta2m^+$ mosaic tumours in mice show that long-distance effects of IFNγ within the tumour are able to suppress outgrowth of antigen-negative cells in these tumours.[209] Lastly, loss in MHC-I-dependent recognition may be overcome by $CD4^+$ T cell cytotoxicity, which has been demonstrated in MHC-I^-/MHC-II^+ tumours.[210] As MHC-I acts as a primarily ligand for NK inhibitory receptors, strategies to boost NK-dependent anti-tumour functions are also of considerable importance.[211]

Given the important effects of IFNγ on tumour immunity, clinical trials have attempted to administer IFNγ systemically or locally in patients to treat solid tumours. Clinical responses were unfortunately very limited in the absence of other therapies.[212–214] IFNγ therapy was also hindered by detrimental side effects experienced by patients which included leukopenia and fever, likely due to non-specific systemic immune activation.

However, biweekly intraperitoneal injections over 3-4 months showed some response in a third of patients with ovarian cancer, indicating certain modes of delivery and tumour types may be amenable to IFNγ treatment.[215] Although it is not known for certain why IFNγ therapies have largely failed, it is likely that IFNγ itself cannot overcome the immunosuppressive mechanisms present in the tumour microenvironment, and may even contribute to pro-tumour effects. More recent trials (NCT03063632 and NCT02614456) have attempted to combine IFNγ with ICB in multiple tumour types, although these studies have not yet concluded.

1.6 Thesis rationale and objectives

As resistance to IFNγ is a primary and acquired immune escape mechanism found in nearly all solid cancers, a novel approach is needed for patients who are not responsive to treatment, or develop resistance to treatment over time. Furthermore, the role of IFNγ in shaping anti-tumour immunity and how it affects the efficacy of checkpoint blockade show seemingly paradoxical roles in literature and clinical observations.

To better understand how IFNγ-deficiency on tumour cells shape the tumour microenvironment over time, we aimed to address the following objectives:

1) Establish a IFNγ-insensitive murine tumour model whereby IFNGR1 expression is ablated using CRISPR-Cas9, and investigate the immunological changes which are involved in the anti-tumour response
2) Assess an admixture tumour model consisting of wild-type and IFNGR1 knockout cells, and investigate the effects of immune selective pressure on immune escape
3) Characterize the immune infiltrating populations in the established WT and IFNGR1KO tumour models using an unbiased transcriptomic approach and validate preliminary findings with experimental data

Materials and Methods

2.1 Mice.

C57BL/6J (B6) WT male mice from 6 to 10 weeks old were purchased from Charles River (JAX number – 000664) and housed 1-2 weeks before experimentation. IFNγ-GREAT^{YFP} (JAX number – 017580), CD8 KO (JAX number – 002665), and IFNγ KO (JAX number – 002287) mice were housed and bred under specific pathogen-free/SPF conditions in the in-house animal facilities at the University of Oxford. Experimental and control animals were co-housed. For bone marrow chimeras, recipient CD45.1 mice (JAX number – 002014) were irradiated with 4.25Gy per cycle for two irradiation cycles 4 hours apart. Bone marrow from WT B6, IFNγ KO, or NKp46^{iCre}R26R^{DTR} (NK-DTR, a kind gift from the group of Prof. Tal Arnon) mice were isolated from the femurs of 8–10-week-old male mice. Isolated bone marrow was mixed 1:1 WT:IFNγKO or NK-DTR:IFNγKO at a final concentration of 1x10^6 cells per 100µL and administered intravenously to irradiated hosts. For CB6F1 mice, male C57Bl/6 mice were bred with female Balb/c mice (JAX number – 000651) to generate F1 offspring.

All experiments involving mice were conducted in agreement with the United Kingdom Animal Scientific Procedures Act of 1986 and performed in accordance with approved experimental procedures by the Home Office and the Local Ethics Reviews Committee (University of Oxford) under UK project license P4BEAEBB5 and PP3609558. In all instances, mice were euthanized by CO_2 asphyxiation followed by cervical dissociation.

2.2 Cell lines and culture conditions.

In chapters 3 and 5, the B16F10 murine melanoma cell line expressing mCherry, ovalbumin and containing a knockout of tyrosinase (B16-OVA-mCherry) kindly provided by Dr. Edward Roberts from the Beatson Institute (Glasgow, UK) was used. For chapter 4, the B16F10 cell line originating from the lab of Prof. Vincenzo Cerundolo was modified to express ZsGreen-minOVA or mCherry-minOVA. minOVA constructs (sequence kindly provided by Dr. Ed

Roberts) were generated by molecular cloning of minimal OVA epitopes for $CD4^+$ ($OVA_{329-337}$) and $CD8^+$ ($OVA_{257-264}$) T cells fused to the C-terminus of the individual fluorescent protein sequences. Constructs were subcloned into a pHRSIN lentiviral backbone for stable transduction of cell lines. Transduced cell lines were sorted for positive expression of ZsGreen or mCherry by fluorescence activated cell sorting (FACS). CT26 murine colon adenocarcinoma obtained from the lab of Prof. Cerundolo were modified to express OVA or human NY-ESO1 antigens using pHRSIN lentiviral vectors encoding for expression of the given protein. All cell lines were cultured in RPMI 1640 (Gibco, Cat. 21870-076) supplemented with 10% FCS (Sigma, Cat. F9665-500ML), and 1X penicillin/streptomycin/L-glutamine (Gibco, Cat. 10378-016) (referred to as R10 medium). Cell lines were kept at 37°C in 5% CO_2.

2.3 CRISPR-Cas9 knockout of IFNGR1.

Knockout of murine IFNGR1 in the aforementioned cell lines was completed using CRISPR-Cas9-mediated gene editing described by Ran *et al.* (2013).[216] Briefly, the single guide RNA (sgRNA) design tool CRISPOR[217] was used to generate candidate sgRNAs against exon 1 or 2 of murine IFNGR1. Double stranded sgRNA oligos were cloned into pX458 backbone (Addgene) containing Cas9 expression and GFP expression, followed by validation via Sanger sequencing. Target murine cell lines were transiently transfected using Lipofectamine 3000 (Invitrogen, Cat. L3000001) with pX458 vectors containing the sgRNA against IFNGR1. After 48 hours, cells were single-cell sorted into individual wells of a 96-well plate. Single cell clones were expanded and stimulated with 1 ng/mL recombinant murine IFNγ (Peprotech, Cat. 315-05). Clones were stained for MHC-I H2-D^b (or H2-K^d for CT26) expression by flow cytometry analysis. Five individual clones unresponsive to IFNγ stimulation were pooled to form the final cell line used in subsequent experiments.

2.4 Tumour induction and administration of immune-modifying agents.

Cell lines were harvested at 50-70% confluency on the day of tumour injections using trypsin-EDTA (Sigma, Cat. T3924-500ML) and washed twice in PBS prior to resuspension at desired cell concentrations in PBS or PBS + 25% Matrigel (Corning, Cat. 354262, or Cat. 256231). Mice were anaesthetized using isoflurane (Zoetis) and flanks were shaved prior to injection. Tumour were typically implanted subcutaneously in the right and/or left ventral flanks at a cell concentration of 1.00-1.25x10^6 cells per mL, resulting in implantation of 1x10^5 or 1.25x10^5 cells per 100 µL injection. Alternative cell doses are indicated by specific experiment. Tumours were measured after 5-7 days post-injection using callipers and monitored for humane endpoints continuously until experimental termination. Tumour volumes were calculated using L^xW^xH in mm^3. For experiments involving administration of blocking or depleting antibodies (BioXCell) or diphtheria toxin (Sigma, Cat. D0564), agents were resuspended in sterile PBS at desired concentrations. Mice were injected intraperitonially and monitored daily.

2.5 Tissue processing and immune cell isolation.

At experimental or humane endpoints of animal experiments, mice were sacrificed and tumours were measured, excised, and weighed before processing. Experimental endpoints ranged from day 7 to 15 post-implantation, and are independently described in corresponding figures. Humane endpoints were defined as any dimension in tumour length, width or height which exceeded 12mm by calliper measurement. Tumours were dilacerated using scalpels to obtain <1mm sized pieces and resuspended in R10 supplemented with 1 mg/mL Liberase TL (Roche, Cat. 5401020001) and 10 µg/mL DNase I (Roche, Cat. 11284932001) for enzymatic digestion. Tumour suspensions were incubated at 37°C for 30 minutes before physical dissociation of remaining fragments through 70µm cell strainers to obtain single cell suspensions. Cells were counted by haemocytometer and trypan blue exclusion. For experiments where lymph node cells or splenocytes were collected, collected

organs were mechanically dissociated using syringe plungers and 70µm cell strainers. Cells were filtered again to obtain single cell suspensions and counted prior to assaying or flow cytometry analysis.

2.6 ELISAs.

Tumour supernatants were collected prior to enzymatic digestion following mechanical dilaceration in minimal volumes of R10 media (i.e., approx. 1mL supernatant per tumour). Samples were frozen at -20°C prior to assaying. IFNγ concentrations were determined using an IFNγ mouse uncoated ELISA kit (Invitrogen, Cat. 88-7314-77) following manufacturer's protocols. Obtained IFNγ concentrations using the standard curve were normalized to tumour weights.

2.7 Flow cytometry.

Single cell suspensions from cell lines, tumours, lymph nodes, or splenocytes were plated into 96-well V bottom plates at concentration of $2.5x10^6$ cell or less. Cells were washed 1X using PBS prior to addition of viability dyes (Biolegend, Zombie NIR, Cat. 423106, or Zombie UV, Cat. 423108) according to manufacturers' instructions. Samples were incubated with anti-CD16/anti-CD32 blocking antibodies (Biolegend, Cat. 101302) for 20 minutes at 4°C, followed by fluorochrome-conjugated antibodies against extracellular markers for 30 minutes at 4°C. Cells were washed with FACS-EDTA buffer (2% FCS, 2.5 mM EDTA, and 0.01% sodium azide in PBS) and resuspended in 2% paraformaldehyde (Alfa Aesar, Cat. 43368.9M) in PBS for a 20-minute fixation at 4°C. Cells were washed before resuspension in FACS-EDTA buffer and stored until analysis. For experiments where tetramers were used, tetramers were diluted in FACS-EDTA and incubated with samples in-between the Fc-blocking and antibody staining steps. Tetramers were obtained from the NIH Tetramer Core Facility (Atlanta, GA, USA). For experiments where intracellular cytokines were detected, cells were fixed and permeabilized with BD Cytofix/Cytoperm (BD, Cat. 554714) following extracellular marker staining for 20 minutes at 4°C and washed with 1X PermWash. Cells

were then incubated with intracellular antibodies diluted in 1X PermWash for 30 minutes at 4°C, and then washed with FACS-EDTA before being resuspended for analysis. For samples where calculation of absolute cell numbers was required, 20,000 Polybead polystyrene Black Dyed Microspheres (Polyscience, Cat. 24293-15) were added to the samples prior to analysis. Absolute counts (cells/µL) were calculated as ((Cell count ˣ counting beads volume) / (Counting beads ˣ Cell volume)) ˣ Counting beads concentration (beads/µL). All flow cytometry samples were analysed by BD Fortessa X-20, BD LSRII, or Cytek Aurora as indicated per experiment. Flow cytometry data was analysed using FlowJo V.10 (BD), or OMIQ (Dotmatics).

2.8 Antibodies.

Antibodies used for flow cytometry, confocal microscopy, or *in vivo* depletion are listed in the table below. Full antibody panels used for flow cytometry are detailed in the corresponding appendices for each study, at the dilutions indicated per experimental condition.

Flow Cytometry				
Specificity	**Fluorochrome**	**Clone**	**Manufacturer**	**Cat. No.**
B220/CD45R	BV510	RA3-6B2	Biolegend	103248
B220/CD45R	BUV615	RA3-6B2	eBioscience	366-0452-82
CD103	BV605	2E7	Biolegend	121433
CD103	BV785	2E7	Biolegend	121439
CD119 (IFNGR1)	PE	REA189	MACS Miltenyi Biotec	130-104-987
CD11b	BV510	M1/70	Biolegend	101245
CD11b	APC-Fire810	M1/70	Biolegend	101288
CD11c	FITC	N418	Biolegend	117305
CD11c	BV605	N418	Biolegend	117333
CD11c	PB	N418	Biolegend	117321
CD11c	Spark387	N418	Biolegend	117370
CD11c	APC	N418	Biolegend	117309
CD163	PE/Cy7	S15049I	Biolegend	155320
CD19	Alexa Fluor 647	6D5	Biolegend	115525
CD19	APC/Cy7	6D5	Biolegend	115529
CD206	BV421	C068C2	Biolegend	141717
CD223 (LAG3)	PE-Cy7	C9B7W	Biolegend	125225

CD274 (B7-H1, PD-L1)	PerCP/Cy5.5	10F.9G2	Biolegend	124334
CD274 (B7-H1, PD-L1)	BV650	10F.9G2	Biolegend	124333
CD279 (PD-1)	FITC	29F.1A12	Biolegend	135213
CD279 (PD-1)	BV605	29F.1A12	Biolegend	135219
CD3	FITC	17A2	Biolegend	100203
CD335 (NKp46)	Alexa Fluor 647	29A1.4	Biolegend	137628
CD366 (TIM3)	APC	RMT3-23	Biolegend	119706
CD4	PerCP/Cy5.5	GK1.5	Biolegend	100433
CD4	BUV 661	RM4-5	eBioscience	376-0042-82
CD44	BV785	IM7	Biolegend	103059
CD44	BUV737	IM7	eBioscience	367-0441-82
CD45	PE-Cy7	30-F11	Biolegend	103113
CD45	BV785	30-F11	Biolegend	103149
CD45	BUV805	30-F11	eBioscience	368-0451-82
CD62L	BV605	MEL-14	Biolegend	
CD62L	BV711	MEL-14	Biolegend	104438
CD68	PerCP-Vio700	FA-11	MACS Miltenyi Biotec	130-102-926
CD86	BV605	GL-1	Biolegend	105037
CD8α	BV650	53-6.7	Biolegend	100742
CD8α	Spark387	53-6.7	Biolegend	100798
CX3CR1	APC-Cy7	SA011F11	Biolegend	149048
F4/80	BV785	BM8	Biolegend	123141
F4/80	APC	BM8	Biolegend	123115
H2-K^b	AF700	AF6-88.5	Biolegend	116521
IFNγ	APC	XMG1.2	Biolegend	505810
Ly6C	PE-Cy7	HK1.4	Biolegend	128018
Ly6C	APC	HK1.4	Biolegend	128015
Ly6G	PB	1A8	Biolegend	127612
MHC-Class I (H2-K^b)	APC	AF6-88.5	Biolegend	116517
MHC-Class I (H2-K^b)	AF700	AF6-88.5	Biolegend	116521
MHC-Class I (H2-D^b)	eF450	28-14-8	Invitrogen	48-5999-80
MHC-Class II	AF700	M5/114.15.2	Biolegend	107621
MHC-Class II	BV421	M5/114.15.2	Biolegend	107631
MHC-Class II	PE-Cy5	M5/114.15.2	Biolegend	107611
NK1.1	PE-Cy7	PK136	Biolegend	108714
TCRβ	PE	H57-597	Biolegend	109207
TNFα	BV785	MP6-XT22	Biolegend	506341
TREM2	PE	237920	R&D systems	FAB17291P

Immunofluorescent Confocal Microscopy				
Specificity	**Fluorochrome**	**Clone**	**Manufacturer**	**Cat. No.**
CD8β	N/A	EPR22331-54	Abcam	ab228965
CD8α	AF647	EPR21769	Abcam	ab237365
Donkey Anti-Rabbit IgG	AF647	Polyclonal	Biolegend	Poly4064

***In vivo* Antibodies**				
Specificity	**Fluorochrome**	**Clone**	**Manufacturer**	**Cat. No.**
NK1.1	N/A	PK136	BioXCell	BE0036
Mouse IgG2a isotype	N/A	C1.18.4	BioXCell	BE0085

2.9 *Ex vivo* T cell stimulation.

For experiments where $CD8^+$ T cells were isolated from tumour single cell suspensions, mouse CD8 (TIL) microbeads (Miltenyi, Cat. 130-116-478) were used following manufacturer's protocols. Otherwise, splenocytes from tumour-bearing mice were collected and co-incubated in the presence or absence of the appropriate peptides (10 ng/mL, ProteoGenix), or PMA (1 µg/mL) + ionomycin (5 nM), and brefeldin A (5 µg/mL, Santa Cruz, Cat. sc-200861) for 4-6 hours at 37°C. At the end of the incubation period, cells were stained for flow cytometry analysis of surface and intracellular cytokines. For experiments where OT-I T cells were stimulated with B16F10 cell lines, $CD45^+$ cells isolated from the tumour or *ex vivo*-isolated tumour cells, OT-I $CD8^+$ T cells were isolated from splenocytes of OT-I mice using Mojosort CD8 isolation kit (Biolegend, Cat. 480035).

2.10 Tissue fixation, cryosectioning, and confocal imaging

Tumours were harvested at indicated timepoints days 10-17 post-engraftment as described previously. Whole intact tumours were immersed in fixative solution (1% PFA, 75 mM L-

lysine [Sigma, Cat. L5501], 10 mM sodium m-periodate [Thermo Scientific Pierce, Cat. 20504], diluted in 0.2M PBS adjusted to pH 7.4) for 16-20 hours at 4°C under gentle agitation. Fixative solution was discarded and tumours were washed using 1X PBS for 1 hour at 4°C under gentle agitation to remove remaining PFA. Tumours were then resuspended in 30% sucrose (w/v, diluted in pH 7.4 PBS) for 24-36 hours at 4°C without agitation, until tissue was no longer floating. Tumours were cryogenically frozen in OCT compound (Thermo Fisher, Cat. 15212776) using methanol and dry ice bath, and stored at -80°C until cryosectioning. Frozen tumour blocks were cryosectioned at 10 µm thickness using a Leica CM1900UV and mounted onto glass slides (VWR, Cat. 631-0108). Cryosections were stored at -80°C until staining. For staining, sections were washed with PBS to remove OCT compound on the slides, and blocked with solutions containing imaging buffer (2% FCS, 0.1% Triton X-100 (Sigma, Cat. X100), 0.01% sodium azide), FcBlock, and species-specific serum depending on the fluorochrome-conjugated antibodies used in each staining panel. Sections were blocked for a minimum of 3 hours at room temperature, before incubation with primary or secondary conjugated antibodies diluted in blocking solution overnight at 4°C. If secondary antibodies were required, sections were washed twice, 15 minutes each, with imaging buffer before incubation with secondary antibodies for 2 hours at room temperature. When required, sections were incubated with DAPI for nuclear staining for 10 minutes at room temperature. A final wash was performed twice using imaging buffer before the sections were mounted using Fluoromount G (Southern Biotech, Cat. 0100-01) and glass coverslips were placed on top of the sections. Images were collected using Zeiss LSM 880 or 980 confocal microscope, and analysed using Imaris software (Bitplane, V9.9).

2.11 Single-cell RNA sequencing.

Single cell suspensions from B16F10 tumours were harvested as previous described. Cells from B16-mCherry-OVA WT tumours were labelled with TotalSeq(TM)-C0301 antibody (Biolegend, Cat. 155861), and IFNGR1KO tumours were labelled with TotalSeq(TM)-C0302 (Biolegend, Cat. 155863). Samples were then stained for live/dead using Zombie NIR, and

$CD45^+$ prior to single cell sorting using a BD FACSAria II. Approximately 10,000 cells were loaded onto a 10X Genomics Chromium Controller (Chip K). Gene expression, feature barcoding and TCR sequencing libraries were prepared using the 10x Genomics Single Cell 5' Reagent Kits v2 (Dual Index) following manufacturer user guide (CG000330 Rev B). The 10 nM library was denatured and further diluted prior to loading on the NovaSeq6000 sequencing platform (Illumina, v1.5 chemistry, 28 bp/98 bp paired end for gene expression and feature barcoding).

2.12 Analysis of scRNAseq datasets.

Sequence reads were mapped using CellRanger multi (version 6.0.0) and the 10x mouse reference transcriptome (version 2020-A). The R package Seurat v4 was used in conjunction with other tools for QC, demultiplexing, filtering, and annotation of the dataset. Briefly, singlets were extracted from the dataset, and counts were log normalized and variable features were scaled. Cells having fewer than 500 or greater than 6000 detected genes were filtered out. Cells in which 5% of the UMIs represent mitochondrial protein-coding genes or more than 20% of large gene contents were also filtered. Lastly, decontX was used to determine contamination of droplets with ambient RNA. The filtered dataset was scaled, log normalized and variable features were identified using the functions in Seurat. Principle component analysis was performed and the number of PCs used for clustering was determined using the ElbowPlot function. Clusters and markers for clustered was identified using the Louvain algorithm embedded in the FindNeighbours and FindClusters functions, at a resolution of 0.5. UMAP projections were computed using the first 10 principal components. Clusters were annotated using the FindAllMarkers function to determine differentially expressed genes for each cluster, then cluster identities were verified using the package SingleR. Heatmaps, violin plots, and UMAP projections were generated using Seurat. The FindMarkers function was used to find differentially expressed genes within each cluster between WT and IFNGR1KO conditions. Pathway analysis and plotting of results was performed using the tool fgsea. Volcano plots and bar plots were created using

ggplot2. Module scoring of different TAM subsets was done using the package UCell. Trajectory analysis for $CD8^+$ T cell and macrophage clusters was completed and visualized using the package monocle3. Finally, analysis of cell-cell communication networks and plotting of results were done using the package CellChat.[218]

2.13 Statistical analysis

Statistics were done with GraphPrism v9 software. In general, comparisons between two groups was done using non-parametric Mann-Whitney *t*-tests. Kruskal-Wallis tests were used to compare three or more unmatched groups. Dunn's test for non-parametric groups was used to correct for multiple comparisons, and adjusted *p*-values are reported. Two-way ANOVA was performed for multiple groups of more than two cell types, followed by Tukey's test for correction of multiple comparisons. Details of statistical test performed are provided for each figure individually.

Establishing an IFNγ-resistant model of B16F10 murine melanoma model and immunophenotyping of the anti-tumour response

3.1 Introduction

This chapter describes the establishment of IFNγ-resistant murine tumour models *in vivo* and phenotyping the resulting endogenous immune response. In brief, a subcutaneous model of B16F10 (B16) modified to express a fluorescent marker mCherry and exogenous antigen ovalbumin was used to study IFNγ-insensitivity in C57BL/6 (B6) mice. Wild-type and IFNGR1-deficient B16 mCherry-OVA (hereafter, B16-OVA) tumours were evaluated for their tumour growth and immunogenicity. Although IFNGR1KO tumours were expected to grow faster in mice compared to WT, they surprisingly remained similar in tumour volume during tumour progression. This effectively provided us with a model by which tumour control may not be solely dependent on $CD8^+$ T cell cytotoxicity, due to the low MHC class I levels detected on IFNGR1KO tumours.

3.1.1 Origins of the B16F10 murine melanoma and its use as an orthotopic tumour model

B16 melanoma was originally isolated as a spontaneous tumour forming on the ear pinnae of a B6 mouse, which was subsequently passaged *in vitro*. Used primarily as a model for metastasis during the 1970s, individual clones of B16 melanoma cells were cultured *in vitro* and intravenously administered to B6 mice.[219,220] These experiments showed that not only can lung metastases form from individual cells, but independent clones also resulted in different numbers of pulmonary tumour colonies.[221] B16F10 was derived from the parental cell line B16F1, and was the result of successive *in vitro* cultures of explanted pulmonary tumours, followed by re-injection of passaged cells intravenously into new mice.[221] As such, B16F10 is considered a highly metastatic line due to its reliability in producing pulmonary tumours when administered intravenously.

When implanted subcutaneously or intradermally, B16 can be considered an orthotopic model which forms palpable tumours approximately 5 days following injection.[222] Compared to human melanoma, however, mutations found in B16F10 do not recapitulate common mutations found in human melanoma such as proto-oncogenes *Nras* and *Braf*, which occur in 20% and 50% of cases, respectively.[223] This difference is likely due to environmental factors initiating carcinogenesis, such as the association of UV damage in the occurrence of *Braf* mutations.[224] Nevertheless, B16F10 remains an important model due to its B6 background and versatility of transgenic murine strains available.

3.1.2 B16F10 as a model of IFNγ-dependent tumour growth

One characteristic of B16F10 observed early on was that variants of the cell line harboured differential sensitivity to killing by syngeneic T cells, which could be explained by either loss of tumour-specific antigens, or selective loss of MHC class I expression over time. B16 melanoma is widely recognized as a poorly immunogenic tumour model due to its comparatively low expression of MHC class I.[225] However, numerous *in vitro* and *in vivo* studies have shown that IFNγ stimulation can restore MHC-I expression and subsequently, T cell-mediated immune responses.[226] The MHC-I deficiency in B16 is attributed to significant RNA and protein downregulation of almost all members of the antigen processing family, including LMP2/7/10 and PA28a/28b, and peptide transporters tapasin and TAP1. The suppression of these transcripts was found to be caused by epigenetic repression through DNA methylation or histone acetylation. As such, restoration of MHC-I expression can be achieved by treatment with epigenetic modifiers[227], or IFNγ stimulation.

Previous studies have shown the IFNγ derived from T cells alone is sufficient to induce upregulation of gamma-dependent genes by tumour cells *in vivo.*[228] Furthermore, sensing of IFNγ is not restricted to cells which can be targeted by T cells. In a model where OVA-specific transgenic T cells, also known as OT-I, were transferred into $Rag2^{-/-}$ mice bearing mixed B16-WT and B16-OVA tumours, all tumour cells expressed the same level of

MHC-I and PD-L1, indicating that direct T cell engagement is not necessary and IFNγ diffuses widely within the tumour microenvironment.

Given that the B16F10 cell line is the result of multiple rounds of *in vivo* passaging, it is also useful to keep in mind that many immune escape mechanisms are already present in the model upon implantation into a immunocompetent host. The immune escape strategies found within B16 tumours are not unique to the model but shared by many others. However, **c**ompared to other syngeneic models across different mouse strains, B16F10 had the lowest immune infiltration, regardless of tumour size.[225] Although partially explained by the low mutational burden of B16, low immune infiltration is likely driven by MHC-I downregulation, which in turn reduces $CD8^+$ T cell infiltration and influx of inflammatory cytokines which are required for infiltration of other immune cells.[225,229] It would also be useful to note that modification of the cell line to express ovalbumin has strong implications on cell- and humoral-mediated immunity, and likely mitigates some immune escape mechanisms which have been previously observed.

3.1.3 B16F10 response to checkpoint blockade

Response rates of anti-PD-1/PD-L1 therapy remains highly variable in humans, despite pre-screening protocols which attempt to increase chances of success. Although one would expect that a syngeneic tumour model in a controlled genetic background would produce comparable results, the literature surrounding whether B16 responds to ICB, either as a monotherapy or in combination, remains discordant. For anti-PD1/PD-L1, an equal number of studies show no response to therapy[229–233], as compared to partial reduction in tumour burden.[97,234–236] Although these differences may at first be attributed to incongruent drug dosing or administration schedules, recent clinical data has furthermore uncovered that parameters from human trials such as microbiome[237], diet[238], and age[239], are also important considerations for animal studies. These parameters although controlled independently, likely vary between different studies and institutions, therefore affecting overall outcomes. In

general, only combination therapies which involve vaccination, radiotherapy, or a second ICB agent is required for significant reduction of B16F10 tumour growth *in vivo*.

The experiments presented in this chapter sought to investigate IFNγ-dependent pathways of anti-tumour immunity in B16F10. We hypothesized that IFNGR1KO tumours would outgrow WT counterparts as ample literature suggested that B16F10 can only elicit a strong anti-tumour response when MHC-I is induced. These data showed instead that spontaneous tumour control can be achieved even when MHC-I expression was at baseline due to ablation of IFNγ-signalling in tumour cells.

3.2 Results

3.2.1 IFNGR1 KO B16F10 melanoma exhibits comparable growth rates to WT tumours *in vivo* despite decreased expression of MHC molecules

In order to evaluate an IFNγ-insensitive tumour model, knockout of the IFNGR1 chain was undertaken using CRISPR-Cas9 methodology (**Figure 9A**). Complete knockout of IFNGR1 in B16F10 mCherry-OVA-expressing cells was validated through immunostaining of the cell lines for MHC class I and II 48 hours post-stimulation with recombinant murine IFNγ (**Figure 9B**). The *in vivo* model for subcutaneous B16F10 involves injection of WT of IFNGR1KO cell lines into the flanks of wild-type C57Bl/6 (B6) mice, and subsequent harvest of tumours 10-15 days after implantation (**Figure 9C**).

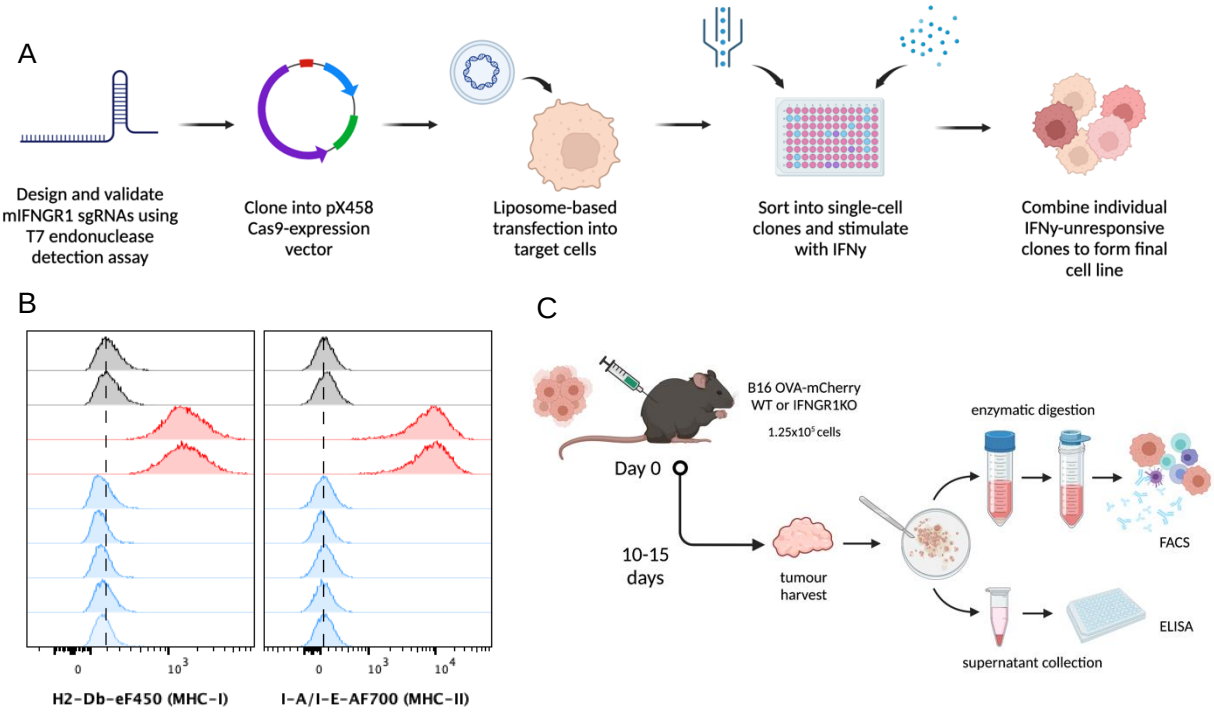

Figure 9. Overview and characterization of a B16-OVA IFNGR1KO tumour model. (A) Workflow for generating the cell lines using CRISPR-Cas9 editing and selection of single cell clones. (B) Stimulation of five individual clones using recombinant murine IFNγ (1ng/mL) and immunostaining for MHC class I and II expression via flow cytometry analysis. Non-stimulated WT in grey, IFNγ-stimulated WT in red, and IFNγ-stimulated CRISPR-Cas9-treated clones in blue. Each histogram represents one sample or cell clone. (C) Workflow for the B16F10 tumour model and methods for subsequent analysis of tumour phenotype and immune infiltrates. Diagrams created with BioRender.com.

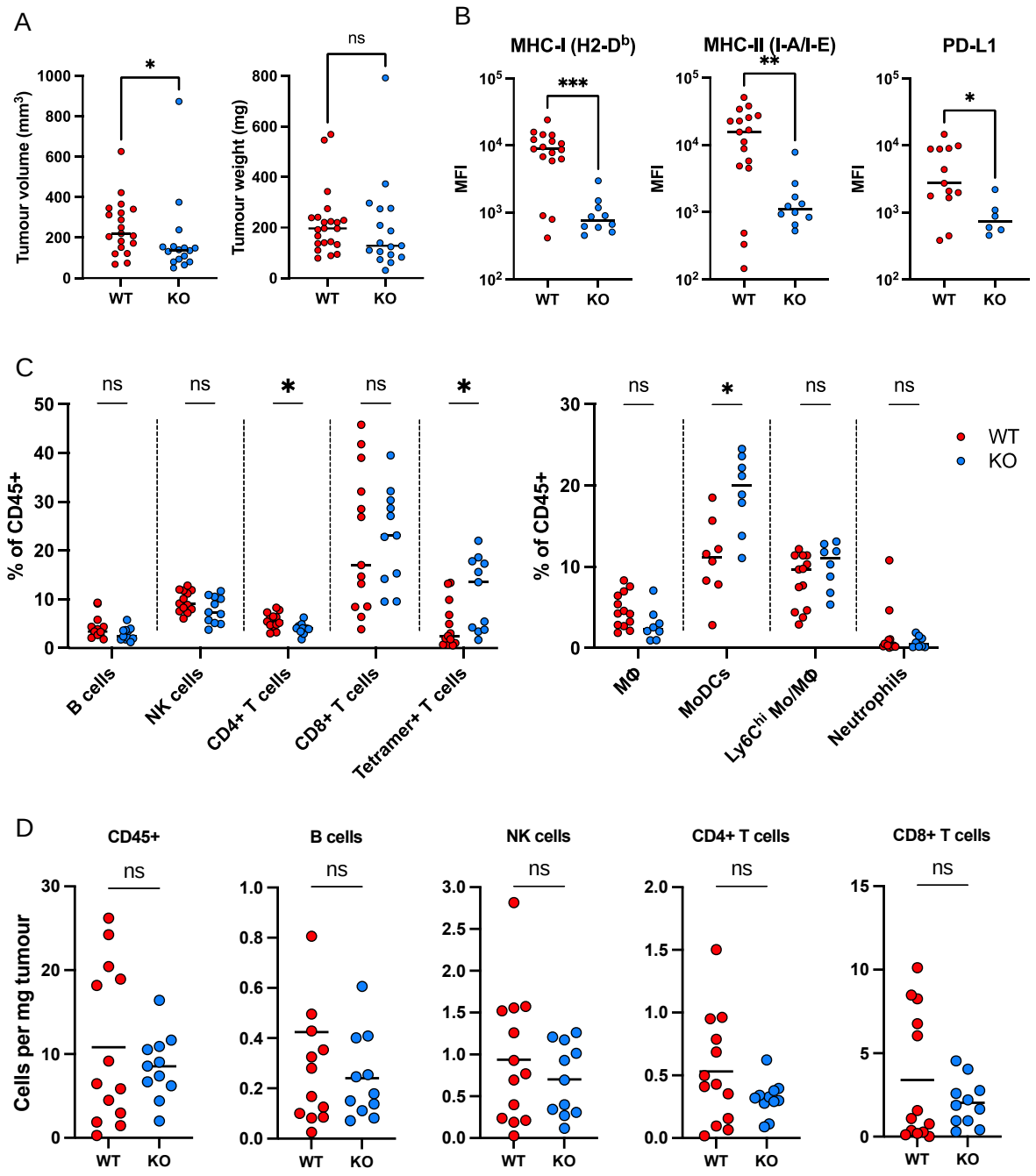

Figure 10. Phenotype of B16-OVA WT vs IFNGR1KO tumours measured by tumour volume, surface expression of IFNγ-dependent genes, and immune infiltration. (A) Tumour volumes and weights measured from B16-OVA WT and IFNGR1KO tumour-bearing mice on days 12-13 post-implantation. Data for B16-OVA WT (n=19) and IFNGR1KO (n=16) tumours were pooled from five independent experiments. (B) Surface expression of MHC-I, MHC-II, and PD-L1 on WT or IFNGR1KO tumour cells isolated from *ex vivo* dissociated tumours. Values shown are median fluorescence intensity. (C) Immune infiltration of WT and IFNGR1KO tumours by lymphoid and myeloid populations measured by flow cytometry as a percentage of live CD45$^+$ cells. Gating strategy and markers used for classification summarized in **Figure S1**. (D) Absolute counts of immune cells per mg of tumour tissue. Data are pooled from three independent experiments for A and B, and two independent experiments for C and D. Data show mean with *p*-values by non-parametric Mann-Whitney *t* tests, **p*≤0.05; ***p*≤0.01; ****p*≤0.001.

IFNGR1KO tumours were modestly smaller in tumour volume at time of harvest, but not statistically significant in tumour weight difference compared to WT (**Figure** 10**A**). Immunostaining for MHC-I, MHC-II, and PD-L1 showed that KO tumours expressed significantly lower levels of these IFNγ-dependent markers (**Figure** 10**B**). Antibody panels used for staining of tumour cells and immune cells isolated *ex vivo* are detailed in Table S1. To investigate the effects of diminished antigen presentation on the infiltration of lymphocyte populations such as NK cells and $CD8^+$ T cells, infiltration of immune populations relative to the whole $CD45^+$ population within the tumour, as well as cell density, were analysed. Relative frequencies of infiltrating lymphoid populations were similar between WT and IFNGR1KO, except for a modest decrease in $CD4^+$ T cells and increase in OVA-specific (i.e., tetramer positive) T cells (**Figure** 10**C**). Furthermore, a significant increase in monocyte-derived DCs, defined as MHC-II^+ $CD11b^+$ $Ly6C^+$ $CD11c^+$, was observed in KO tumours compared to WT. Total cell counts normalized by tumour weight were similar between WT and IFNGR1KO tumours, indicating that loss of IFNγ signalling by tumour cells did not significantly impact overall immune infiltration in this model (**Figure** 10**D**).

3.2.2 Intratumoural production of IFNγ by $CD8^+$ T cells and NK cells leads to accumulation of IFNγ in IFNGR1 KO tumours

Using a murine fluorescent reporter strain where production of the expression of enhanced yellow fluorescent protein (EYFP) was driven by the IFNγ promoter, production of IFNγ was tracked across different immune populations within the tumour microenvironment over time. During early timepoints following tumour implantation (days 7-8), EYFP-positive cells were comprised equally of NK cells and $CD8^+$ T cells. Over time, the proportion of IFNγ-$EYFP^+$ cells which were $CD8^+$ T cells increased, while NK cells decreased (**Figure 11A**). Using mean fluorescence intensity as a surrogate measure of the level of IFNγ being produced per cell, MFI was two-to-five-fold higher in $CD8^+$ T cells compared to NK cells on days 7-10 post-tumour implantation (**Figure 11B**). Although T cells from WT tumours appeared to produce more IFNγ when using EYFP MFI as a measure, ELISAs performed on

tumour supernatants showed high levels of IFNγ present in IFNGR1KO compared to WT (**Figure 11C**).

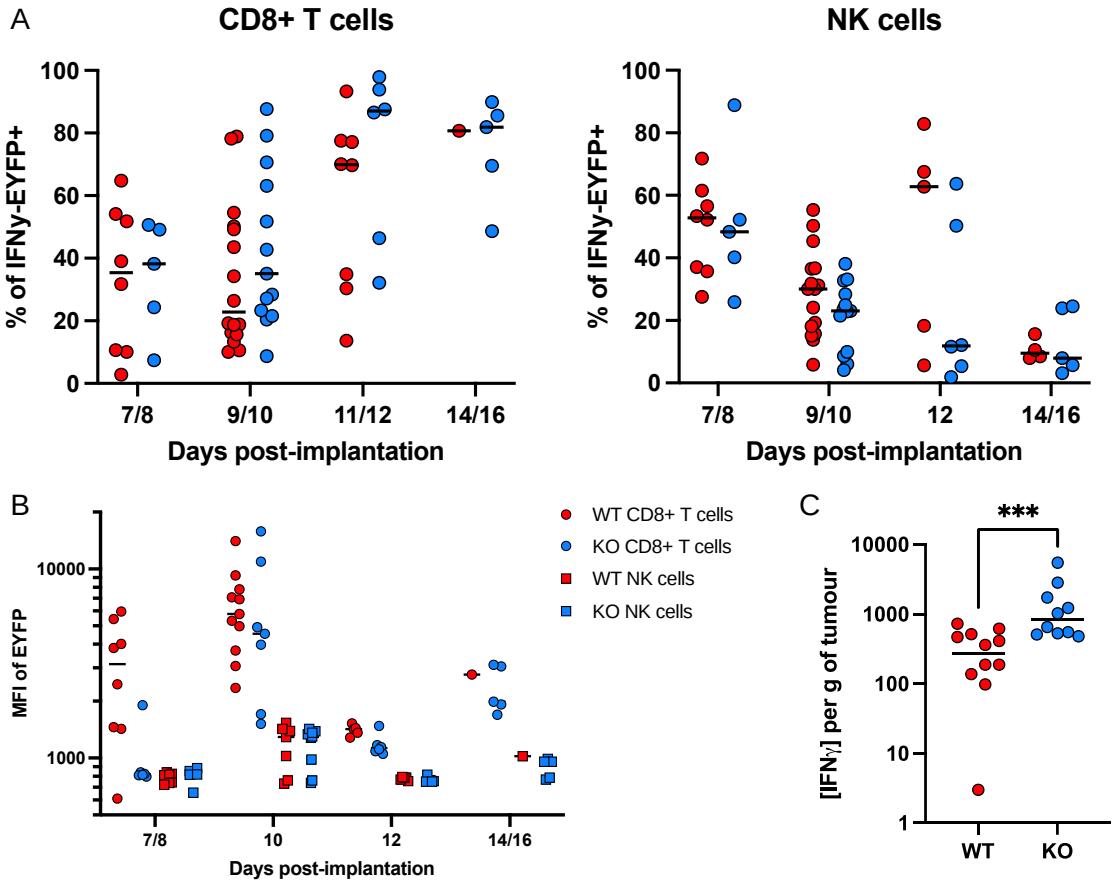

Figure 11. IFNγ production by tumour-infiltrating CD8⁺ T cells and NK cells measured using a EYFP reporter mouse. (A) Proportion of EYFP⁺ immune cells which are identified as CD8⁺ T cells (TCRß⁺/CD8⁺) or NK cells (TCRß⁻/NK1.1⁺) measured at indicated time points following tumour implantation. (B) Comparison of EYFP mean fluorescence intensity between CD8⁺ T cells and NK cells from B16-OVA WT and IFNGR1KO tumours. (C) Intratumoural concentration of IFNγ from tumour supernatants following mechanical dissociation of tumours collected on days 9-12 post-implantation, measured via ELISA. Data are pooled from three independent experiments, and show mean with *p*-values by non-parametric Mann-Whitney *t* tests, **p*≤0.05; ***p*≤0.01; ****p*≤0.001.

3.2.3 Characterising the CD8$^+$ T cell response in B16-OVA

To investigate whether CD8$^+$ T cells from IFNGR1KO tumours were functionally different than WT, tumour-infiltrating CD8$^+$ T cells were isolated from WT or KO tumours and re-stimulated using H-2K^b-restricted OVA peptide (**Figure 12A**). During T cell stimulation, the TCR is downmodulated for signal transduction, and to limit T cell overstimulation.[240] As expected, surface TCRβ expression by CD8$^+$ T cells in the tumour-draining lymph nodes (tdLNs) was similar regardless of the type of tumour implanted. Infiltrating CD8$^+$ T cells from IFNGR1KO tumours had modestly higher TCRβ expression compared to WT (**Figure 12B**). However, tetramer binding for OVA-specific T cells from IFNGR1 tumours was significantly higher compared to WT (**Figure 12C**). In this scenario, higher tetramer MFI could be indicative of higher T cell affinity, or less TCR downregulation due to reduced stimulation. Using intracellular cytokine staining to measure T cell activation, higher affinity T cells would activate and respond to lower affinity peptides with greater sensitivity than lower affinity counterparts. At present, we observed no difference in the proportion of CD8$^+$ TILs that responded to PMA/ionomycin or OVA peptide stimulation, measured as IFNγ (**Figure 12D**) or TNFα (**Figure 12E**) production. However, our assay would benefit from dose-dependent titration of the stimuli to better understand whether EC_{50} (i.e., the peptide concentration which results in half maximum responding T cells) differs between WT and KO tumours. T cells were also unresponsive to stimulation with cultured, IFNγ-stimulated B16F10 cells above baseline (data not shown). As these assays were preliminary in evaluating endogenous CD8$^+$ T cell function, further experiments will be required to ascertain differences in cytotoxicity such as granule release, etc.

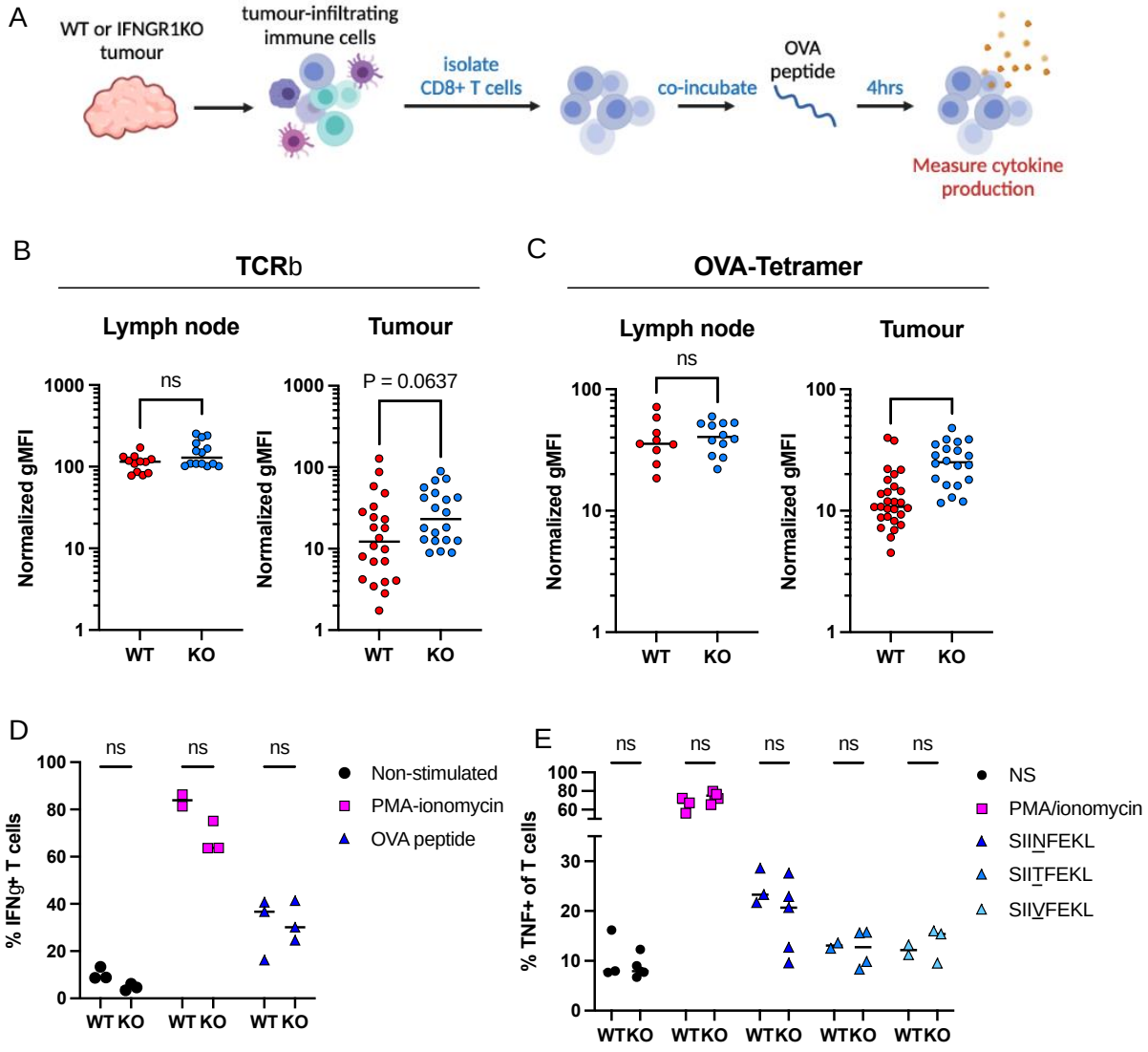

Figure 12. Isolation and *ex vivo* re-stimulation of CD8⁺ T cell from B16-OVA WT and IFNGR1KO tumours. (A) Workflow for isolation and re-stimulation of CD8⁺ T cells from tumours collected on days 10-12 post-implantation. Surface expression of TCRß (B) or OVA-specific TCR via tetramer staining (C) was normalized to the mean fluorescence intensity of the TCRß⁻ or tetramer-negative population within each sample, respectively. Samples were gated on live CD8⁺ T cells from the lymph node or tumour-infiltrating cells. Data are pooled from two or three experiments for lymph nodes and tumour, respectively. (D) Intracellular cytokine staining of IFNγ production by intratumoural CD8⁺ T cells following stimulation via PMA (1µg/mL) + ionomycin (5nM) or SIINFEKL peptide stimulation (1µg/mL). Data is from one experiment. (E) TNFα production by intratumoural CD8⁺ T cells following stimulation via PMA+ionomycin, or OVA peptide variants. Data is from one experiment. All data show mean with *p*-values by non-parametric Mann-Whitney *t* tests in B, and two-way ANOVA in C and D, ****$p \leq 0.0001$.

While CD8⁺ T cells from KO tumours appear to have similar fitness than T cells from WT, we next assessed whether WT and KO tumours would display a difference in the capacity to prime those cells. Our above assessment of surface levels of IFNγ-inducible proteins such as MHC-I/II and PD-L1 between WT and IFNGR1KO tumours suggests that KO tumours would not be able to efficiently stimulate T cells. Therefore, the relative

immunogenicity of *in vivo* vs. *in vitro* B16 tumours was investigated using OT-I activation as a surrogate for antigen presentation (**Figure 13A**). Maximal IFNγ-inducible levels of MHC-I and PD-L1 was measured following *in vitro* stimulation of the cell lines, and compared with expression on isolated tumour cells *ex vivo* (**Figure 13B**). When co-incubated with naïve OT-I T cells, the B16F10 WT cell line was highest in activation potential whereas the IFNGR1KO counterpart did not elicit any response above baseline (**Figure 13C**). *Ex vivo* isolated WT tumour cells were two-fold less stimulatory compared to the cell lines despite significant MHC-I expression, suggesting that inhibitory mechanisms such as PD-L1 expression may be limiting activation of OT-I *in vitro.* Interestingly, CD45+ immune cells isolated from WT and IFNGR1KO tumours showed a significant difference in their ability to activate OT-I T cells, indicating a possible discrepancy in antigen presentation, or suppression of activation by immune counterparts of each tumour microenvironment.

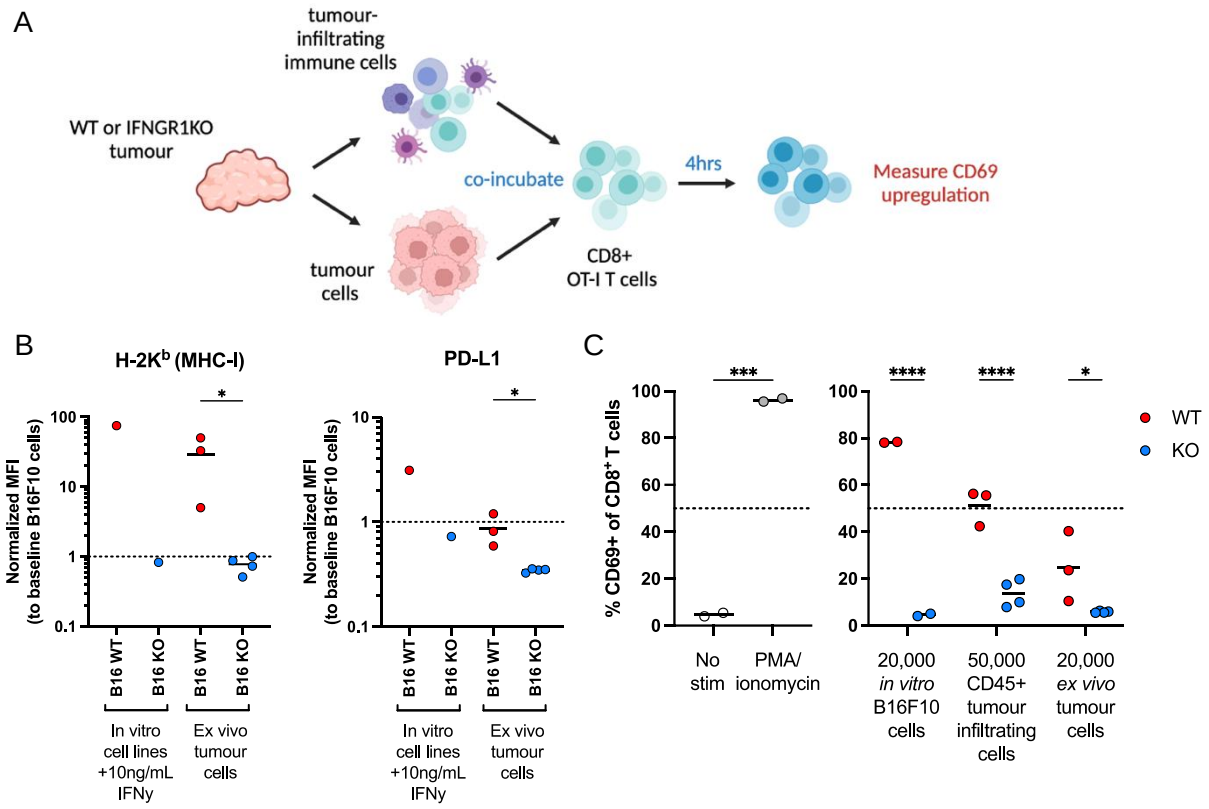

Figure 13. Stimulation of OT-I T cells using *ex vivo* tumour single cell suspensions. (A) Workflow for isolation of tumour and CD45$^+$ populations from B16-OVA WT and IFNGR1 day 10 tumours and stimulation of OT-I T cells *in vitro*. (B) Comparison of MHC-I and PD-L1 levels on IFNγ-stimulated B16-OVA cell lines, and single-cell suspensions of B16-OVA tumour cells isolated *ex vivo*. (C) Upregulation of CD69 by naïve OT-I CD8$^+$

T cells following 4-hour co-incubation with *in vitro* IFNγ-stimulated cell lines or *ex vivo*-isolated $CD45^+$ immune cells, or $CD45^-$ tumour cells from WT or IFNGR1KO tumours. Data is from one experiment and show mean with *p*-values by non-parametric Mann-Whitney *t* tests in B, and two-way ANOVA in C, **p*≤0.05, ****p*≤0.001, *****p*≤0.0001.

3.2.4 Control of B16 IFNGR1KO tumours is not dependent on ovalbumin expression

Ovalbumin, although a useful tool for tracking *in vivo* cellular and humoral responses, represents a wholly foreign antigen which can increase overall tumour immunogenicity. To ensure that the observed phenotype whereby B16-OVA IFNGR1KO tumours do not grow faster than WT, similar experiments using the parental B16F10 cell line were completed. IFNGR1 was deleted from parental B16F10 cells using the same method as described in Figure 9A. Compared to WT, parental B16 IFNGR1KO tumour were similar in volume (**Figure 14A**), and displayed similar phenotype to previously experiments where tumours failed to upregulate MHC-I/II and PD-L1 (**Figure 14B**). IFNGR1 levels were higher in WT compared to B16 IFNGR1KO to further verify tumour phenotype. Due to the low number of replicates, the difference in relative infiltration of $CD45^+$ cells could not be accurately determined. However, the present data recapitulates the cell frequencies previously observed in the B16-OVA model (**Figure 14C**). As a result, it did not appear that the use of OVA as an exogenous antigen significantly impacted the immune phenotype observed in the models under investigation.

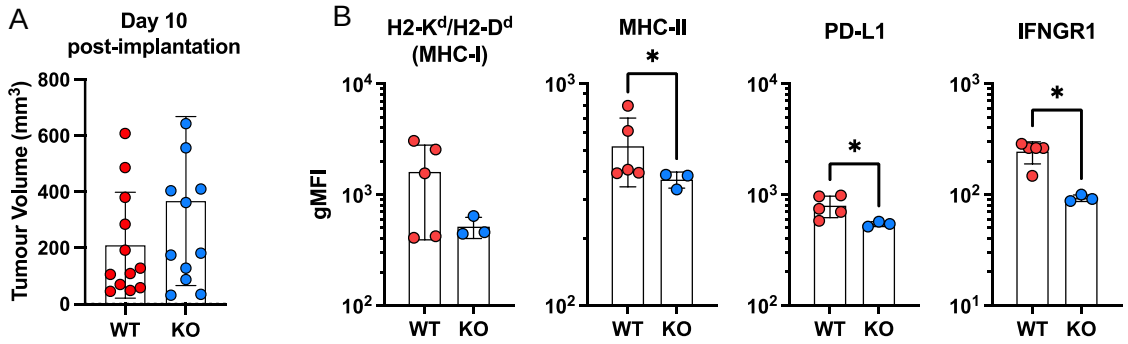

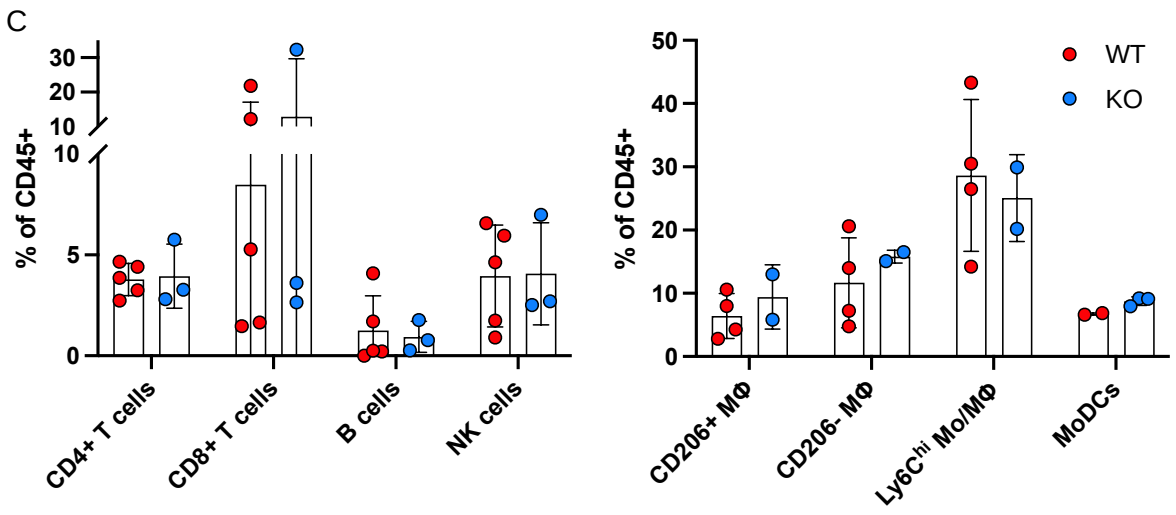

Figure 14. Implantation of parental B16F10 WT or IFNGR1KO tumours in B6 WT mice. (A) Tumour volumes of B16 WT or IFNGR1KO measured at endpoint, day 10 post-implantation. Data are from two independent experiments. (B) Surface expression of MHC-I, MHC-II, PD-L1 and IFNGR1 on B16 WT or IFNGR1KO tumour cells measured as geometric mean fluorescence intensity by flow cytometry. (C) Relative infiltration of lymphoid and myeloid immune populations in B16 WT or IFNGR1KO tumours, as measured by flow cytometry. Data in B & C are from one experiment, representative of two independent experiments. Data show mean ± SD and with *p*-values by non-parametric Mann-Whitney *t* tests, *$p \leq 0.05$.

3.2.5 Anti-PD-L1 does not affect B16-OVA WT or IFNGR1 tumour growth or immune infiltration

Given reports in literature which have shown either no response or partial response of B16 to anti-PD-1 or PD-L1 treatment, a similar experiment was performed to determine whether it would have an effect on our WT or IFNGR1KO tumours. Mice were dosed with anti-mouse PD-L1 monoclonal antibodies 5 days following tumour implantation, and every 3 days thereafter (**Figure 15A**). The experiment ended when no difference in tumour volume was detected day 15 post-implantation (**Figure 15B**). Similar to the lack of distinct effect of anti-PD-L1 on tumour growth rates, the composition of immune infiltration cells also remained unchanged (**Figure 15C**). Due to the variability in the tumour volumes in this study, this experiment would benefit from being repeated with changes in the antibody dosing schedule as other studies have shown that earlier or later dosing may have a significant impact on B16 tumour growth.[241]

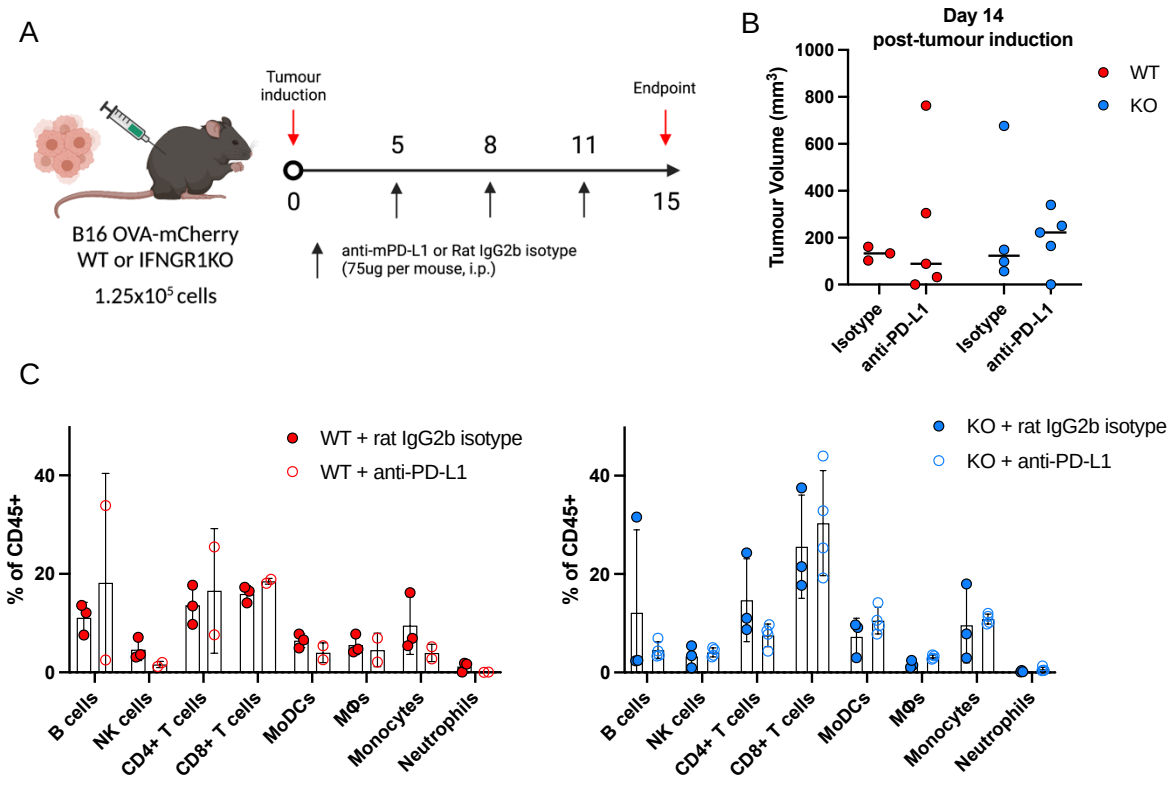

Figure 15. Administration of anti-PD-L1 monoclonal antibody therapy in B16 OVA tumour-bearing mice. (A) Dosing schedule of anti-PD-L1 monoclonal antibody or isotype control following B16 OVA WT of IFNGR1 tumour induction. (B) Tumour volumes of treated and non-treated tumours on day 15 post-tumour implantation. (C) Relative frequencies of tumour-infiltrating immune populations determined by flow cytometry. Samples were gated on live CD45^{+} cells. Data is from one experiment and show mean with statistical testing performed by non-parametric Mann-Whitney *t* tests.

3.2.6 Investigating the effects of increased intratumoural IFNγ on cross-presentation of tumour-specific antigens

The B16F10 OVA model showed that relative infiltration of OVA-specific T cells was higher in IFNGR1KO tumours compared to WT, which was contrary to expectations due to the significant lack of MHC-I upregulation. To investigate whether this increase was due to direct antigen presentation at the tumour site, or enhanced cross-presentation by APCs distally within tdLNs, a cross-presentation model was adopted to delineate the two independent processes. It was hypothesized that enhancement of intratumoural IFNγ levels in IFNGR1KO tumour would also promote greater antigen cross-presentation distally, resulting in more tumour-specific T cells.

C57Bl/6 male mice were crossed with Balb/c female mice, resulting in a hybrid CB6F1 (F1) generation which expresses both H2-^{b} and H2-^{d} MHC haplotypes (**Figure 16A**). All APCs, including DCs, from F1 mice would express both H2-^{b} and H2-^{d} for priming of independent H2-^{b}- or ^{d}-specific T cells *in vivo* (**Figure 16B**). B16F10 was engineered to express NY-ESO1, which has a well-characterized H2-D^{d} epitope.[242] As B16 only expresses H2-^{b}, direct presentation of NY-ESO1 by tumour cells to H2-^{d}-specific T cells would not be possible. Therefore, the resulting H2-D^{d} NY-ESO1-specific T cells are present only as a result of cross-presentation. Similarly, H2-^{d}-restricted CT26 colon adenocarcinoma engineered to express OVA would only give rise to H2-K^{b} OVA-specific T cells through cross-presentation *in vivo*. Detection of cross-primed T cells from the tumour, lymph nodes, or spleen were detected via tetramer staining *ex vivo*, or restimulation using the cognate peptide and intracellular staining for cytokine production.

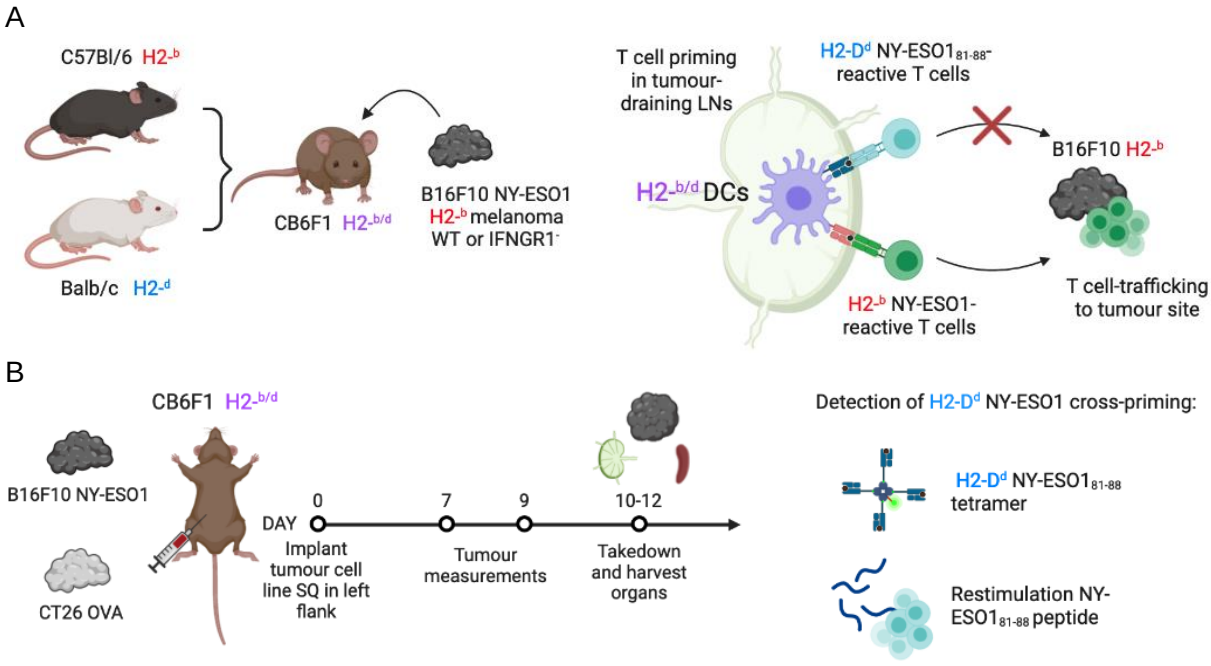

Figure 16. Schemata of the CB6F1 H2-$^{b/d}$ hybrid murine tumour model using B16F10 NY-ESO1 and CT26 OVA. (A) Crossing of male C57Bl/6 mice with female Balb/c mice to produce hybrid CB6F1 mice which express both H2-^{b} and H2-^{d} alleles on all somatic cells. Subsequent implantation of H2-^{b}-positive B16F10 cells allows for direct presentation of NY-ESO1 epitopes only via H2-^{b} molecules. Lymph node priming of both H2-^{d}- or H2-^{b}-NY-ESO1-specific T cells would result in only one population which can be directly stimulated by the B16 tumour. (B) Proposed tumour models of H2-^{b}-positive B16F10 or H2-^{d}-positive CT26 cell lines in CB6F1 mice. Detection of cross-primed T cells is performed using NY-ESO1 or OVA tetramers, or re-stimulation of CD8^{+} T cells *ex vivo* with the appropriate peptides.

Initial experiments sought to test whether tetramer binding or restimulation using peptide was sufficient in detection of NY-ESO1-specific T cells in a model of CT26 NY-ESO1 implanted into Balb/c mice (**Figure 17A**). However, CT26 NY-ESO1 proved to be highly immunogenic and was spontaneously rejected in all animals. Peptide stimulation of dissociated lymph nodes and splenocytes showed that indeed IFNγ-positive tumour-specific T cells could be detected (**Figure 17B**). However, tetramer-binding of T cells could not be detected, possibly because peptide-MHC and TCR interactions are much more dependent on TCR avidity, and limited by optimal staining conditions.

In the following experiment, F1 mice were implanted with B16 NY-ESO1 WT or IFNGR1KO tumours (**Figure 17C**). No differences in tumour volume at day 10 post-implantation was observed between WT and IFNGR1KO (**Figure 17D**). Furthermore, splenocytes from tumour-bearing mice restimulated with NY-ESO1$_{81\text{-}88}$ peptide did not elicit a cytokine response (**Figure 17E**). Similarly, no tetramer binding for H2-D^{d} NY-ESO1$_{81\text{-}88}$ could be observed for tumour-infiltrating lymphocytes, splenocytes, or T cells from tdLNs (data not shown). Despite testing different staining conditions, varying time, temperature and whether anti-CD8α antibodies were blocking the pMHC-TCR interaction, H2-D^{d}-NY-ESO-1-specific T cells could not be detected. In conclusion, tools for detecting cross-presentation were insufficient in the B16 NY-ESO1 model, and tetramer-specific cross-primed T cells could not be found.

Due to the robustness of the H2-K^{b} OVA tetramer in detecting OVA-specific T cells, the CT26 OVA cross-presentation model was tested in lieu of B16 NY-ESO1. CT26 is not considered an IFNγ-sensitive model due to its high basal level of MHC-I expression. However, it remained mechanistically possible that IFNγ consumption by the tumour would result in intratumoural IFNγ accumulation during tumour development, thereby enhancing antigen cross-presentation through our original hypothesis.

F1 mice were implanted with CT26 OVA WT or IFNGR1. At a cell dose of 6x10^{5}, IFNGR1KO tumours began to regress in tumour volume by day 11, and were rejected by day 18 post-implantation in all mice (**Figure 17F**). In comparison, 5 out of 6 WT tumours

were still present at day 18. At the higher cell dose of $1x10^6$ cells, WT and IFNGR1KO tumours grew at similar rates, and cross-presentation of OVA was analysed at day 13. No difference in tumour volume was observed (**Figure 17G**), and surface staining of tumour cell following *ex vivo* dissociation revealed similar levels of MHC-I, MHC-II, and PD-L1 expression (**Figure 17H**). Although CT26 were unable to present the H2-K^b OVA peptide, H2-K^b-OVA-specific T cells were still found in significant numbers within the tumour. However, no difference in frequency of H2-K^b-OVA-primed T cells were found in the tdLNs or at the tumour site (**Figure 17I**). Lastly, we checked whether tumour antigens could be found in the tdLNs of WT or IFNGR1 tumour-bearing mice. Using B16 expressing a pH-resistant variant of GFP, ZsGreen was found in roughly equal proportions of tdLN immune cells, indicating that antigens from both tumours are being trafficked (Figure S2).

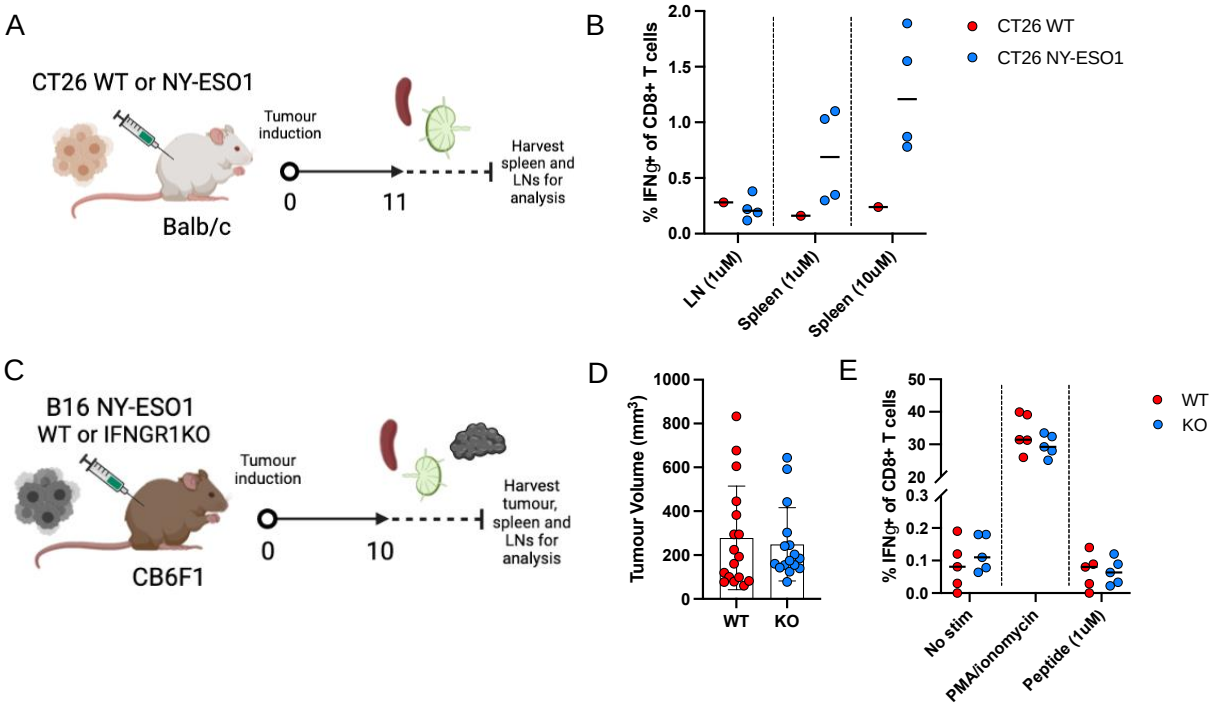

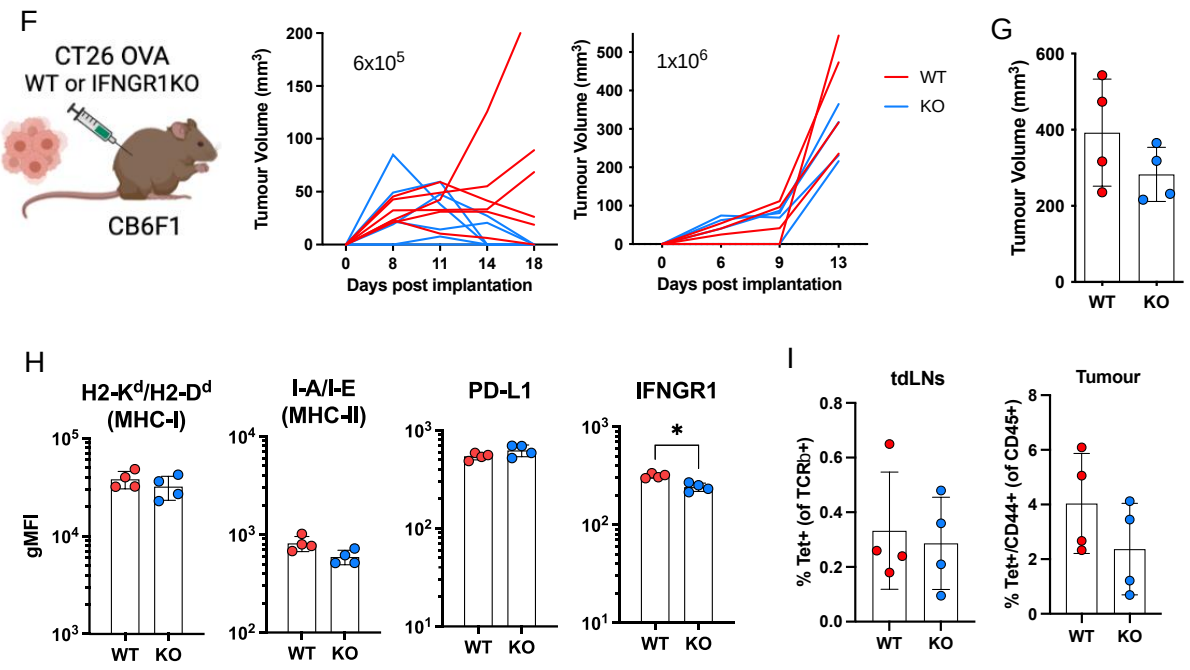

Figure 17. Evaluation of an *in vivo* tumour cross-presentation model using hybrid CB6F1 mice. (A) Workflow for testing of NY-ESO1 expression by the CT26 syngeneic tumour model via implantation of $1x10^6$ cells per mouse. (B) Re-stimulation of cells isolated from lymph nodes and spleen of tumour-bearing mice with NY-ESO1$_{81-88}$ peptide at indicated concentrations for 6 hours, and analysis of IFNγ response via intracelullar cytokine staining. (C) Workflow for implantation of $2.5x10^5$ B16 NY-ESO1 WT of IFNGR1KO cells in CB6F1 mice and harvest of tissues for analysis at endpoint. (D) Tumour volumes of B16 NY-ESO1 tumours at endpoint. Data are pooled from three independent experiments. (E) Intracellular cytokine staining of splenocytes from B16 NY-ESO1 tumour-bearing mice stimulated with PMA + ionomycin or NY-ESO1$_{81-88}$ peptide for 6 hours. Data is from one experiment. (F) Tumour growth curves for CT26 OVA WT or IFNGR1KO implanted into CB6F1 mice at two indicated cell doses. (G) Tumour volumes for CT26 OVA tumours at day 13 post-implantation. (H) Analysis of MHC-I, MHC-II, PD-L1 and IFNGR1 expression on CT26 OVA tumour cells indicated by geometric mean fluorescence intensity by flow cytometry. (I) Detection of OVA-specific T cells from CT26 OVA tumour-bearing mice from the tumour-draining lymph nodes or intratumoural $CD8^+$ T cells via *ex vivo* tetramer staining. Data from F-I are from one experiment. All data show mean with p-values by non-parametric Mann-Whitney *t* tests, *$p \leq 0.05$.

3.3 Discussion and conclusion

3.3.1 Confounding effects of IFNGR ablation in murine models compared to clinical observations

This chapter presented a model of B16F10 melanoma whereby IFNγ signalling was abolished through deletion of IFNGR1 from the cell line. Previous publications which have undertaken similar methodologies have resulted in varying conclusions. In one publication, IFNGR2 was ablated in B16 engineered to express model antigen SIY, and demonstrated that IFNGR2KO resulted in complete tumour regression following formation of palpable tumours.[243] Our IFNGR1 model does not result in significant outgrowth, nor regression, compared to WT controls, which is intriguing when comparing the relative differences in expression of MHC and PD-L1 which should impact tumour immunogenicity. Furthermore, the IFNGR2 model was sensitive to anti-PD-L1 ICB, as treatment of IFNGR2:WT admixed tumours with anti-PD-L1 resulted in significant tumour rejection compared to controls.

Other papers describing a similar phenomenon have highlighted the possibility that IFNγ-dependent, PD-L1-independent pathways are instead driving ICB resistance. Benci *et al.* showed that tumour cells which are resistant to ICB develop resistance through chronic IFNγ stimulation, which upregulate additional non-PD-L1 immune-inhibitory genes.[241] In their murine model, which was derived from a radiotherapy/anti-CTLA4 resistant B16F10 variant, IFNGR1KO tumours responded better to anti-CTLA4/anti-PD-1 mono- and combination therapy. This supports their hypothesis that IFNγ-signalling in tumour cells ultimately contribute to immune escape. Intriguingly, these studies would indicate that checkpoint blockade should be administered alongside anti-IFNγ in order to mitigate the inhibitory effects of IFNγ-signalling which would otherwise dampen ICB mode of action. It remains to be seen whether clinical trials combining ICB and IFNγ administration would have a beneficial effect given the findings from these large-scale animal studies.

Results from these previous studies are especially difficult to understand as human melanomas demonstrate loss of IFNγ sensitivity as an immune escape mechanism to anti-

PD-L1 therapy, rather than enhancement of responses currently observed in murine models. Some murine models using IFNGR1 knockdown showed that loss of IFNγ-signalling in tumour cells reduces anti-CTLA4 efficacy.[105] Similarly, human clinical studies have shown acquired resistance to ICB manifest as JAK1/JAK2 loss of function mutations which rendered the tumours insensitive to IFN-dependent pathways.[105,201,202] Furthermore, clinical evidence appears to support that transcriptomic signatures of IFNγ-signalling are positively correlated with ICB response.[128,183] Despite the amount of research dedicated to understanding the role IFNγ plays in anti-tumour (or equally pro-tumour) immunity, it has been difficult to ascertain the true effects of IFNγ-signalling and its role in inhibiting or enhancing disease progression. As multiple murine studies imply that presence of IFNγ-insensitive mutants makes WT cells more susceptible to monotherapies, it would seem that further scrutiny of the models would be important in determining their clinical relevance.

3.3.2 Choice of model for ablation of IFNγ signalling and sequestration of IFNγ as an immune escape mechanism

The predicted phenotypic difference that would result in ablating IFNGR1 versus IFNGR2 comes from integration of previous biochemical and biological knowledge. Early structural studies showed that IFNγ homodimers can bind IFNGR1 dimers in solution with high affinity in the absence of IFNGR2.[244] At the cell surface, IFNγ uptake is strongly mediated by IFNGR1, whereas uptake was only slightly decreased when IFNGR2 was deleted.[245] In some cell types, IFNγ degradation only occurs following internalization [246]; however, whether this process occurs in tumour cells and in the absence of IFNGR2 is unknown. Taken together, we surmised that IFNGR2 deletion would significantly affect downstream IFNγ signalling, but perhaps transient IFNγ uptake and recycling may remain intact due to constitutive IFNGR1 expression. This in turn affects the concentration of unbound IFNγ present in the tumour microenvironment which may stimulate other cells present. For example, previous studies have shown that IFNγ acting on endothelial cells to induce vasculature regression was sufficient in restricting tumour growth.[144] Whether these

mechanisms can explain the differences observed between IFNGR1 and IFNGR2KO in this present model remains to be tested.

One unique observation of our IFNGR1-deficient model is the detection of increased intratumoural IFNγ in B16 IFNGR1KO tumours compared to WT. However, it remains unclear whether this is due to higher immune activation status resulting in more IFNγ, or decreased IFNγ consumption by IFNGR1KO tumour cells present. These preliminary data allowed us to hypothesize a novel mechanism by which tumour cells may be 'absorbing' or sequestering IFNγ in the tumour microenvironment, thereby restricting available IFNγ necessary for anti-tumour immune function. To test this theory, a signalling mutant of murine IFNGR1 has been generated, whereby tyrosine 445 was changed to an alanine residue to ablate binding of STAT1. The mutant Y445A IFNGR1 will be re-introduced into IFNGR1KO B16 cells. While the Y445A mutant can bind and sequester IFNγ from the microenvironment, downstream signalling is inhibited and neither MHC-I nor PD-L1 will be upregulated. B16 WT, IFNGR1KO and IFNGR1Y445A will be incubated with rmIFNγ *in vitro* and unconsumed IFNγ can be quantified by ELISA. If a detectable difference is observed *in vitro*, then this would warrant testing of the cell lines *in vivo*. Compared to WT tumours, we would expect that absorption of IFNγ, which does not result in upregulation of MHC class I on the Y445A mutant, would be detrimental to tumour control over time. This mechanism would provide greater insight into how IFNγ is utilized by tumour cells, and whether IFNγ consumption by the tumour cells inhibits anti-tumour immunity.

Compared to similar models in literature, loss of IFNγ-signalling in B16F10 in our experiments did not result in overt tumour growth compared to WT, and also did not enhance anti-PD-L1 therapy as observed by others. While other papers have focused on the unexpected effects of IFNγ-resistance in enhancing ICB, our current data indicates that certain immune mechanisms may have been overlooked, such as the accumulation of IFNγ which may alter the tumour microenvironment significantly. As $CD8^+$ T cell immunity itself was not specifically enhanced in KO vs. WT, chapter 4 and 5 employ several unbiased

approaches using high dimensional flow cytometry and scRNAseq to focus on other immune cell types which may be modulating the tumour microenvironment.

3.4 Appendix

Table S1. Antibody panels for tumour cell surface staining or immune infiltration analysis by flow cytometry.

Tumour cell staining panel:

Fluorochrome	Marker	Clone	Manufacturer	Cat. No.	Dilution (1:X)
BV421	MHC-Class II	M5/114.15.2	Biolegend	107631	400
BV785	CD45	30-F11	Biolegend	103149	400
PerCP-Cy5.5	PD-L1	10F.9G2	Biolegend	124334	400
PE	CD119	REA189	MACS Miltenyi Biotec	130-104-987	20
APC	MHC-Class I (H2-K^b)	AF6-88.5	Biolegend	116517	200
NIR	Zombie NIR	--	Biolegend	423106	500

Lymphocyte staining panel:

Fluorochrome	Marker	Clone	Manufacturer	Cat. No.	Dilution (1:X)
BV421	OVA-Tetramer	--	NIH	--	500
BV510	B220 (CD45R)	RA3-6B2	Biolegend	103248	100
BV605	CD62L	MEL-14	Biolegend	104437	200
BV650	CD8α	53-6.7	Biolegend	100742	200
BV785	CD44	IM7	Biolegend	103059	400
FITC	PD-1	29F.1A12	Biolegend	135213	200
PerCP-Cy5.5	CD4	GK1.5	Biolegend	124334	400
PE	TCRβ	H57.597	Biolegend	109207	400
PE-Cy7	CD45	30-F11	Biolegend	103113	400
AF647	NKp46	29A1.4	Biolegend	137628	100
NIR	Zombie NIR	--	Biolegend	423106	500

Myeloid staining panel:

Fluorochrome	Marker	Clone	Manufacturer	Cat. No.	Dilution (1:X)
PB	Ly6G	1A8	Biolegend	127612	400
BV510	CD11b	M1/70	Biolegend	101245	200
BV650	CD8α	53-6.7	Biolegend	100742	200
BV785	CD103	2E7	Biolegend	121439	200
FITC	CD11c	N418	Biolegend	117309	200
PerCP-Cy5.5	PD-L1	10F.9G2	Biolegend	124334	400
PE	CD45.2	30-F11	Biolegend	109807	400
PE-Cy7	Ly6C	N418	Biolegend	117305	400
APC	F4/80	BM8	Biolegend	123115	100
AF700	MHC-Class II	M5/114.15.2	Biolegend	107621	200
NIR	Zombie NIR	--	Biolegend	423106	500

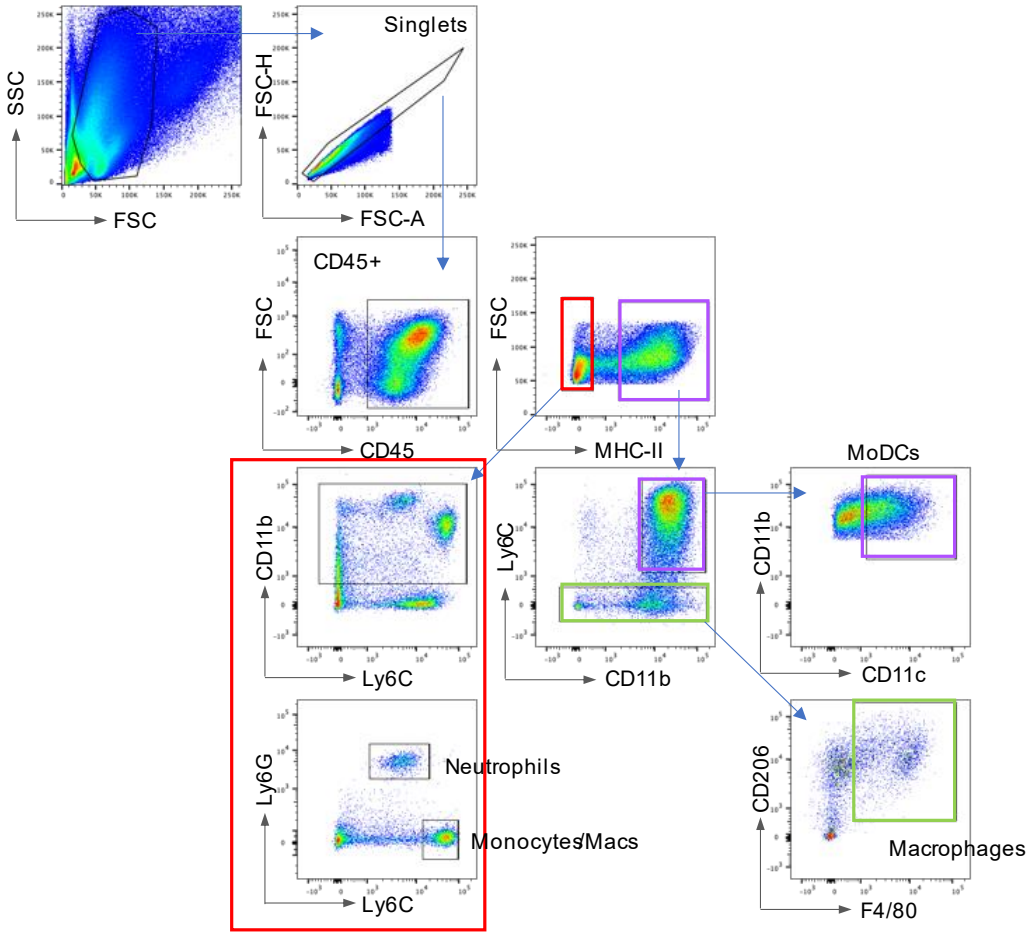

Figure S1. Gating strategy for myeloid populations from B16-OVA tumours.

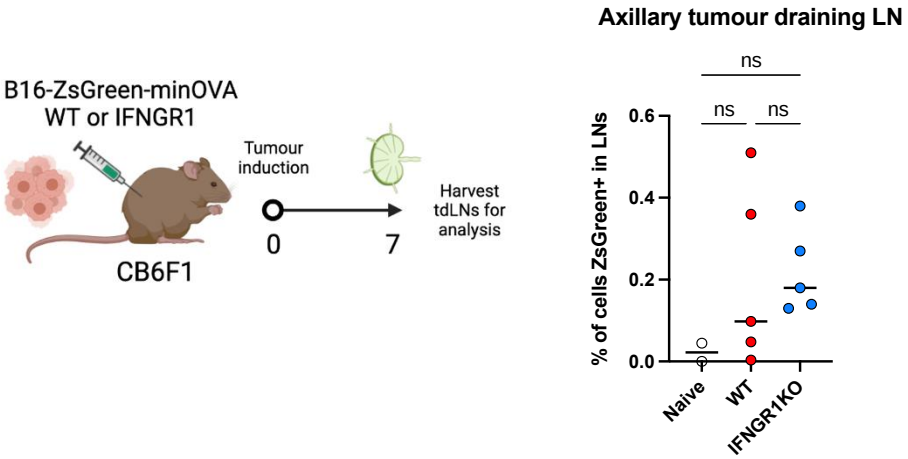

Figure S2. Detection of ZsGreen-positive cells in tumour-draining lymph nodes of WT and IFNGR1KO tumour-bearing mice. Tumour-draining axillary lymph nodes were harvested from mice implanted with $5x10^5$ B16-ZsGreen-minOVA cells (described in 4.2.1) at day 7 post-implantation and cells were analysed by flow cytometry. Cells were plotted as live, $ZsGreen^+$ of total population.

Admixture of IFNGR1KO and WT cells potentiates intratumoural competition which allows for immune escape

4.1 Introduction

This chapter introduces a model where B16-OVA WT and IFNGR1KO cells are implanted simultaneously in equal proportions. From the previous chapter where WT and KO tumours grew at equivalent rates, we predicted that the admixed tumours starting at a 1:1 ratio of WT:KO would maintain the same ratio over the course of tumour progression. Instead, a phenotype emerged where admixed tumours became increasingly KO-dominant over time, suggesting that presence of both cells would result in clearance of the one over the other. Interestingly, this model recapitulates the clinically relevant observation that cells with an advantageous mutation will eventually out-survive others in the immediate environment. The model was further tested in CD8KO and IFNγKO mice to elucidate whether $CD8^+$ T cells, or IFNγ, is involved in the outgrowth of KO cells.

4.1.1 Contributions of cell-cell competition to immune escape

In the admixed model, we sought to study the mechanisms of cell-cell competition which can result in the outgrowth of one cellular species to another. Cell-cell competition is described as a general biological mechanism where 'survival of the fittest' results in elimination of less fit or suboptimal cells within a population over time.[247] In the context of cancer, cancer cells that are more fit may arise due to acquisition of mutations following immune pressure, which promotes tumour growth and immune escape. Cell-cell competition manifests in several different ways, many of which involve proliferation or apoptosis. An example of how IFNγ potentiates cellular competition is through Myc, a proto-ongogene which has been shown to be a major driver of most human tumours.[248,249] The growth inhibitory effects of IFNγ are partially explained by its suppression of c-*myc* mRNA levels, which in turn reduces cell proliferation.[250] As a result, Myc overexpression would allow for enhanced competition, and override the direct effects of IFNγ in some tumour cells. Apart

from cell-cell competition which exists between adjacent tumour cells, tumour cells have also been observed to induce apoptosis of stromal cells or neighbouring peritumour tissues, which then allows tumour cells to continuing growing and invading surrounding healthy tissues.[251]

The admixed model presented in this chapter introduces an element of cell-cell competition which is not present when tumours are in separate environments. IFNGR1KO cells are likely more 'fit' than wild-type cells when given the same microenvironment due to its resistance against IFNγ. With the knowledge that human tumours often contain a similar type of heterogeneity and clonal competition between tumour cells, this admixed model becomes an interesting microcosm which we can manipulate and subsequently investigate the resulting phenotype. In this chapter, we refer to immune escape as resistance of one cell type towards immune-dependent killing despite successful clearance of the other, rather than escape of the entire tumour due to lack of host response.

4.1.2 Immunological consequences of CD8 and IFNγ ablation in tumourigenesis

Given the importance of $CD8^+$ T cells in IFNγ production, and the role of IFNγ itself in mediating anti-tumour immunity, we sought to test our tumour models in CD8KO and IFNγKO mice which would serve as controls lacking tumour control. Here, we review the anticipated effects of ablating $CD8\alpha^+$ cells or IFNγ on tumourigenesis.

In the $CD8\alpha^{-/-}$ mouse strain, $CD8^+$ T cells are not present in the periphery, but $CD4^+$ T cell development and function are unaltered.[252] However, MHC-I-mediated immune responses were still observed by $CD4^+$ $TCR\alpha\beta^+$ T cells, and mice lacking CD8 T cells were able to reject MHC-mismatched skin grafts at the same frequency as WT mice.[253] CD8KO mice infected with mouse polyoma virus were able to generate virus-specific MHC-I-restricted T cells, albeit at a 10-fold lower frequency compared to WT mice.[254] Most of these responses show that double-negative ($CD4^-/CD8^-$) T cells are capable of becoming MHC-I-restricted cytotoxic lymphocytes which share some of the functions of conventional $CD8^+$ T cells. Of note, the absence of $CD8^+$ T cells leads to priming of Th2-biased $CD4^+$ T cells by

DCs, which produce high levels of IL-4, IL-5, IL-10 and TGFβ upon antigen recognition.[255] Tumour implantation into CD8KO mice may result in an overtly immunosuppressive TME, driven by the lack of IFNγ-dependent suppression of Th2 pathways. In the context of tumour immunology, the success of checkpoint blockade is heavily dependent on the presence and infiltration of $CD8^+$ T cells.[256–258] However, other methods of augmenting the anti-tumour response such as DC vaccines have shown that $CD8^+$ T cells are not required for efficacy[259], demonstrating that multiple cell types are capable of exerting anti-tumour functions.[260]

In IFNγKO mice, it has been shown previously that there was no difference in the frequency of antigen-specific $CD8^+$ T cells generated between WT and IFNγKO mice during acute infection by *Listeria monocytogenes*.[261] IFNγ produced by $CD8^+$ T cells is required for their expansion, memory formation, and motility, which are all markedly impaired in IFNγKO mice, as demonstrated by different models of acute infection.[262–264] $CD4^+$ T cells were found to be inherently Th2 skewed despite antigens which would normally lead to Th1 differentiation, such as in bacterial or parasite infection.[265,266] In the context of cancer, several different pathways including antigen presentation by tumour cells, and Fas/FasL-dependent apoptosis are greatly affected in IFNγKO mice. For B16F10 specifically, cells which co-expressed Fas/FasL following *in vitro* IFNγ stimulation became irreversible apoptotic, which is a mechanism of cell death that is immune-independent.[267] This type of tumour cell death is likely diminished in IFNγKO mice. This is a brief and non-exhaustive overview of the major immunological phenotypes observed in these two mouse models, and provides a basis in understanding how the anti-tumour responses against B16F10 WT or IFNGR1KO may be altered in our studies. Although the two models are not interchangeable, a comparison of the resulting tumour phenotypes and immune infiltrates will be used to dissect the roles of each independently of one another.

Previously, we observed that loss of IFNγ-signalling by tumour cells did not confer a growth advantage in the presence of selective pressure. In this chapter, we hypothesized that insensitivity to IFNγ confers a growth advantage only when cell-cell competition is

present, thereby restoring immune escape under selective pressure by an active anti-tumour response.

4.2 Results

4.2.1 Implantation of B16 WT and IFNGR1KO admixed tumours results in outgrowth of KO cells over time

In order to create an admixed model of WT and IFNGR1KO tumours where tumour cells could be later identified *ex vivo*, B16F10 WT or IFNGR1KO were lentivirally transduced to express mCherry-minOVA or ZsGreen-minOVA (hereafter referred to as B16-OVA mCherry or ZsGreen; the structure of the ZsGreen- and mCherry-minOVA transgene is detailed in Figure S3). For *in vivo* experiments, WT and IFNGR1KO expressing ZsGreen and mCherry, or vice versa, were mixed 1:1 and implanted subcutaneously similar to previous experiments. Tumour were harvested at indicated time points (**Figure 18A**), and analysed by flow cytometry or confocal microscopy. As previously observed, WT and KO were similar in tumour volume at experimental endpoint (**Figure 18B**). A majority of admixed tumours were the same size as unmixed controls; however, a small number of tumours grew to over twice the average volume. Differences in tumour growth rates between the three models were not abundantly clear (**Figure 18C**). Approximately 1 in 10 tumours from all groups grew rapidly and reached humane endpoints by day 9 to 11 post tumour-implantation. A majority of all tumours hit a stationary phase of growth between days 7-14 before growing exponentially in volume.

Interestingly, the composition of the admixed tumours changed over time compared to single-mixture controls, where the proportion of KO tumour cells eventually overtook WT in each tumour (**Figure 18D**). To ensure that the effect was intrinsic to the IFNGR1KO rather than the fluorescent proteins, the same effect was observed in the opposite admixture (i.e., mCherry-WT, ZsGreen-KO). The effect was increasingly pronounced in tumours analysed at late time points, such as 14 days post-implantation.

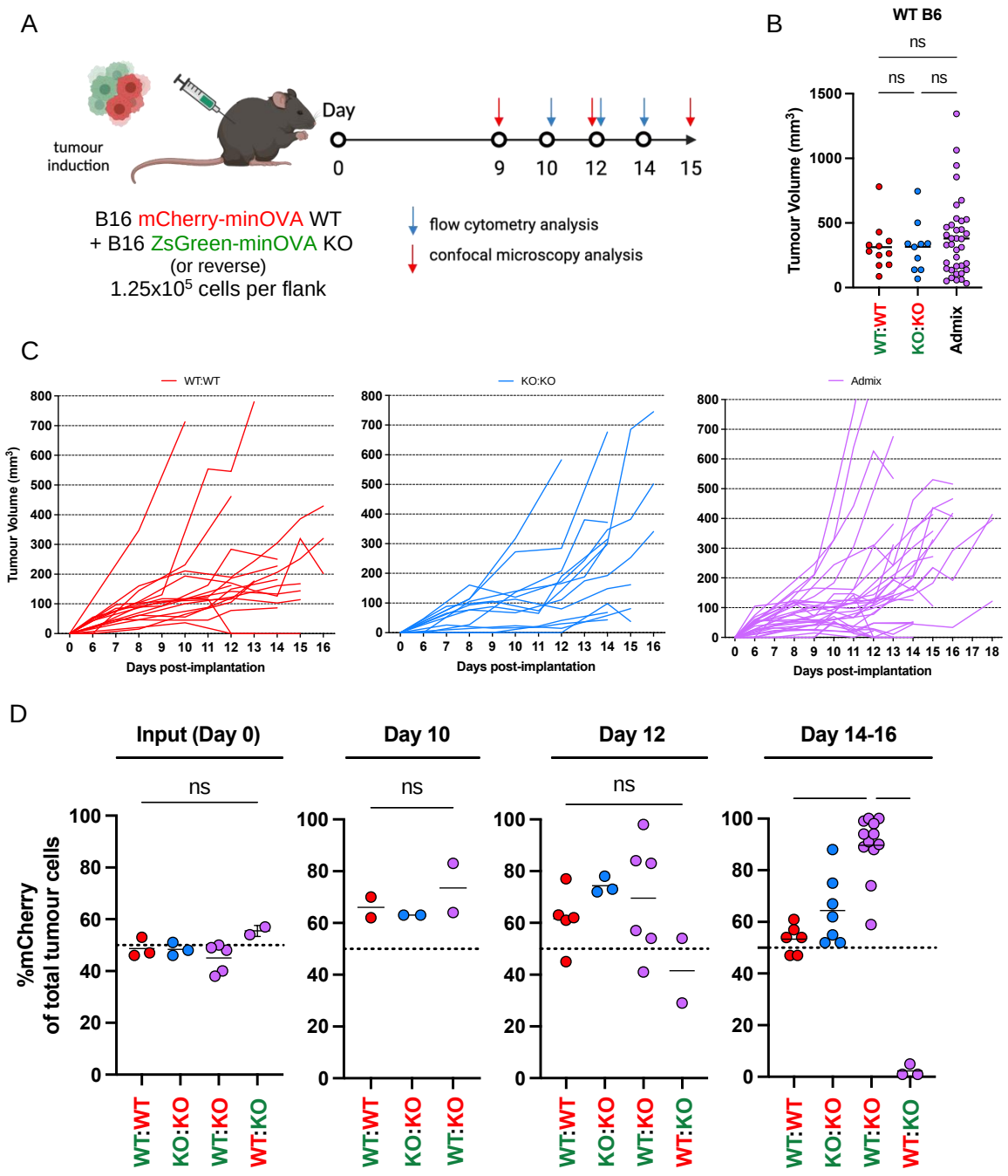

Figure 18. Overview of the B16F10 WT and IFNGR1 admixture model with tumour growth curves and change in composition over time. (A) Workflow for implantation of B16-OVA WT and IFNGR1KO admixed tumours *in vivo* and timeline for collection of tissues for flow cytometry or confocal microscopy analysis. (B) Tumour volumes of WT (n=11), IFNGR1KO (n=10) or admixed tumours (n=37) taken at endpoint on days 12-14 post-implantation from three independent experiments for WT:WT and KO:KO, and six independent experiments for admixed tumours. Admixed tumours include both ZsGreen-WT:mCherry-KO, and mCherry-WT:ZsGreen-KO combinations. (C) Growth curves of individual tumours from each of the three models plotted as tumour volume in mm^3 over time following implantation. (D) Tumour composition gated on the live $CD45^-$ population of *ex vivo* harvested tumours at various days post-implantation. Colour of the label denotes ZsGreen (green) or mCherry (red) expression by the respective cell lines. Data show mean with *p*-values by one-way ANOVA using Kruskal-Wallis multiple comparisons test, $^{**}p \leq 0.01$.

To determine whether WT cells from admixed tumours were phenotypically different to WT cells from WT:WT control tumours, MHC-I and PD-L1 expression was measured by flow cytometry (**Figure 19A**). It was hypothesized that the presence of KO cells in the admixed model would enable for higher intratumoural IFNγ accumulation which was observed previously in Chapter 2.3.1. However, no difference in MHC-I or PD-L1 expression was observed, indicating that both WT:WT and admixed tumours are equally capable of producing an environment which enables IFNγ-signalling. Similar to KO:KO tumours which produced OVA-specific T cells in higher frequencies than WT:WT, admixed tumours were similar to KO:KO tumours and also showed elevated presence of OVA-tetramer^{+} T cells (**Figure 19B**). Other lymphocyte populations, in both frequency and absolute count (**Figure 19C**), were unchanged in all three models.

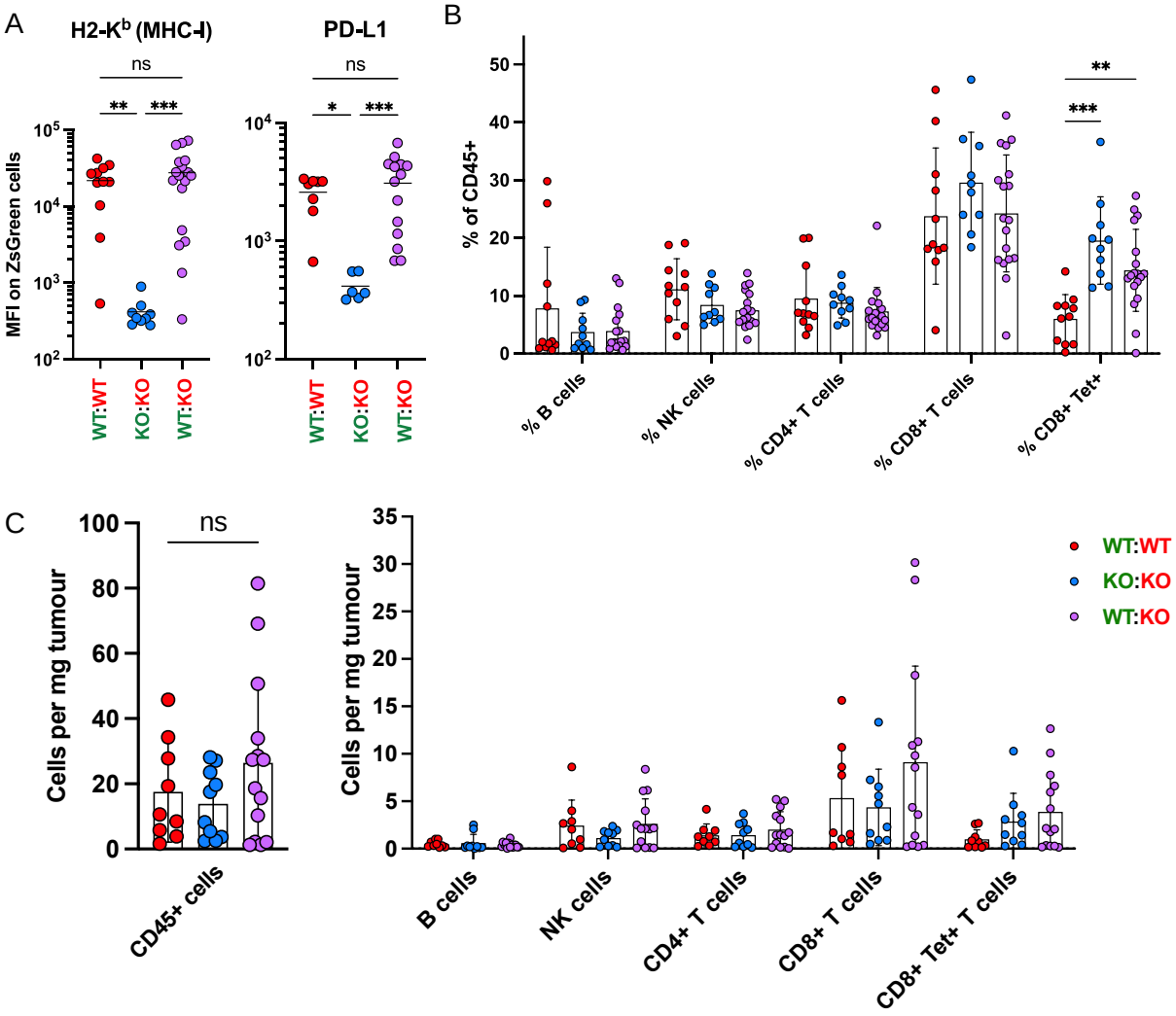

Figure 19. Phenotype of admixed tumours compared to single-mixture controls. (A) Surface expression of H2-K^{b} and PD-L1 as measured by flow cytometry on WT, IFNGR1KO or admixed tumours on days 12-14 post-implantation. Data shows geometric MFI gated on ZsGreen^{+} cells. (B) Relative frequencies of tumour-infiltrating immune populations determined by flow cytometry. Samples were gated on live CD45^{+} cells. (C) Absolute counts of immune cells per mg of tumour tissue. Data are pooled from five independent experiments, and show mean ± SD with *p*-values by one-way ANOVA using Kruskal-Wallis multiple comparisons test in A, and two-way ANOVA for B & C. *p≤0.05; **p≤0.01; ***p≤0.005.

To identify potential immune populations which may be enabling the outgrowth of IFNGR1KO cells in admixed tumours, high dimensional flow cytometry using a 21-colour pan-immune panel (Table S2) was performed on tumour cell suspensions. Dimensionality reduction using opt-SNE, an improved and optimized form of T-distributed stochastic neighbour embedding (t-SNE), was performed on the dataset to create a visual representation (**Figure 20A**). Using an algorithmic tool called FlowSOM, metaclustering was performed on the resulting minimal spanning tree maps (Figure S4) to find the smallest number of informative clusters in the dataset.

Overall, the high dimensional flow cytometry data reflected on previous data that admixed tumours share more similar infiltration patterns to IFNGR1KO tumours compared to WT:WT tumours lacked two distinct populations present in KO and admixed tumours; the first was a tetramer-high CD8^{+} T cell population from cluster 11, and a second MHC-II^{+} TIM-3^{+} PD-L1^{+} myeloid population which are present in clusters 13 and 14 (**Figure 20B**). Unsupervised clustering of all markers in the panel also clustered WT tumours separately from the majority of admixed and IFNGR1KO tumours (**Figure 20C**).

A

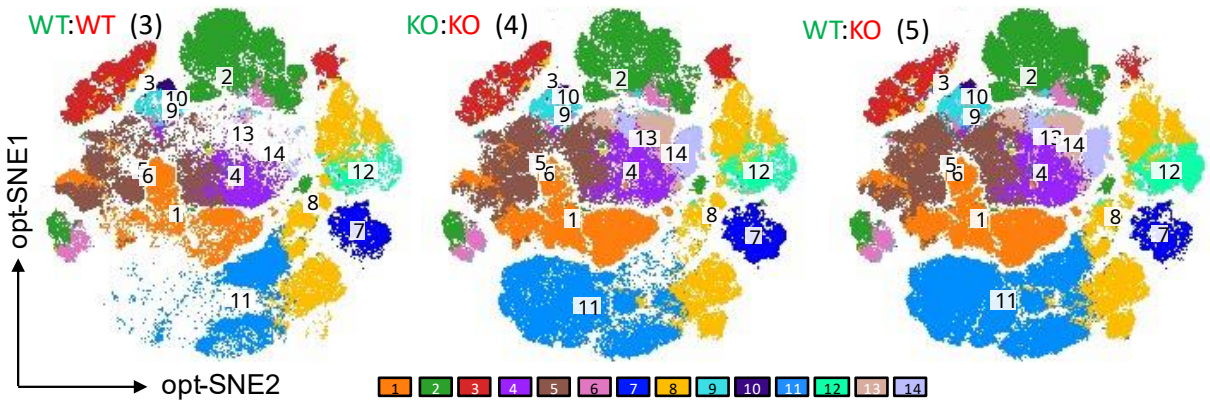

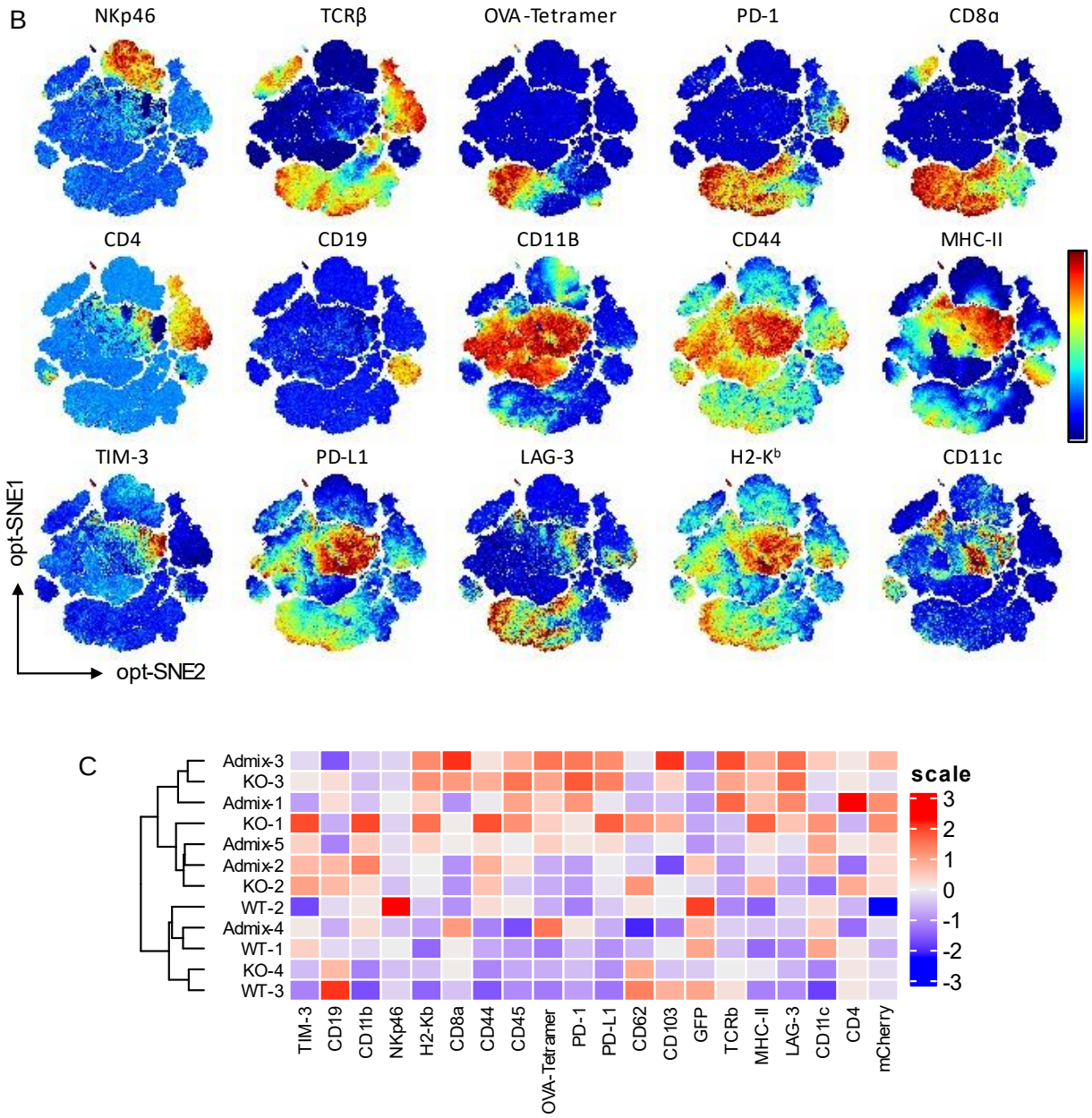

Figure 20. High dimensional spectral flow cytometry analysis of CD45^{+} infiltrating cells in WT, IFNGR1KO and admixed tumours. (A) opt-SNE plots of live CD45^{+} immune cells analysed from a 21-colour Cytek Aurora flow cytometry panel using the OMIQ software platform. Each plot contains an equivalent number of cells downsampled from a given number of samples per tumour type, indicated by the number in brackets. Plots are coloured by FlowSOM metaclustering which determines the optimal number of nodes which best describe the dataset. (B) opt-SNE plots by continuous colour scale where each marker is represented by an independent scale. Highest expression in the dataset is shown by red, and lowest expression in blue. (C) Unsupervised hierarchical clustering of the individual samples in the dataset by marker expression heatmap. Marker expression is globally scaled for comparison. Data are from one experiment, representative of two independent experiments.

4.2.2 Presence of WT and IFNGR1KO tumour cells in admixed tumours enables competition which results in a distinct tumour phenotype

Admixed tumours were observed to be highly heterogeneous in terms of tumour volume, composition, and immune control following implantation (**Figure 21A&B**). As IFNGR1KO tumour cells are already present at the time of implantation, this model does not recapitulate the different phases of the cancer immunoediting, which would in theory develop this resistance over time. However, the admixed model still appeared to give rise to tumours resembling each phase based on the tumour volumes measured over time (**Figure 21B**). The three types of tumours which fall along the spectrum of immune elimination, control, and escape are highlighted in **Figure 21C**. The ratio of IFNGR1KO to WT tumour cells, as well as tumour volume, are used as an indicator of disease progression.

In brief, tumours may grow exponentially by around day 9 post-implantation, in which case no tumour control by the immune response is possible. Alternatively, a strong immune response may be mounted, whereby some tumours remain small, but palpable, or are eliminated completely despite their original presence. Lastly, the majority of tumours are in equilibrium, which is generally the phase in which they are analysed experimentally and we look for clues as to which tumours may be controlled or not.

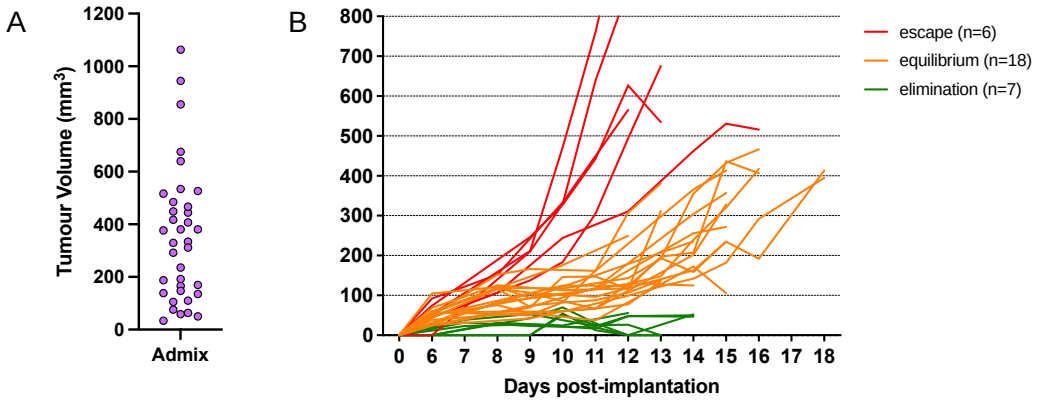

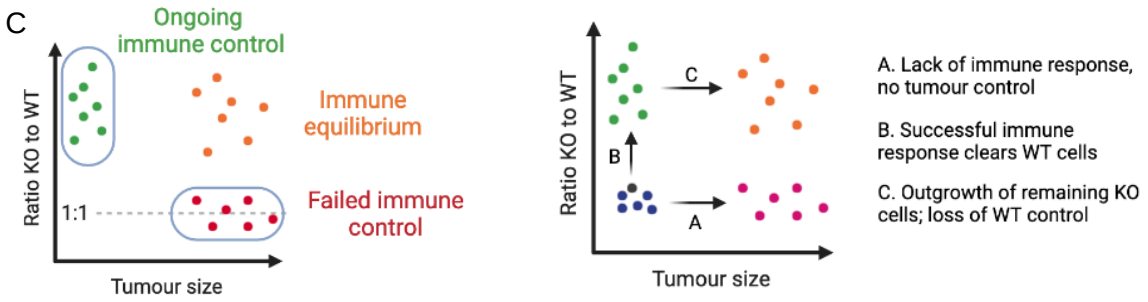

Figure 21. Phases of immune escape as modelled by B16 WT and IFNGR1 admixed tumours. (A) Variability in tumour volume of admixed tumours measured at experimental or humane endpoint, between days 10-18 post-implantation. (B) Experimentally acquired growth curves of individual admixed tumours coloured by the proposed immunoediting phase. (C) Schematic of the types of tumours which may arise during tumour growth and progression. Two pathways are proposed, the first of which is caused by the lack of immune response, and therefore an increase in tumour size is observed without a change in the ratio of KO to WT cells. The second is initial immune control of the tumour which depletes WT cells in the admixture, but tumour progression proceeds due to growth of KO cells.

We attempted to stratify 20 admixed tumours across five independent experiments to analyse the different outcomes of the tumours which were implanted in experimentally similar conditions (i.e., cell number, cell passage, etc.). A pattern similar to our model emerged, where three groups could be distinguished from the tumours analysed (**Figure 22A**). Tumours which were roughly 50/50 WT and IFNGR1KO cells and larger in volume represented a lack of successful immune control. The remaining two groups of tumours experienced outgrowth of KO cells, but differed in tumour volume. Generally, low WT presence and higher tumour volume samples were harvested at later timepoints (**Figure 22B**). To gauge whether these groups of tumours were immune-responsive, levels of MHC-I on the tumour cells were measured by flow cytometry. As expected, IFNGR1KO cells were not observed to upregulate MHC-I regardless of tumour volume (**Figure 22C**). Levels of MHC-I on WT cells, however, were similar between small (<100mm^3) and moderate (200-500 mm^3) tumours (**Figure 22D**), indicating that the tumour cells were recently IFNγ-responsive. We compared relative infiltration of lymphocytes between small and moderate sized tumours with a high proportion of IFNGR1KO cells, and found that although the proportion of CD8$^+$ T cells were lower in moderate-sized tumours, a significant proportion of them were OVA-specific (Figure S5).

In general, tumours of the same WT:KO ratio and tumour volume had very similar immunological footprints (e.g., MHC-I expression, CD4/CD8/NK infiltration). While we had initially assumed that tumour volume was a highly stochastic measure, stratification of our admixed tumours showed us that tumours of similar size and composition often elicited very similar immune responses. This ultimately allows us to create models of cell competition with limited parameters based on experimental data. Models such as these with heuristic value may have some merit in the field of immunotherapy where patient data and meaningful biomarkers are difficult to obtain.

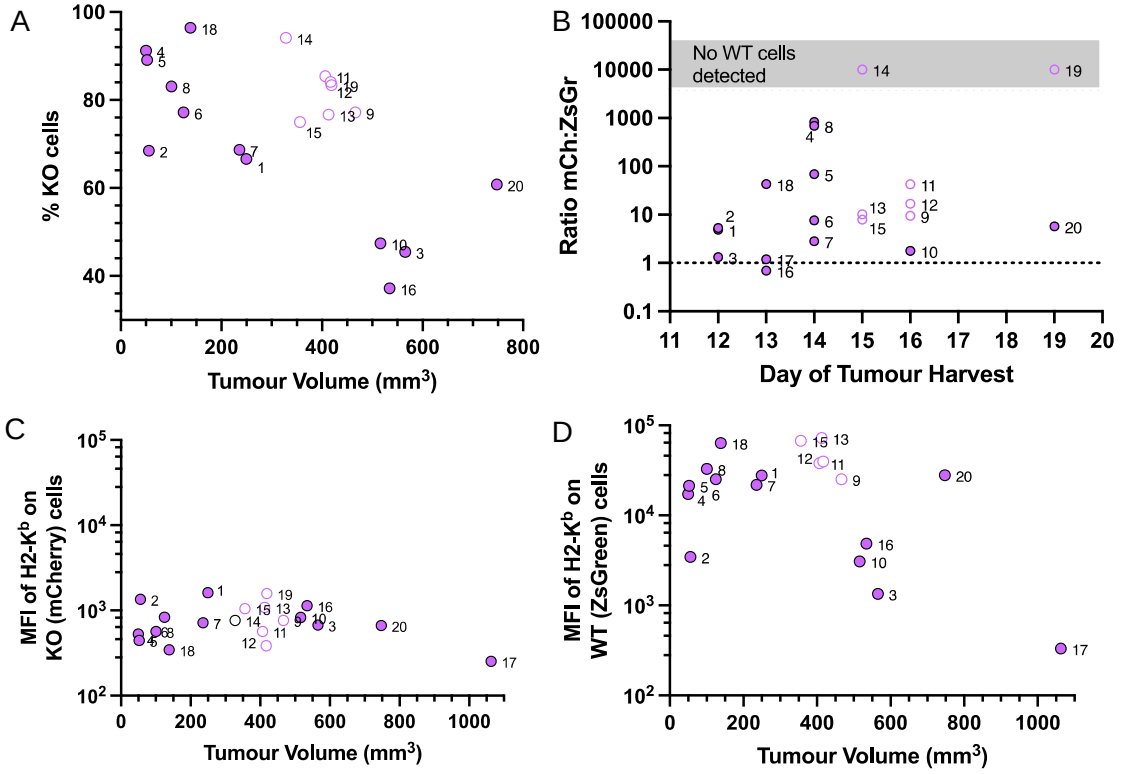

Figure 22. Stratification of B16-OVA ZsGreen-WT:mCherry-KO tumours. (A) Percentage of mCherry-KO tumour cells present in the live CD45$^-$ proportion of tumours analysed by flow cytometry plotted against tumour volume at time of harvest. (B) Ratio of mCherry-KO to ZsGreen-WT cells versus day of tumour harvest. Surface expression of H2-K^b on mCherry-KO cells (C) or ZsGreen-WT cells (D) versus tumour volume. Each point represents one tumour, and labels for each tumour are consistent between all graphs.

4.2.3 B16 admixed tumours are insensitive to single agent anti-PD-L1 checkpoint blockade

From Figure 19A, we observed that PD-L1 expression levels on WT cells from both WT:WT and admixed tumours were similar despite the presence of IFNGR1KO cells in the admixed tumours. To investigate the possibility that intratumoural expression of PD-L1 influences the ratio of WT to KO cells in admixed tumours, anti-PD-L1 was administered to mice following implantation (**Figure** 23**A**). Similar to previous experiments with independent WT or KO tumours in chapter 3.2.5, anti-PD-L1 did not significantly influence the tumour volume (**Figure** 23**B**), nor the degree by which WT cells were cleared from the tumours (**Figure** 23**C**). Further profiling of the infiltration of immune cells into admixed tumours showed no differences either in the frequency (**Figure** 23**D**) nor absolute numbers (**Figure** 23**E**) of the lymphocyte populations analysed. The effects of anti-PD-L1, despite the high levels of PD-L1 expressed by the WT tumour cells, appear to be null in our current models.

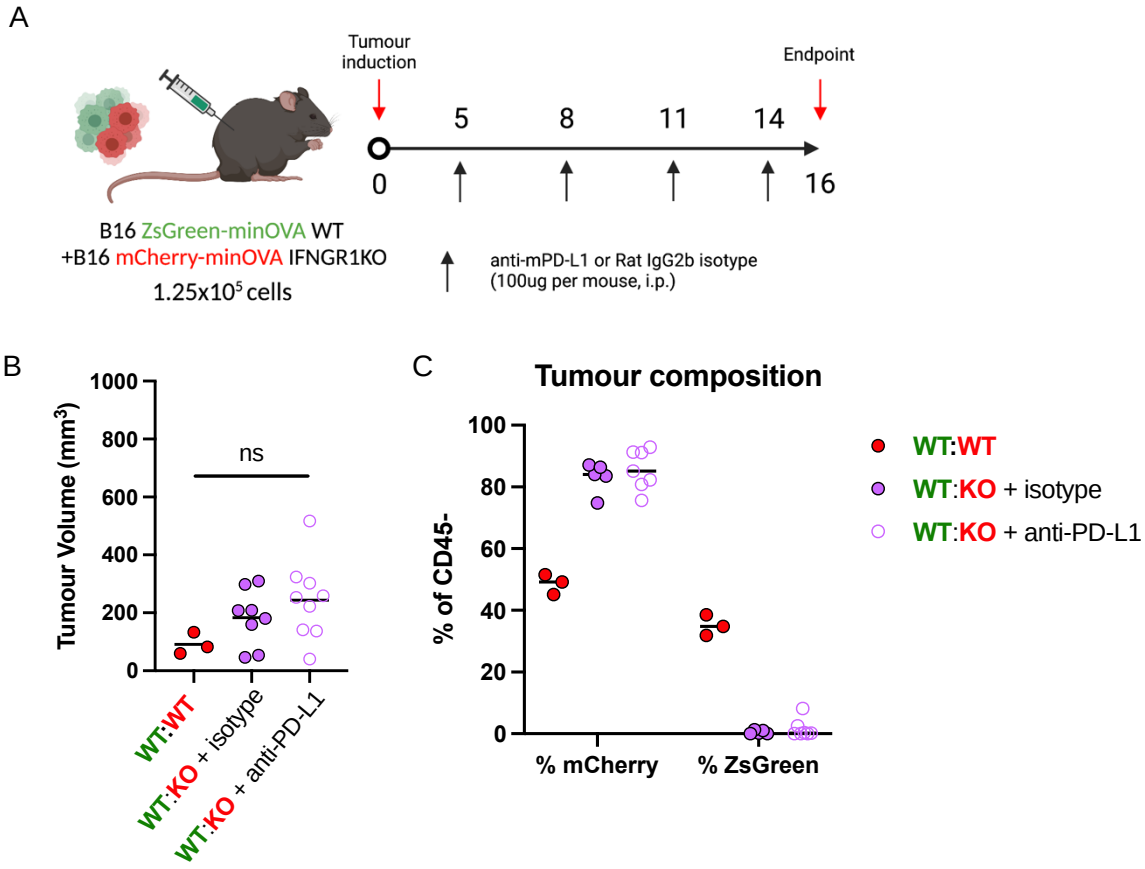

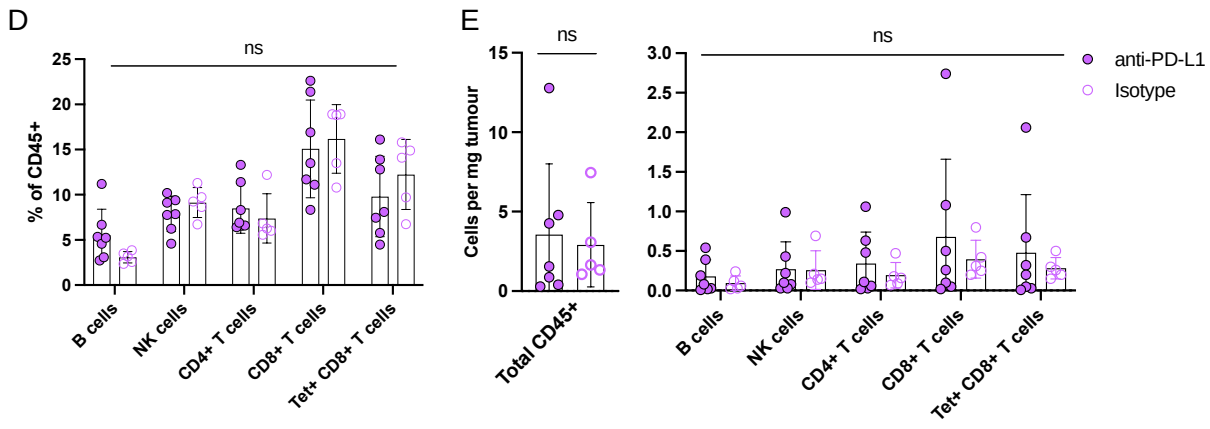

Figure 23. Administration of anti-PD-L1 does not have an effect on the progression of admixed tumours *in vivo*. (A) Dosing schedule of anti-PD-L1 monoclonal antibody or isotype control following B16-OVA ZsGreen-WT/mCherry-KO tumour induction. Control WT:WT tumours were not administered either antibody and used as a negative control. (B) Tumour volumes of treated and non-treated tumours on day 16 post-tumour induction. (C) Percentage of tumour cells which were mCherry or ZsGreen at experimental endpoint, measured by flow cytometry. Sample were gated on live $CD45^-$ population. Frequencies of tumour-infiltrating lymphocyte populations by percentage of $CD45^+$ (D) and absolute count (E) determined by flow cytometry. Samples were gated on live $CD45^+$ cells. Data is from one experiment and show mean with statistical testing performed by one-way ANOVA in B, and two-way ANOVA in D and E.

4.2.4 Confocal microscopy of admixed tumours show spatial segregation of WT and IFNGR1KO cells

Following the observation that presence of WT tumour cells diminished over time in admixed tumours, we used confocal microscopy to gain spatial information of how tumour cells were organized over time (**Figure 24A**). Cryosectioning of tumours at days 9, 12 and 15 post-implantation and subsequent imaging showed that single-mixture WT:WT or KO:KO tumours were uniformly mCherry and ZsGreen and sporadically unpatterned. In comparison, admixed tumours were non-uniform and showed segregation of WT from KO cells (**Figure 24B**). Admixed tumours at late stages featured a unique pattern where WT cells formed an internal core, surrounded by KO tumour cells. This prompted further investigation using confocal microscopy to analyse the stages at which tumour cells became segregated, and where immune cells are localized within each tumour.

A

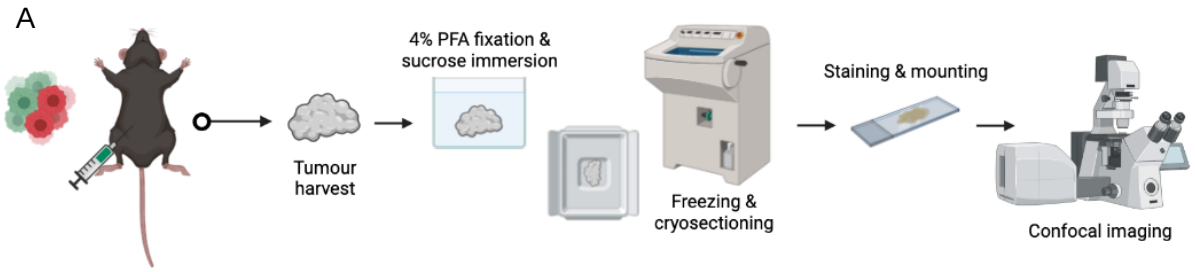

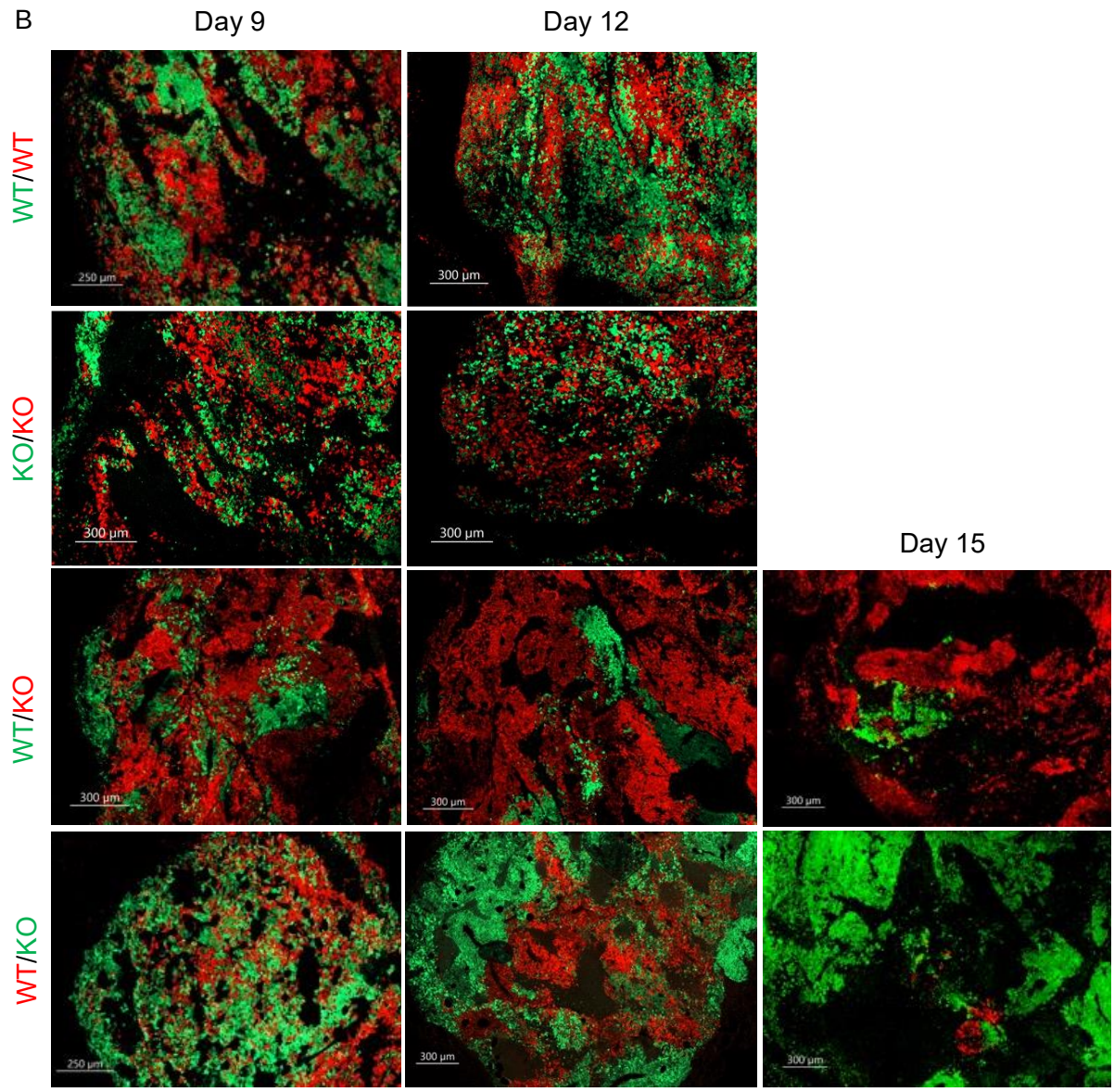

Figure 24. Confocal imaging of B16-OVA WT and IFNGR1KO admixed tumours. (A) Workflow for collection, fixation, sucrose immersion, freezing, cryosectioning, staining, and mounting, of tumour samples for microscopy. (B) Images of control WT:WT, KO:KO, and admixed ZsGreen-WT:mCherry-KO, or mCherry-WT:ZsGreen-KO tumours collected on days 9, 12, or 15 post-implantation. Each image represents one individual tumour, and are representative of 3-6 tumours collected per time point from two independent experiments.

Early stages (days 9-12 post-implantation) of admixed tumours were well infiltrated by both $CD4^+$ and $CD8^+$ T cells, and both WT and KO 'zones' contained both T cell subsets in equal proportion (**Figure 25A-C**). We attempted to use the machine learning function in Imaris image analysis software to identify the number of $CD4^+$ and $CD8^+$ T cells observed per tumour section from a set of tumours imaged on day 12 post-implantation (**Figure 25D**). Overall, there were no immediate differences in the number of $CD4^+$ or $CD8^+$ T cells per tumour section analysed, the counts of which were normalized to the total tumour area in

each image. However, this analysis is limited by the single section taken per tumour, and is likely not representative of the whole tumour nor the degree of segregation present in each.

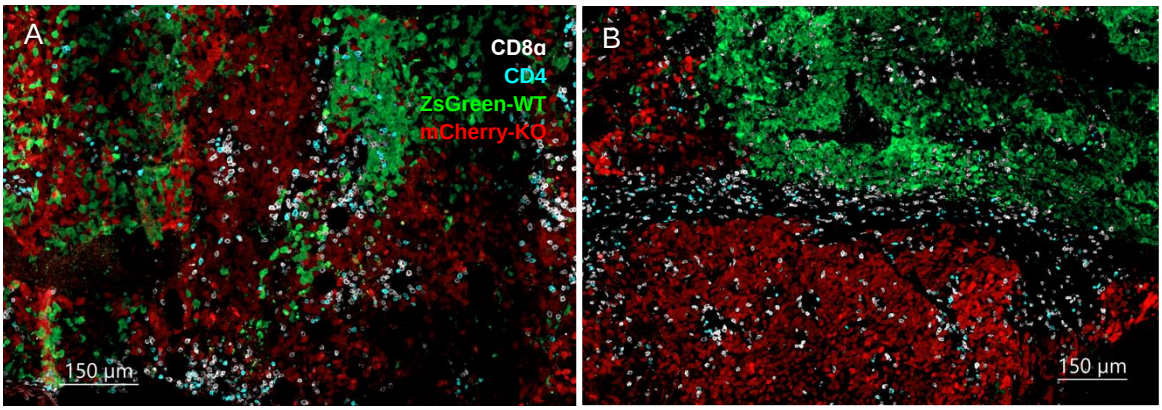

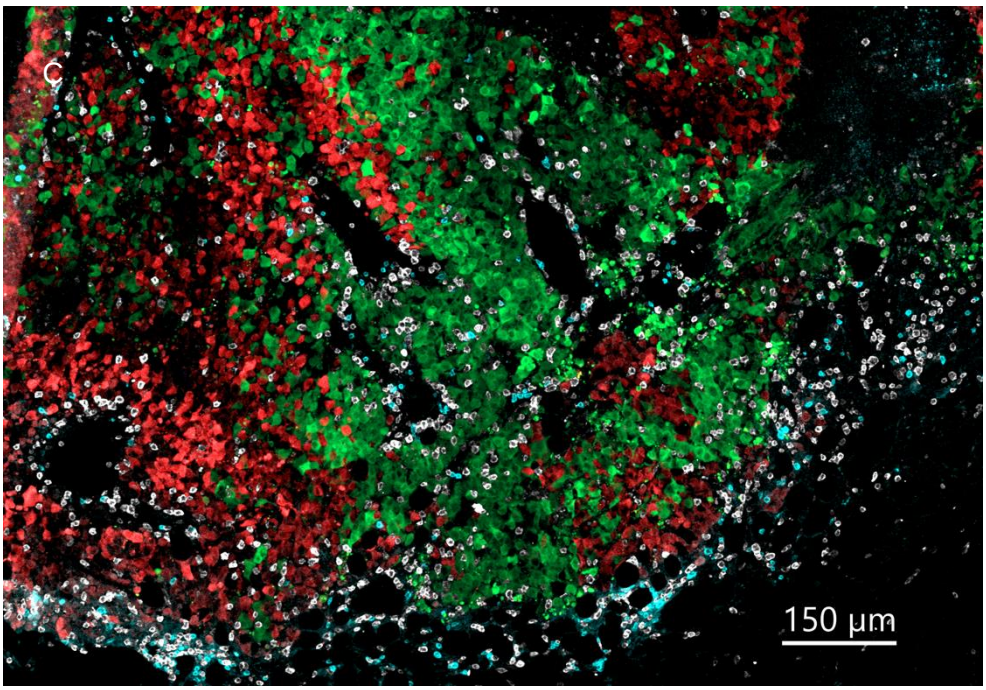

D

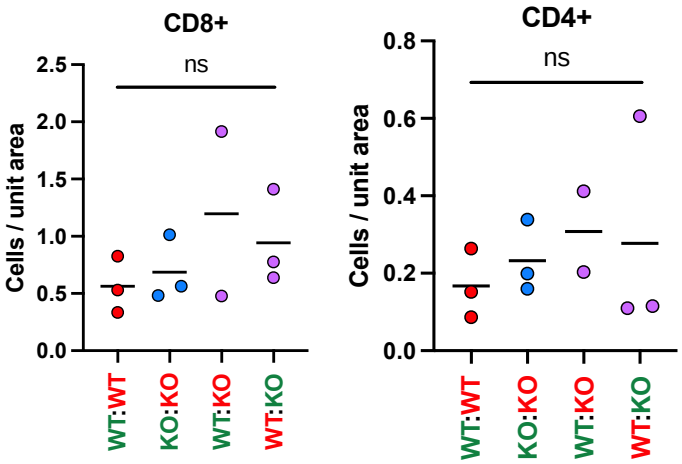

Figure 25. Confocal images of ZsGreen-WT:mCherry-KO tumours immunostained for CD8α and CD4 antibodies. Each panel from A-C show an individual tumour from day 15 post-implantation. Sections were stained with anti-CD8α AF647 and anti-CD4 PE antibodies for detection of T cells. (D) Quantification of the $CD4^+$ or $CD8^+$ T cells per unit area of the images. Each dot represents one section from one tumour. Data is from one experiment, and show the mean for each set of samples.

During late stages of segregation, some, but not all, tumours showed preferential clustering of $CD8^+$ T cells within WT zones, leaving adjacent KO zones less well infiltrated (**Figure 26A**). In admixed tumours where WT cells were not found during imaging, $CD8^+$ T cells showed greater infiltration into the tumour compared to $CD4^+$ T cells, which were mostly retained at the periphery of the tumour tissue (**Figure 26B&C**). This may indicate an advantage in these tumours where $CD8^+$ T cells have improved tumour infiltration, compared to tumours where both WT and KO cells remain.

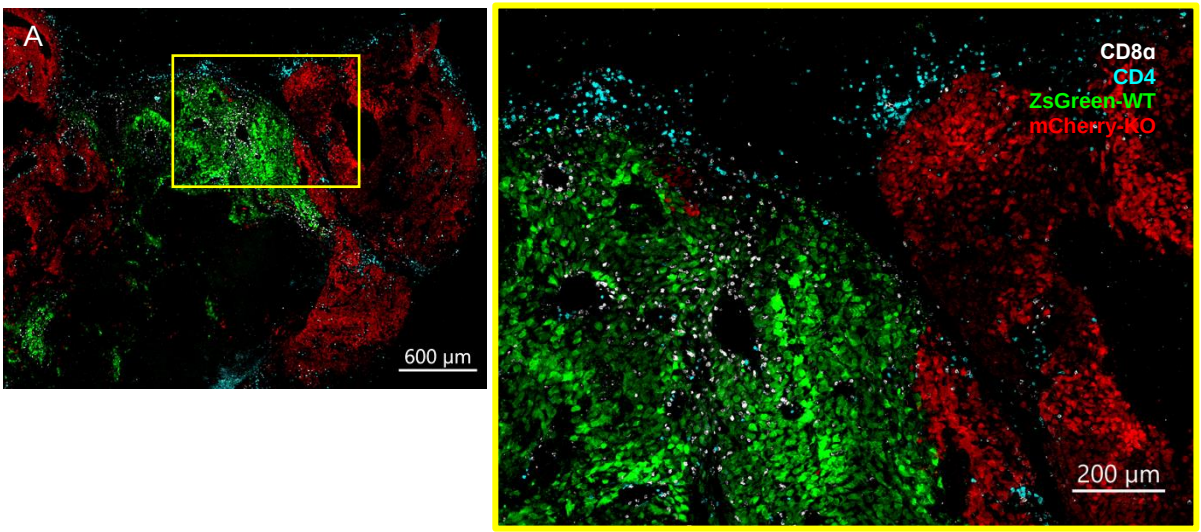

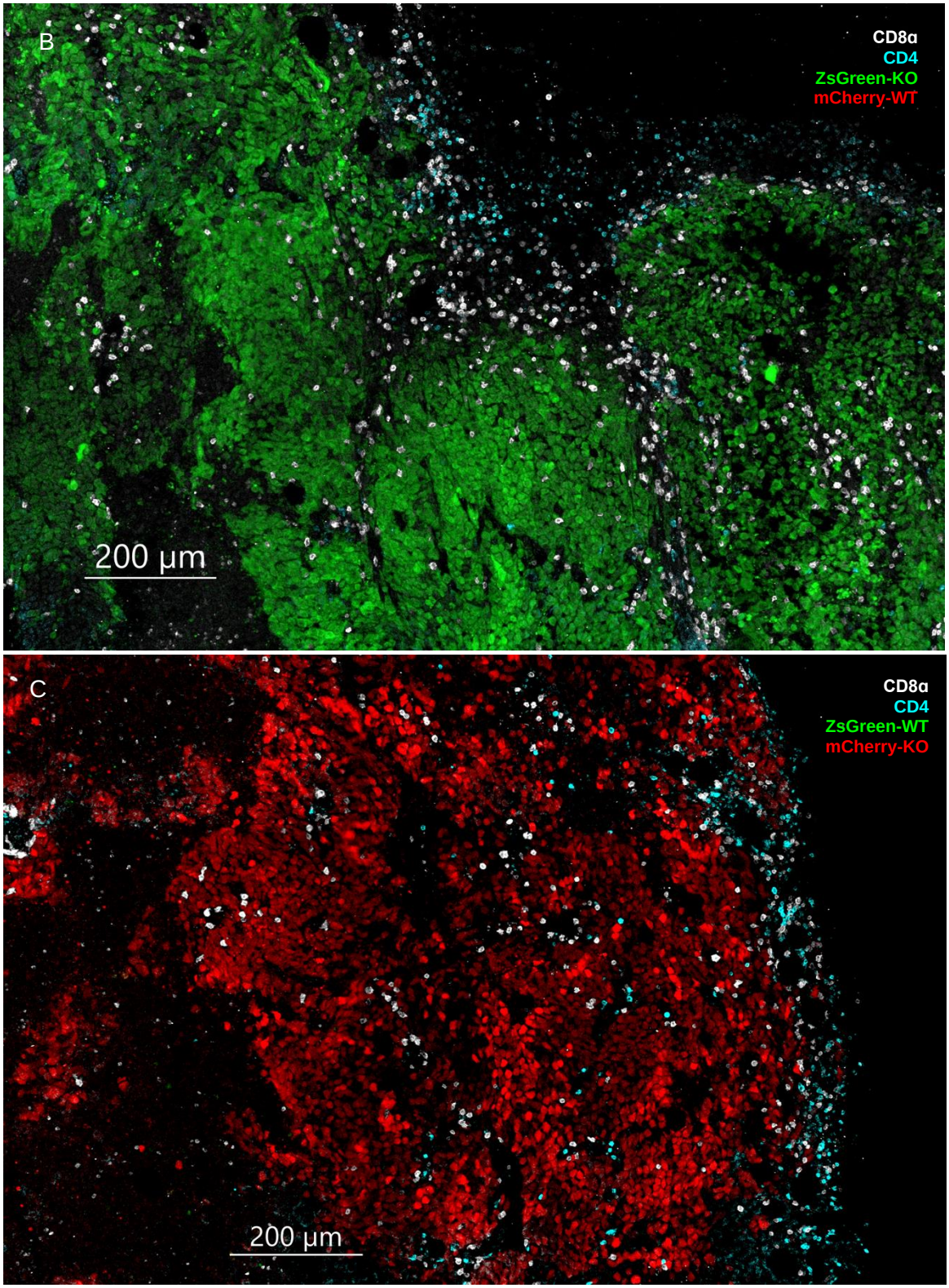

Figure 26. Confocal images of admixed tumours taken at day 15 which show a high degree of tumour cell segregation. Images of ZsGreen-WT:mCherry-KO tumours (A and C), or a mCherry-WT:ZsGreen-KO tumour (B) which shows anti-CD8α and anti-CD4 staining. Each image is from one individual tumour. Data are from one experiment.

4.2.5 Immune escape of IFNGR1KO tumour cells in admixed tumours requires the presence of CD8$^+$ T cells and/or IFNγ *in vivo*

We proceeded to test the admixed model in CD8 knockout (*Cd8a*^{tm1Mak}) and IFNγ knockout (*Ifng*^{tm1Ts}) mice to determine whether the major producers of IFNγ, or IFNγ itself, are important factors in the segregation phenotype. Similar to previous experiments, mice were implanted with a 1:1 mixture of B16-OVA ZsGreen-WT and mCherry-IFNGR1KO. Tumours were on average larger than in WT mice (shown in Figure 18C) as most tumours did not experience a 'stationary' period of growth (**Figure 27A&B**). Interestingly, the admixed phenotype whereby IFNGR1KO cells outgrow WT cells over time was reversed (i.e., WT outgrows IFNGR1KO cells) in about half of the CD8KO mice (**Figure 27C**). In comparison, no significant outgrowth of either WT nor IFNGR1KO cells was observed in IFNγKO mice. The levels of MHC-I (H2-K^b) upregulation were measured on both ZsGreen and mCherry tumour cells isolated from the tumours implanted in CD8KO and IFNγKO mice. Compared to WT mice, MHC-I levels on WT cells were 10-to-20-times lower in CD8KO mice, which was indicative of the overall effect that CD8$^+$ T cells normally have on tumour cells *in vivo* (**Figure 27D**). No significant H2-K^b was measured on either cell type from IFNγKO mice, demonstrating that MHC-I expression is primarily driven by IFNγ *in vivo*.

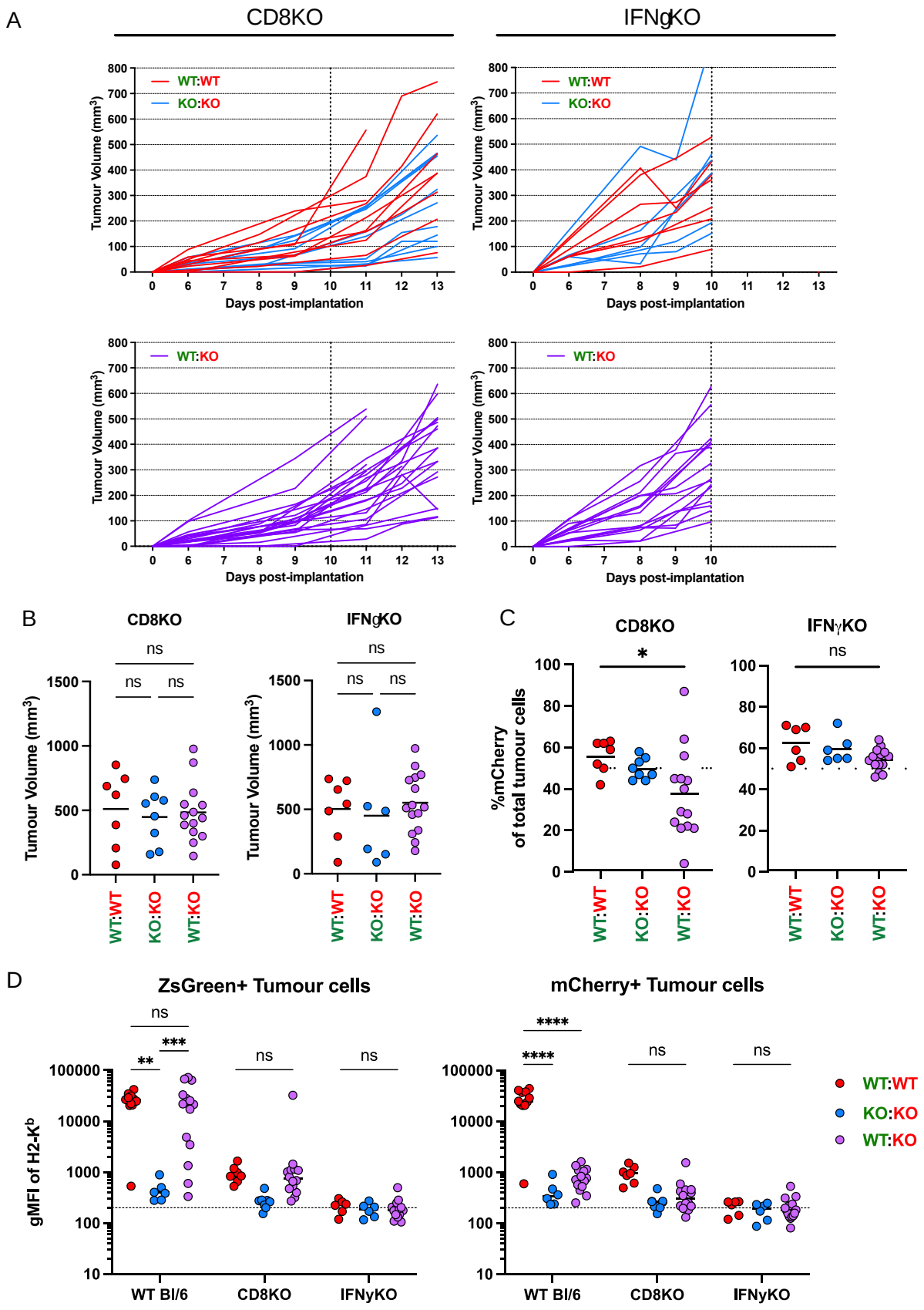

Figure 27. B16-OVA WT and IFNGR1KO admixed model in CD8KO and IFNγKO mice. (A) Tumour volumes measured by day of control WT:WT or KO:KO tumours, and admixed WT:KO tumours, in CD8KO and IFNγKO

mice. Mice were implanted with $1x10^5$ total tumour cells subcutaneously per flank. (B) Tumour volumes in CD8KO and IFNγKO mice at endpoint, on day 13 and day 10, respectively. (C) Ratio of mCherry and ZsGreen cells measured by flow cytometry of tumours isolated from CD8KO and IFNγKO mice. (D) Levels of $H2\text{-}K^b$ MHC-I by geometric MFI measured on $ZsGreen^+$ or $mCherry^+$ tumour cells gated by live $CD45^-$ population. Data are pooled from two independent experiments, and show mean with *p*-values by one-way ANOVA using Kruskal-Wallis multiple comparisons test in B & C. $^{**}p \leq 0.01$; $^{***}p \leq 0.005$; $^{****}p \leq 0.001$.

Spectral flow cytometry and metaclustering analysis of infiltrating immune populations showed a lack of difference between WT:WT or KO:KO control and admixed tumours (**Figure 28A**). Compared to previous opt-SNE plots from the same tumour mixtures in WT mice, there were no detectable changes in the frequencies of clusters identified nor specific immune populations which differed between the conditions. This indicated overall that the admixed phenotype was primarily $CD8^+$ T cell- and IFNγ-driven. Overall tumour infiltration of $CD45^+$ cells was significantly diminished in CD8KO mice (Figure S6), and affected to a lesser extent in IFNγKO mice.

The metaclustering analysis showed a loss in the differences within the $CD8^+$ T cell population between WT:WT and KO:KO/admixed in IFNγKO mice. This prompted a more in-depth comparison of the tetramer-positive T cell populations between the two models. The difference in percentage of tetramer-positive T cells between WT:WT and KO:KO/admixed was lost in IFNγKO mice (**Figure 28B**). Furthermore, no difference in MFI of the tetramer staining was observed (**Figure 28C**), a phenotype which was preserved in previous experiments as well as in the admixed model. This indicates that IFNγ-driven MHC-I expression is likely required for downregulation of OVA-specific TCRs, as lack of MHC-I expression on the tumours of IFNγKO mice maintains a similar tetramer MFI across all groups. This would also imply that the higher tetramer MFI of T cells in IFNGR1KO tumours in WT mice is due to lack of TCR-dependent stimulation, rather than increased TCR affinity.

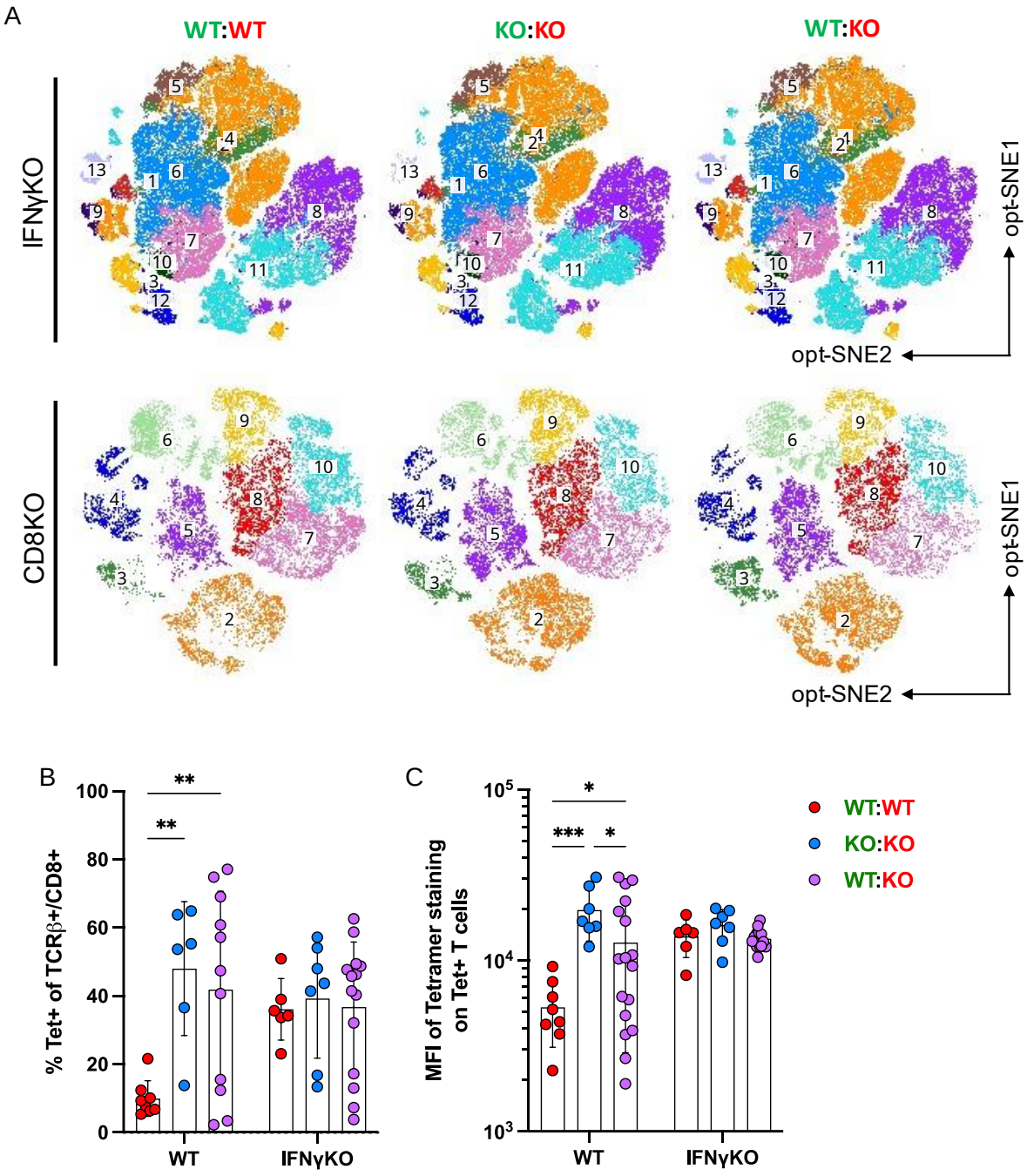

Figure 28. High dimensional flow cytometry analysis of CD45⁺ cells from IFNγKO or CD8KO tumours. (A) opt-SNE plots of live CD45⁺ immune cells analysed from a 20-colour Cytek Aurora flow cytometry panel (Table S3) using the OMIQ software platform. Individual metaclusters of cells were determined using FlowSOM and indicated by different colours and labels. Plots shown are concatenated from 3-5 samples of the same tumour type. Data are from one experiment per mouse strain, representative of two independent experiments each. (B) Percentage of CD8⁺ T cells which were tetramer⁺, gated on live CD45⁺ cells. (C) Geometric MFI of tetramer⁺ T cells, gated on CD8⁺ T cells. Samples are grouped by mouse strain (i.e., WT of IFNγKO). Data are pooled from two independent experiments using IFNγKO mice, and three independent experiments using WT mice. Data show mean ± SD with *p*-values by two-way ANOVA using multiple comparisons testing in B & C. **p*≤0.05; ***p*≤0.01; ****p*≤0.001.

Finally, we used confocal microscopy to determine whether admixed tumours formed any particular patterns in CD8KO and IFNγKO mice. In IFNγKO mice, although there was some evidence that some tumours showed 'patchiness' of WT or IFNGR1KO cells in some areas (**Figure 29A**), there were frequently tumour regions where cells remained well-mixed, and did not exhibit the same exclusionary pattern as in WT mice where WT cells were corralled into the core of the tumour (**Figure 29B-C**). Similar observations were found in CD8KO mice (**Figure 29D-F**), which indicates that there may be some preference for each cell type to grow around similar cells, which produces a less speckled pattern than found previously in Figure 24B.

For admixed tumours in CD8KO mice where WT cells outgrew IFNGR1KO cells, we imaged two independent tumours. Interestingly, these tumours showed the reverse pattern of cell segregation, where IFNGR1KO cells were closer to the centre of the tumour, and WT cells formed the majority of cells in the tumour (**Figure 29G-I**). These images, together with the segregation patterns from WT mice, provide a clue as to how tumour cells which are vulnerable to immune pressure are cleared over time. Further work is needed to clarify the types of immune cells which are involved in clearance of KO cells in the model, which may provide a key in understanding an CD8-independent pathway of tumour control.

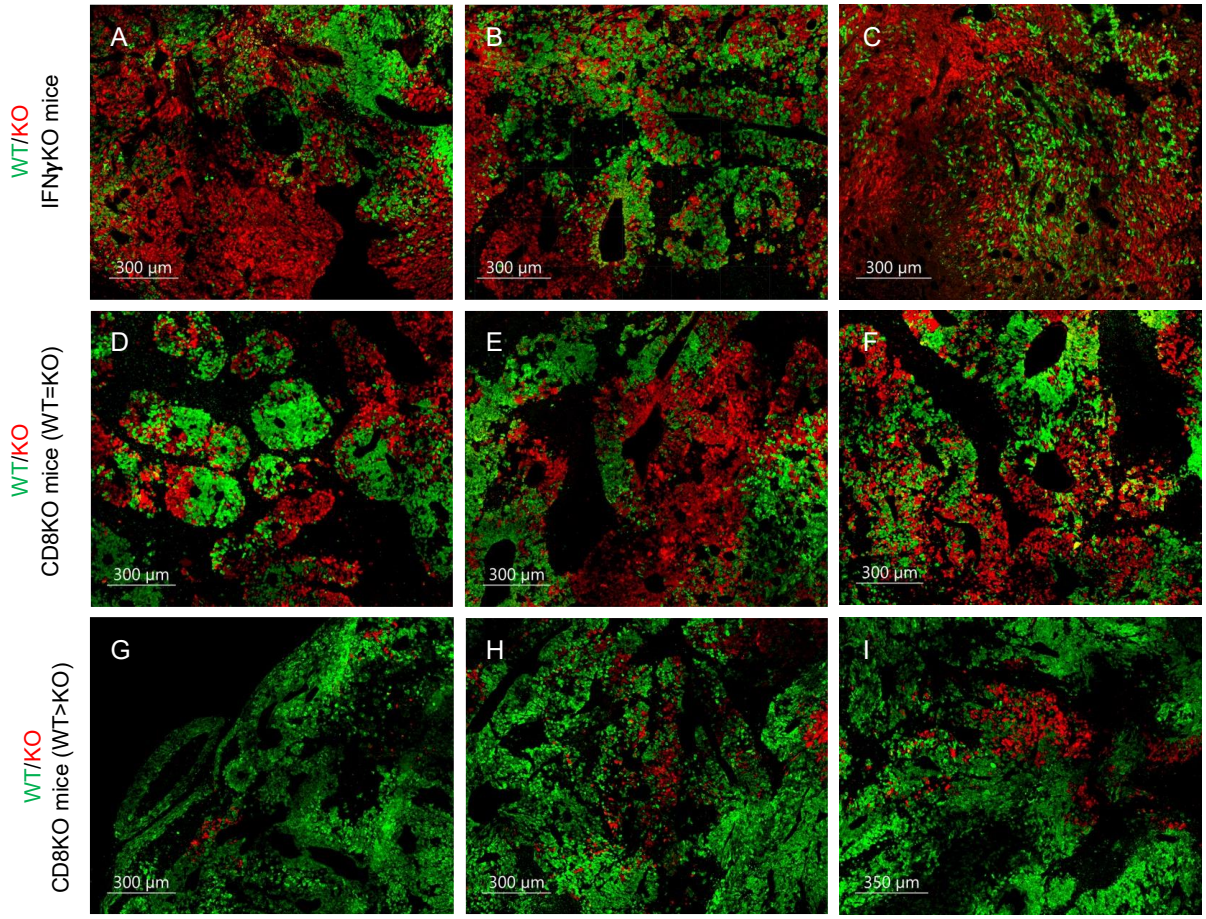

Figure 29. Confocal microscopy images of admixed tumours in IFNγKO and CD8KO mice. Representative sections taken from B16-OVA ZsGreen-WT and mCherry-IFNGR1KO tumours in IFNγKO mice (A-C), and CD8KO mice (D-I) are shown. Each image per mouse strain is taken from 3 mice per group, except for images in G-I which are taken from two mice.

4.3 Discussion and conclusion

4.3.1 Observations from the CD8KO and IFNγKO murine models

The CD8KO and IFNγKO murine models initially served as a negative control for the admixed tumours as we hypothesized that the phenotype was IFNγ-driven. Instead, the two strains provided more interesting insights into the data obtained in the previous chapter, as well as the findings described in the current chapter, as the effects of losing $CD8^+$ T cells or IFNγ appeared more nuanced than anticipated. Although loss of IFNγ did not abolish the presence of OVA-specific $CD8^+$ T cells in the tumour, it did result in complete failure of tumour control as humane endpoints were reached by day 10 post-implantation.

In Chapter 3.2.5, we attempted to uncover whether IFNγ-signalling in tumour cells affected cross-priming of T cells. Although this model suggests that IFNγ is indispensable for the priming of OVA-specific T cells, the lack of IFNγ signalling in tumour cells also rendered WT and KO tumours similar to one another. Therefore, the important dimensionality of how the tumour itself contributes to T cell priming is lost. Without IFNγ present, no significant differences in the proportion of OVA-specific T cells in between WT and IFNγKO mice was observed, supporting the idea that IFNγ is dispensable for cross-priming of tumour-specific T cells. The infiltration of OVA-specific T cells in these tumours also indicate that while $CD8^+$ T cells are able to arrive at the tumour site, cytotoxic functions which result in tumour control are IFNγ-dependent. Lastly, there was no longer a separation in the quantity nor MFI of the $tetramer^+$ T cells between WT and KO tumours in IFNγKO mice. While it remains a possibility that these T cells are of higher TCR affinity, and therefore stain for higher MFI, it is more likely that the lack of MHC-I upregulation in IFNγKO mice would reduce T cell receptor engagement, and subsequent downregulation.

The CD8KO model was uniquely compelling for admixed tumours as an unexpected reversal of the phenotype was observed. The main differences were that admixed tumours in WT mice may have little to no WT cells remaining (0.5 to 10%) whereas 5 to 30% of KO cells would remain in the reversed admixed tumours from CD8KO mice. However, this would

mean that there is some CD8-independent mechanism which is capable of inhibiting KO cell growth, or promoting KO cell death. It would be intriguing if the same cell type or mechanism plays a role in the control of KO tumours when implanted independently, which remains to be uncovered. Future experiments will be focused on repeating the phenotype using an anti-CD8β depletion antibody to deplete $CD8^+$ T cells specifically, rather than ablating all CD8α-expressing cells *in vivo.*

4.3.2 Tumour-intrinsic mechanisms underlying tumour cell segregation

One striking observation is the reliability with which WT cells are increasingly segregated from IFNGR1KO cells over time when both cell types are present in the same microenvironment. Tumour-intrinsic factors are likely to enhance or accelerate this process, with IFNγ-dependent pathways taken into further consideration. Key chemokines expressed by the tumour cells themselves may directly enhance T cell infiltration. B16 cells have been found to express CXCL9 and 10[243], which are upregulated by IFNγ stimulation. This chemoattraction may explain the clustering of $CD8^+$ T cells preferentially around WT cells in admixed tumours which have an abundance of IFNGR1KO cells present, and also provide a clue as to how WT cells become the preferential target. We can determine intrinsic chemoattractant properties of B16F10 using transwell migration assays, and incubation with immune subsets derived from pure cultures or sorted by flow cytometry from the tumour. Additionally, stimulation of B16F10 with IFNγ followed by a wash-out period would 'prime' the tumour cells for production of chemoattractants regulated only by IFNγ.

Recent studies have also highlighted the importance of IFNγ-dependent pathways which increase the adhesion between tumour cells and effector T cells, as demonstrated by the use of CAR T cells against solid tumours.[268,269] Success of these therapies hinges on the upregulation of ICAM-1 by IFNγ on tumour cells, which allows for T cell entry and promotion of interaction between T cells and target cells. Although B16F10 is not known to express ICAM-1[270], they do express CD44, and integrins α1, α4, αV, and β1.[271] Some of these

integrins are directly upregulated by IFNγ[272,273], but it is currently unknown which integrins and binding partners are used by T cells for direct adhesion.

Whole-mount immunolabelling, tissue clearing, and imaging of tumours by light-sheet microscopy has been recently demonstrated by different groups.[274–276] Volumetric 3D imaging of admixed tumours would greatly enhance our understanding of the cell segregation patterns, as current 2D imaging is limited to sampling of small tumour sections at a time. Furthermore, immunolabelling of T cells within the tumour, or detection of myeloid populations using fluorescent reporters would provide spatial information on whether these interactions contribute to the observed admixed phenotype.

4.3.3 Immune mechanisms enabling the admixed phenotype

Based on the observation that independent WT and IFNGR1KO tumours remained similar in size during tumour progression, we surmised the possibility that the same immune factors would control both types of tumours with equal effectiveness. This would result in admixed tumours retaining a 50:50 WT:KO composition overtime, which was not experimentally observed. An alternative model, where independent factors control WT and KO tumours, would better explain how both may be present in an admixed context (**Figure 30**). Although the independent factors may be difficult to narrow down, we have experimental clues as to which cell types and pathways are most worthwhile exploring.

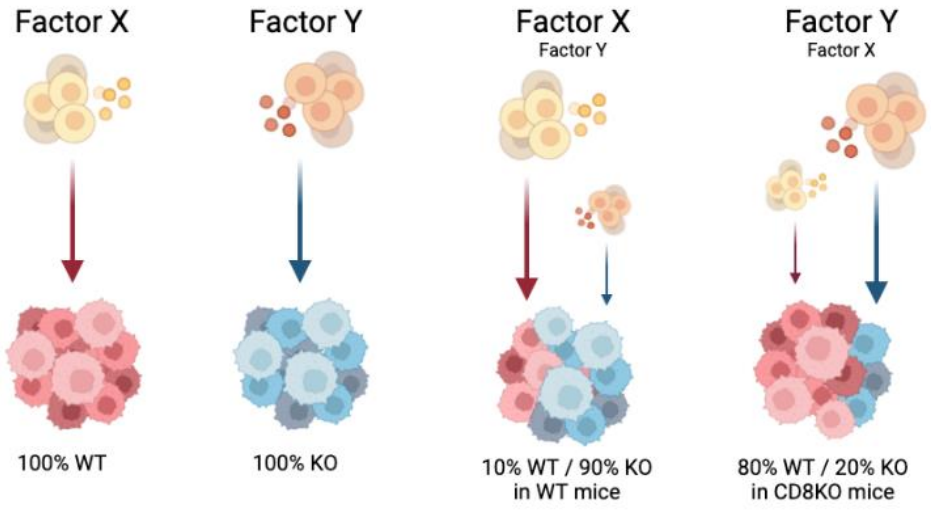

Figure 30. Independent factors controlling B16 WT and IFNGR1 tumours may be used to explain the phenotypes observed in the admixed model.

The factors controlling WT cells are more likely to be $CD8^+$ T cell-based, based on previous literature which have reported that $CD8^+$ T cells are necessary for efficacy of checkpoint therapy in B16F10 models.[277,278] Supporting this is the observation that loss of $CD8^+$ T cells also results in outgrowth of WT in our admixed model. The factors controlling KO cells are more difficult to ascertain. It is possible that outgrowth of WT cells in some CD8KO tumours are due to improved NK cell cytotoxicity against IFNGR1KO cells, which could be experimentally tested using NK depletion methods *in vivo*. Our analysis of high dimensional flow cytometry data from WT mice also proposes that the factor may be myeloid in origin, due to the presence of a MHC-II^{hi} population in the KO which is not present in the WT. Indeed, MHC-II^{hi} TAMs have been reported to be present during the early phase of tumour suppression, and transition to a MHC-II^{lo} phenotype was associated with tumour progression.[279]

In chapter 5, our single-cell dataset was used to identify dichotomous monocyte and macrophages present in WT and KO tumours. Taken together, these data point to an intermediary between lymphocytes which can control the tumour, and a myeloid component which enables, or hinders, their anti-tumour function.

4.4 Appendix

Table S2. Cytek Aurora panel for admixed experiments in WT mice.

Peak Channel	Fluorochrome	Marker	Clone	Manufacturer	Cat. No.	Dilution (1:X)
UV2	Spark387	CD8a	53-6.7	Biolegend	100798	200
UV6	Zombie UV	--	--	Biolegend	423108	1000
UV14	BUV737	CD44	IM7	eBioscience	367-0441-82	400
UV16	BUV805	CD45	30-F11	eBioscience	368-0451-82	400
V1	BV421	OVA-Tetramer	--	NIH	--	500
V3	PB	CD11c	N418	Biolegend	117231	400
V10	BV605	PD-1	29F.1A12	Biolegend	135219	200
V11	BV650	PD-L1	10F.9G2	Biolegend	124333	400
V13	BV711	CD62L	MEL-14	Biolegend	104438	200
V15	BV785	CD103	2E7	Biolegend	121439	200
B2	ZsGreen	Tumour	--	--	--	--
B9	PerCP-Cy5.5	CD4	GK1.5	Biolegend	124334	400
YG1	PE	TCRβ	H57.597	Biolegend	109207	400
YG3	mCherry	Tumour	--	--	--	--
YG5	PE-Cy5	MHC-II	M5/114.15.2	Biolegend	107611	1000
YG9	PE-Cy7	LAG-3	C9B7W	Biolegend	125225	200
R1	APC	TIM-3	RMT3-23	Biolegend	119706	200
R2	AF647	NKp46	29A1.4	Biolegend	137628	100
R4	AF700	H2-K^{b}	AF6-88.5	Biolegend	116521	200
R7	APC/Cy7	CD19	6D5	Biolegend	115525	200
R8	APC-Fire810	CD11b	M1/70	Biolegend	101288	400

Table S3. Cytek Aurora panel for admixed experiments in CD8KO and IFNγKO mice.

Peak Channel	Fluorochrome	Marker	Clone	Manufacturer	Cat. No.	Dilution (1:X)
UV2	Spark387	CD8a	53-6.7	Biolegend	100798	200
UV6	Zombie UV	--	--	Biolegend	423108	1000
UV14	BUV737	CD44	IM7	eBioscience	367-0441-82	400
UV16	BUV805	CD45	30-F11	eBioscience	368-0451-82	400
V1	BV421	OVA-Tetramer	--	NIH	--	500
V3	PB	CD11c	N418	Biolegend	117231	400
V10	BV605	PD-1	29F.1A12	Biolegend	135219	200
V11	BV650	PD-L1	10F.9G2	Biolegend	124333	400
V13	BV711	CD62L	MEL-14	Biolegend	104438	200
V15	BV785	CD103	2E7	Biolegend	121439	200
B2	ZsGreen	Tumour	--	--	--	--
B9	PerCP-Cy5.5	CD4	GK1.5	Biolegend	124334	400
YG1	PE	TCRβ	H57.597	Biolegend	109207	400
YG3	mCherry	Tumour	--	--	--	--
YG9	PE-Cy7	Ly6C	HK1.4	Biolegend	128018	400
R1	APC	F4/80	BM8	Biolegend	123115	200
R2	AF647	NKp46	29A1.4	Biolegend	137628	100
R4	AF700	MHC-II	M5/114.15.2	Biolegend	107621	400
R7	APC/Cy7	CD19	6D5	Biolegend	115525	200
R8	APC-Fire810	CD11b	M1/70	Biolegend	101288	400

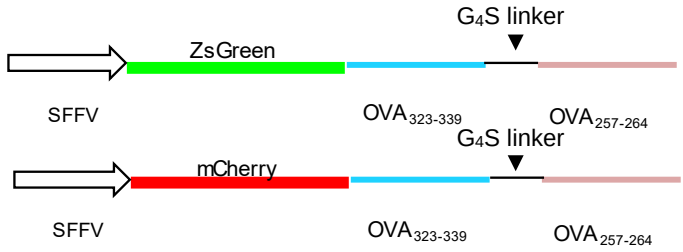

Figure S3. Structure of the ZsGreen- and mCherry-minOVA transgene used in transduction of B16F10 cells. The gene fragments were cloned into a pHRSIN lentiviral backbone under a SFFV constitutive promoter.

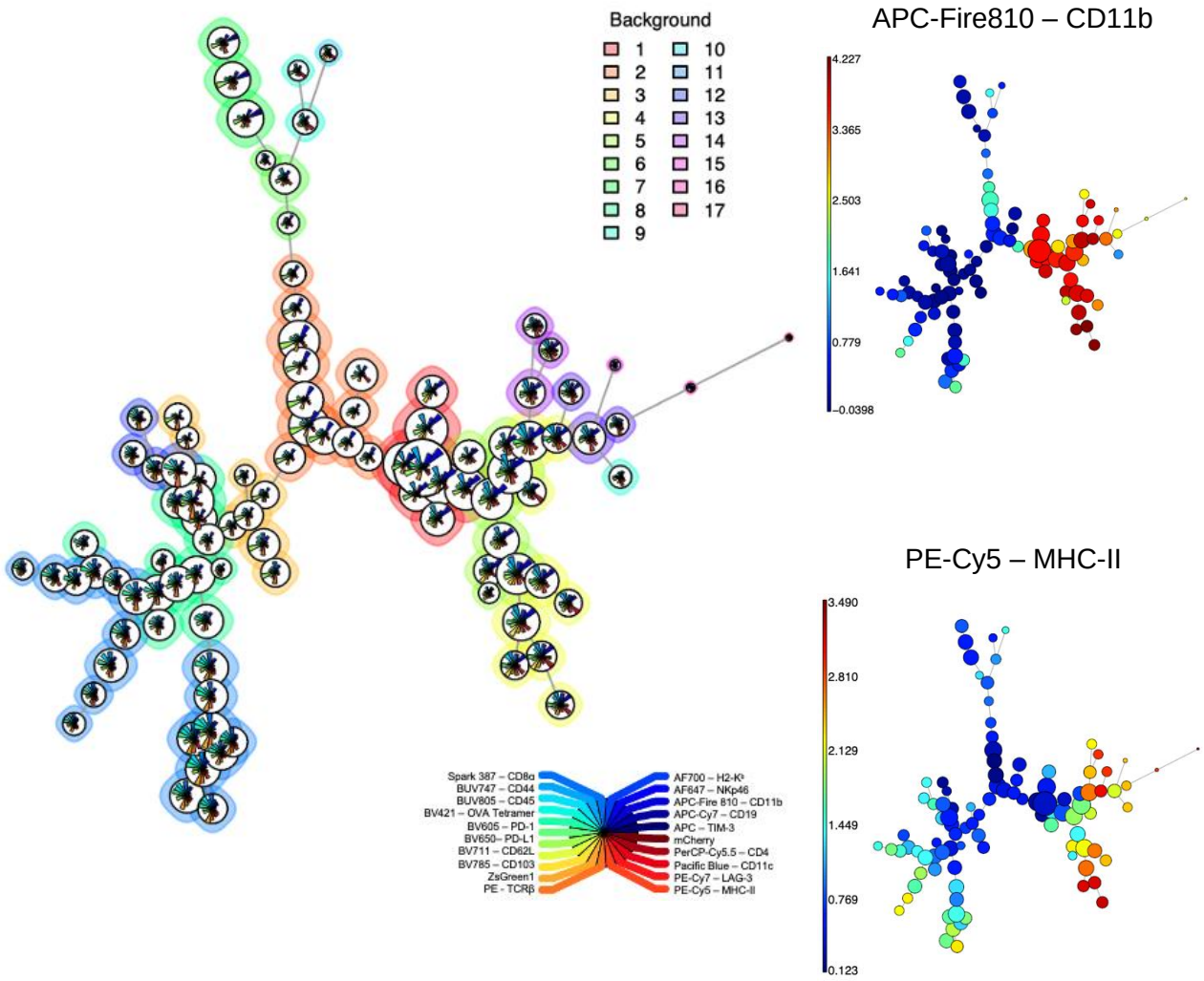

Figure S4. Example of FlowSOM metaclustering using the OMIQ analysis software. Tree-structure visualization used for determining each uniquely coloured metacluster. Sample trees (right) show relative expression of two representative markers in the flow panel.

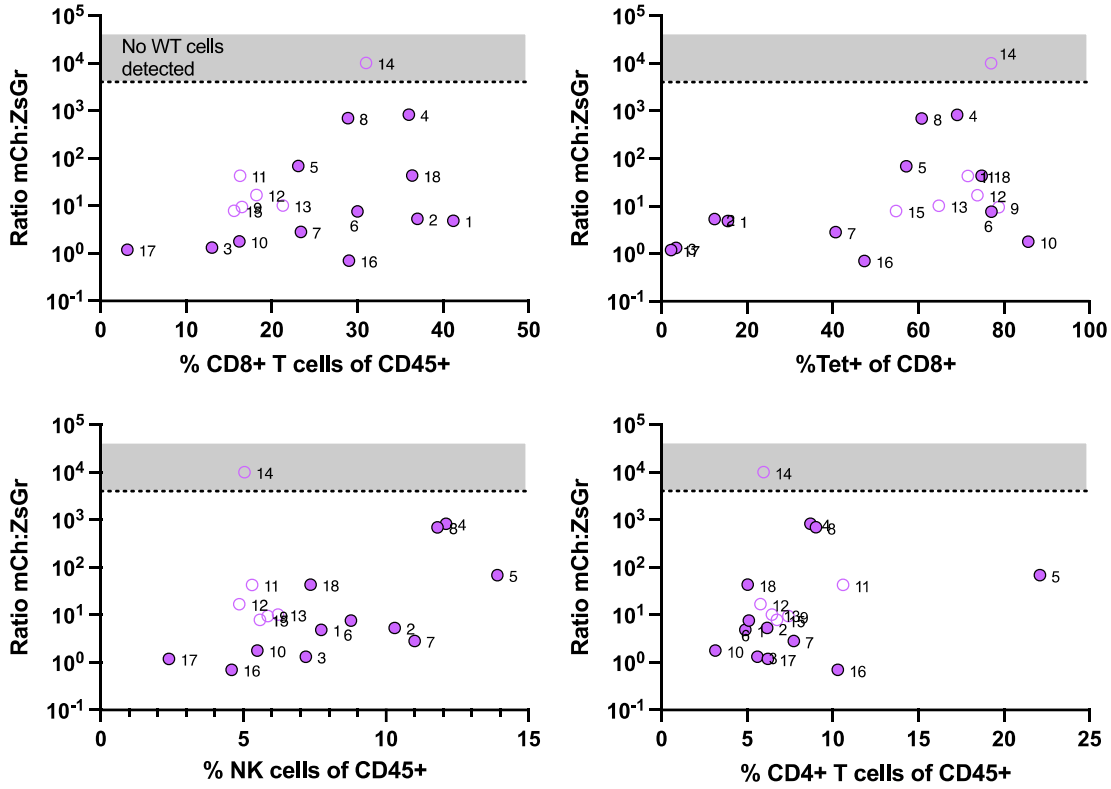

Figure S5. Comparison of mCherry:ZsGreen ratio from admixed tumours and infiltration of lymphocyte populations. Each dot represents one tumour and tumours are labelled with the same number or symbol throughout. All lymphocyte populations shown are gated on live CD45⁺ cells.

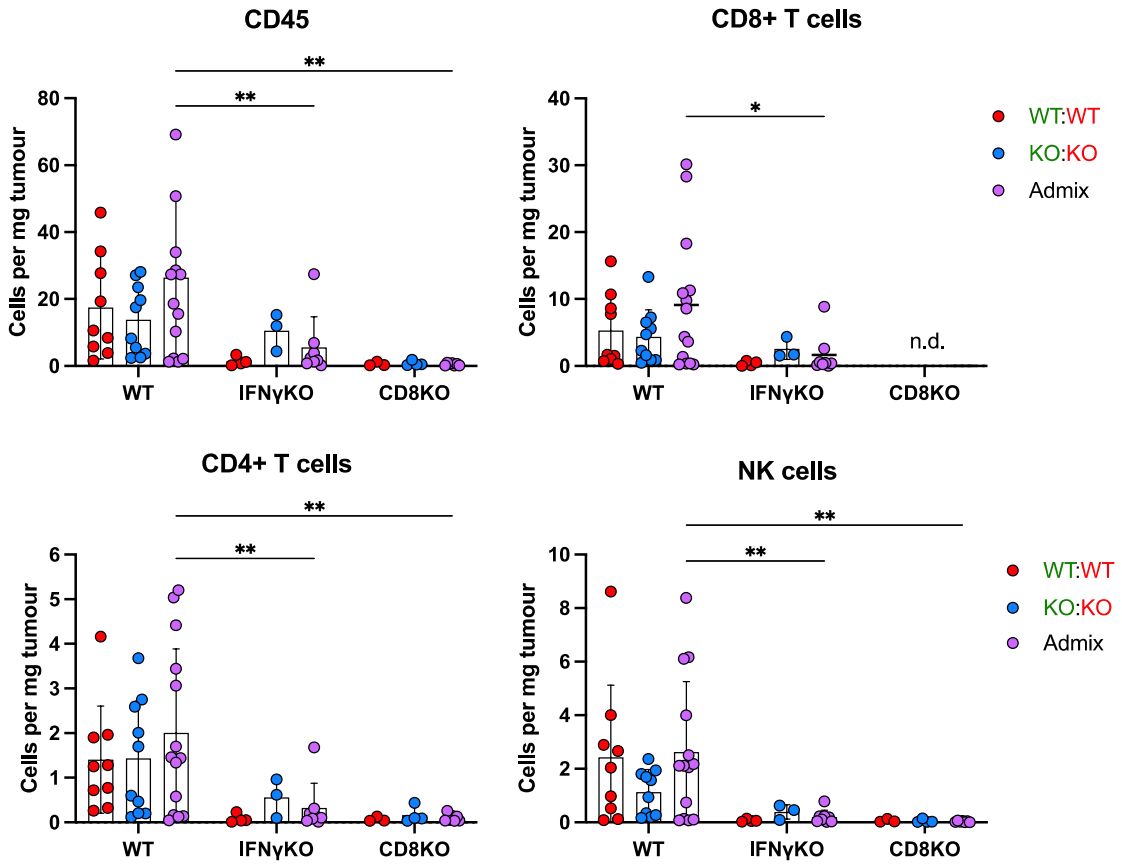

Figure S6. Absolute counts of CD45 cells, or lymphocyte populations found in control or admixed tumours compared between three mouse strains. Data are pooled from two independent experiments for each mouse strain, and showed mean ± SD with statistics by two-way ANOVA using Kruskal-Wallis multiple comparisons test, *$p \leq 0.05$, **$p \leq 0.01$, ***$p \leq 0.001$, ****$p \leq 0.0001$.

Single-cell analysis of infiltrating CD45$^+$ immune cells from B16-OVA WT and IFNGR1KO tumours

5.1 Introduction

This chapter describes the single-cell sequencing experiment and analysis of CD45$^+$ immune cells infiltrating the B16-OVA WT or IFNGR1KO tumours. Using different bioinformatic tools to interrogate the dataset in an unbiased manner, we found that the single-cell dataset supported our experimental findings where CD45$^+$ cells were experiencing a more IFNγ-rich environment in IFNGR1KO tumours compared to WT. Sequencing data allowed us perform unbiased characterization of immune subsets which have adapted to IFNGR1 ablation on tumour cells. By doing so, we hypothesized that one or more immune subsets (e.g., CD8$^+$ T cells) may be responsible for the increase in intratumoural IFNγ, and this increase also causes transcriptional changes in other cells.

5.1.1 Utility of single-cell sequencing over conventional transcriptomic methods

The transcriptome is the set of RNA transcripts present in a cell at any given time, which can be used to interrogate cellular function and molecular components specific to the physiological state in question. Bulk RNA sequencing (referred to as RNAseq) measures the transcriptome of a population of cells and enables both identification and quantification of transcripts present.[280] The most common type of analysis following RNAseq is differential gene expression, which is measured by the change in read counts between samples. Pathway analysis, or gene set enrichment analysis, gives greater meaning to groups or sets of differentially expressed genes which may belong to similar functional, metabolic, or signalling pathways, as examples.[281] However, the transcriptomes from unique cell populations are often lost, and rare or low abundance transcripts may be overlooked due to highly expressed common or ubiquitous transcripts.

Single-cell RNAseq (scRNAseq) overcomes many cell-specific limitations, and was developed following technology which allows for the capture and sequencing of

transcriptomes from single cells.[282] Compared to RNAseq which may pool many cell types together and millions of cells at once, scRNAseq is limited by the number of cells it can profile, which is currently 10,000 cells per lane of an eight-lane chip by 10X Genomics.[283] Furthermore, between 500-1000 unique genes are often sequenced per cell, meaning that rarer transcripts are unlikely to be picked up.[284] Although sampling of cells is much more limited in single-cell compared to bulk sequencing, scRNAseq has been instrumental in identifying rare, previously undescribed cell types from heterogeneous populations. Examples of single-cell profiling in immunology have allowed for extensive profiling of dendritic cell subtypes[285], exploring TCR clonality with respect to antigen specificity[286], and sampling of cell populations from 20 organs to reveal vast immune heterogeneity between tissues.[287]

5.1.2 Using single-cell RNAseq to infer intratumoural interactions

Specific to the field of cancer immunology, single-cell sequencing has great utility in analysing pre- and post-immunotherapy samples to identify biomarkers of clinical response and resistance.[288] Our interest in studying IFNGR1KO tumour cells was in part driven by sequencing experiments which identified IFNγ-signalling as a pathway downregulated in several murine cancer models to evade cytotoxic T cell-dependent killing.[289,290]

IFNγ-signalling is one type of cell-cell interaction which has both paracrine and autocrine functions. scRNAseq is increasingly being used to infer cell-cell interactions at both secreted, and cell-contact dependent levels, which provides information on both signal senders and receivers in a heterogeneous population.[291] At present, however, these ligand-receptor pairs must be manually curated from previous publications into single databases, which may include non-validated protein-protein interactions.[292] Tools to analyse the ligand-receptor pairs present in a scRNAseq dataset, such as CellPhoneDB[293], NicheNet[294], or CellChat[218], calculate communication scores or probabilities based on gene expression of the ligand-receptor pairs. Although powerful in determining cell-cell interactions which are not otherwise possible during bulk sequencing, findings must be experimentally validated as

gene expression is not always indicative of protein levels especially for receptors which have low mRNA abundance.

Nevertheless, recent publications have shown the utility of analysing these signalling networks in the context of tumour microenvironments, and demonstrates the feasibility in which ligand-receptor pairs can be identified and subsequently validated in syngeneic tumour models.[295]

5.1.3 Using single-cell RNAseq to identify influential myeloid populations

Mononuclear phagocytes present in the tumour range from monocytes and macrophages to dendritic cells which traffic to the tumour from blood or lymph nodes. Cell surface marker expression used in gating strategies for flow cytometry are largely insufficient for defining all the subsets of myeloid cells present. As a result, scRNAseq has been useful in delineation of myeloid subtypes which are not limited to those within tumour tissues.

The M1/M2 model of macrophage differentiation proposed in the early 2000's is now thought to be insufficient in describing TAMs.[296] The arrival of monocytes and subsequent differentiation into classical or TAM phenotypes cause the cells to exist on a continuum, rather than distinct, independent states.[297] M1 and M2 signatures are found simultaneously in TAMs from all cancer types, which shows the need for an improved model which groups TAMs based on functional characteristics rather than gene expression.[296,298] A recent review of TAMs using the single-cell omics data aimed to categorize TAMs based on their function, rather than the M1/M2 dichotomy (**Figure 31**), and their respective functions are summarized in **Table 2**. Correspondingly, similar reviews have also begun to use functional definitions in order to classify TAMs.[299]

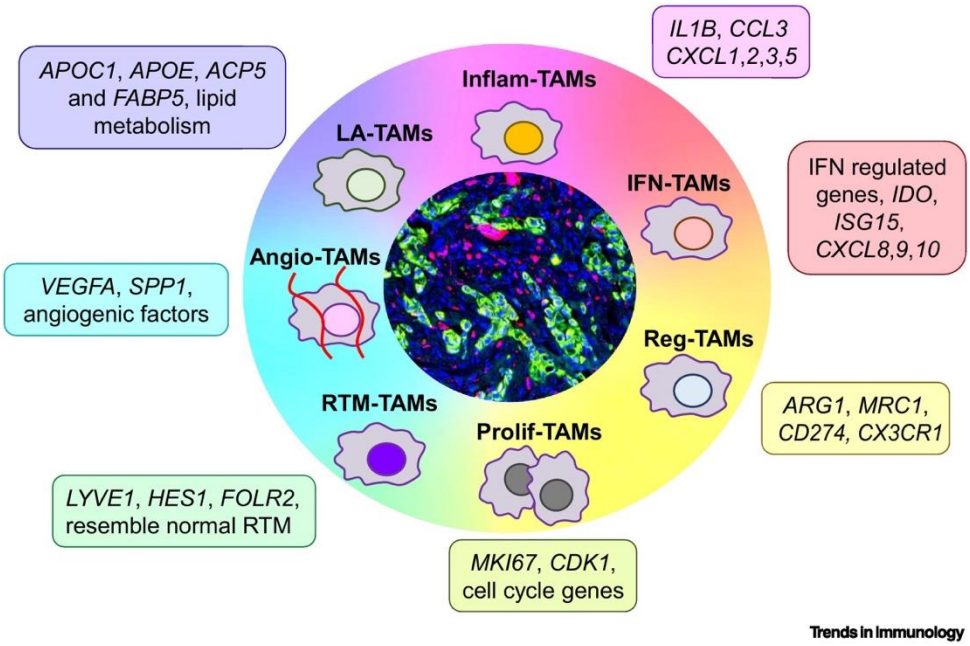

Figure 31. Characterization of TAMs in to seven functional subsets using single-cell omic datasets. Distinctive molecular features of TAM subsets were identified across many different human and mouse cancer types. These transcriptomic subsets exist on a continuum rather than distinct subsets, contrary to previous models which attempt to classify TAMs as pro-inflammatory or immunosuppressive. Figure retrieved from [298].

Table 2. Descriptions of TAM subsets by function.

TAM Subset	Description	Functions in the TME
IFN-TAMs (Interferon-primed TAMs)	High expression of IFN-regulated genes, resembling M1-like macrophages but are not anti-tumour	Tryptophan degradation, recruitment of Tregs, high expression of immune checkpoint molecules
Reg-TAMs (immune regulatory TAMs)	Resemble alternatively activated macrophages, high expression of *Arg1*, *Mrc1*, and *Cx3cr1*	Non-exclusive immune regulatory functions, including immunosuppression via *Trem2* expression
Inflam-TAMs (inflammatory cytokine-enriched TAMs)	Inflammatory cytokine signature, including *Il1b, Cxcl1/2, Ccl3, Ccl3l1*	Recruitment of monocytes and lymphocytes via secretion of chemokines during tumour-associated inflammatory responses
LA-TAMs (lipid-associated TAMs)	Enrichment of genes in lipid metabolism and oxidative phosphorylation pathways	Lipid catabolism in macrophages is associated with immunosuppression and tolerance of other immune cells; lipid accumulation are required for proliferation and activation of TAMs
Angio-TAMs (proangiogenic TAMs)	High expression of angiogenic signature *Vegfa* and *Spp1*, along with angiogenic factors *Vcan, Fcn1* and *Thbs1*	Promotion of angiogenesis; facilitate metastasis through promotion of tumour cell intra- and extravasation, and chemotherapy resistance
RTM-TAMs (resident-tissue macrophage-like TAMs)	Resembles normal tissue-resident macrophages, but also have high embryonic precursor signature	Enriched in adjacent tissues from tumour cells, and induces epithelial-mesenchymal transition and tumour invasiveness

Prolif-TAMs (proliferating TAMs)	Expression of *Mki67* and cell cycle-dependent genes such as cyclins	Pro-inflammatory functions and expands through proliferation to promote tumour progression; promotes a profibrotic tumour phenotype

Almost all cell types and aspects of the tumour microenvironment are capable of modulating TAM activity (**Figure 32**). As macrophages are highly plastic cells which respond to their environment, several TAM-targeted treatments have attempted to reprogram their functionality and promote anti-tumour functions. Use of monoclonal antibodies which modulate their ability to phagocytose target cells have been shown to enhance killing of cancer cells in murine xenograft models.[300] Intratumoural delivery of Toll-like receptor agonists have been tested for activating innate immune pathways in TAMs, as classical TLR agonists are known for their ability to polarize macrophages *in vitro* and *in vivo.*[301] Lastly, agonists for the CD40-CD40L pathway utilized broadly by innate and adaptive cells is known to upregulate MHC molecules and production of IL-12, which leads to activation of cytotoxic lymphocytes.[302,303] Anti-CD40 agonistic antibodies are tested for their ability to induce macrophage and other APC activation as a method of bolstering the adaptive anti-tumour response.

Understanding of how such a heterogeneous population of cells with diverse functionality are recruited and sustained in the tumour microenvironment is of significant interest, as their differentiation is in direct response of cytokine and chemokines present. As a result, studying macrophage diversity and function within a tumour would be indicative of the overall state of the TME, and made easier by their relative abundance compared to other cell types.

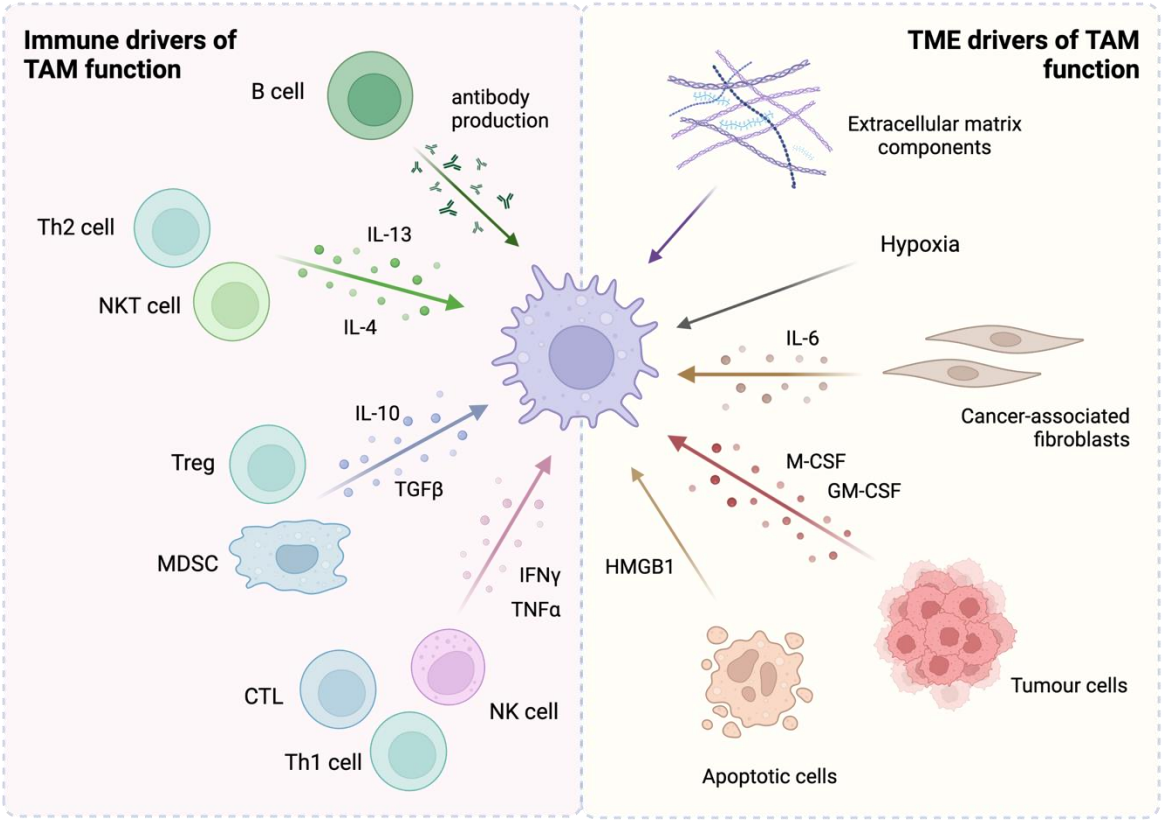

Figure 32. Immune and non-immune drivers of the TAM phenotype in the tumour microenvironment. (Left) Innate and adaptive cells both produce primarily Th2 cytokines which contribute to TAM function, with the exception of IFNγ and TNFα which exert pro-tumour functions in this scenario. (Right) Non-immune drivers such as fibrosis by cancer-associated fibroblasts, hypoxic conditions, and cell stress from apoptotic cells also drive the TAM phenotype. Tumour cells, and other immune cells secrete M-CSF to recruit monocytes, and promote differentiation into TAMs. Created with BioRender.com.

In our current studies, we integrated different and complementary types of analyses to fully characterise how IFNGR1KO tumours alter the cell-cell communication of immune cells during tumour development in an unbiased manner. We further analysed the differences in TAM subsets present in WT and KO tumours transcriptionally and made preliminary efforts in validating these phenotypes *ex vivo* with the hopes of understanding whether TAMs are a key cell type in enabling anti-tumour immunity in IFNGR1KO tumours.

5.2 Results

5.2.1 Single-cell sequencing of B16 OVA WT and IFNGR1KO tumour reveals diverse CD45$^+$ infiltrating populations

As flow cytometry-based analysis was limited in the unique markers useful for distinguishing independent immune cell types, we performed single-cell RNA sequencing (scRNAseq) analysis on the CD45$^+$ infiltrating populations within WT and IFNGR1KO tumours. Incorporation of a cell hashing step during sample preparation mitigated downstream batch effects which would require additional batch correction algorithms during data analysis (**Figure 33A**). Following data quality control steps and filtering, dimensionality reduction was performed to allow for clustering of single-cell populations. UMAP projection of data structure shows equal distribution of both lymphoid and myeloid populations which are present in both WT and IFNGR1KO samples (**Figure 33B**). Proportional bar graphs comparing frequencies of each annotated cell type showed similar infiltration of lymphoid populations, and approximately 10% more cells identified as ‘macrophage 2’ in WT compared to KO (**Figure 33C**). Reassuringly, the populations identified from scRNAseq recapitulated the major immune cell types and their respective proportions previously found in our flow cytometry data in Chapter 3.2.1.

A

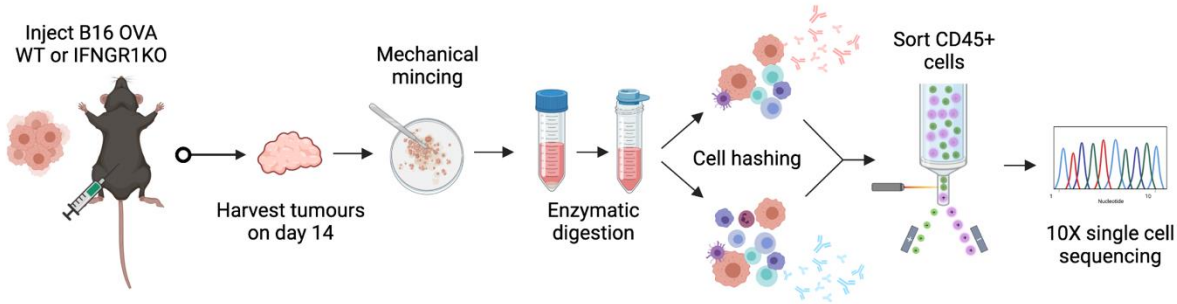

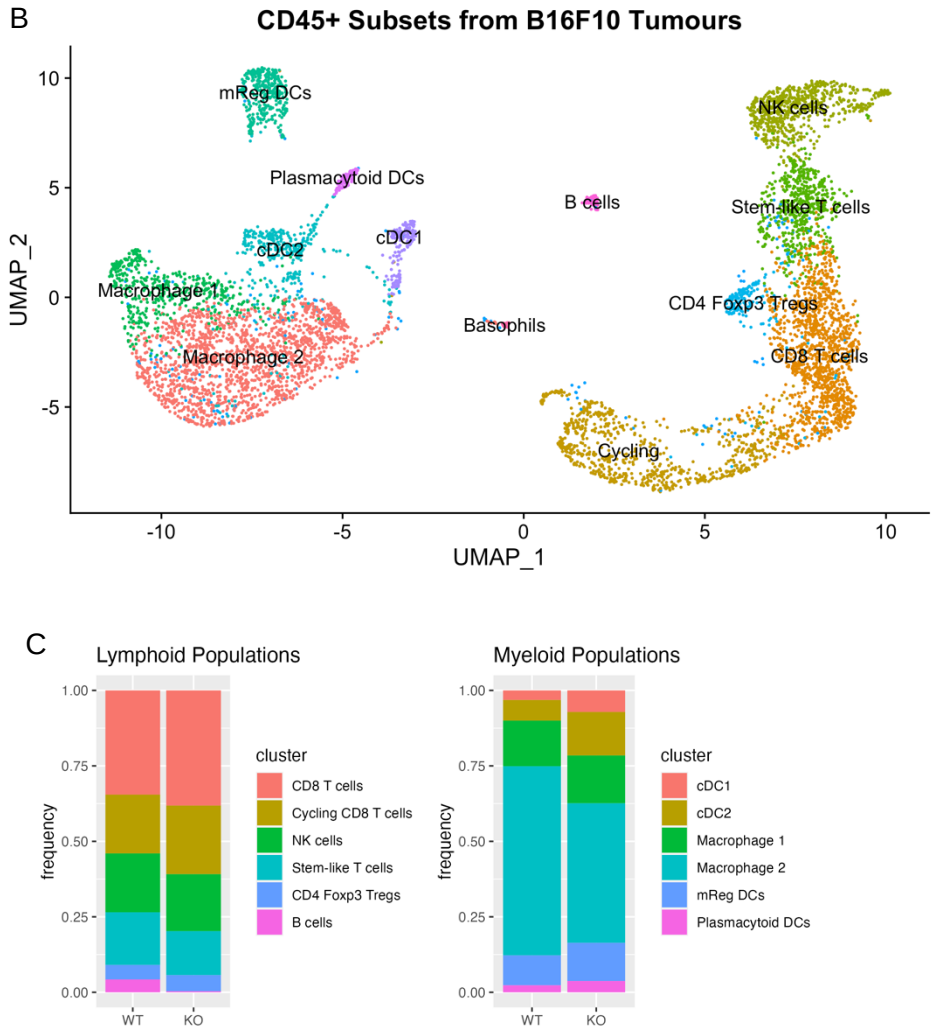

Figure 33. Single-cell RNAseq analysis of CD45⁺ tumour-infiltrating cells from B16-OVA WT and IFNGR1KO tumours. (A) Workflow for tumour implantation and tissue processing at endpoint. Mice were implanted with 2.5x10^5 cells per flank. Single-cell suspensions of following enzymatic digestion of tumours were labelled with TotalSeqC cell hashing antibodies prior to fluorescence-activated cell sorting (FACS). (B) UMAP projection of the single-cell dataset analysed using the R package seurat. (C) Relative proportions of the cell clusters, separated by lymphoid and myeloid populations.

For simpler interpretation of global differential expression of genes between WT and KO, gene set enrichment (GSEA) was performed on the dataset to reveal the most significant pathways which define each condition (**Figure 34A&B**). Concordantly, both the hallmark gene sets and Reactome pathway databases independently identified IFNγ signalling as the top hit in the IFNGR1KO condition (i.e. normalized enrichment scores <0), indicating that those immune cells were indeed more likely to be experiencing an IFNγ-

enriched microenvironment compared to WT. Enrichment plots for the 'interferon gamma response' pathway shows that gene overrepresentation is present in multiple cell subsets, rather than concentration on one cell type alone (**Figure 34C**).

Pathways which appeared in the WT tumours were indicative of a cytokine-rich environment, however, several of these were Th2-skewed, such as IL-6 or TGFβ-signalling from hallmark pathways, or IL-4/IL-10-signaling from the Reactome database. These cytokines have well-known immunosuppressive functions[304], and prompted further analysis into which cell types are producing and receiving these signals within the tumour microenvironment.

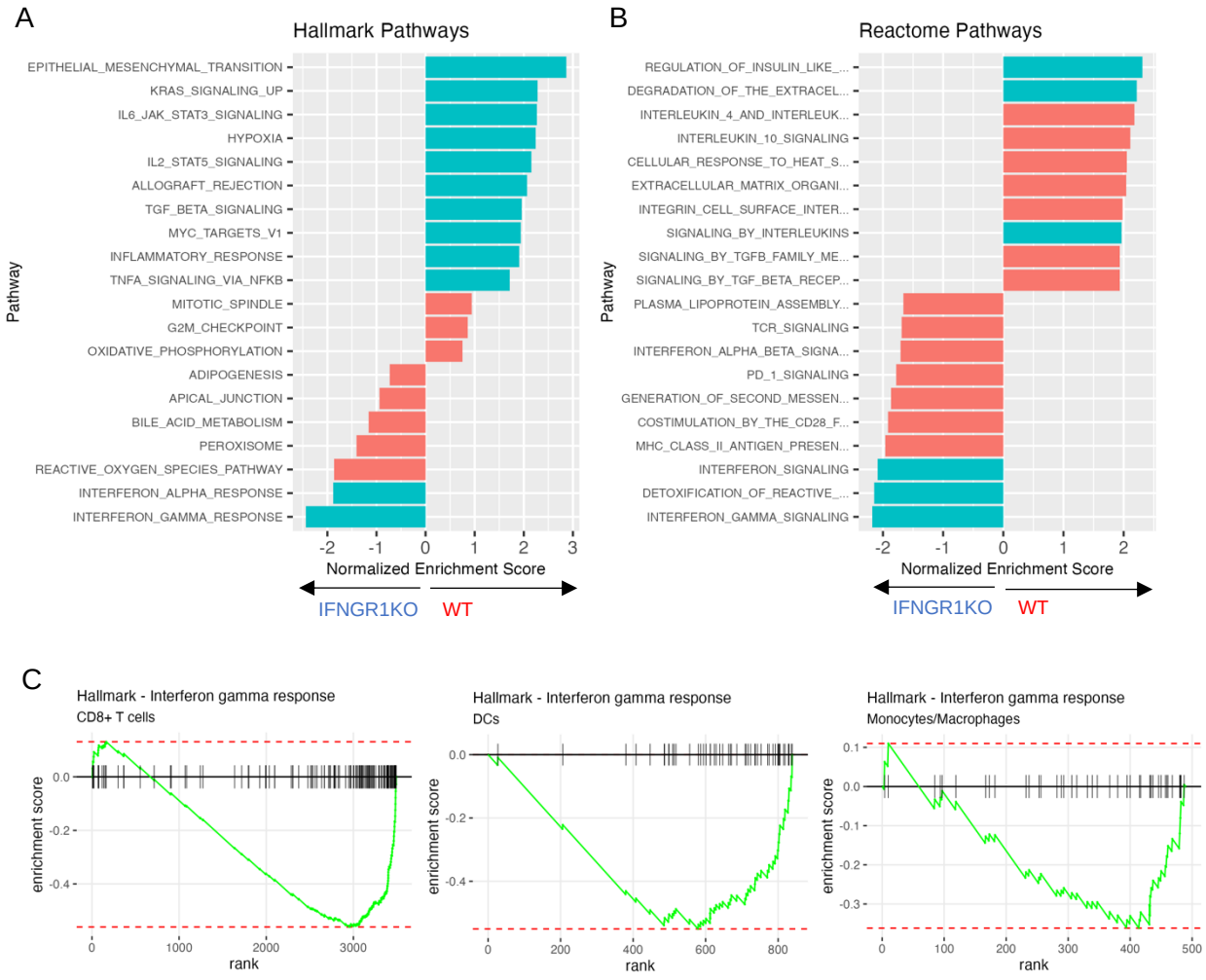

Figure 34. Pathway analysis of differentially expressed genes using GSEA and Reactome databases. Normalized enrichment scores for (A) GSEA hallmark pathways and (B) Reactome pathways. Pathways in blue have an adjusted p-value of <0.05. Scores greater than 0 show significant enrichment in WT tumours, whereas scores less than 0 are significantly enriched in IFNGR1KO tumours. (C) Enrichment plots for the 'Interferon gamma response' pathway from the hallmarks database of GSEA, independently generated for each cell subset (ie. $CD8^+$ T cells, DCs, or monocyte/macrophage clusters).

5.2.2 Analysis of CD8$^+$ T cell clusters from WT and IFNGR1KO tumours

Following the observation that CD8$^+$ TILs did not show a functional difference when stimulated *ex vivo*, we subset the CD8$^+$ T cell clusters from the scRNAseq dataset to assess whether there is an apparent difference in transcriptional programmes (**Figure 35A**). Analysis of transcripts belonging to T cell receptor α/β variable gene segments showed significant T cell clonality within the population of TILs (**Figure 35B**), which likely drove the difference between clusters 0 and 5 unique to each model. Furthermore, exhaustion scoring showed that clusters 0 and 5 were indeed transcriptionally similar as it identifies effector T cells expressing high levels of checkpoint inhibitory receptors (**Figure 35C**). Cluster 1 was identified as a stem-like T cell cluster which expressed the transcription factor *Tcf7*, and cluster 2 was an actively proliferating *Mki67*-positive subcluster (**Figure 35D**). Twice the number of CD8$^+$ TILs from KO tumours were in cluster 4 compared to WT, which corresponded to a *Gzmk^{hi}* population (analysis of cluster genes by heatmap Figure S7.).

Differential gene expression analysis showed expression of multiple genes which were unique to each tumour microenvironment (**Figure 35E**). Interestingly, CD8$^+$ TILs from KO tumours expressed *Gzmk* and *Gzmf*, which are distinctly produced by activated T cells, and function as both inflammatory and cell cytotoxic molecules.[305,306] Conversely, WT CD8$^+$ TILs expressed higher levels of *Ifng* and *Csf1*, and *Ptpn6* which encodes for SHP-1, a negative regulator of TCR signalling. Taken together, TILs originating from WT and KO tumours both appeared to be activated by distinctly different pathways. T cells from WT tumours appeared to display a more classical TCR-dependent activation pathway, including genes such as *Ifng*, *Ptpn6*, and *Lat2*. It is not yet known whether T cells from KO tumours are responding to TCR-dependent or independent signals, and whether this alternative transcriptional signature may be the result of IFNγ-signalling and APC-dependent activation as tumour cells themselves are not expressing MHC class I molecules in abundance.

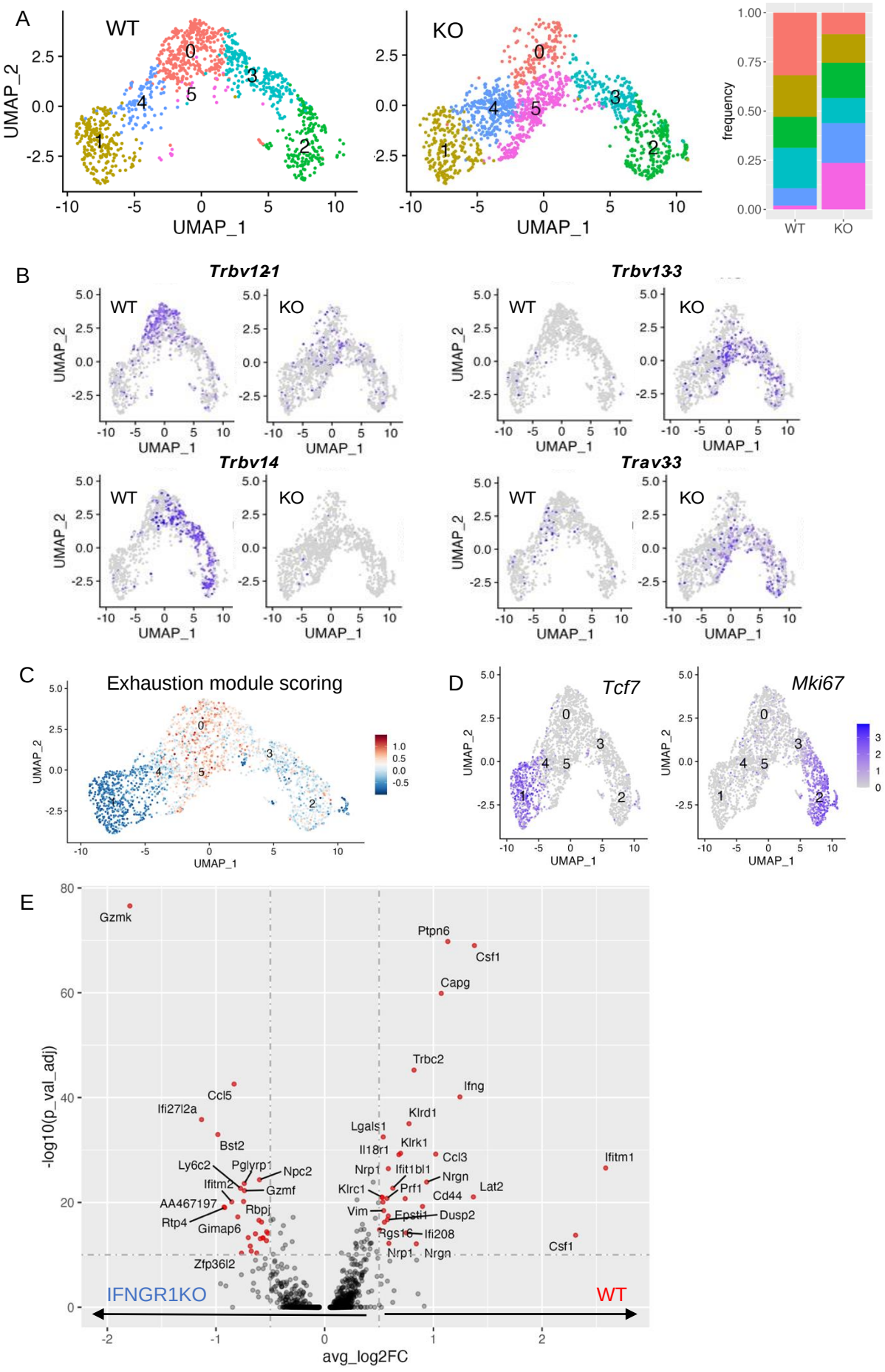
A
WT
KO
UMAP_1
UMAP_2
frequency
B
Trbv121
Trbv133
Trbv14
Trav33
C
Exhaustion module scoring
D
Tcf7
Mki67
E
-log10(p_val_adj)
avg_log2FC
IFNGR1KO
WT
Gzmk
Ptpn6
Csf1
Capg
Trbc2
Ifng
Ccl5
Ifi27l2a
Klrd1
Lgals1
Klrk1
Il18r1
Ccl3
Ifitm1
Bst2
Ly6c2
Pglyrp1
Npc2
Nrp1
Ifit1bl1
Nrgn
Ifitm2
Gzmf
Klrc1
Prf1
Cd44
Lat2
AA467197
Rbpj
Vim
Epsti1
Dusp2
Rtp4
Gimap6
Rgs16
Ifi208
Nrp1
Nrgn
Csf1
Zfp36l2

Figure 35. Analysis of CD8⁺ T cell clusters from the scRNAseq dataset. (A) UMAP projection of CD8⁺ T cell subset clusters, separated by model. Relative frequencies of cells in each cluster are shown as a stacked bar graph to highlight differences in cluster distribution between WT and IFNGR1KO tumours. (B) Expression of TCR α or β variable segment genes overlaid on UMAP projections highlighting model-specific T cell clones which express the same alleles. (C) Exhaustion module scoring on CD8⁺ T cells using the gene signature *Pdcd1, Lag3, Havcr2, Tigit, Ctla4, Klrg1,* and *Prdm1*. Results are overlaid on the UMAP projection which encompasses TILs from both WT and IFNGR1KO tumours. (D) Expression patterns of *Tcf7* and *Mki67* by clusters 1 and 2, respectively. Expression is scaled independently by gene. (E) Volcano plot for differentially expressed genes found within the CD⁺ T cell clusters, where positive values are upregulated by CD8⁺ TILs from WT tumours, and negative values from KO.

5.2.3 Global analysis of cell-cell communication modes and networks

Prompted by the number of pathways from GSEA which were related to cytokine signalling, the tool CellChat[218] was used to explore cell-to-cell communication within the scRNAseq data which may provide clues for relevant cell types in each model. CellChat consists of a database of known ligand-receptor pairs, which is then used to quantitatively infer intra- and intercellular communication networks from single-cell data. For this dataset, we were most interested in communication between lymphoid and myeloid populations.

The quantity and quality (i.e., inferred interaction strengths) of putative ligand-receptor pairs were compared between WT and KO for secreted signalling, ECM-receptor, and cell-cell contact databases as categorized by CellChat. Similar to earlier pathway analysis, secreted signalling (i.e., chemokine or interleukin signalling) showed the greatest differences between WT and KO (Figure S8). Quantifying the differential number of interactions within secreted signalling showed that there were more interactions overall between multiple cell types in WT tumours compared to IFNGR1KO, indicated by blue lines in a circle plot, which connects different cells types located on different nodes on the circle (**Figure 36A**). Differential interaction strength showed that monocytes and macrophages (labelled simply as macrophages in these plots) interacted more strongly with multiple T cell types in WT, whereas DC to lymphoid signalling was more prominent in the KO (**Figure 36B**).

The same analysis visualized as a heatmap features a barplot at the top, which represents the sum of incoming signals for each cell type (**Figure 36C**). Barplots at the right

of each heatmap represents the sum of outgoing signals for each sender cell type, which shows that monocytes and macrophages were the most abundant source of secreted cytokine signals in both quantity and strength. Plotting of all the soluble ligand-receptor pairs present in the dataset showed several signals which were WT tumour-specific, including *Spp1*, *Tnf*, and *Csf* (**Figure 36D**). The majority of soluble signals were chemokines, present in both WT and KO tumours and roughly equal in proportion (**Figure 36E**). **T**hese visualizations indicated that much of the signal sending was done by monocytes/macrophages in the dataset, which were further analysed as a subset.

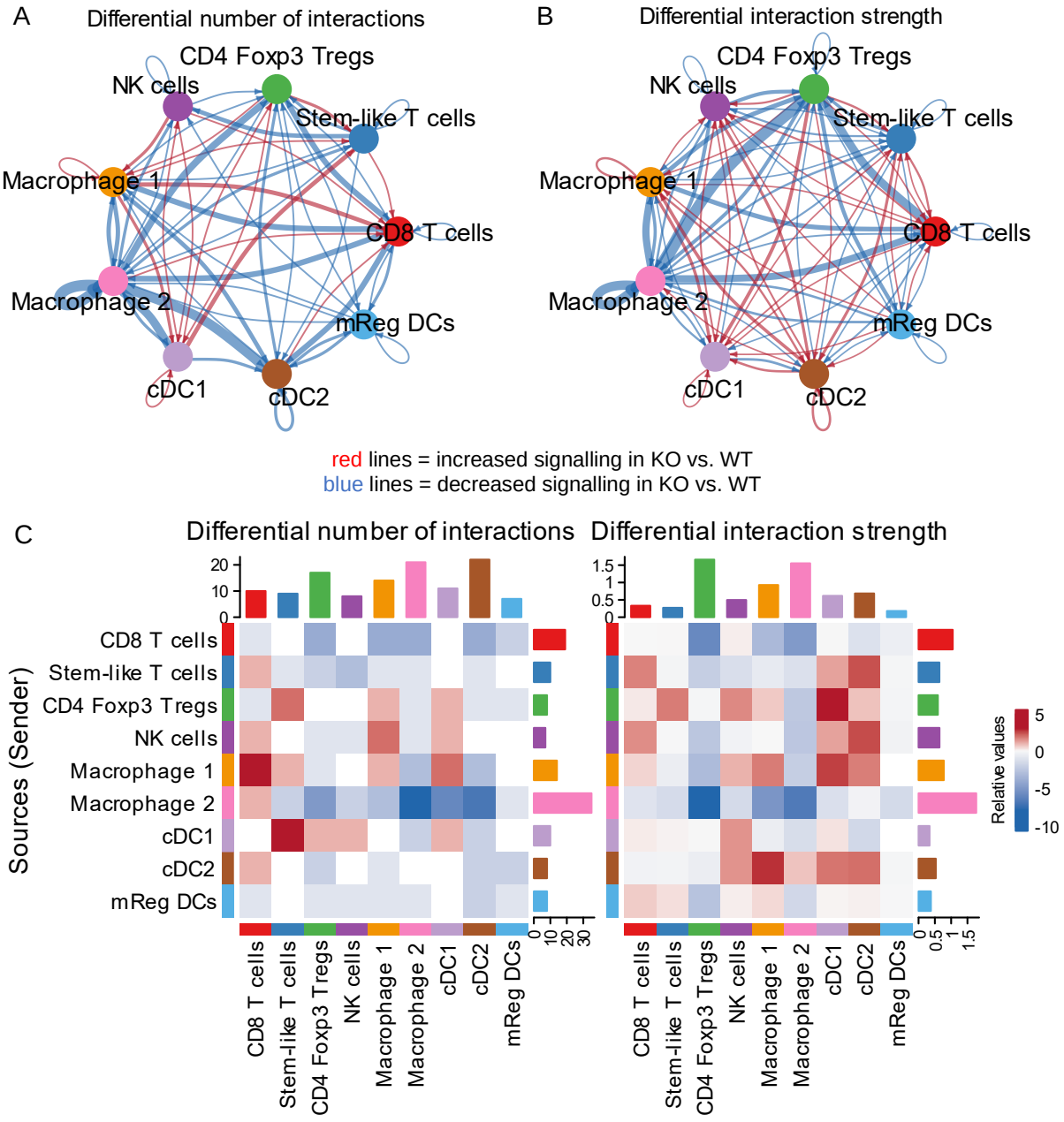

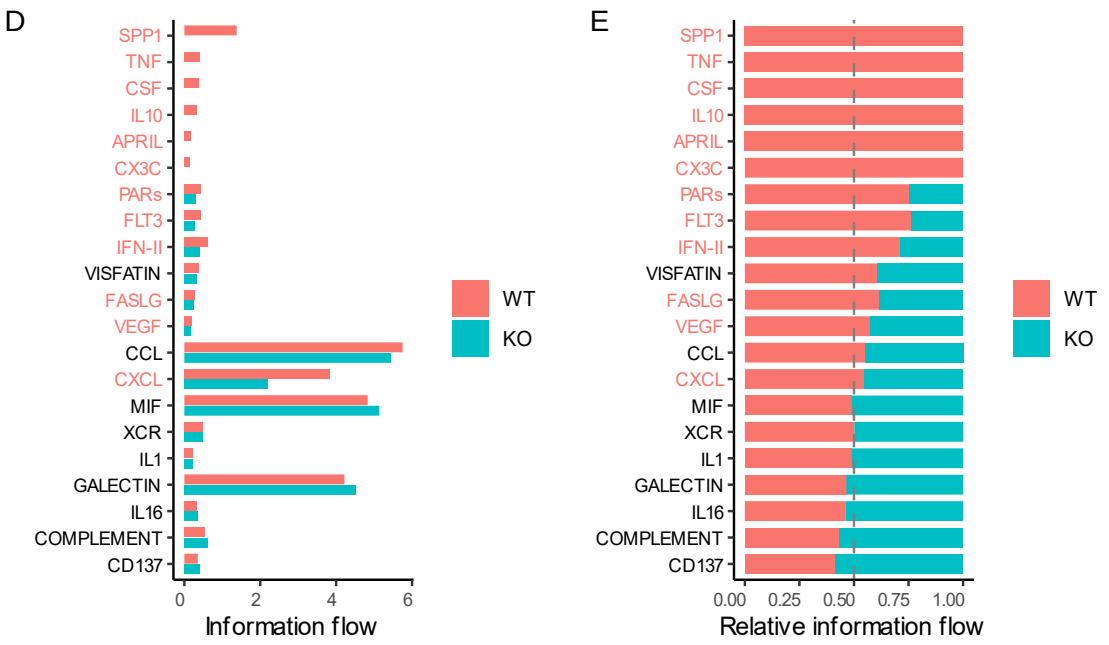

Figure 36. CellChat analysis of ligand-receptor pairs for secreted signalling pathways present in the scRNAseq dataset. Circle plots showing (A) differential number of interactions, or (B) differential interaction strength, between WT and KO where arrows represent an increase in signals from one vertex (cell type) to another. Red arrows indicate increase in signals for KO tumours, and blue arrows in WT tumours. (C) Heatmap showing the sources, or senders, of signals on the y-axis and receivers on the x-axis. Red and blue squares indicate increase in signalling for KO or WT tumours, respectively. Coloured top bar plot at the top and right-side of the heatmap represents the sum of the column of values displayed to show total signals sent or received by a cell type. (D) Bar plot showing total information flow of all soluble ligand-receptor interaction types found in the dataset for WT and KO tumours individually. (E) Stacked bar plot for relative information flow between WT and KO tumours for soluble ligand-receptor signals to indicate interactions which are found in one condition but not the other.

5.2.4 NK cells from IFNGR1KO tumours are more transcriptionally active compared to WT

Following the observation that B16 IFNGR1KO tumours failed to upregulate MHC-I following *in vivo* implantation, we hypothesized that effective control of KO tumours compared to WT may be dependent on NK cell activity rather than $CD8^+$ T cell-based immunity. Based on the principle of 'missing self', the presence of MHC-I molecules on virtually all nucleated host cells serves as an inhibitory ligand, thereby preventing activation against healthy host tissues during homeostasis.[307] On aberrant cells, such as virally infected cells during HIV infection or tumour cells which have downregulated MHC-I, NK cells are capable of killing these cells directly as a rapid innate response. Furthermore, a

previous study where B2m was knocked out from B16F10 showed greater stimulation of activated NK cells during *in vitro* co-culture compared to the parental line.[308]

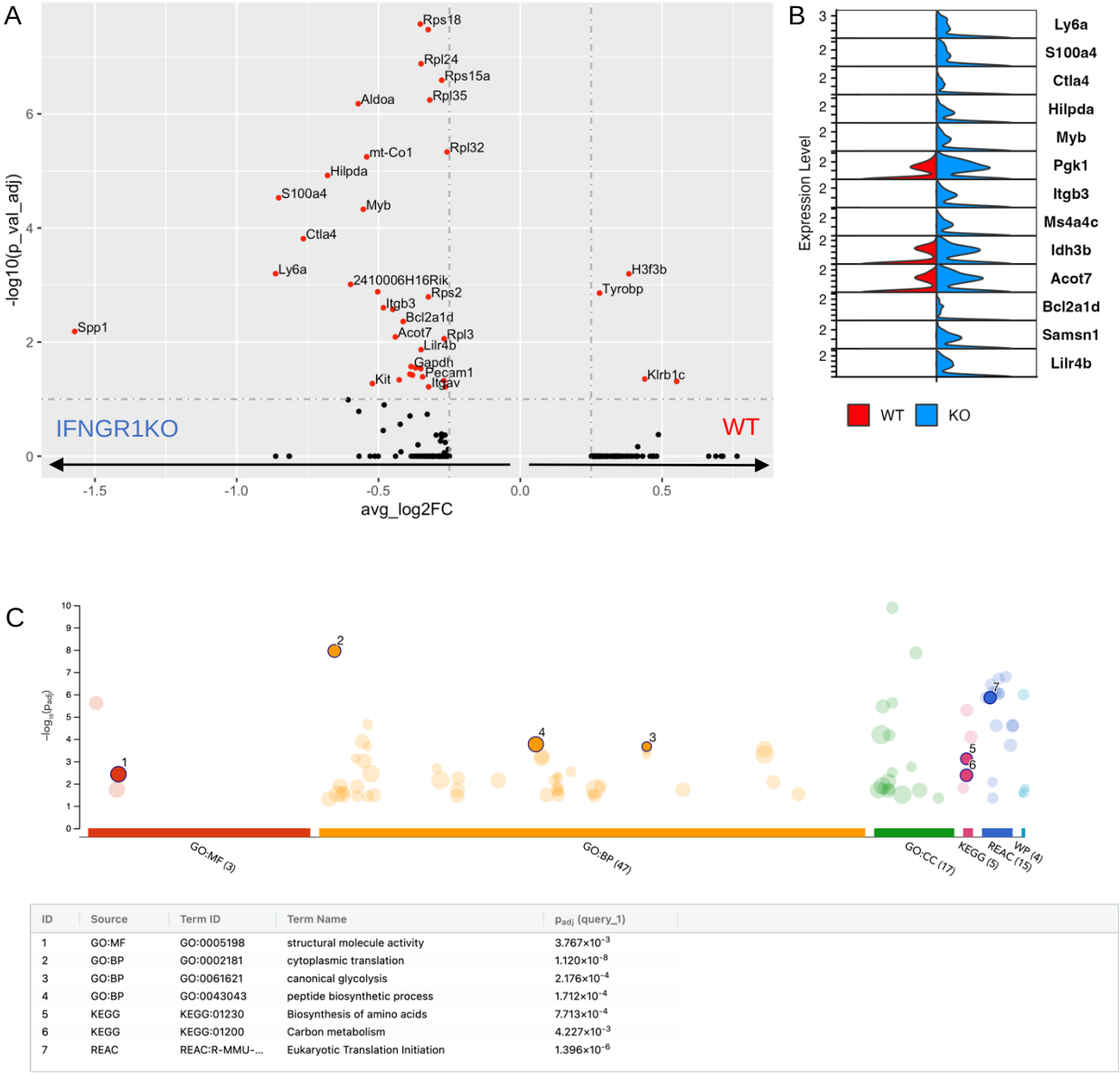

ID	Source	Term ID	Term Name	p_{adj} (query_1)
1	GO:MF	GO:0005198	structural molecule activity	3.767×10^{-3}
2	GO:BP	GO:0002181	cytoplasmic translation	1.120×10^{-8}
3	GO:BP	GO:0061621	canonical glycolysis	2.176×10^{-4}
4	GO:BP	GO:0043043	peptide biosynthetic process	1.712×10^{-4}
5	KEGG	KEGG:01230	Biosynthesis of amino acids	7.713×10^{-4}
6	KEGG	KEGG:01200	Carbon metabolism	4.227×10^{-3}
7	REAC	REAC:R-MMU-...	Eukaryotic Translation Initiation	1.396×10^{-6}

Figure 37. Differential gene expression analysis within the NK cell cluster from scRNAseq. (A) Volcano plot for differentially expressed genes found within the NK cell cluster, where positive values are upregulated by NK cells from WT tumours, and negative values from KO. (B) Split violin plots showing expression of the top 13 genes which are differentially expressed by NK cells from WT and KO tumours. (C) Functional enrichment analysis dot plot for differentially expressed genes in KO tumours using g:Profiler. Pathways are from multiple databases separated along the y-axis. Highlighted dots are shown as individual pathways in the table underneath with adjusted p-values.

We investigated transcriptional changes within the NK cell cluster and found significantly more genes upregulated by NK cells from IFNGR1KO tumours than WT (**Figure 37A**). Among the top 10 differentially expressed genes (DEGs) were genes specific to KO,

several of which were indicative of NK cell activation such as *Myb* and *Ctla4* (**Figure 37B**). Functional enrichment analysis using the tool g:Profiler[281] yielded pathways related to metabolic function and protein biosynthesis (**Figure 37C**). This led to the hypothesis that NK cells had a key role in controlling IFNGR1KO tumours *in vivo*.

We sought to validate our findings experimentally via antibody-mediated NK cell depletion *in vivo* for tumour-bearing mice. In this model, NK cells were depleted prior to and after tumour induction to investigate the role of NK cells in overall tumour control (**Figure 38A**). Near complete depletion of NK cells was verified by blood, lymph nodes, and intratumourally at endpoint (**Figure 38B**), whereas $CD8^+$ T cell levels remained comparable to control animals treated with a corresponding isotype antibody (**Figure 38C**). Tumours grew much faster in NK-depleted mice compared to isotype controls, reducing overall survival by at least three days in more than half the animals in both cohorts (**Figure 38D**). However, no difference in tumour size by weight at endpoint was observed between B16 WT and IFNGR1KO mice (**Figure 38E**), indicating a lack of dependence on NK cells in the control of KO tumours *in vivo*.

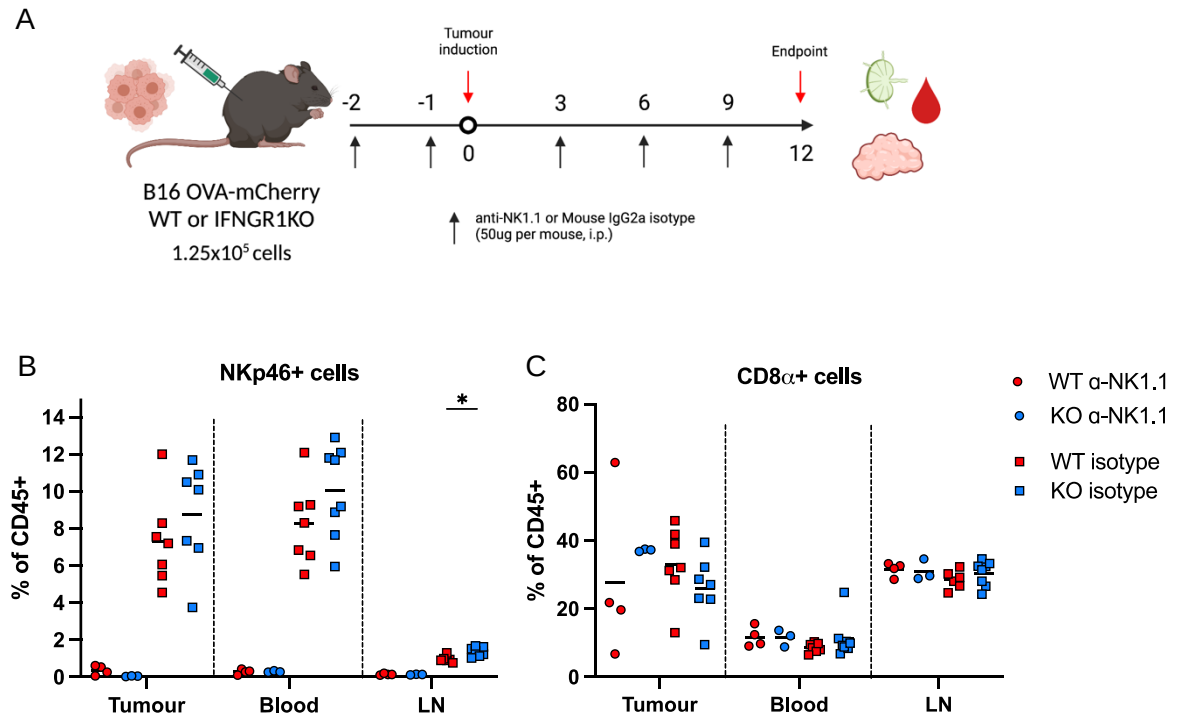

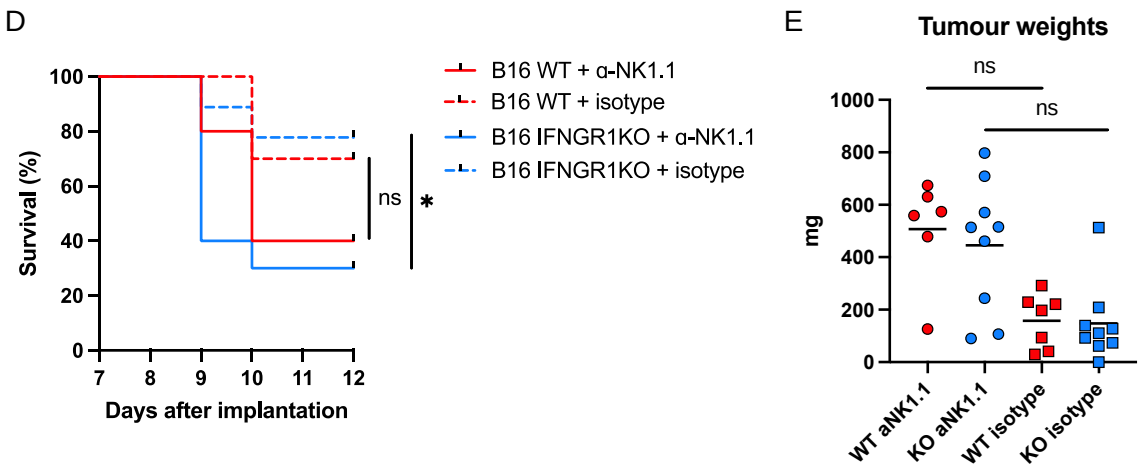

Figure 38. Antibody-mediated NK depletion in B16-OVA WT or IFNGR1KO tumour-bearing mice. (A) Experimental outline with anti-NK1.1 (clone PK136) or mouse IgG2a isotype antibody dosing schedule in C57Bl/6 mice. (B) Tumour weights of NK-depleted, or isotype-treated mice at experimental endpoint day 12 post-implantation. (C) Survival curves of all mice in the cohorts. Percentage of NKp46-positive cells (D) or CD8α^{+} cells (E) gated on live CD45^{+} flow cytometry analysis of immune populations collected from the tumour, blood, or lymph nodes of tumour-bearing mice. Data is from one experiment and show mean with statistical testing performed by non-parametric Mann-Whitney *t* test in B, logrank (Mantel-Cox) test for each pair of survival curves in C, and two-way ANOVA in D&E. *$p \leq 0.05$.

From earlier experiments using IFNγ-GREAT mice to track intratumoural production of IFNγ (Figure 11), NK cells comprised up to half of immune cells producing IFNγ at the earliest measured time points. To determine whether NK-derived IFNγ was important in the control of IFNGR1KO tumours specifically, CD45.1 mice were reconstituted with bone marrow from CD45.2 donor mice as illustrated in **Figure 39A**. Specific deletion of IFNγ-producing NK cells was undertaken in mice reconstituted with 50% IFNγ$^{-/-}$ and 50% NKp46^{iCre}R26R^{DTR} (NK-DTR) bone marrow, thereby allowing for deletion of IFNγ-producing NK cells via administration of diphtheria toxin. Deletion of NK cells was confirmed by observation of a two-fold reduction in tumour-infiltrating NK cells in NK-DTR mice compared to WT (**Figure 39B**). Ideally, an intracellular stain for IFNγ production by these isolated NK cells following *ex vivo* re-stimulation would be more diagnostic in assessing specific deletion. However, surface NKp46 could not be detected during intracellular cytokine staining, possibly due to receptor downregulation following stimulation. Furthermore, no difference in tumour growth was observed between NK-DTR and WT bone marrow chimera mice, which reduced the likelihood that NK-derived IFNγ was a significant factor in maintaining tumour

control (**Figure 39C**). Further analysis of tumour-infiltrating immune populations showed no differences between the NK-DTR/IFNγKO and WT/IFNγKO bone marrow chimeras (**Figure 39D**). Overall, our bone marrow chimera model was either not robust enough to demonstrate a significant role for NK-derived IFNγ in the IFNGR1KO tumours, or indeed the biological effects were negligible. Future repeats of the model would benefit from functional assessment of whether NK cells from NK-DTR/IFNγKO splenocytes retain the ability to produce IFNγ *ex vivo.*

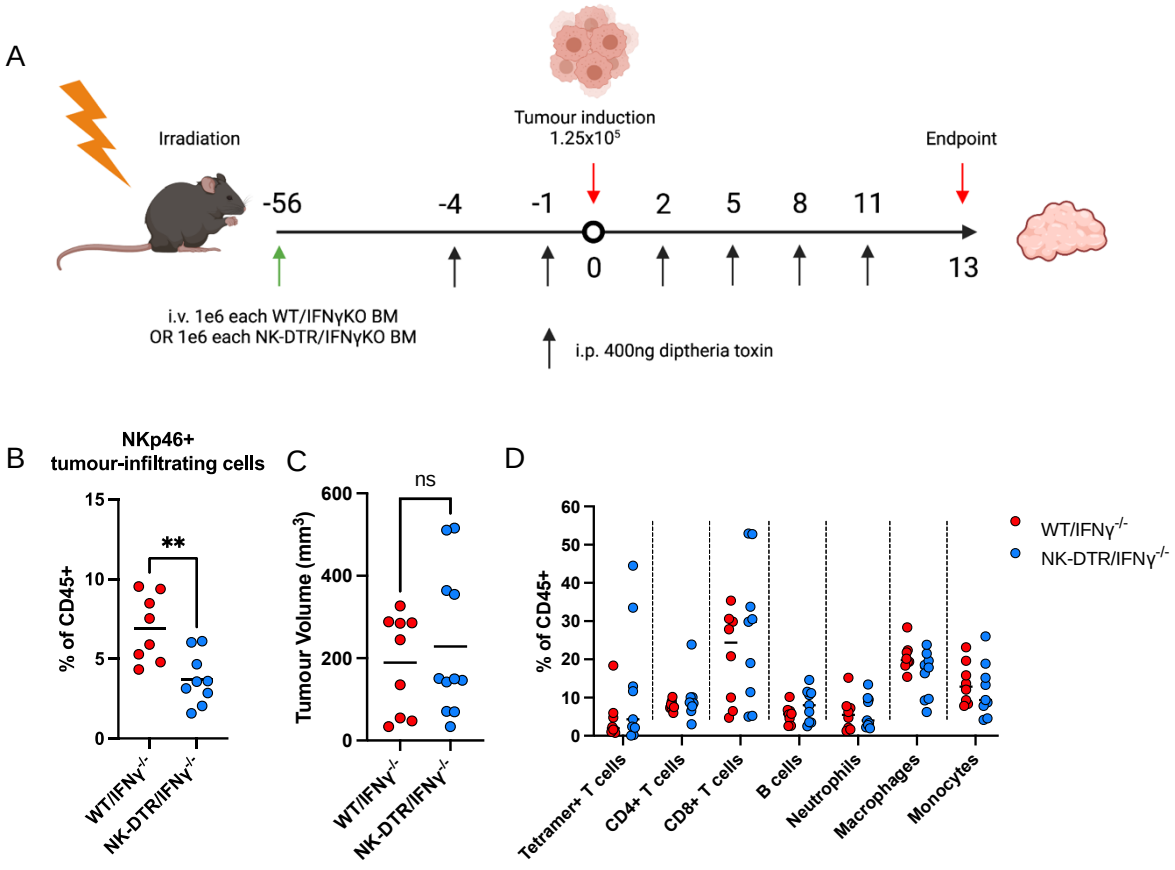

Figure 39. Depletion of IFNγ-producing NK cells using bone marrow chimeras. (A) Host C57Bl/6 mice expressing the pan leukocyte marker CD45.1 were gamma irradiated at a dose of 10,000 cGy. After 24 hours, mice were reconstituted with $1x10^6$ 50:50 bone marrow mixtures from WT/IFNγKO mice, or NK-DTR/IFNγKO mice. NK-DTR refers to $NKp46^{iCre}R26R^{DTR}$ mice which express the diphtheria toxin receptor under the Ncr1 promoter. After 52 days, all mice were given 400ng of diphtheria toxin intraperitonially every 3 days thereafter. B16-OVA WT or IFNGR1KO tumours were implanted 56 days post-irradiation. (B) Comparison of tumour-infiltrating $NKp46^+$ cells between WT/IFNγKO or NK-DTR/IFNγKO bone marrow chimera mice. (C) Tumour volumes of mice reconstituted with WT/IFNγKO or NK-DTR/IFNγKO bone marrow at experimental endpoint. (D) Relative tumour-infiltrating populations gated on live $CD45^+$ cells from flow cytometry analysis. Data is from one experiment and show mean with statistical testing performed by non-parametric Mann-Whitney *t* test in B&C, and two-way ANOVA in D. $^{**}p \leq 0.01$.

5.2.5 Tumour-infiltrating monocyte and macrophage populations show distinct transcriptional differences between WT and IFNGR1KO tumours

We had previously observed changes in the myeloid compartment between WT and KO tumours, namely in the monocytes as detected by flow cytometry. We sought to determine whether clusters labelled “macrophages” from our scRNAseq dataset differed between WT and KO. Indeed, the clusters present in each model appeared to be dichotomous, with limited overlap between clusters of cells (**Figure 40A**). Clusters 1, 2 and 3 were unique to KO, whereas cluster 0 was derived primarily from WT tumours. A heatmap of the top 6 genes representative of each cluster is shown in **Figure 40B**, although many of the genes were not specific to one cluster alone. We used recent literature sources to categorize the monocyte and macrophage subsets present in our scRNAseq dataset (**Table 3**) and observed that two of the three KO-specific clusters were likely to be monocyte-like, or pre-macrophage populations. Categorization of clusters was further validated by observing the pattern of expression for canonical genes across the UMAPs (Figure S9).

We used the tool monocle for pseudotime trajectory analysis which allowed for visualizing of the differentiation path between adjoining clusters from monocytes to macrophages. Based on the trajectory, differentiation of monocytes in cluster 6 did not proceed linearly to each of the macrophage clusters, but instead showed interconnections between them (**Figure 40C**). Cluster 1 appeared to be central to all other surrounding macrophage clusters 0, 4 and 5, with 5 being the most differentiated cluster by pseudotime analysis (**Figure 40D**). Module scoring for transcriptional signatures for previously reported TAM populations[298] was performed on the entire monocyte/macrophage dataset, which would be unbiased by the naming or selection of the clusters. We found that myeloid cells from WT tumours showed higher scoring for genes related to both immune regulatory functions, as well as angiogenesis within the tumours (**Figure 40E&F**). This suggests that the WT tumours enable for differentiation of more previously annotated or characterized

TAMs, whereas the cytokine environment of KO tumours may result in alternative TAM phenotypes.

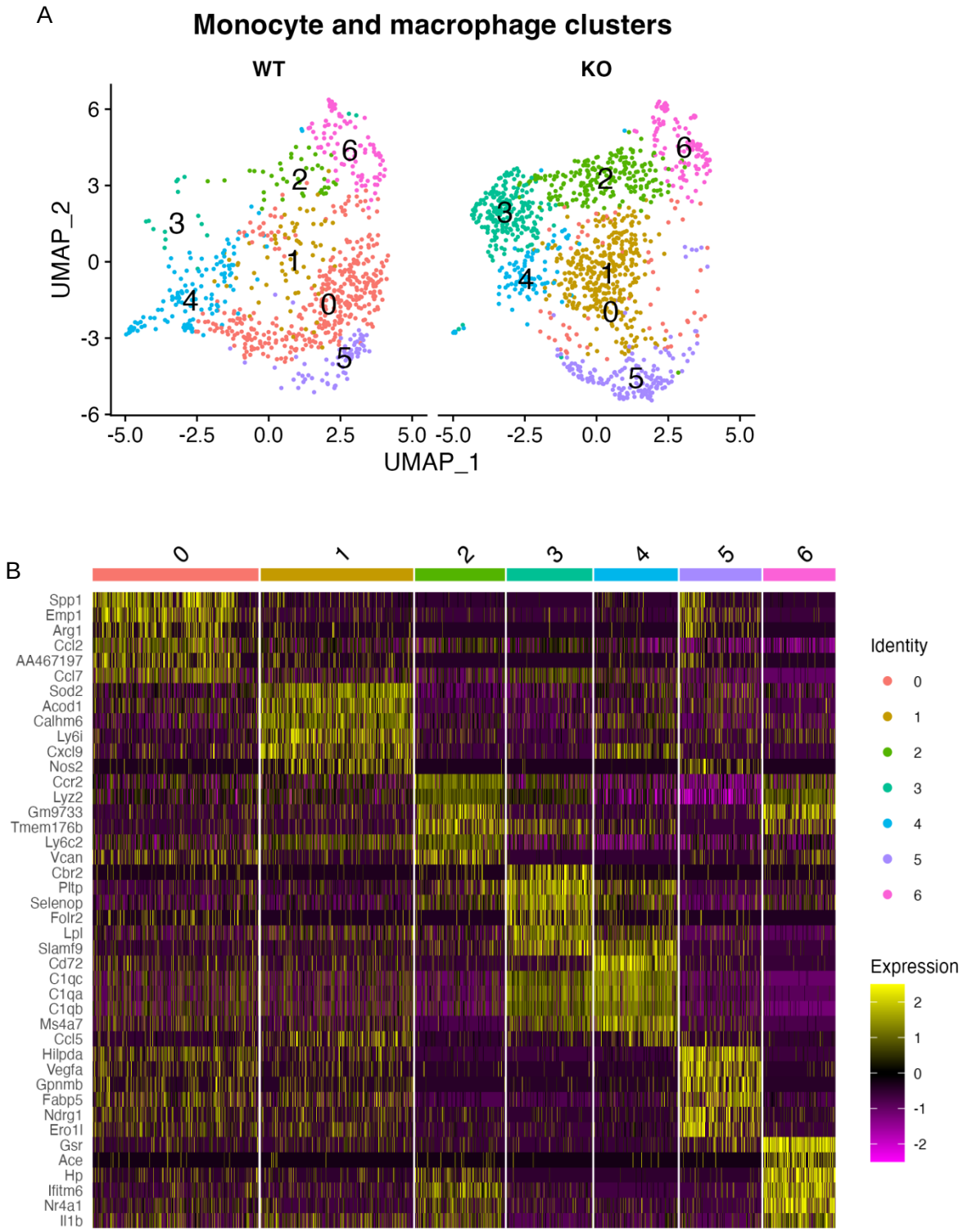

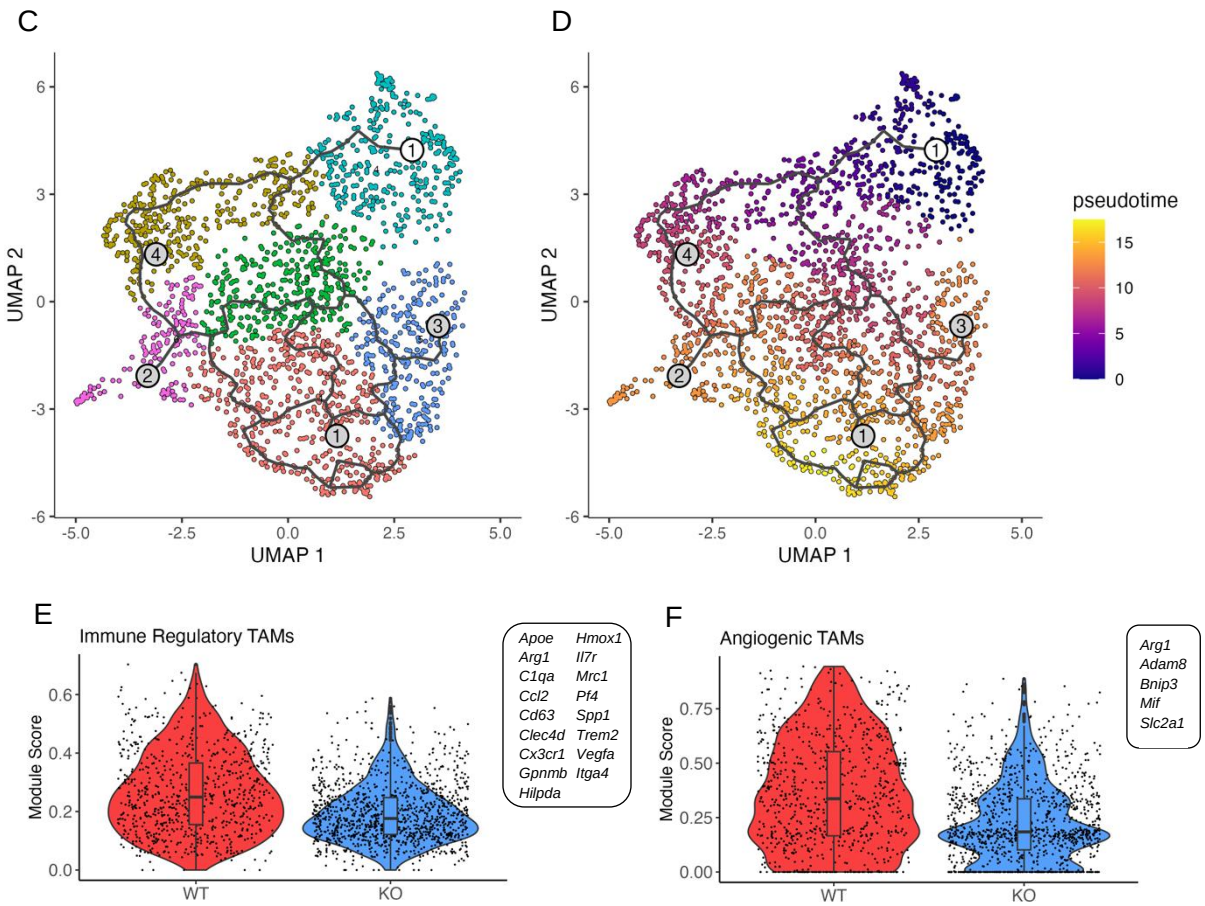

Figure 40. Analysis of monocyte and macrophage clusters from the scRNAseq dataset. (A) UMAP projection of the monocyte/macrophage cell subsets, re-clustered to show differences between WT and IFNGR1KO tumours. (B) Heatmap of the top 6 genes differentially expressed between the one cluster compared to all other clusters in the subset of cells. Trajectory analysis using the R package monocle3 overlaid on the UMAP projection of monocyte/macrophage cell clusters (C) or coloured by pseudotime (D). Pseudotime is an abstract measure of how much progress an individual cell has made through the learned trajectory. White numbered circle indicates the starting node, and grey numbered circles are 'leaves' of the branches which represent a unique outcome (i.e., cell fate). Violin plots comparing module scoring of the immune regulatory TAM (E) or angiogenic TAM (F) gene signatures, which are listed alongside each graph.

Table 3. Cluster annotations of the monocyte/macrophage cell subset from scRNAseq.

Cluster	Annotation	Proposed functions and/or characteristics	Key genes
0	Regulatory TAMs	Immunosuppression of NK cells and CD8 T cells	*Spp1, Arg1, Ccl2, Ccl7, Hmox1*
1	Interferon-stimulated TAMs	IFNγ-responsive TAMs	*Cxcl9, Cxcl10, Nos2, Il7r*
2	Tumour-infiltrating monocytes	IFNγ-responsive monocytic cells	*Ccr2, Lyz2, Ly6c2, Ifitm6, Vcan, Fn1*
3	Non-classical Monocytes/Pre-macrophages	Induction of TAMs, infiltration of adjacent tissues	*C1q, Ms4a7, Slamf9*
4			
5	Angiogenic TAMs	Promotes angiogenesis within the tumour; extracellular matrix remodeling	*Vegfa, Adam8, Clec4d, Il7r, Bnip3*

6	Classical monocytes	Monocytes from peripheral circulation; within circulation of the tumour vasculature	*Ace, Gsr, Hp, Il1b, Fn1, Nr4a1*

CellChat was used to identify ligand-receptor pairs which are relevant in macrophage signalling to other immune populations within the tumour microenvironment. Earlier analysis of the dataset had indicated that a majority of the secreted signals were by Ccl chemokine signalling. Bubble plots provided a visual comparison of soluble signals which had increased signalling in WT compared to KO tumours (**Figure 41A&B**). We found that signals with the highest communication probability were from WT macrophages towards lymphocyte populations including Tregs and NK cells. Visual representation of the signal senders and receivers by chord diagram also showed that macrophages in WT tumours may be recruiting Foxp3 $CD4^+$ Tregs into the tumour to a greater extent than in KO (**Figure 41C**). In comparison, signalling to Tregs in KO tumours was minimal compared to WT.

Finally, violin plots comparing chemokine expression between WT and KO for each cell subtype were created for an overall view of all chemoattractants present (**Figure 41D**). Higher expression of *Ccr2* and *Ccr5* in WT Tregs corresponded with higher expression of ligands *Ccl2* and *Ccl7*, which were also more highly expressed by WT macrophages. These ligand-receptor pairs have shown to support Treg trafficking from lymph nodes[309], and homing into the tumour.[310]

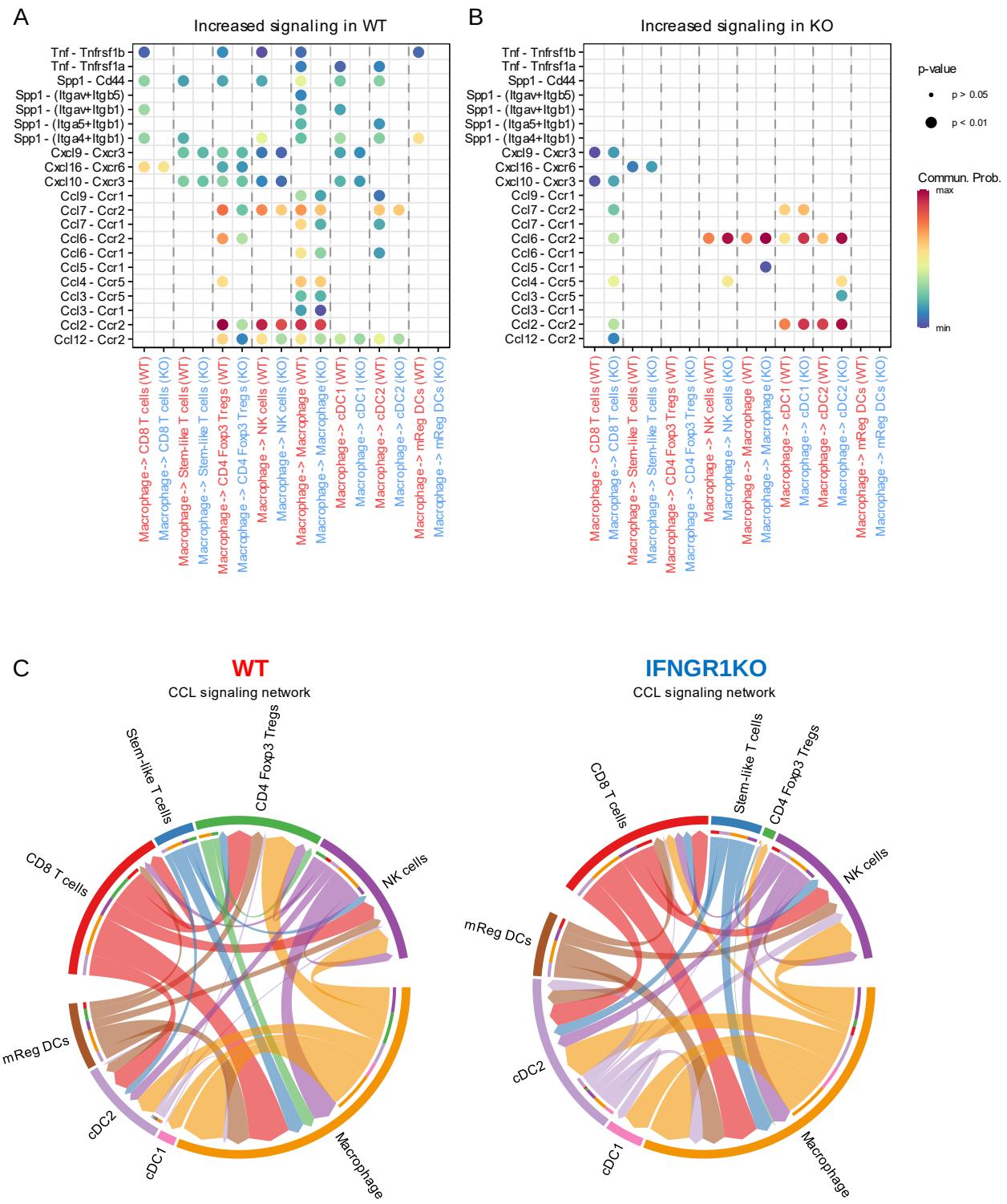
A
Increased signaling in WT
B
Increased signaling in KO
Tnf - Tnfrsf1b
Tnf - Tnfrsf1a
Spp1 - Cd44
Spp1 - (Itgav+Itgb5)
Spp1 - (Itgav+Itgb1)
Spp1 - (Itga5+Itgb1)
Spp1 - (Itga4+Itgb1)
Cxcl9 - Cxcr3
Cxcl16 - Cxcr6
Cxcl10 - Cxcr3
Ccl9 - Ccr1
Ccl7 - Ccr2
Ccl7 - Ccr1
Ccl6 - Ccr2
Ccl6 - Ccr1
Ccl5 - Ccr1
Ccl4 - Ccr5
Ccl3 - Ccr5
Ccl3 - Ccr1
Ccl2 - Ccr2
Ccl12 - Ccr2
Macrophage -> CD8 T cells (WT)
Macrophage -> CD8 T cells (KO)
Macrophage -> Stem-like T cells (WT)
Macrophage -> Stem-like T cells (KO)
Macrophage -> CD4 Foxp3 Tregs (WT)
Macrophage -> CD4 Foxp3 Tregs (KO)
Macrophage -> NK cells (WT)
Macrophage -> NK cells (KO)
Macrophage -> Macrophage (WT)
Macrophage -> Macrophage (KO)
Macrophage -> cDC1 (WT)
Macrophage -> cDC1 (KO)
Macrophage -> cDC2 (WT)
Macrophage -> cDC2 (KO)
Macrophage -> mReg DCs (WT)
Macrophage -> mReg DCs (KO)
p-value
p > 0.05
p < 0.01
Commun. Prob.
max
min
C
WT
CCL signaling network
IFNGR1KO
CCL signaling network
CD8 T cells
Stem-like T cells
CD4 Foxp3 Tregs
NK cells
mReg DCs
cDC2
cDC1
Macrophage

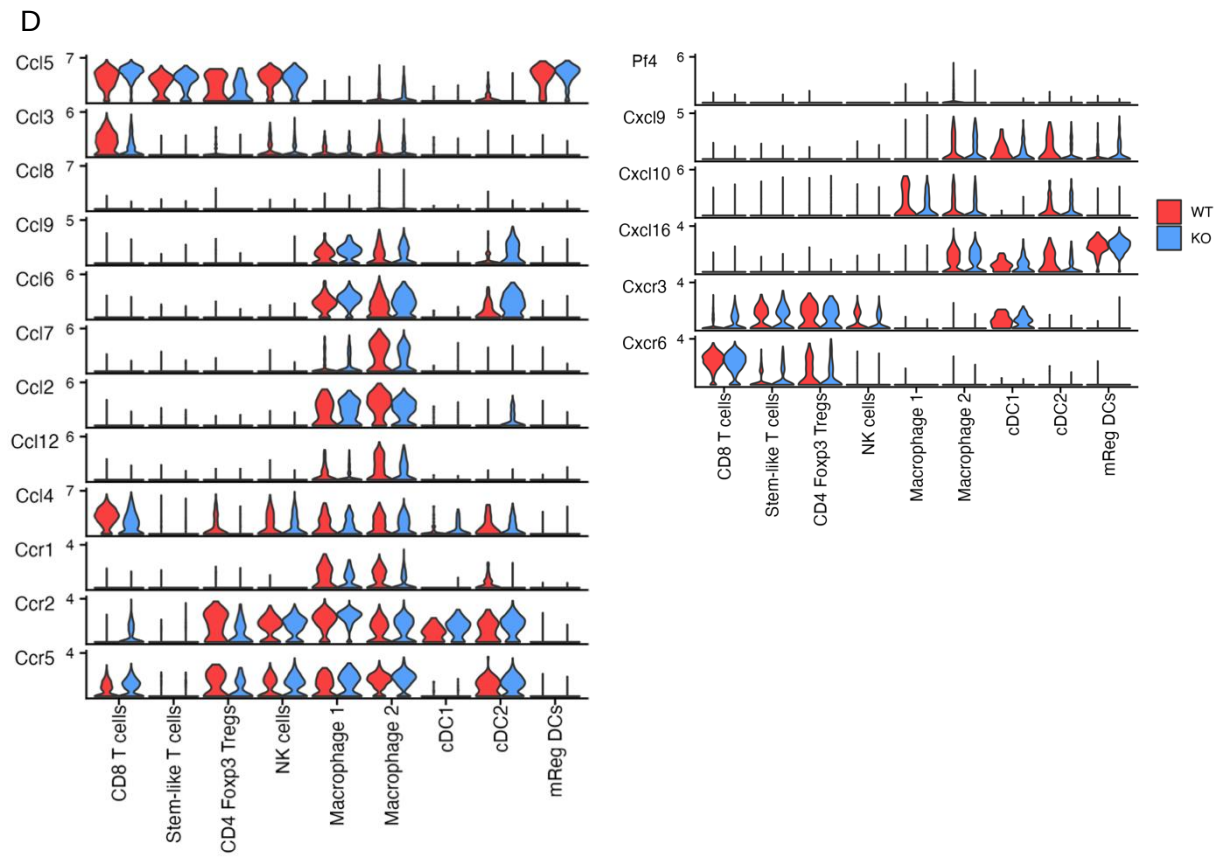

Figure 41. Identifying soluble ligand-receptor interactions within the monocyte/macrophage scRNAseq subsets. Bubble plots from CellChat analysis showing increased signalling of soluble ligand-receptor pairs in WT (A), or KO tumours (B), based on signals sent by monocytes/macrophages to all other cell types. Colour of the bubbles corresponds to the communication probability, which is calculated depending on ligand and receptor expression levels of senders (i.e., monocytes/macrophages) and receivers. (C) Chord diagrams showing signal senders and receivers of Ccl family chemokines, where each cell type forms an independent outer arc and colour. Thinner, inside arcs represent the targets receiving signal from the corresponding outer arc. (D) Violin plots showing the expression of C- and CXC-type chemokines for each cell cluster in the dataset. Data is scaled per row for expression.

5.2.6 Validation of scRNAseq macrophage phenotypes in B16-OVA WT and IFNGR1KO TAMs

To validate our observations from the scRNAseq data set on the major differences in myeloid cells between WT and IFNGR1KO tumours, a 22-colour myeloid-centric flow cytometry panel (detailed in Table S4.) was tested on immune cells isolated from the tumour. Data was gated on $CD11b^{+}$ and subsampled for analysis of an equal number of cells per tumour model. opt-SNE dimensionality reduction was performed to create a visual comparison of the datasets (**Figure 42A**). WT tumours showed a higher cell density within

the metaclusters 1 and 14, which were F4/80^{hi}, CD206^{hi} clusters found within the dataset likely to be TAMs (**Figure 42B**). Myeloid cells from KO tumours were concentrated in clusters 2, 6 and 13, which were Ly6C^{hi}, CX3CR1^{hi}, and CD86^{+}, which were indicative of an inflammatory monocyte-like phenotype. Markers chosen from the panel were overlaid on the opt-SNE plots to identify cell subsets by surface protein expression (**Figure 42C**). Due to limitations of fluorochrome compatibility and staining only for surface-expressed proteins, it was not possible to determine the subtypes of TAMs or tumour-infiltrating monocytes present with the same detail as in RNA analysis.

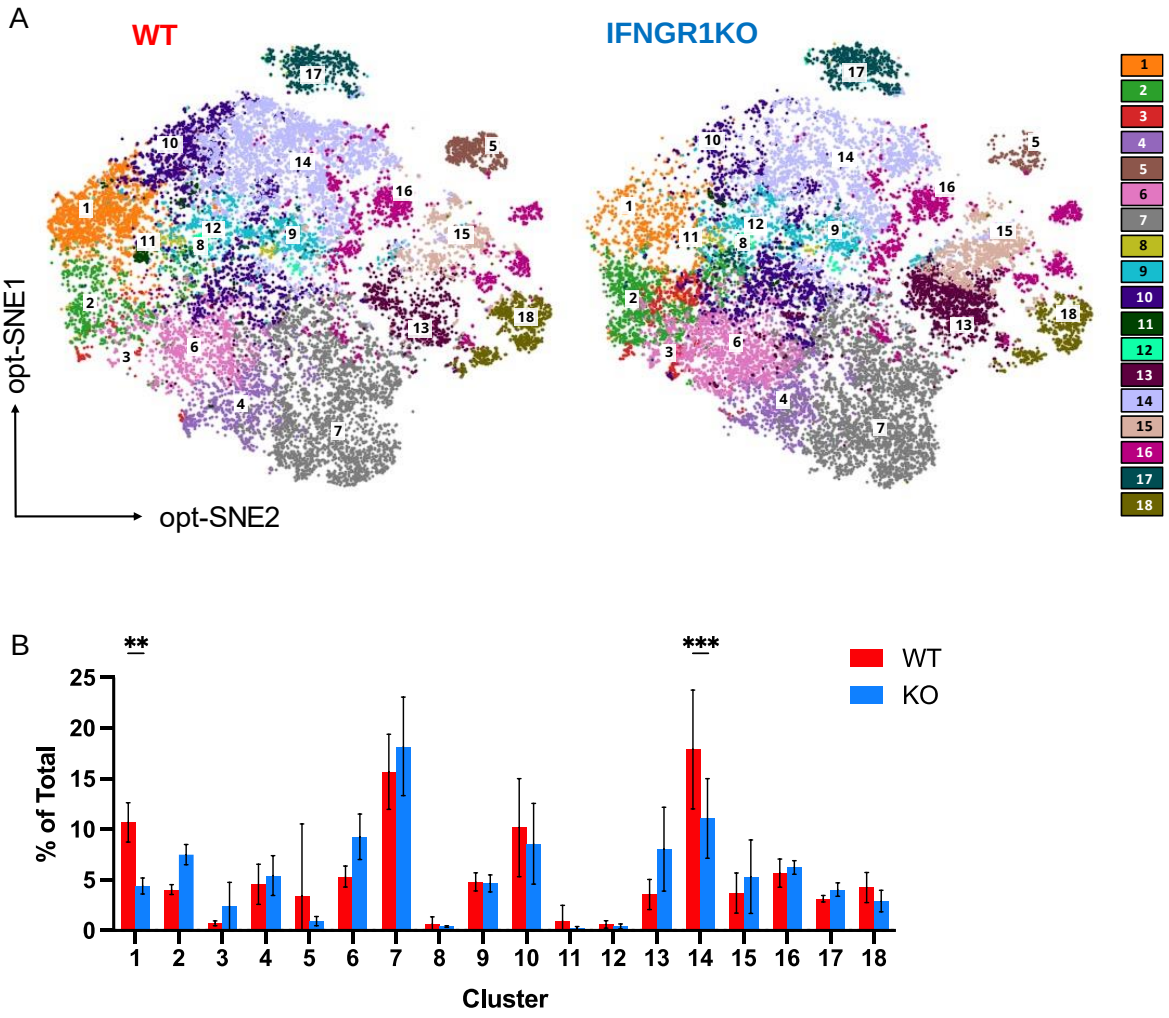

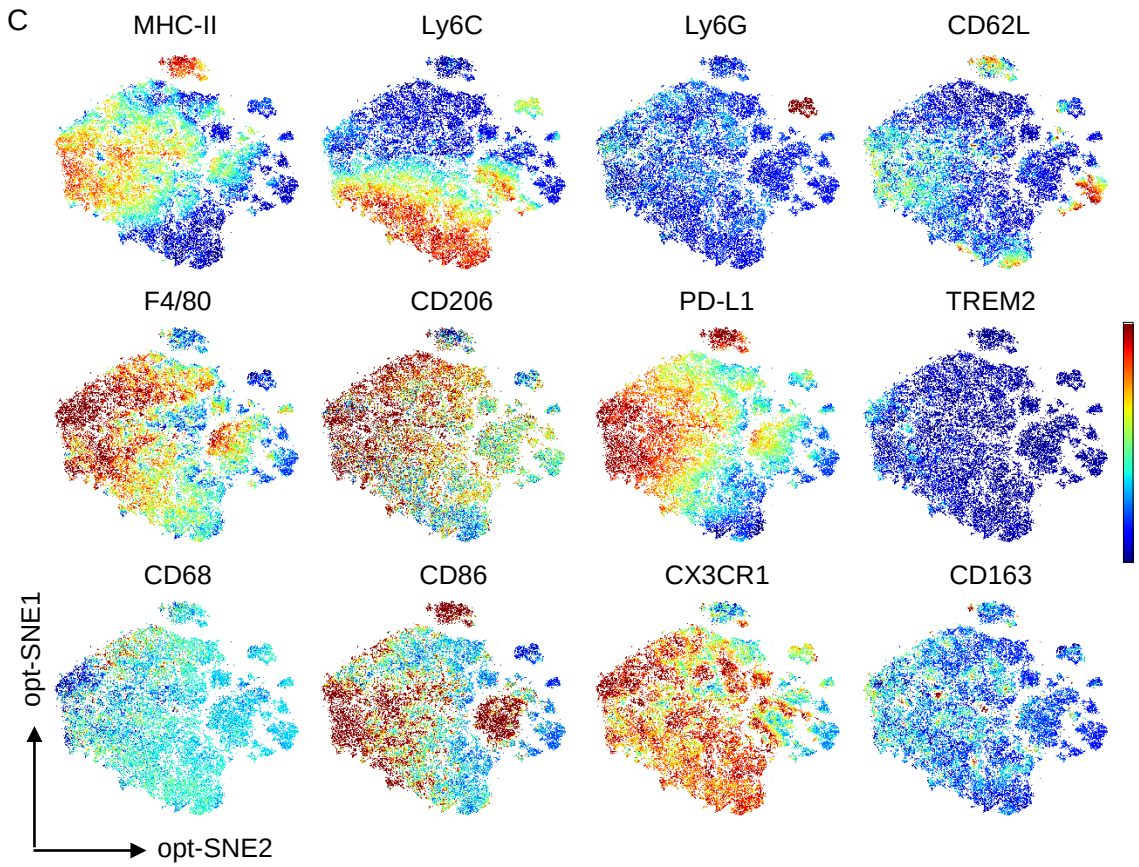

Figure 42. High dimensional flow cytometry analysis of CD11b$^+$ infiltrating cells in B16-OVA WT or IFNGR1KO tumours. (A) opt-SNE plots of live CD45$^+$ immune cells gated on CD11b$^+$ cells, analysed from a 22-colour Cytek Aurora flow cytometry panel using the OMIQ software platform. Each plot contains an equivalent number of cells downsampled from WT (6 tumours, from n=3 mice) and IFNGR1KO (5 tumours, from n=3 mice). Plots are coloured by FlowSOM metaclustering which determines the optimal number of nodes which best describe the dataset. (B) Relative percentages of cells in each metacluster. Two-way ANOVA was used for statistical analysis, $^{**}p \leq 0.01$, $^{***}p \leq 0.001$. (C) opt-SNE plots by continuous colour scale where each marker is represented by an independent scale. Highest expression in the dataset is shown by red, and lowest expression in blue. Data are from one experiment.

We also followed up on scRNAseq data which showed that *Trem2* expression was higher in macrophages clusters from WT tumours compared to KO (**Figure 43A**). TREM2 has recently been described as a marker of immunosuppressive TAMs, and TREM2-blockade appears to improve preclinical tumour models.[311] We analysed TREM2 expression by flow cytometry of macrophages, identified as a CD11b$^+$/F4/80$^+$/MHC-II$^+$ population in both WT and IFNGR1KO tumours, and found expression was indeed higher in WT tumours (**Figure 43B**). Using the 22-colour panel which was better able to identify macrophage populations by inclusion of multiple markers, we found that CD11b$^+$/F4/80/MHC-II$^+$

macrophages were more abundant in KO than WT tumours, along with elevated monocytes (**Figure 43C**). We also measured the relative abundance of TAM subsets gated on CD11b^{+}/F4/80^{+}/MHC-II^{+} macrophages which may be indicative of more M1 pro-inflammatory phenotypes (i.e., CD86, CD68 or CX3CR1 expression) or M2 pro-tumourigenic phenotypes (i.e., TREM2, CD206, or CD163 expression) (**Figure 43D**). Overall, IFNGR1KO tumours showed higher relative infiltration of CD86^{+}/CX3CR1^{+} TAMs, and lower relative infiltration of CD206^{+}/CD163^{+} TAMs.

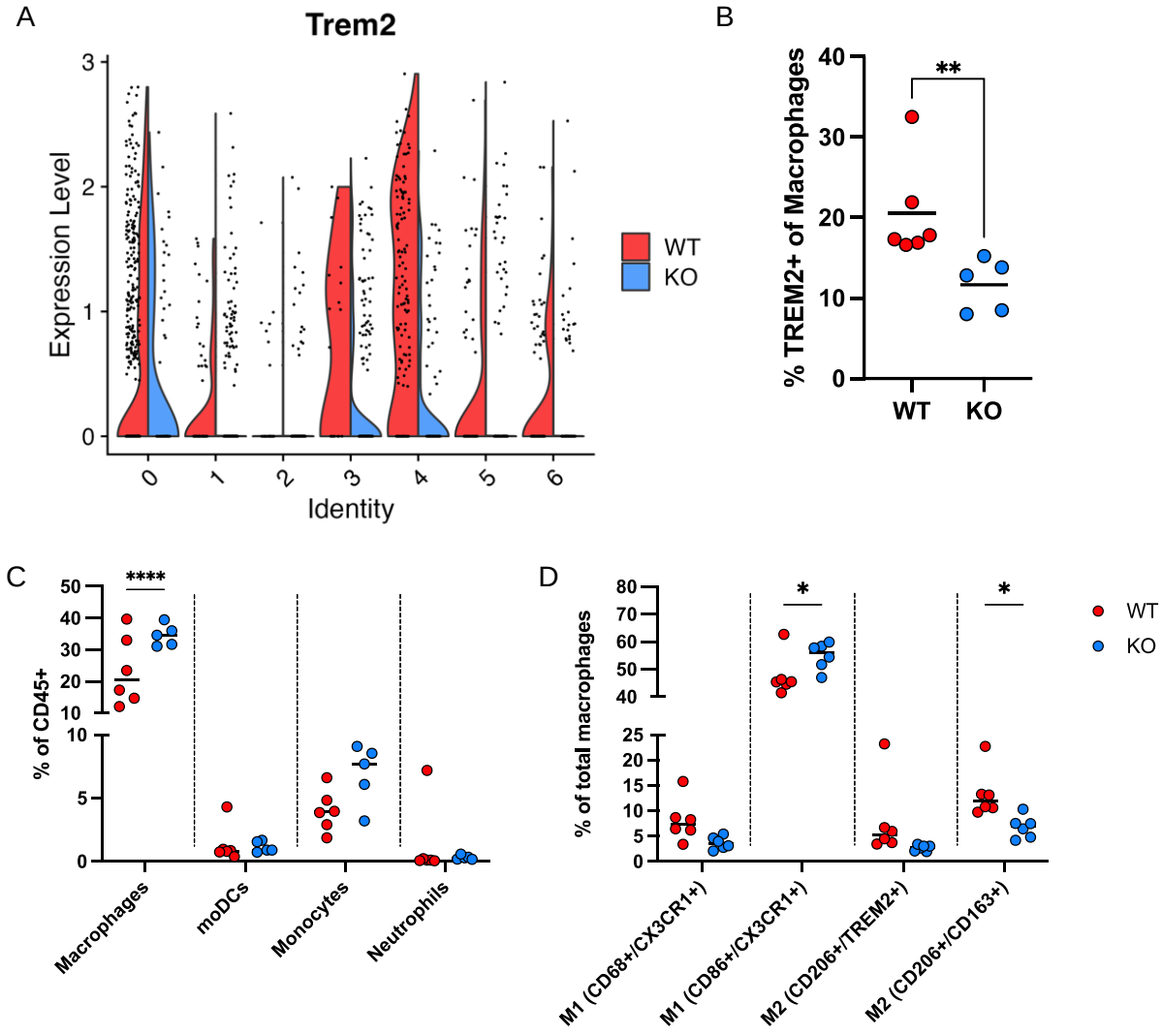

Figure 43 . Experimental validation of tumour-associated macrophage phenotypes from WT or IFNGR1KO tumours. (A) Violin plot for Trem2 expression from the scRNAseq dataset, by monocyte/macrophage cluster. (B) Surface TREM2 expression on tumour-associated macrophages (MHC-II^{+}/CD11b^{+}/F4/80^{+}) as measured by flow cytometry. (C) Relative proportions of myeloid populations found in WT or IFNGR1KO tumours, using the 22-colour spectral flow cytometry panel. Gating strategies are shown in Figure S10. (D) Expression of M1 or M2 markers gated on tumour-associated macrophages. Data are from one experiment, and show mean with statistical testing performed by non-parametric Mann-Whitney *t* test in B, and two-way ANOVA in C&D. *$p\leq0.05$, **$p\leq0.01$, ****$p\leq0.0001$.

5.3 Discussion and conclusion

5.3.1 Current limitations and strengths of single-cell analysis in our model

The exploratory nature of single-cell analysis meant that it could be used as a tool for hypothesis generation when it was not clear which cell subset contributed most to our *in vivo* phenotype. In our dataset, analysing signalling networks was highly useful in discovering ligand-receptor interactions which may be altered in immune cells when IFNγ-signalling is absent on tumour cells. Bioinformatic tools such as CellChat provided insight on the significance of macrophage-dependent signalling, which was not immediately apparent at the conclusion of the first results chapter. Finding that IFNγ-signalling pathways were more transcriptionally prominent in KO tumours also lent confidence to our experimental model, and shed light on how increased IFNγ could influence other immune cell populations. Ultimately, the single-cell experiment led us to form hypotheses surrounding myeloid cells rather than $CD8^+$ T cells or NK cells which are traditionally thought of as being the most influential in anti-tumour response. Instead, it appears that IFNγ significantly alters the myeloid landscape which we hypothesize may enable better $CD8^+$ T cell responses.

The main limitation of scRNAseq for our study was low sequencing throughput during sampling, meaning that we lose resolution of rare transcripts and signalling pathways, or cell populations which are low in abundance. As a result, non-immune components such as stromal, endothelial, or tumour cells themselves could not be sequenced in the same experiment. As these cell types are significant responders of IFNγ which can lead to suppression of angiogenesis[312,313] or tumour cell senescence.[164,314] Bulk or single-cell sequencing on these non-immune cell types would allow for a more complete picture of the tumour models as a whole.

5.3.2 The CD8-macrophage axis of anti-tumour immunity

T cell and TAM cooperation have been found in human tumours which are responsive to immune checkpoint blockade.[315,316] Unexpectedly, the transcriptomic data

indicates that IFNGR1KO tumours are capable of maintaining a pro-inflammatory tumour microenvironment, supported by the presence of *Nos2*-expressing monocytes. There is evidence that a IFNγ-rich environment induces a tumouricidal macrophage phenotype which is driven by nitric oxide production.[317,318] This may be an MHC-I-independent, IFNγ-dependent mode of tumour control in our IFNGR1KO model where $CD8^+$ T cells play an important role in sustaining a pro-inflammatory microenvironment.

Conversely, TAM-T cell interactions have also been shown to re-enforce independent immunosuppressive mechanisms.[319] Although exhausted T cells are thought to be functionally limited in the tumour microenvironment, recent studies show that TAMs can prime $CD8^+$ T cells for exhaustion in an antigen-dependent manner via prolonged synapses in the tumour microenvironment. *Apoe*^{hi}, *Ms4a7*^{hi}, and proliferating macrophages preferentially occupied the interior regions of the TME along with exhausted T cells. Other groups have previously reported similar patterns where different TAM subtypes occupy the tumour centre versus the invasive margin.[320] In our model where antigen presentation by tumour cells is disparate, we aim to investigate whether $CD8^+$ T cells are finding alternate sources of antigen stimulation which may enhance or diminish the overall anti-tumour response. Ideally, confocal microscopy will be used to show colocalization of TAM and $CD8^+$ populations on existing tumour sections from previous chapters.

5.3.3 Future directions on TAMs in the IFNGR1KO tumour model

Our dataset shows significant bifurcation of monocyte-macrophage subsets between B16-OVA WT and IFNGR1KO tumours. However, it is not known whether IFNγ itself is the factor which causes this difference. In chapter 3.2.1, harvested tumour supernatants contained higher concentrations of IFNγ in KO tumours versus WT. Future experiments will focus on whether these supernatants are capable of differentiating bone marrow and blood murine monocytes *in vitro*, as well as the macrophage phenotypes which ensue.

Furthermore, it is not clear *in vivo* whether KO tumours have higher abundance of monocytic populations due to increased chemoattraction of peripheral monocytes from

circulation, or reduced differentiation into macrophages due to the cytokine microenvironment present in the tumour. Transwell assays using tumour supernatants will be useful in determining the relative chemoattractant properties present in each model, as WT tumours showed higher transcription of chemokines such as *Ccl2* and *Ccl7*. In both differentiation and migration assays, blocking antibodies (e.g., against IFNγ or CXCL9) would be a simple and viable strategy *in vitro* to determine the effects of a specific chemokine or cytokine in question. Ultimately, finding a candidate soluble factor which modulates monocyte or macrophage function would support a novel mechanism by which control of IFNGR1KO tumours depend on myeloid differentiation or migration.

5.4 Appendix

Table S4. Cytek Aurora panel for staining of myeloid populations.

Peak Channel	Fluorochrome	Marker	Clone	Manufacturer	Cat. No.	Dilution (1:X)
UV2	Spark387	CD11c	53-6.7	Biolegend	100798	400
UV6	Zombie UV	--	--	Biolegend	423108	1000
UV9	BUV615	B220	RA3-6B2	eBioscience	366-0452-82	200
UV10	BUV661	CD4	RM4-5	eBioscience	376-0042-82	200
UV14	BUV737	CD44	IM7	eBioscience	367-0441-82	400
UV16	BUV805	CD45	30-F11	eBioscience	368-0451-82	400
V1	BV421	CD206	C068C2	Biolegend	141717	200
V3	PB	Ly6G	1A8	Biolegend	127612	800
V10	BV605	CD86	GL-1	Biolegend	105037	200
V11	BV650	PD-L1	10F.9G2	Biolegend	124333	400
V13	BV711	CD62L	MEL-14	Biolegend	121439	200
V15	BV785	F4/80	BM8	Biolegend	123115	200
B2	ZsGreen	Tumour	GK1.5	Biolegend	124334	400
B10	PerCP-Vio770	CD68	FA-11	Miltenyi Biotec	130-102-926	20
YG1	PE	TREM2	237920	R&D Systems	FAB17291P	200
YG3	mCherry	Tumour	--	--	--	--
YG9	PE-Cy7	CD163	S15049I	Biolegend	155320	200
R1	APC	Ly6C	HK1.4	Biolegend	128015	400
R2	AF647	NKp46	29A1.4	Biolegend	137628	100
R4	AF700	MHC-II	M5/114.15.2	Biolegend	107621	400
R7	APC/Cy7	CX3CR1	SA011F11	Biolegend	149048	200
R8	APC-Fire810	CD11b	M1/70	Biolegend	101288	400

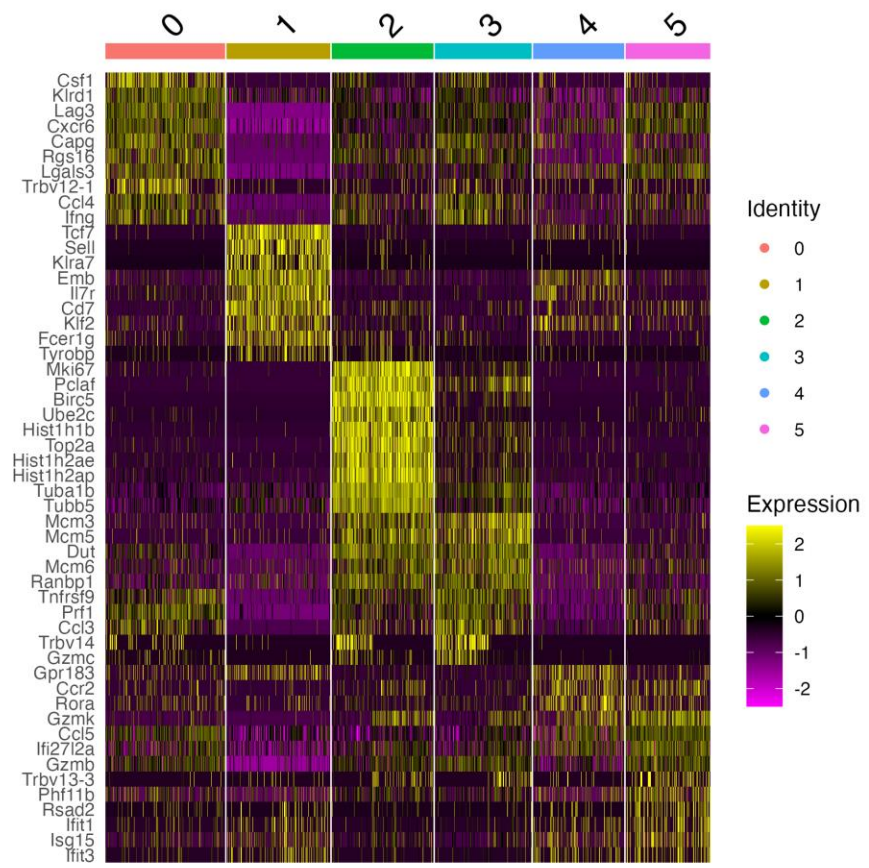

Figure S7. Heatmap of genes expressed by the subset of CD8⁺ T cell clusters.

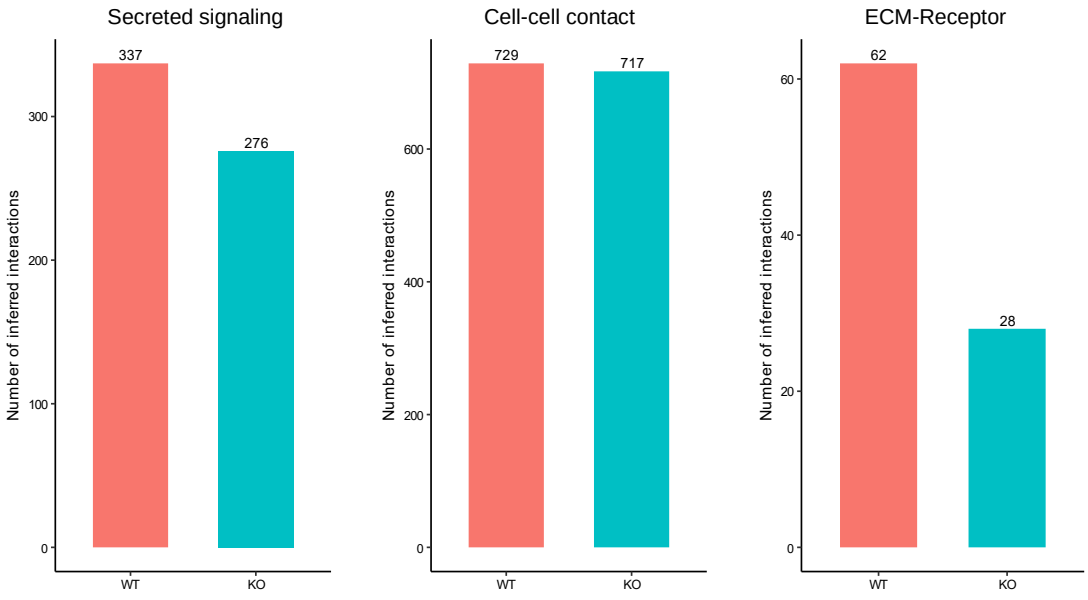

Figure S8. Comparison of the number of interactions between immune cells from WT and IFNGR1KO tumours for each cell-cell communication database in CellChat.

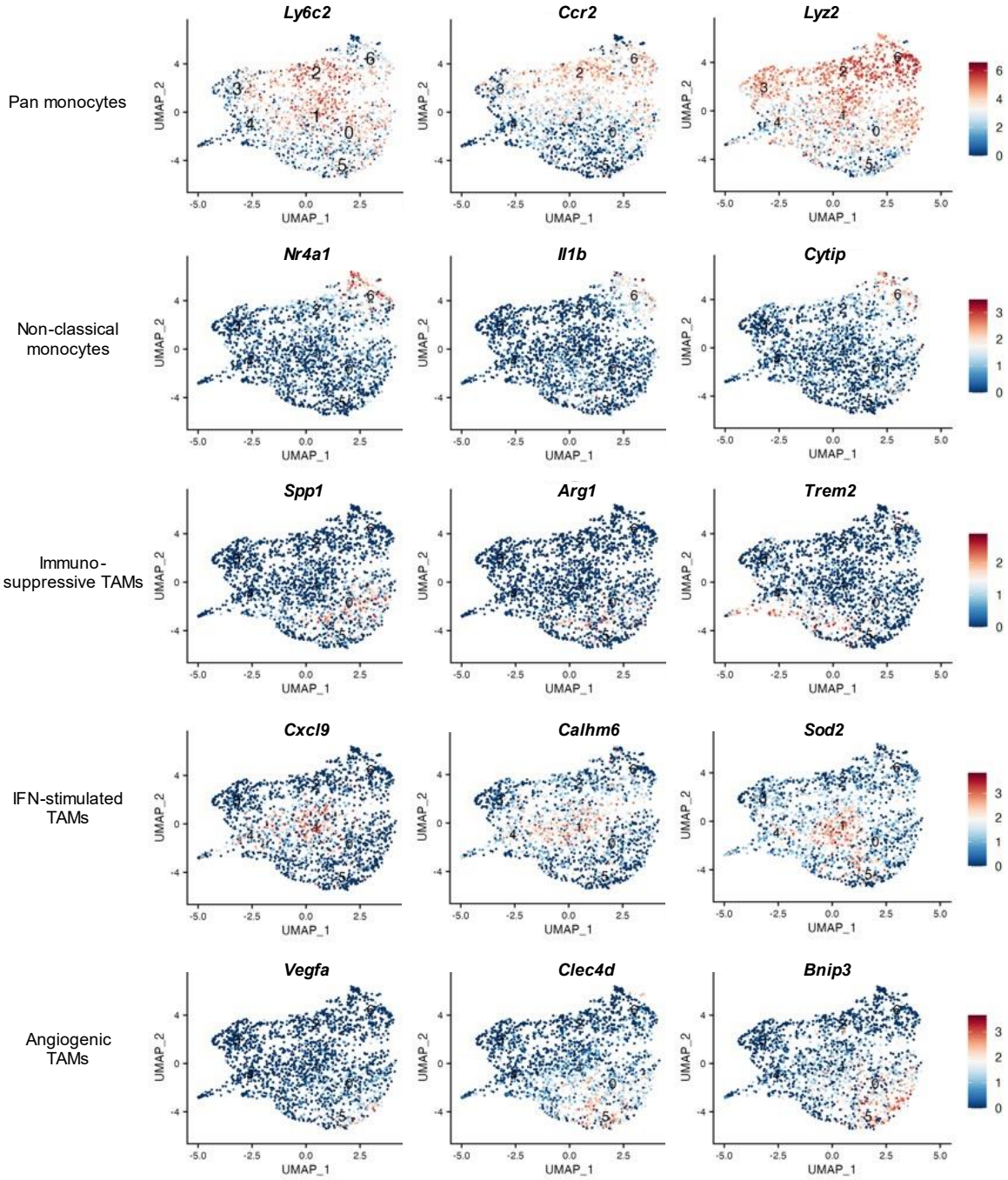

Figure S9. Visualization of genes expressed by different myeloid subsets by row, overlaid onto UMAP projections. Colours indicate relative expression per gene.

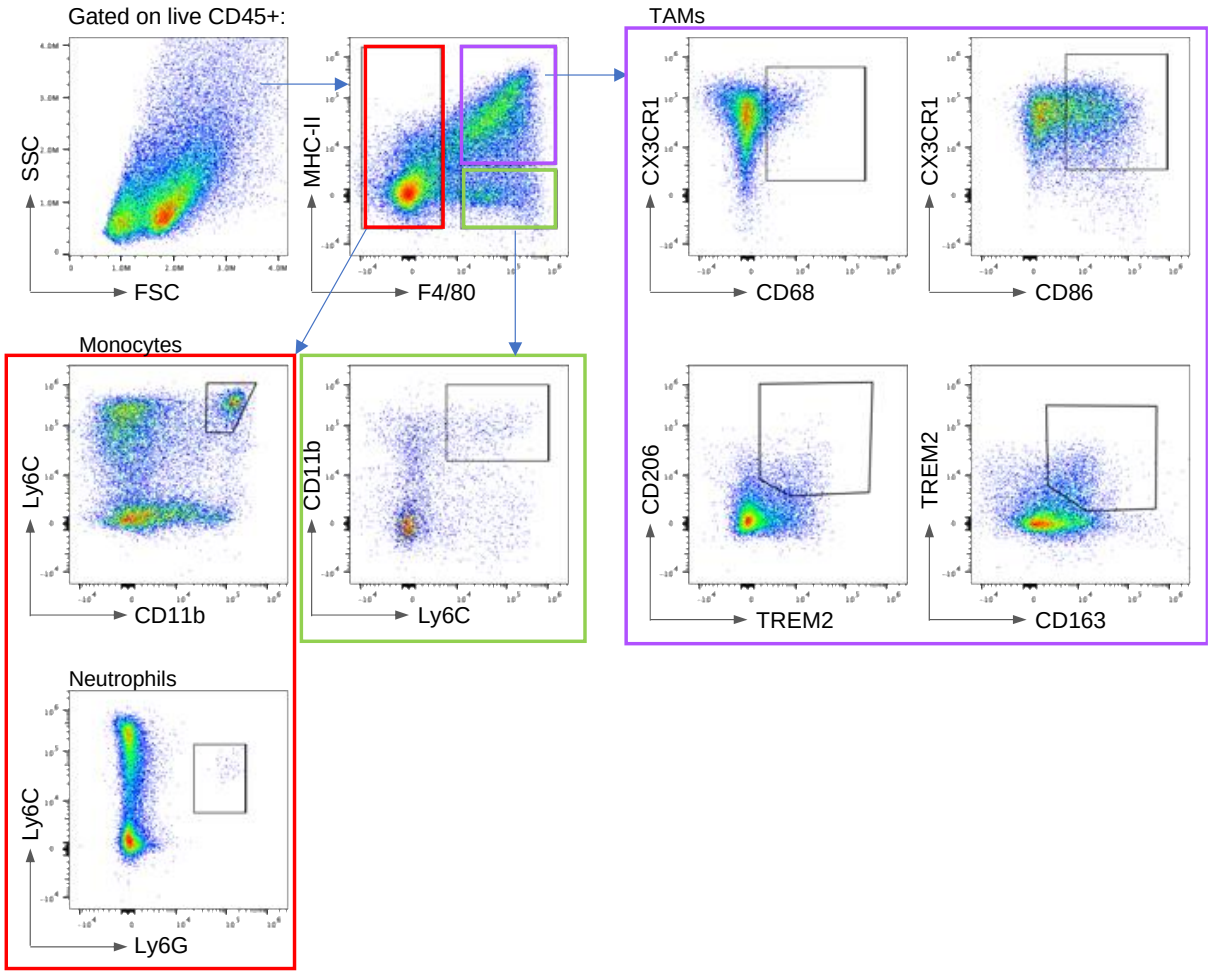

Figure S10. Gating strategy for flow cytometry data of tumour-infiltrating immune cells stained with the Cytek Aurora myeloid panel in Table S4.

General Discussion and Conclusion

In this thesis, we explored the role of IFNγ in shaping the tumour microenvironment, and how loss of IFNγ-signalling on the side of the tumour affects disease control over time. In chapter 3, we established an IFNγ-insensitive tumour model by ablating IFNGR1 expression on B16F10 melanoma, and began to phenotype the immune response and changes to the anti-tumour response which ensued. Unexpectedly, the tumour volumes remained equal over time in animals bearing WT or IFNGR1KO tumours, indicating that loss of IFNγ-stimulated gene expression such as MHC class I expression did not overly impact mechanisms of tumour control in this model. Following this, we observed in chapter 4 that mixing of the two cell types prior to injection restored the immune escape phenotype whereby IFNGR1KO cells would outgrow WT cells over time in immunocompetent mice. Implantation of these tumours in mice deficient in $CD8\alpha^+$ cells or IFNγ production resulted in loss of the escape phenotype, indicating that the phenomenon was driven by immune selection. This ultimately gave us a model which recapitulates more closely the mechanisms which may be resulting in primary immune escape of tumour immunity in clinical settings.

Lastly, we utilized scRNAseq in an unbiased manner to identify the cell types and signalling pathways which may differ from loss of IFNγ-sensitivity by tumour cells. We found that although multiple immune cell subsets were altered, we were able to validate phenotypic changes to the tumour-associated macrophage populations with preliminary flow cytometry studies. In the future, we aim for follow-up these studies primarily with monocyte differentiation assays *in vitro* using tumour supernatants, and functionally determining whether macrophages play a role in altering $CD8^+$ T cell-dependent anti-tumour immunity.

6.1 Assessing T cell avidity in the control of MHC class I-low tumours

We initially hypothesized that WT tumours would be more immunogenic than IFNGR1KO tumours based on differences in MHC-I expression which would enable $CD8^+$ T cell-dependent cytotoxicity. However, as overall tumour control appeared to be equal in both

models, alternative mechanisms must be at play. Although PD-L1 levels are also significantly different between WT and KO cells, we and others who have tested anti-PD-1 or anti-PD-L1 checkpoint blockade in B16F10 have observed that the model is not responsive to monotherapy. Hence, PD-L1 expressed by the tumour (or other immune cells) is not likely to be the primary immunosuppressive factor which hinders $CD8^+$ T cell cytotoxicity.

From the scRNAseq data, it is evident that $CD8^+$ TILs from KO tumours are not dormant, and can actively produce effector molecules. Furthermore, tumours implanted into the CD8KO mice also demonstrated that $CD8^+$ T cell immunity is not easily substituted in either tumour model, and readily impacts the infiltration of all other immune populations. One interpretation of how tumour control is achieved in the IFNGR1KO model is that $CD8^+$ T cells may be capable of adapting to MHC-I-low target cells. Higher TCR avidity is able to respond to lower antigen doses (i.e., fewer MHC-I molecules)[321], and studies have also shown that higher avidity T cells confer greater tumour eradication.[322] Furthermore, it has been demonstrated *in vitro* that priming of T cells with low dose peptide enabled greater sensitization towards targets loaded with >100-fold less peptide than T cells primed with high dose peptide.[323] Taken together, these observations make it plausible that priming with lower antigen doses, combined with IFNγ accumulation in the tumour, may result in more functional and higher avidity tumour-specific T cells in IFNGR1KO tumours compared to WT.

Although we have used tetramers to identify and quantify OVA-specific T cells, tetramer-TCR interactions are inaccurate measures of T cell avidity due to dependence on the physiological state of the T cells at the time of staining and variability in staining conditions.[324] Instead, our lab has previously used a platform called z-Movi analyser by Lumicks to measure functional TCR avidity using applied acoustic force. The system binds target cells (antigen-pulsed APCs, or tumour cells) onto a chip, and T cells are co-incubated on top. The rate at which T cells become unbound is measured after acoustic force is applied at increasing intervals, which allows the avidity to be inferred.[268] Ensuring pure cell populations isolated from the tumour samples would be important, and avidity measurements using OT-I T cells or B16 cell lines serve as benchmarks in our experiments.

If T cells from WT and KO tumours show no difference in their avidity, then the importance of other factors such as T cell trafficking and recruitment, or immunosuppression by myeloid populations, become increasingly important. ‘Double-implantation’ experiments (i.e., implantation of WT and KO tumours on separate flanks of the same animal), described in the next section, would be helpful in elucidating mechanisms in the TME intrinsic to each tumour model.

6.2 Using a double-implantation model of WT and IFNGR1KO tumours to study the role of IFNγ in lymph node dynamics, T cell trafficking and bystander T cells in cancer immunology

A model we have not yet explored is whether implantation of WT and IFNGR1KO tumours as separate tumours in the same animal would result in both tumours growing equally, or regression of one tumour and outgrowth of the other. This ‘double-implantation’ model would provide insight into whether the local tumour microenvironments can be retained if both tumours share the same systemic immune response (**Figure 44**). Interestingly, we have several distinct biomarkers, such as the tetramer MFI, increase in pro-inflammatory macrophages, or accumulation of IFNγ, which are specific to IFNGR1KO tumours. It would be of interest to determine which of these observations are intrinsic to the tumour microenvironment itself, or is lost to peripheral systemic effects.

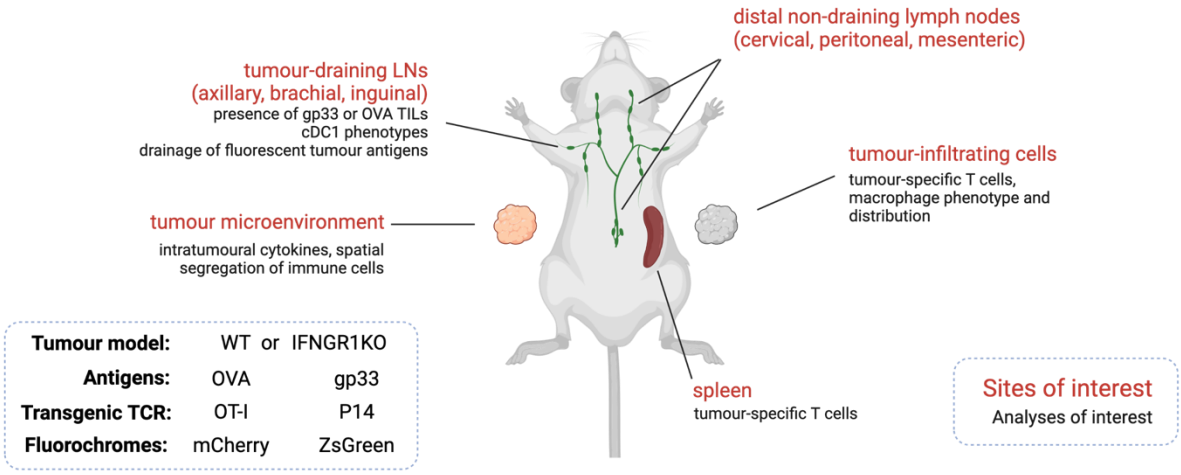

Figure 44. Overview of double-implantation experiments. A combination of tumour antigens, transgenic T cells which recognize tumour antigens, and fluorochromes used to track distribution of tumour antigens can be used in the proposed model. Tumour-intrinsic factors which affect immune responses can be evaluated via analysis of the tumours themselves, or tumour-extrinsic factors which take place in peripheral lymphoid organs may be of interest.

Although our cross-priming model was unable to determine whether cross-priming was affected by IFNγ-resistant tumours, we nevertheless observe significant infiltration of T cells in both WT and IFNGR1KO tumours, indicating that there is no overt dysfunction in priming in one model compared to the other. Interestingly, we may be able to use the double-implantation model to study whether local tumour-draining lymph nodes which are more closely located to the site of implantation also experience changes. Human clinical studies which sampled lymphocytes from regional lymph nodes of patients with melanoma or breast cancer showed that cells closer to the tumour were less responsive to thymidine uptake or IL-2 production upon stimulation than those further away.[325] More recent studies have shown that an IFNγ transcriptional signature found within the tumour-draining lymph nodes of melanoma patients also result in an increase in PD-L1^{+} DCs.[326] Intriguingly, these may or may not be phenotypically similar to the immunoregulatory DC phenotype reported by Maier *et al*., which also confer reduced tumour antigen uptake in mice and humans.[58] It would be interesting to explore whether the IFNγ-high environment of IFNGR1KO tumours extend to the tdLNs, and whether cells such as DCs which traffic between the tumour and tdLNs experience improved antigen presentation functions or costimulatory properties. At present, our scRNAseq data analysis of pathways upregulated by intratumoural immune

cells (in chapter 5.2.1) appears to support the hypothesis that APCs from IFNGR1KO tumours may be better at presenting tumour antigen, as IFN-response pathway genes are differentially expressed. Furthermore, if WT and IFNGR1KO tumours are tagged with different fluorescent proteins, then drainage of tumour-specific antigens to distal sites may also be tracked by flow cytometry or microscopy.

Trafficking of T cells to the tumour and subsequent infiltration into the tumour bed is an indispensable component of the anti-tumour response. As efficacy of immunotherapies against solid cancers continue to improve, understanding factors which overcome immunosuppression and enable T cell infiltration is of significant clinical interest.[327] Furthermore, this is not limited to trafficking of endogenously responding T cells as genetically engineered T cell therapies also face the same T cell-limiting mechanisms upon transfer into the host.[328] Analysis of our scRNAseq data using CellChat supports our hypothesis that differential expression of chemokine ligands and receptors exists between WT and IFNGR1KO tumours, which may be shaped by IFNγ-dependent signalling. We aim to assess relative chemoattractive properties inherent to each tumour model using double-implantation of OVA-expressing WT and IFNGR1KO tumours into CD45.1 hosts, followed by transfer of activated CD45.2 OT-I $CD8^+$ T cells after establishment of palpable tumours (**Figure 45**). Within the same host, activated OT-I $CD8^+$ T cells would home to the tumours directly without requiring T cell priming. Furthermore, dye-labelled OT-I T cells may also be used to track relative differences in proliferation which would be indicative of antigen-dependent stimulation in each tumour. Although endogenous T cells may play a role in activation of OT-I T cells in these scenarios, aiming to study the immediate effects of antigen stimulation at shorter time scales (i.e., 24- or 48-hours post-transfer) would provide a more accurate representation of antigen-dependent stimulation.

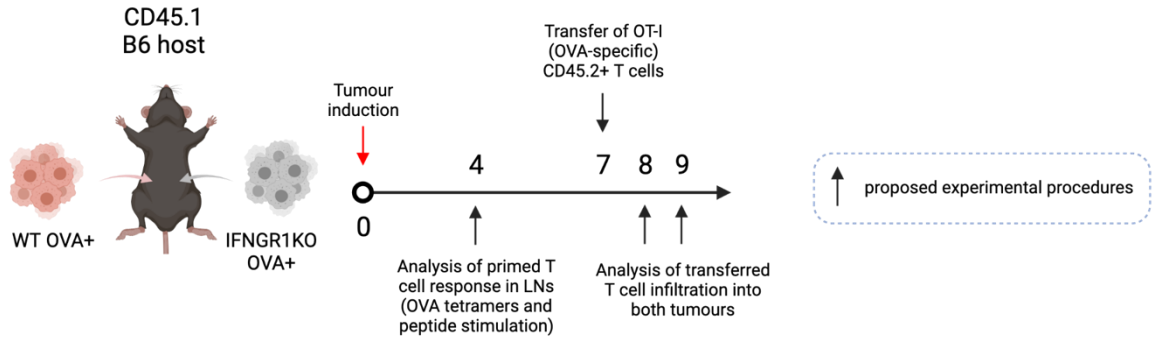

Figure 45. Schemata for tumour-specific T cell transfer experiments into the double-implantation model.

Lastly, recent studies have identified many TILs to be 'bystander' in the sense that they do not respond to tumour itself, but are recruited to the tumour regardless of antigen-specificity. [329,330] In human tumours, cancer-non-specific T cells comprise vary from 20-80% of all tumour-infiltrating T cells, dependent on the tumour type and method of detection.[331] In murine models, transfer of an activated mixture of tumour-specific and non-specific $CD8^+$ T cells showed that both populations were capable of infiltrating the tumour at comparable levels.[332] For our double-implantation model, expressing a different tumour-specific antigen such as gp33 and ovalbumin in each tumour independently would allow for tracking of T cell responses within the same animal (**Figure 46**). Initially, double-implantation of the same tumour (i.e., both WT, or both IFNGR1KO) would be used to track whether gp33-specific T cells infiltrate an OVA-expressing tumour, and vice versa. As this would be our baseline bystander infiltration when both tumours are the same, implantation of a WT tumour in one flank and KO tumour in the other would allow us to determine whether preferential recruitment of tumour-specific and non-specific T cells occurs in either tumour. Furthermore, the transfer of P14 (gp33-specific) or OT-I (OVA-specific) T cells described previously would allow us to differentiate endogenously primed T cells versus recent T cell infiltrates. Ultimately, this experimental system would be a useful tool in exploring whether IFNγ-dependent signalling by the tumour changes chemoattractant properties of the tumour microenvironment. The use of $Rag2^{-/-}$ mice which lack T and B cells as a host would also be

useful in isolating tumour-intrinsic properties which are not influenced by endogenous T or B cell responses.

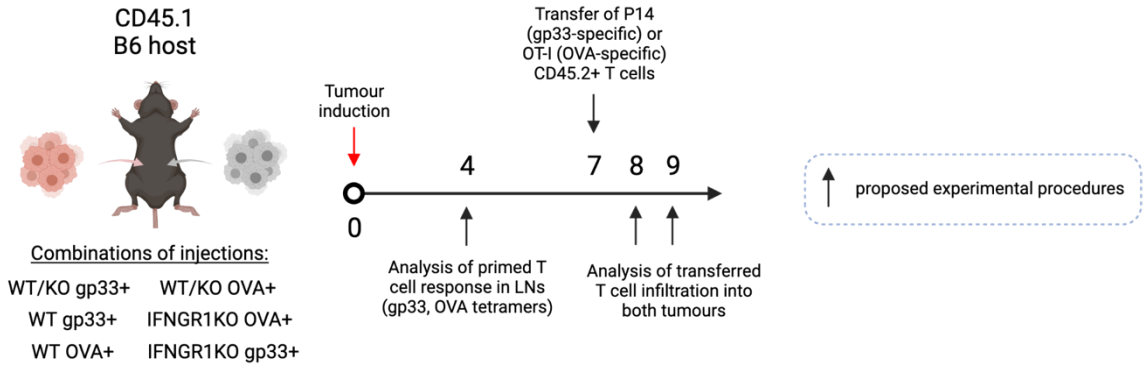

Figure 46. Schemata for double-implantation of tumours expressing different antigens.

6.3 Predicting the mechanisms which result in immune escape of the admixed model

The main caveat of using IFNGR-deficient models is that human tumours do not start with a pool of IFNγ-resistant cells. Instead, these mutations are acquired over time alongside immune selective pressure, which calls into question whether utility of these murine models are recapitulating the same mechanisms of immune escape. We and others who have ablated IFNγ-signalling in B16F10 melanoma through deletion of IFNGR1 or IFNGR2 have observed similar findings in that tumour growth was largely unaffected, or suppressed.[105,241,243] A recently published meta-analysis showed a significant difference in the conclusions between *in vitro* and *in vivo* models, where CRISPR screens were used to investigate the impact of IFNγ on anti-tumour immunity.[333] Alteration of IFNγ-signalling *in vivo* and *in vitro* had seemingly opposing effects; whereas 17/19 *in vitro* immune and tumour cell co-cultures indicated positive selection of IFNγ-signalling mutations, only 3/14 *in vivo* tumour screens showed similar findings following host immune pressure. A review of these *in vivo* CRISPR screens indeed supports the finding that mutations in IFNγ-signalling sensitizes tumours to the host immune system. Consequently, there is a pressing need to identify more clinically relevant animal models than previously anticipated.

Our admixed model is unique in that it spontaneously exhibits an immune escape dynamic, and allows us to perturb the model to study one component of the immune response at a time. Given a model such as B16F10 which is notorious for its variability in tumour growth[334,335], the reliability and reproducibility by which the cell segregation and escape of KO cells occurs is somewhat remarkable. Cell competition theory dictates that fitter cells would outcompete less-fit cells when they share the same resources, if the mechanism for competition was cell-intrinsic (e.g., carrying a mutation in a gene).[336] From our CD8KO and IFNγKO experiments, we were able to determine that outgrowth of KO cells was not cell-intrinsic or self-selecting, and indeed requires immune selection through IFNγ. However, it is not obvious which IFNγ-dependent mechanisms are enabling the phenotype.

The observation that the escape phenotype requires more than 7 days to develop indicates that WT cells are not targeted and cleared at early timepoints immediately following implantation. Tumour cells likely receive IFNγ stimulation much earlier, as IFNγ-EYFP$^+$ T cells were found in abundance in the tumour as early as day 7. This implies that IFNγ-dependent suppression of WT cell proliferation is not sufficient, since the tumour was still 50/50 WT and KO at day 7. In chapter 4.2.5, quantifying the proportion of OVA-specific T cells infiltrating into IFNγKO tumours demonstrates that it is likely CD8$^+$ T cell function that is hindered in the absence of IFNγ, as priming and/or recruitment of T cells appears unaffected by the lack of IFNγ.

One major question for the admixed model is whether IFNGR1KO cells are outgrowing WT due to inhibition of WT proliferation, or induction of WT cell death. Using the proliferation marker Ki-67 and cleaved caspase-3, a marker of apoptosis, we aim to measure the proportion of cells undergoing proliferation or cell death by microscopy or flow cytometry. What we would expect to see experimentally is highlighted in **Figure 47**. We hypothesize that WT and KO tumours would result in the same levels of proliferation and/or apoptosis as their tumour growth is the same in independent animals. In the admixed model, if the

proportion of proliferating cells is the same, then this would likely indicate more WT cells are dying over time to allow KO cells to overtake the tumour.

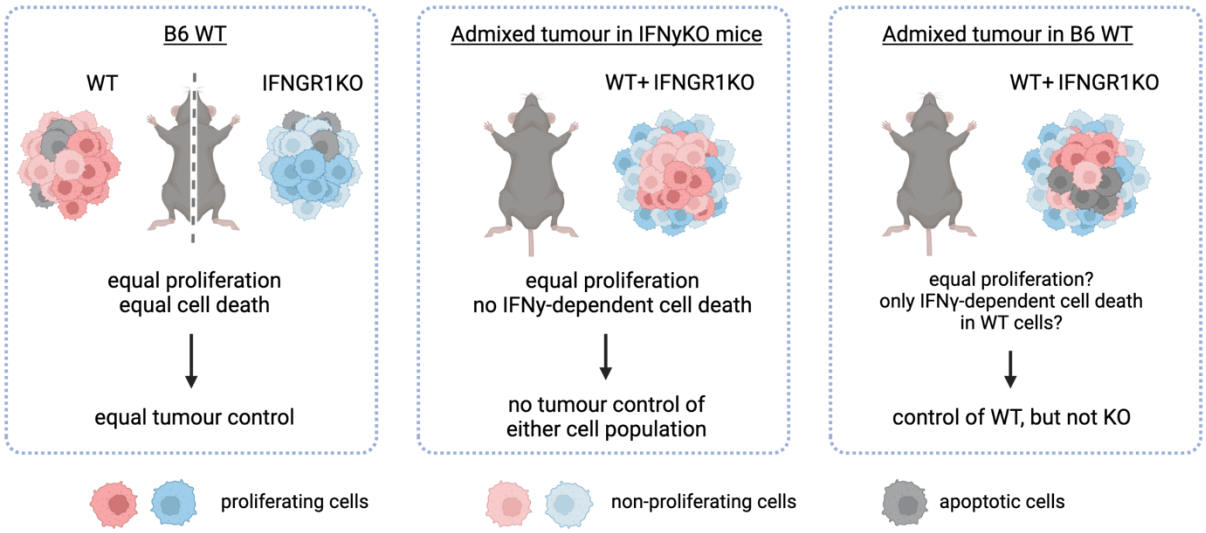

Figure 47. Proposed patterns of tumour cell proliferation and cell death in the tumour models previously tested.

Because these experiments do not ultimately point to a cell population which may be modulating tumour cell apoptosis in the admixed tumours, immunophenotyping of the anti-tumour response from day 7, before the admixed tumours change, and after, at day 14 and beyond, may give an indication of immune populations which have changed over time. Following the hypothesis where TAM populations are modulated by the local IFNγ concentrations present in the tumour, comparing TAM signatures in admixed tumours to WT:WT and KO:KO controls may also be indicative of whether TAMs are involved in the escape phenotype. Based on our hypothesis that monocyte and macrophage populations are vastly altered by the presence of IFNGR1KO tumour cells which cannot sequester IFNγ, we aim to first deplete monocytes by antibody, or macrophages by liposome-encapsulated clodronate.[337,338] These experiments aim to determine whether we may be able to relate our findings from scRNAseq to the immune escape phenotype observed in the admixed model.

6.4 Thesis outlook and conclusion

There are many more questions raised in the data presented in this thesis owing to the complexity of the models present by our group, and others, which are not fully understood. The main questions to be answered would likely require a model responsive to checkpoint blockade, as the key pathways which enable therapy success remain unclear for all patients. Recent studies have also demonstrated that ICB likely operates within a therapeutic window; too little of a response can result in failure of disease control, and too much of a response can trigger unwanted regulatory mechanisms. Even so, it has been shown that immunotherapy-resistant models can be useful for finding pathways which are amenable to alternative treatments. Furthermore, there are no standards of treatment at the moment which utilizes a strategy of switching treatment regimens once acquired resistance develops. Understanding which immune cells to target, and how to eliminate clones such as those which are IFNγ resistant, would allow these patients to overcome immunotherapy resistance.

At present, we have managed to identify a novel tumour model which we hope to use in order to understand the main questions relevant for clinical applications. The strength of this model is that we may study the causality between IFNγ resistance and loss of anti-tumour immunity, especially as technologies are advancing in the field of functional genomics. It is our hope that our work, as well as the work of others, may be able to bridge this gap in the near future.

References

1. Hanahan, D. & Weinberg, R. A. The hallmarks of cancer. *Cell* **100**, 57–70 (2000).
2. Fouad, Y. A. & Aanei, C. Revisiting the hallmarks of cancer. *Am. J. Cancer Res.* **7**, 1016–1036 (2017).
3. Hanahan, D. Hallmarks of Cancer: New Dimensions. *Cancer Discov.* **12**, 31–46 (2022).
4. Burnet, F. M. Immunological aspects of malignant disease. *Lancet* **289**, 1171–1174 (1967).
5. PREHN, R. T. & MAIN, J. M. Immunity to methylcholanthrene-induced sarcomas. *J. Natl. Cancer Inst.* **18**, 769–78 (1957).
6. KLEIN, G., SJOGREN, H. O., KLEIN, E. & HELLSTROM, K. E. Demonstration of resistance against methylcholanthrene-induced sarcomas in the primary autochthonous host. *Cancer Res.* **20**, 1561–72 (1960).
7. Smyth, M. J. *et al.* Differential tumor surveillance by natural killer (NK) and NKT cells. *J. Exp. Med.* **191**, 661–668 (2000).
8. Kaplan, D. H. *et al.* Demonstration of an interferon gamma-dependent tumor surveillance system in immunocompetent mice. *Proc. Natl. Acad. Sci. U. S. A.* **95**, 7556–7561 (1998).
9. Dighe, A. S., Richards, E., Old, L. J. & Schreiber, R. D. Enhanced in vivo growth and resistance to rejection of tumor cells expressing dominant negative IFNγ receptors. *Immunity* **1**, 447–456 (1994).
10. Opelz, G. & Döhler, B. Lymphomas after solid organ transplantation: a collaborative transplant study report. *Am. J. Transplant. Off. J. Am. Soc. Transplant. Am. Soc. Transpl. Surg.* **4**, 222–230 (2004).
11. Grulich, A. E., van Leeuwen, M. T., Falster, M. O. & Vajdic, C. M. Incidence of cancers in people with HIV/AIDS compared with immunosuppressed transplant recipients: a meta-analysis. *Lancet (London, England)* **370**, 59–67 (2007).
12. Barnd, D. L., Lan, M. S., Metzgar, R. S. & Finn, O. J. Specific, major histocompatibility complex-unrestricted recognition of tumor-associated mucins by human cytotoxic T cells. *Proc. Natl. Acad. Sci. U. S. A.* **86**, 7159–7163 (1989).
13. Türeci, O., Sahin, U. & Pfreundschuh, M. Serological analysis of human tumor antigens: molecular definition and implications. *Mol. Med. Today* **3**, 342–349 (1997).
14. Dunn, G. P., Bruce, A. T., Ikeda, H., Old, L. J. & Schreiber, R. D. Cancer immunoediting: from immunosurveillance to tumor escape. *Nat. Immunol.* **3**, 991–998 (2002).
15. Böttcher, J. P. & Reis e Sousa, C. The Role of Type 1 Conventional Dendritic Cells in Cancer Immunity. *Trends in Cancer* **4**, 784–792 (2018).
16. Hamann, D. *et al.* Phenotypic and functional separation of memory and effector human CD8+ T cells. *J. Exp. Med.* **186**, 1407–1418 (1997).
17. Raskov, H., Orhan, A., Christensen, J. P. & Gögenur, I. Cytotoxic CD8+ T cells in cancer and cancer immunotherapy. *Br. J. Cancer* **124**, 359–367 (2021).
18. O'Connell, J., Bennett, M. W., O'Sullivan, G. C., Collins, J. K. & Shanahan, F. The Fas Counterattack: A Molecular Mechanism of Tumor Immune Privilege. *Mol. Med.* **3**, 294–300 (1997).
19. Chen, D. S. & Mellman, I. Oncology meets immunology: The cancer-immunity cycle. *Immunity* **39**, 1–10 (2013).
20. Murphy, K. M. & Weaver, C. *Janeway's Immunobiology: Tenth Edition*. (W.W. Norton, 2022).
21. Curtsinger, J. M. & Mescher, M. F. Inflammatory cytokines as a third signal for T cell activation. *Curr. Opin. Immunol.* **22**, 333–340 (2010).
22. Greenwald, R. J., Freeman, G. J. & Sharpe, A. H. The B7 family revisited. *Annu. Rev. Immunol.* **23**, 515–548 (2005).
23. Hildner, K. *et al.* Batf3 deficiency reveals a critical role for CD8α+ dendritic cells in

cytotoxic T cell immunity. *Science (80-.).* **322**, 1097–1100 (2008).
24. Roberts, E. W. *et al.* Critical Role for CD103+/CD141+ Dendritic Cells Bearing CCR7 for Tumor Antigen Trafficking and Priming of T Cell Immunity in Melanoma. *Cancer Cell* **30**, 324–336 (2016).
25. Broz, M. L. *et al.* Dissecting the Tumor Myeloid Compartment Reveals Rare Activating Antigen-Presenting Cells Critical for T Cell Immunity. *Cancer Cell* **26**, 638–652 (2014).
26. Sim, M. J. W. & Sun, P. D. T Cell Recognition of Tumor Neoantigens and Insights Into T Cell Immunotherapy. *Front. Immunol.* **13**, 1–12 (2022).
27. Schumacher, T. N. & Schreiber, R. D. Neoantigens in cancer immunotherapy. *Science (80-.).* **348**, 69–74 (2015).
28. Zhang, Z. *et al.* Neoantigen: A New Breakthrough in Tumor Immunotherapy. *Front. Immunol.* **12**, 1–9 (2021).
29. Maleki Vareki, S. High and low mutational burden tumors versus immunologically hot and cold tumors and response to immune checkpoint inhibitors. *J. Immunother. Cancer* **6**, 4–8 (2018).
30. McLane, L. M., Abdel-Hakeem, M. S. & Wherry, E. J. CD8 T Cell Exhaustion During Chronic Viral Infection and Cancer. *Annu. Rev. Immunol.* **37**, 457–495 (2019).
31. Omilusik, K. D. & Goldrath, A. W. The origins of memory T cells. *Nature* **552**, 337–339 (2017).
32. Youngblood, B. *et al.* Effector CD8 T cells dedifferentiate into long-lived memory cells. *Nature* **552**, 404–409 (2017).
33. Kaech, S. M. & Cui, W. Transcriptional control of effector and memory CD8+ T cell differentiation. *Nat. Rev. Immunol.* **12**, 749–761 (2012).
34. Wherry, E. J. *et al.* Molecular signature of CD8+ T cell exhaustion during chronic viral infection. *Immunity* **27**, 670–684 (2007).
35. Schietinger, A. *et al.* Tumor-Specific T Cell Dysfunction Is a Dynamic Antigen-Driven Differentiation Program Initiated Early during Tumorigenesis. *Immunity* **45**, 389–401 (2016).
36. Wherry, E. J. & Kurachi, M. Molecular and cellular insights into T cell exhaustion. *Nat. Rev. Immunol.* **15**, 486–499 (2015).
37. Greaves, M. & Maley, C. C. Clonal evolution in cancer. *Nature* **481**, 306–313 (2012).
38. Li, H. *et al.* Dysfunctional CD8 T Cells Form a Proliferative, Dynamically Regulated Compartment within Human Melanoma. *Cell* **176**, 775-789.e18 (2018).
39. Singer, M. *et al.* A Distinct Gene Module for Dysfunction Uncoupled from Activation in Tumor-Infiltrating T Cells. *Cell* **166**, 1500-1511.e9 (2016).
40. Philip, M. *et al.* Chromatin states define tumour-specific T cell dysfunction and reprogramming. *Nature* **545**, 452–456 (2017).
41. Duan, Q., Zhang, H., Zheng, J. & Zhang, L. Turning Cold into Hot: Firing up the Tumor Microenvironment. *Trends in Cancer* **6**, 605–618 (2020).
42. Zhang, J., Huang, D., Saw, P. E. & Song, E. Turning cold tumors hot: from molecular mechanisms to clinical applications. *Trends Immunol.* **43**, 523–545 (2022).
43. *Tumor Microenvironment*. (Springer Cham, 2020).
44. Hedrick, C. C. & Malanchi, I. Neutrophils in cancer: heterogeneous and multifaceted. *Nat. Rev. Immunol.* **22**, 173–187 (2022).
45. Wculek, S. K., Bridgeman, V. L., Peakman, F. & Malanchi, I. Early Neutrophil Responses to Chemical Carcinogenesis Shape Long-Term Lung Cancer Susceptibility. *iScience* **23**, 101277 (2020).
46. Cristinziano, L. *et al.* Anaplastic Thyroid Cancer Cells Induce the Release of Mitochondrial Extracellular DNA Traps by Viable Neutrophils. *J. Immunol.* **204**, 1362–1372 (2020).
47. Hirschhorn, D. *et al.* T cell immunotherapies engage neutrophils to eliminate tumor antigen escape variants. *Cell* **186**, 1432-1447.e17 (2023).
48. Matlung, H. L. *et al.* Neutrophils Kill Antibody-Opsonized Cancer Cells by Trogoptosis. *Cell Rep.* **23**, 3946-3959.e6 (2018).
49. Olingy, C. E., Dinh, H. Q. & Hedrick, C. C. Monocyte heterogeneity and functions in

cancer. *J. Leukoc. Biol.* **106**, 309–322 (2019).
50. De Palma, M. & Naldini, L. Tie2-expressing monocytes (TEMs): novel targets and vehicles of anticancer therapy? *Biochim. Biophys. Acta* **1796**, 5–10 (2009).
51. Chittezhath, M. *et al.* Molecular profiling reveals a tumor-promoting phenotype of monocytes and macrophages in human cancer progression. *Immunity* **41**, 815–829 (2014).
52. Kuhn, S., Yang, J. & Ronchese, F. Monocyte-derived dendritic cells are essential for CD8+ T cell activation and antitumor responses after local immunotherapy. *Front. Immunol.* **6**, 1–14 (2015).
53. Dungan, L. S., McGuinness, N. C., Boon, L., Lynch, M. A. & Mills, K. H. G. Innate IFN-γ promotes development of experimental autoimmune encephalomyelitis: a role for NK cells and M1 macrophages. *Eur. J. Immunol.* **44**, 2903–2917 (2014).
54. Liu, J., Geng, X., Hou, J. & Wu, G. New insights into M1/M2 macrophages: key modulators in cancer progression. *Cancer Cell Int.* **21**, 1–7 (2021).
55. Lu, H. *et al.* A breast cancer stem cell niche supported by juxtacrine signalling from monocytes and macrophages. *Nat. Cell Biol.* **16**, 1105–1117 (2014).
56. Petty, A. J. *et al.* Hedgehog-induced PD-L1 on tumor-associated macrophages is critical for suppression of tumor-infiltrating CD8+ T cell function. *JCI insight* **6**, (2021).
57. Kim, C. W., Kim, K.-D. & Lee, H. K. The role of dendritic cells in tumor microenvironments and their uses as therapeutic targets. *BMB Rep.* **54**, 31–43 (2021).
58. Maier, B. *et al.* A conserved dendritic-cell regulatory program limits antitumour immunity. *Nature* **580**, 257–262 (2020).
59. Ruffell, B. *et al.* Macrophage IL-10 blocks CD8+ T cell-dependent responses to chemotherapy by suppressing IL-12 expression in intratumoral dendritic cells. *Cancer Cell* **26**, 623–637 (2014).
60. Binnewies, M. *et al.* Unleashing Type-2 Dendritic Cells to Drive Protective Antitumor CD4(+) T Cell Immunity. *Cell* **177**, 556-571.e16 (2019).
61. Munn, D. H. Indoleamine 2,3-dioxygenase, Tregs and cancer. *Curr. Med. Chem.* **18**, 2240–2246 (2011).
62. Groth, C. *et al.* Immunosuppression mediated by myeloid-derived suppressor cells (MDSCs) during tumour progression. *Br. J. Cancer* **120**, 16–25 (2019).
63. Schlecker, E. *et al.* Tumor-infiltrating monocytic myeloid-derived suppressor cells mediate CCR5-dependent recruitment of regulatory T cells favoring tumor growth. *J. Immunol.* **189**, 5602–5611 (2012).
64. Huang, B. *et al.* Gr-1+CD115+ immature myeloid suppressor cells mediate the development of tumor-induced T regulatory cells and T-cell anergy in tumor-bearing host. *Cancer Res.* **66**, 1123–1131 (2006).
65. Movahedi, K. *et al.* Identification of discrete tumor-induced myeloid-derived suppressor cell subpopulations with distinct T cell-suppressive activity. *Blood* **111**, 4233–4244 (2008).
66. Lichterman, J. N. & Reddy, S. M. Mast Cells: A New Frontier for Cancer Immunotherapy. *Cells* **10**, (2021).
67. Poto, R. *et al.* Basophils from allergy to cancer. *Front. Immunol.* **13**, 1056838 (2022).
68. Varricchi, G. *et al.* Eosinophils: The unsung heroes in cancer? *Oncoimmunology* **7**, e1393134 (2018).
69. Böttcher, J. P. *et al.* NK Cells Stimulate Recruitment of cDC1 into the Tumor Microenvironment Promoting Cancer Immune Control. *Cell* **172**, 1022-1037.e14 (2018).
70. Bryceson, Y. T., Ljunggren, H.-G. & Long, E. O. Minimal requirement for induction of natural cytotoxicity and intersection of activation signals by inhibitory receptors. *Blood* **114**, 2657–2666 (2009).
71. Lo Nigro, C. *et al.* NK-mediated antibody-dependent cell-mediated cytotoxicity in solid tumors: biological evidence and clinical perspectives. *Ann. Transl. Med.* **7**, 105 (2019).

72. Speiser, D. E., Chijioke, O., Schaeuble, K. & Münz, C. CD4(+) T cells in cancer. *Nat. cancer* **4**, 317–329 (2023).
73. Wing, K. *et al.* CTLA-4 control over Foxp3+ regulatory T cell function. *Science* **322**, 271–275 (2008).
74. Ferris, S. T. *et al.* cDC1 prime and are licensed by CD4(+) T cells to induce anti-tumour immunity. *Nature* **584**, 624–629 (2020).
75. Noël, G. *et al.* Functional Th1-oriented T follicular helper cells that infiltrate human breast cancer promote effective adaptive immunity. *J. Clin. Invest.* **131**, (2021).
76. Horowitz, A., Behrens, R. H., Okell, L., Fooks, A. R. & Riley, E. M. NK cells as effectors of acquired immune responses: effector CD4+ T cell-dependent activation of NK cells following vaccination. *J. Immunol.* **185**, 2808–2818 (2010).
77. Kim, P. S. & Ahmed, R. Features of responding T cells in cancer and chronic infection. *Curr. Opin. Immunol.* **22**, 223–230 (2010).
78. Iwahori, K. Cytotoxic CD8+ Lymphocytes in the Tumor Microenvironment. in *Tumor Microenvironment: Hematopoietic Cells -- Part A* (ed. Birbrair, A.) 53–62 (Springer International Publishing, 2020). doi:10.1007/978-3-030-35723-8_4.
79. Yi, L. & Yang, L. Stem-like T cells and niches: Implications in human health and disease. *Front. Immunol.* **13**, 907172 (2022).
80. Olkhanud, P. B. *et al.* Tumor-evoked regulatory B cells promote breast cancer metastasis by converting resting $CD4^+$ T cells to T-regulatory cells. *Cancer Res.* **71**, 3505–3515 (2011).
81. Wei, X. *et al.* Regulatory B cells contribute to the impaired antitumor immunity in ovarian cancer patients. *Tumour Biol. J. Int. Soc. Oncodevelopmental Biol. Med.* **37**, 6581–6588 (2016).
82. Sautès-Fridman, C., Petitprez, F., Calderaro, J. & Fridman, W. H. Tertiary lymphoid structures in the era of cancer immunotherapy. *Nat. Rev. Cancer* **19**, 307–325 (2019).
83. Kroeger, D. R., Milne, K. & Nelson, B. H. Tumor-Infiltrating Plasma Cells Are Associated with Tertiary Lymphoid Structures, Cytolytic T-Cell Responses, and Superior Prognosis in Ovarian Cancer. *Clin. cancer Res. an Off. J. Am. Assoc. Cancer Res.* **22**, 3005–3015 (2016).
84. Cassetta, L. & Pollard, J. W. Targeting macrophages: Therapeutic approaches in cancer. *Nat. Rev. Drug Discov.* **17**, 887–904 (2018).
85. Bain, C. C. *et al.* Constant replenishment from circulating monocytes maintains the macrophage pool in the intestine of adult mice. *Nat. Immunol.* **15**, 929–937 (2014).
86. Schulz, C. *et al.* A lineage of myeloid cells independent of myb and hematopoietic stem cells. *Science (80-.).* **335**, 86–90 (2012).
87. Sheng, J., Ruedl, C. & Karjalainen, K. Most Tissue-Resident Macrophages Except Microglia Are Derived from Fetal Hematopoietic Stem Cells. *Immunity* **43**, 382–393 (2015).
88. Chen, Z. *et al.* Cellular and Molecular Identity of Tumor-Associated Macrophages in Glioblastoma. *Cancer Res.* **77**, 2266–2278 (2017).
89. Loyher, P.-L. *et al.* Macrophages of distinct origins contribute to tumor development in the lung. *J. Exp. Med.* **215**, 2536–2553 (2018).
90. Zhu, Y. *et al.* Tissue-Resident Macrophages in Pancreatic Ductal Adenocarcinoma Originate from Embryonic Hematopoiesis and Promote Tumor Progression. *Immunity* **47**, 323-338.e6 (2017).
91. Cortese, N., Carriero, R., Laghi, L., Mantovani, A. & Marchesi, F. Prognostic significance of tumor-associated macrophages: past, present and future. *Semin. Immunol.* **48**, 101408 (2020).
92. Lee, H.-W., Choi, H.-J., Ha, S.-J., Lee, K.-T. & Kwon, Y.-G. Recruitment of monocytes/macrophages in different tumor microenvironments. *Biochim. Biophys. Acta* **1835**, 170–179 (2013).
93. Lenzo, J. C. *et al.* Control of macrophage lineage populations by CSF-1 receptor and GM-CSF in homeostasis and inflammation. *Immunol. \& Cell Biol.* **90**, 429–440 (2012).

94. Van Overmeire, E. *et al.* M-CSF and GM-CSF Receptor Signaling Differentially Regulate Monocyte Maturation and Macrophage Polarization in the Tumor Microenvironment. *Cancer Res.* **76**, 35–42 (2016).
95. Yang, H. *et al.* CCL2-CCR2 axis recruits tumor associated macrophages to induce immune evasion through PD-1 signaling in esophageal carcinogenesis. *Mol. Cancer* **19**, 41 (2020).
96. Arakaki, R. *et al.* CCL2 as a potential therapeutic target for clear cell renal cell carcinoma. *Cancer Med.* **5**, 2920–2933 (2016).
97. Lin, H. *et al.* Host expression of PD-L1 determines efficacy of PD-L1 pathway blockade–mediated tumor regression. *J. Clin. Invest.* **128**, 805–815 (2018).
98. Mantovani, A., Marchesi, F., Malesci, A., Laghi, L. & Allavena, P. Tumour-associated macrophages as treatment targets in oncology. *Nat. Rev. Clin. Oncol.* **14**, 399–416 (2017).
99. Mantovani, A., Allavena, P., Marchesi, F. & Garlanda, C. Macrophages as tools and targets in cancer therapy. *Nat. Rev. Drug Discov.* **21**, 799–820 (2022).
100. Chen, L. *et al.* Inflammatory responses and inflammation-associated diseases in organs. *Oncotarget* **9**, 7204–7218 (2018).
101. Coussens, L. M. & Werb, Z. Inflammation and cancer. *Nature* **420**, 860–7 (2022).
102. Wroblewski, L. E., Peek, R. M. & Wilson, K. T. Helicobacter pylori and gastric cancer: Factors that modulate disease risk. *Clin. Microbiol. Rev.* **23**, 713–739 (2010).
103. Zhao, H. *et al.* Inflammation and tumor progression: signaling pathways and targeted intervention. *Signal Transduct. Target. Ther.* **6**, (2021).
104. Kartikasari, A. E. R., Huertas, C. S., Mitchell, A. & Plebanski, M. Tumor-Induced Inflammatory Cytokines and the Emerging Diagnostic Devices for Cancer Detection and Prognosis. *Front. Oncol.* **11**, 692142 (2021).
105. Gao, J. *et al.* Loss of IFN-γ Pathway Genes in Tumor Cells as a Mechanism of Resistance to Anti-CTLA-4 Therapy. *Cell* **167**, 397-404.e9 (2016).
106. Propper, D. J. & Balkwill, F. R. Harnessing cytokines and chemokines for cancer therapy. *Nat. Rev. Clin. Oncol.* **19**, 237–253 (2022).
107. Schroder, K., Hertzog, P. J., Ravasi, T. & Hume, D. A. Interferon-γ: an overview of signals, mechanisms and functions. *J. Leukoc. Biol.* **75**, 163–189 (2004).
108. Walter, M. R. The Role of Structure in the Biology of Interferon Signaling. *Front. Immunol.* **11**, 1–12 (2020).
109. Pfizenmaier, K. *et al.* High affinity human IFN-gamma-binding capacity is encoded by a single receptor gene located in proximity to c-ros on human chromosome region 6q16 to 6q22. *J. Immunol.* **141**, 856–860 (1988).
110. Soh, J. *et al.* Identification and sequence of an accessory factor required for activation of the human interferon gamma receptor. *Cell* **76**, 793–802 (1994).
111. Johnson, H. M., Noon-Song, E. & Ahmed, C. M. Controlling Nuclear Jaks and Stats for Specific Gene Activation by Ifn γ and Other Cytokines: A Possible Steroid-like Connection. *J. Clin. Cell. Immunol.* **2**, (2011).
112. Bach, E. A. *et al.* Ligand-induced assembly and activation of the gamma interferon receptor in intact cells. *Mol. Cell. Biol.* **16**, 3214–3221 (1996).
113. Babon, J. J., Lucet, I. S., Murphy, J. M., Nicola, N. A. & Varghese, L. N. The molecular regulation of Janus kinase (JAK) activation. *Biochem. J.* **462**, 1–13 (2014).
114. Hu, X. & Ivashkiv, L. B. Cross-regulation of Signaling Pathways by Interferon-γ: Implications for Immune Responses and Autoimmune Diseases. *Immunity* **31**, 539–550 (2009).
115. Satoh, J.-I. & Tabunoki, H. A Comprehensive Profile of ChIP-Seq-Based STAT1 Target Genes Suggests the Complexity of STAT1-Mediated Gene Regulatory Mechanisms. *Gene Regul. Syst. Bio.* **7**, 41–56 (2013).
116. Pestka, S., Krause, C. D. & Walter, M. R. Interferons, interferon-like cytokines, and their receptors. *Immunol. Rev.* **202**, 8–32 (2004).
117. Ivashkiv, L. B. IFNγ: signalling, epigenetics and roles in immunity, metabolism, disease and cancer immunotherapy. *Nat. Rev. Immunol.* **18**, 545–558 (2018).

118. Sakatsume, M. & Finbloom, D. S. Modulation of the expression of the IFN-gamma receptor beta-chain controls responsiveness to IFN-gamma in human peripheral blood T cells. *J. Immunol.* **156**, 4160–4166 (1996).
119. Bach, E. A. *et al.* Ligand-induced autoregulation of IFN-gamma receptor beta chain expression in T helper cell subsets. *Science* **270**, 1215–1218 (1995).
120. Pernis, A. *et al.* Lack of interferon gamma receptor beta chain and the prevention of interferon gamma signaling in TH1 cells. *Science* **269**, 245–247 (1995).
121. Bernabei, P. *et al.* Interferon-gamma receptor 2 expression as the deciding factor in human T, B, and myeloid cell proliferation or death. *J. Leukoc. Biol.* **70**, 950–960 (2001).
122. Oddo, M. *et al.* Fas ligand-induced apoptosis of infected human macrophages reduces the viability of intracellular Mycobacterium tuberculosis. *J. Immunol.* **160**, 5448–5454 (1998).
123. Hu, X., Li, J., Fu, M., Zhao, X. & Wang, W. The JAK/STAT signaling pathway: from bench to clinic. *Signal Transduct. Target. Ther.* **6**, 402 (2021).
124. Liau, N. P. D. *et al.* The molecular basis of JAK/STAT inhibition by SOCS1. *Nat. Commun.* **9**, 1558 (2018).
125. You, M., Yu, D. H. & Feng, G. S. Shp-2 tyrosine phosphatase functions as a negative regulator of the interferon-stimulated Jak/STAT pathway. *Mol. Cell. Biol.* **19**, 2416–2424 (1999).
126. ten Hoeve, J. *et al.* Identification of a nuclear Stat1 protein tyrosine phosphatase. *Mol. Cell. Biol.* **22**, 5662–5668 (2002).
127. Wu, T. R. *et al.* SHP-2 is a dual-specificity phosphatase involved in Stat1 dephosphorylation at both tyrosine and serine residues in nuclei. *J. Biol. Chem.* **277**, 47572–47580 (2002).
128. Grasso, C. S. *et al.* Conserved Interferon-γ Signaling Drives Clinical Response to Immune Checkpoint Blockade Therapy in Melanoma. *Cancer Cell* **38**, 500-515.e3 (2020).
129. Kim, Y. J., Puig-Saus, C. & Ribas, A. Melanoma dedifferentiation induced by IFN-γ epigenetic remodeling in response to anti-PD-1 therapy Graphical abstract The Journal of Clinical Investigation. *J Clin Invest* **131**, (2021).
130. Lighvani, A. A. *et al.* T-bet is rapidly induced by interferon-γ in lymphoid and myeloid cells. *Proc. Natl. Acad. Sci. U. S. A.* **98**, 15137–15142 (2001).
131. Overacre-Delgoffe, A. E. *et al.* Interferon-γ Drives Treg Fragility to Promote Anti-tumor Immunity. *Cell* **169**, 1130-1141.e11 (2017).
132. Metzemaekers, M., Vanheule, V., Janssens, R., Struyf, S. & Proost, P. Overview of the mechanisms that may contribute to the non-redundant activities of interferon-inducible CXC chemokine receptor 3 ligands. *Front. Immunol.* **8**, (2018).
133. House, I. G. *et al.* Macrophage-derived CXCL9 and CXCL10 are required for antitumor immune responses following immune checkpoint blockade. *Clin. Cancer Res.* **26**, 487–504 (2020).
134. Melero, I., Rouzaut, A., Motz, G. T. & Coukos, G. T-cell and NK-cell infiltration into solid tumors: A key limiting factor for efficacious cancer immunotherapy. *Cancer Discov.* **4**, 522–526 (2014).
135. Kashfi, K., Kannikal, J. & Nath, N. Macrophage reprogramming and cancer therapeutics: Role of inos-derived no. *Cells* **10**, 1–22 (2021).
136. Haabeth, O. A. W. *et al.* Inflammation driven by tumour-specific Th1 cells protects against B-cell cancer. *Nat. Commun.* **2**, (2011).
137. Nguyen, K. G. *et al.* Localized Interleukin-12 for Cancer Immunotherapy. *Front. Immunol.* **11**, 1–36 (2020).
138. Harvat, B. L., Seth, P. & Jetten, A. M. The role of p27(Kip1) in gamma interferon-mediated growth arrest of mammary epithelial cells and related defects in mammary carcinoma cells. *Oncogene* **14**, 2111–2122 (1997).
139. Chin, Y. E. *et al.* Cell growth arrest and induction of cyclin-dependent kinase inhibitor p21WAF1/CIP1 Mediated by STAT1. *Science (80-.).* **272**, 719–722 (1996).

140. Vairo, G. *et al.* Deregulated c-myc expression overrides IFN gamma-induced macrophage growth arrest. *Oncogene* **10**, 1969—1976 (1995).
141. Chin, Y. E., Kitagawa, M., Kuida, K., Flavell, R. A. & Fu, X. Y. Activation of the STAT signaling pathway can cause expression of caspase 1 and apoptosis. *Mol. Cell. Biol.* **17**, 5328–5337 (1997).
142. Fulda, S. & Debatin, K. M. IFNγ sensitizes for apoptosis by upregulating caspase-8 expression through the Stat1 pathway. *Oncogene* **21**, 2295–2308 (2002).
143. Listopad, J. J. *et al.* Fas expression by tumor stroma is required for cancer eradication. *Proc. Natl. Acad. Sci. U. S. A.* **110**, 2276–2281 (2013).
144. Kammertoens, T. *et al.* Tumour ischaemia by interferon-γ resembles physiological blood vessel regression. *Nature* **545**, 98–102 (2017).
145. Beatty, G. L. & Paterson, Y. IFN-γ-Dependent Inhibition of Tumor Angiogenesis by Tumor-Infiltrating CD4+ T Cells Requires Tumor Responsiveness to IFN-γ. *J. Immunol.* **166**, 2276–2282 (2001).
146. Qin, Z. *et al.* A critical requirement of interferon γ-mediated angiostasis for tumor rejection by CD8+ T cells. *Cancer Res.* **63**, 4095–4100 (2003).
147. Larionova, I., Kazakova, E., Gerashchenko, T. & Kzhyshkowska, J. New angiogenic regulators produced by tams: Perspective for targeting tumor angiogenesis. *Cancers (Basel).* **13**, 1–40 (2021).
148. Groettrup, M., Standera, S., Stohwasser, R. & Kloetzel, P. M. The subunits MECL-1 and LMP2 are mutually required for incorporation into the 20S proteasome. *Proc. Natl. Acad. Sci. U. S. A.* **94**, 8970–8975 (1997).
149. Hisamatsu, H. *et al.* Newly identified pair of proteasomal subunits regulated reciprocally by interferon γ. *J. Exp. Med.* **183**, 1807–1816 (1996).
150. Tripathi, S. C., Vedpathak, D. & Ostrin, E. J. The functional and mechanistic roles of immunoproteasome subunits in cancer. *Cells* **10**, 1–22 (2021).
151. Amaldi, I., Reith, W., Berte, C. & Mach, B. Induction of HLA class II genes by IFN-gamma is transcriptional and requires a trans-acting protein. *J. Immunol.* **142**, 999–1004 (1989).
152. Steimle, V., Siegrist, C. A., Mottet, A., Lisowska-Grospierre, B. & Mach, B. Regulation of MHC class II expression by interferon-γ mediated by the transactivator gene CIITA. *Science (80-.).* **265**, 106–109 (1994).
153. Pluhar, G. E., Pennell, C. A. & Olin, M. R. CD8 + T Cell – Independent Immune-Mediated Mechanisms of Anti-Tumor Activity. **35**, 153–172 (2015).
154. Meireson, A., Devos, M. & Brochez, L. IDO Expression in Cancer: Different Compartment, Different Functionality? *Front. Immunol.* **11**, 1–17 (2020).
155. Yu, C. P. *et al.* The Clinicopathological and Prognostic Significance of IDO1 Expression in Human Solid Tumors: Evidence from a Systematic Review and Meta-Analysis. *Cell. Physiol. Biochem.* **49**, 134–143 (2018).
156. Curti, A. *et al.* Modulation of tryptophan catabolism by human leukemic cells results in the conversion of CD25- into CD25+ T regulatory cells. *Blood* **109**, 2871–2877 (2007).
157. Wainwright, D. A. *et al.* IDO expression in brain tumors increases the recruitment of regulatory T cells and negatively impacts survival. *Clin. Cancer Res.* **18**, 6110–6121 (2012).
158. Fallarino, F. *et al.* Modulation of tryptophan catabolism by regulatory T cells. *Nat. Immunol.* **4**, 1206–1212 (2003).
159. Song, M. *et al.* Low-dose IFNg induces tumor cell stemness in tumor microenvironment of non–small cell lung cancer. *Cancer Res.* **79**, 3737–3748 (2019).
160. Chang, Y. J., Holtzman, M. J. & Chen, C. C. Interferon-γ-induced epithelial ICAM-1 expression and monocyte adhesion. Involvement of protein kinase c-dependent c-Src tyrosine kinase activation pathway. *J. Biol. Chem.* **277**, 7118–7126 (2002).
161. Roland, C. L., Harken, A. H., Sarr, M. G. & Barnett, C. C. ICAM-1 expression determines malignant potential of cancer. *Surgery* **141**, 705–707 (2007).
162. Ewald, J. A., Desotelle, J. A., Wilding, G. & Jarrard, D. F. Therapy-induced senescence in cancer. *J. Natl. Cancer Inst.* **102**, 1536–1546 (2010).

163. Demaria, M. *et al.* Cellular senescence promotes adverse effects of chemotherapy and cancer relapse. *Cancer Discov.* **7**, 165–176 (2017).
164. Chen, H.-A. *et al.* Senescence Rewires Microenvironment Sensing to Facilitate Antitumor Immunity. *Cancer Discov.* **13**, OF1–OF22 (2023).
165. Saleh, T. *et al.* Therapy-induced senescence: an “old” friend becomes the enemy. *Cancers (Basel).* **12**, 1–38 (2020).
166. Ortiz-Montero, P., Londoño-Vallejo, A. & Vernot, J. P. Senescence-associated IL-6 and IL-8 cytokines induce a self- and cross-reinforced senescence/inflammatory milieu strengthening tumorigenic capabilities in the MCF-7 breast cancer cell line. *Cell Commun. Signal.* **15**, 1–18 (2017).
167. Ohanna, M. *et al.* Secretome from senescent melanoma engages the STAT3 pathway to favor reprogramming of naive melanoma towards a tumor-initiating cell phenotype. *Oncotarget* **4**, 2212–2224 (2013).
168. Sun, C., Mezzadra, R. & Schumacher, T. N. Regulation and Function of the PD-L1 Checkpoint. *Immunity* **48**, 434–452 (2018).
169. Alsaab, H. O. *et al.* PD-1 and PD-L1 checkpoint signaling inhibition for cancer immunotherapy: mechanism, combinations, and clinical outcome. *Front. Pharmacol.* **8**, 1–15 (2017).
170. Abiko, K. *et al.* IFN-γ from lymphocytes induces PD-L1 expression and promotes progression of ovarian cancer. *Br. J. Cancer* **112**, 1501–1509 (2015).
171. Hui, E. *et al.* T cell costimulatory receptor CD28 is a primary target for PD-1-mediated inhibition. *Science (80-.).* **355**, 1428–1433 (2017).
172. Mo, X. *et al.* Interferon-γ signaling in melanocytes and melanoma cells regulates expression of CTLA-4. *Cancer Res.* **78**, 436–450 (2018).
173. Couzin-Frankel, J. Breakthrough of the year 2013. Cancer immunotherapy. *Science* **342**, 1432–3 (2013).
174. He, X. & Xu, C. Immune checkpoint signaling and cancer immunotherapy. *Cell Res.* **30**, 660–669 (2020).
175. Ribas, A. & Wolchok, J. D. Cancer immunotherapy using checkpoint blockade. *Science (80-.).* **359**, 1350–1355 (2018).
176. Larkin, J. *et al.* Combined Nivolumab and Ipilimumab or Monotherapy in Untreated Melanoma. *N. Engl. J. Med.* **373**, 23–34 (2015).
177. Shields, B. D. *et al.* Indicators of responsiveness to immune checkpoint inhibitors. *Sci. Rep.* **7**, 1–12 (2017).
178. Sunshine, J. & Taube, J. M. PD-1/PD-L1 inhibitors. *Curr. Opin. Pharmacol.* **23**, 32–38 (2015).
179. Tumeh, P. C. *et al.* PD-1 blockade induces responses by inhibiting adaptive immune resistance. *Nature* **515**, 568–571 (2014).
180. Chen, P. L. *et al.* Analysis of immune signatures in longitudinal tumor samples yields insight into biomarkers of response and mechanisms of resistance to immune checkpoint blockade. *Cancer Discov.* **6**, 827–837 (2016).
181. Hellmann, M. D. *et al.* Genomic Features of Response to Combination Immunotherapy in Patients with Advanced Non-Small-Cell Lung Cancer. *Cancer Cell* **33**, 843-852.e4 (2018).
182. Hugo, W. *et al.* Genomic and Transcriptomic Features of Response to Anti-PD-1 Therapy in Metastatic Melanoma. *Cell* **165**, 35–44 (2016).
183. Ayers, M. *et al.* IFN-γ-related mRNA profile predicts clinical response to PD-1 blockade. *J. Clin. Invest.* **127**, 2930–2940 (2017).
184. Liu, D. *et al.* Integrative molecular and clinical modeling of clinical outcomes to PD1 blockade in patients with metastatic melanoma. *Nat. Med.* **25**, 1916–1927 (2019).
185. Sharma, P., Hu-Lieskovan, S., Wargo, J. A. & Ribas, A. Primary, Adaptive, and Acquired Resistance to Cancer Immunotherapy. *Cell* **168**, 707–723 (2017).
186. Kluger, H. M. *et al.* Defining tumor resistance to PD-1 pathway blockade : recommendations from the first meeting of the SITC Immunotherapy Resistance Taskforce. 1–12 (2020) doi:10.1136/jitc-2019-000398.

187. Cornel, A. M., Mimpen, I. L. & Nierkens, S. MHC class I downregulation in cancer: Underlying mechanisms and potential targets for cancer immunotherapy. *Cancers (Basel).* **12**, 1–33 (2020).
188. Taylor, B. C. & Balko, J. M. Mechanisms of MHC-I Downregulation and Role in Immunotherapy Response. *Front. Immunol.* **13**, 1–11 (2022).
189. Burr, M. L. *et al.* An Evolutionarily Conserved Function of Polycomb Silences the MHC Class I Antigen Presentation Pathway and Enables Immune Evasion in Cancer. *Cancer Cell* **36**, 385-401.e8 (2019).
190. Restifo, N. P. *et al.* Loss of functional beta2-microglobulin in metastatic melanomas from five patients receiving immunotherapy. *J. Natl. Cancer Inst.* **88**, 100–108 (1996).
191. Sucker, A. *et al.* Genetic evolution of T-cell resistance in the course of melanoma progression. *Clin. Cancer Res.* **20**, 6593–6604 (2014).
192. Zhao, F. *et al.* Melanoma lesions independently acquire t-cell resistance during metastatic latency. *Cancer Res.* **76**, 4347–4358 (2016).
193. Dhatchinamoorthy, K., Colbert, J. D. & Rock, K. L. Cancer Immune Evasion Through Loss of MHC Class I Antigen Presentation. *Front. Immunol.* **12**, (2021).
194. Lorenzi, S. *et al.* IRF1 and NF-kB restore MHC class I-restricted tumor antigen processing and presentation to cytotoxic T cells in aggressive neuroblastoma. *PLoS One* **7**, e46928 (2012).
195. Lazaridou, M.-F. *et al.* Identification of miR-200a-5p targeting the peptide transporter TAP1 and its association with the clinical outcome of melanoma patients. *Oncoimmunology* **9**, 1774323 (2020).
196. Mari, L. *et al.* microRNA 125a Regulates MHC-I Expression on Esophageal Adenocarcinoma Cells, Associated With Suppression of Antitumor Immune Response and Poor Outcomes of Patients. *Gastroenterology* **155**, 784–798 (2018).
197. Al-Batran, S.-E. *et al.* Intratumoral T-cell infiltrates and MHC class I expression in patients with stage IV melanoma. *Cancer Res.* **65**, 3937–3941 (2005).
198. Perea, F. *et al.* The absence of HLA class I expression in non-small cell lung cancer correlates with the tumor tissue structure and the pattern of T cell infiltration. *Int. J. cancer* **140**, 888–899 (2017).
199. Sucker, A. *et al.* Acquired IFNγ resistance impairs anti-tumor immunity and gives rise to T-cell-resistant melanoma lesions. *Nat. Commun.* **8**, 1–15 (2017).
200. Gulhan, D. C. *et al.* Genomic Determinants of De Novo Resistance to Immune Checkpoint Blockade in Mismatch Repair–Deficient Endometrial Cancer. *JCO Precis. Oncol.* 492–497 (2020) doi:10.1200/po.20.00009.
201. Shin, D. S. *et al.* Primary resistance to PD-1 blockade mediated by JAK1/2 mutations. *Cancer Discov.* **7**, 188–201 (2017).
202. Zaretsky, J. M. *et al.* Mutations associated with acquired resistance to PD-1 blockade in melanoma. *N. Engl. J. Med.* **375**, 819–829 (2016).
203. Evans, M. K. *et al.* Expression of SOCS1 and SOCS3 genes is differentially regulated in breast cancer cells in response to proinflammatory cytokine and growth factor signals. *Oncogene* **26**, 1941–1948 (2007).
204. Torrejon, D. Y. *et al.* Overcoming genetically based resistance mechanisms to PD-1 blockade. *Cancer Discov.* **10**, 1140–1157 (2020).
205. Kalbasi, A. *et al.* Uncoupling interferon signaling and antigen presentation to overcome immunotherapy resistance due to JAK1 loss in melanoma. *Sci. Transl. Med.* **12**, (2020).
206. Wang, S. *et al.* Intratumoral injection of a CpG oligonucleotide reverts resistance to PD-1 blockade by expanding multifunctional CD8+ T cells. *Proc. Natl. Acad. Sci. U. S. A.* **113**, E7240–E7249 (2016).
207. Such, L. *et al.* Targeting the innate immunoreceptor RIG-I overcomes melanoma-intrinsic resistance to T cell immunotherapy. *J. Clin. Invest.* **140**, 4266–4281 (2020).
208. Upadhyay, R. *et al.* A critical role for fas-mediated off-target tumor killing in t-cell immunotherapy. *Cancer Discov.* **11**, 599–613 (2021).
209. Hoekstra, M. E., Bornes, L., Dijkgraaf, F. E., Philips, D. & Pardieck, I. N. Long-

distance modulation of bystander tumor cells by CD8 + T cell-secreted IFNγ. *Nat. Cancer* (2020) doi:10.1038/s43018-020-0036-4.
210. Nagasaki, J. *et al.* The critical role of CD41 T cells in PD-1 blockade against MHC-II–expressing tumors such as classic Hodgkin lymphoma. *Blood Adv.* **4**, 4069–4082 (2020).
211. Muntasell, A. *et al.* Targeting NK-cell checkpoints for cancer immunotherapy. *Curr. Opin. Immunol.* **45**, 73–81 (2017).
212. Gleave, M. E. *et al.* Interferon gamma-1b compared with placebo in metastatic renal-cell carcinoma. Canadian Urologic Oncology Group. *N. Engl. J. Med.* **338**, 1265–1271 (1998).
213. Schiller, J. H. *et al.* Eastern cooperative group trial of interferon gamma in metastatic melanoma: an innovative study design. *Clin. cancer Res. an Off. J. Am. Assoc. Cancer Res.* **2**, 29–36 (1996).
214. Von Hoff, D. D. *et al.* Phase II evaluation of recombinant gamma-interferon in patients with advanced pancreatic carcinoma: a Southwest Oncology Group study. *J. Biol. Response Mod.* **9**, 584–587 (1990).
215. Pujade-Lauraine, E. *et al.* Intraperitoneal recombinant interferon gamma in ovarian cancer patients with residual disease at second-look laparotomy. *J. Clin. Oncol. Off. J. Am. Soc. Clin. Oncol.* **14**, 343–350 (1996).
216. Cong, L. & Zhang, F. Genome engineering using crispr-cas9 system. *Chromosom. Mutagen. Second Ed.* **8**, 197–217 (2014).
217. Concordet, J. P. & Haeussler, M. CRISPOR: Intuitive guide selection for CRISPR/Cas9 genome editing experiments and screens. *Nucleic Acids Res.* **46**, W242–W245 (2018).
218. Jin, S. *et al.* Inference and analysis of cell-cell communication using CellChat. *Nat. Commun.* **12**, 1–20 (2021).
219. Fidler, I. J. The relationship of embolic homogeneity, number, size and viability to the incidence of experimental metastasis. *Eur. J. Cancer* **9**, 223–7 (1973).
220. Fidler, I. J. Biological Behavior of Malignant Melanoma Cells Correlated to Their Survival in Vivo. *Cancer Res.* **35**, 218–224 (1975).
221. Fidler, I. J. & Kripke, M. L. Metastasis results from preexisting variant cells within a malignant tumor. *Science (80-.).* **197**, 893–895 (1977).
222. Overwijk, W. W. & Restifo, N. P. B16 as a Mouse Model for Human Melanoma. *Curr. Protoc. Immunol.* **39**, 1–29 (2000).
223. Zhong, W. *et al.* Comparison of the molecular and cellular phenotypes of common mouse syngeneic models with human tumors. *BMC Genomics* **21**, 1–17 (2020).
224. Davis, E. J., Johnson, D. B., Sosman, J. A. & Chandra, S. Melanoma: What do all the mutations mean? *Cancer* **124**, 3490–3499 (2018).
225. Yu, J. W. *et al.* Tumor-immune profiling of murine syngeneic tumor models as a framework to guide mechanistic studies and predict therapy response in distinct tumor microenvironments. *PLoS One* **13**, e0206223 (2018).
226. Seliger, B. *et al.* Characterization of the major histocompatibility complex class I deficiencies in B16 melanoma cells. *Cancer Res.* **61**, 1095–1099 (2001).
227. Khan, A. N. H., Gregorie, C. J. & Tomasi, T. B. Histone deacetylase inhibitors induce TAP, LMP, Tapasin genes and MHC class I antigen presentation by melanoma cells. *Cancer Immunol. Immunother.* **57**, 647–654 (2008).
228. Thibaut, R. *et al.* Bystander IFN-γ activity promotes widespread and sustained cytokine signaling altering the tumor microenvironment. *Nat. Cancer* **1**, 1–13 (2020).
229. Mosely, S. I. S. S. *et al.* Rational selection of syngeneic preclinical tumor models for immunotherapeutic drug discovery. *Cancer Immunol. Res.* **5**, 29–41 (2017).
230. Cho, H.-I., Lee, Y.-R. & Celis, E. Interferon γ limits the effectiveness of melanoma peptide vaccines. *Blood* **117**, 135–144 (2011).
231. Oba, T. *et al.* Overcoming primary and acquired resistance to anti-PD-L1 therapy by induction and activation of tumor-residing cDC1s. *Nat. Commun.* **11**, 5415 (2020).
232. Wculek, S. K. *et al.* Effective cancer immunotherapy by natural mouse conventional

type-1 dendritic cells bearing dead tumor antigen. *J. Immunother. cancer* **7**, 100 (2019).
233. Lasso, P. *et al.* An Immunomodulatory Gallotanin-Rich Fraction From Caesalpinia spinosa Enhances the Therapeutic Effect of Anti-PD-L1 in Melanoma. *Front. Immunol.* **11**, 1–13 (2020).
234. Albershardt, T. C. *et al.* Therapeutic efficacy of PD1/PDL1 blockade in B16 melanoma is greatly enhanced by immunization with dendritic cell-targeting lentiviral vector and protein vaccine. *Vaccine* **38**, 3369–3377 (2020).
235. Hu, Z., Ye, L., Xing, Y., Hu, J. & Xi, T. Combined SEP and anti-PD-L1 antibody produces a synergistic antitumor effect in B16-F10 melanoma-bearing mice. *Sci. Rep.* **8**, 1–13 (2018).
236. Johnson, D. B., Sullivan, R. J. & Menzies, A. M. Immune checkpoint inhibitors in challenging populations. *Cancer* **123**, 1904–1911 (2017).
237. Gopalakrishnan, V. *et al.* Gut microbiome modulates response to anti-PD-1 immunotherapy in melanoma patients. *Science* **359**, 97–103 (2018).
238. Wu, M. *et al.* Improvement of the anticancer efficacy of PD-1/PD-L1 blockade via combination therapy and PD-L1 regulation. *J. Hematol. Oncol.* **15**, 24 (2022).
239. Betof, A. S. *et al.* Impact of Age on Outcomes with Immunotherapy for Patients with Melanoma. *Oncologist* **22**, 963–971 (2017).
240. Escors, D., Bricogne, C., Arce, F., Kochan, G. & Karwacz, K. On the Mechanism of T cell receptor down-modulation and its physiological significance. *J. Biosci. Med.* **1**, (2011).
241. Benci, J. L. *et al.* Tumor Interferon Signaling Regulates a Multigenic Resistance Program to Immune Checkpoint Blockade. *Cell* **167**, 1540-1554.e12 (2016).
242. Muraoka, D. *et al.* Peptide vaccine induces enhanced tumor growth associated with apoptosis induction in CD8+ T cells. *J. Immunol.* **185**, 3768–3776 (2010).
243. Williams, J. B. *et al.* Tumor heterogeneity and clonal cooperation influence the immune selection of IFN-γ-signaling mutant cancer cells. *Nat. Commun.* **11**, 602 (2020).
244. Walter, M. R. *et al.* Crystal structure of a complex between interferon-γ and its soluble high-affinity receptor. *Nature* **376**, 230–235 (1995).
245. Blouin, C. M. *et al.* Glycosylation-Dependent IFN-γR Partitioning in Lipid and Actin Nanodomains Is Critical for JAK Activation. *Cell* **166**, 920–934 (2016).
246. Celada, A. & Schreiber, R. D. Internalization and degradation of receptor-bound interferon-gamma by murine macrophages. Demonstration of receptor recycling. *J. Immunol.* **139**, 147–153 (1987).
247. Madan, E. *et al.* Cell Competition in Carcinogenesis. *Cancer Res.* **82**, 4487–4496 (2022).
248. Gabay, M., Li, Y. & Felsher, D. W. MYC activation is a hallmark of cancer initiation and maintenance. *Cold Spring Harb. Perspect. Med.* **4**, (2014).
249. Di Giacomo, S. *et al.* Human Cancer Cells Signal Their Competitive Fitness Through MYC Activity. *Sci. Rep.* **7**, 1–12 (2017).
250. Ramana, C. V *et al.* Regulation of c-myc expression by IFN-gamma through Stat1-dependent and -independent pathways. *EMBO J.* **19**, 263–272 (2000).
251. Suijkerbuijk, S. J. E., Kolahgar, G., Kucinski, I. & Piddini, E. Cell competition drives the growth of intestinal adenomas in Drosophila. *Curr. Biol.* **26**, 428–438 (2016).
252. Fung-Leung, W. P. *et al.* CD8 is needed for development of cytotoxic T cells but not helper T cells. *Cell* **65**, 443–449 (1991).
253. Dalloul, A. H., Ngo, K. & Fung-Leung, W. P. CD4-negative cytotoxic T cells with a T cell receptor alpha/beta intermediate expression in CD8-deficient mice. *Eur. J. Immunol.* **26**, 213–218 (1996).
254. Andrews, N. P., Pack, C. D. & Lukacher, A. E. Generation of antiviral major histocompatibility complex class I-restricted T cells in the absence of CD8 coreceptors. *J. Virol.* **82**, 4697–4705 (2008).
255. Foucras, G., Coudert, J. D., Coureau, C. & Guéry, J. C. Dendritic cells prime in vivo

alloreactive CD4 T lymphocytes toward type 2 cytokine- and TGF-beta-producing cells in the absence of CD8 T cell activation. *J. Immunol.* **165**, 4994–5003 (2000).
256. Wei, S. C., Duffy, C. R. & Allison, J. P. Fundamental Mechanisms of Immune Checkpoint Blockade Therapy. *Cancer Discov.* **8**, 1069–1086 (2018).
257. Watson, R. A. *et al.* Immune checkpoint blockade sensitivity and progression-free survival associates with baseline CD8(+) T cell clone size and cytotoxicity. *Sci. Immunol.* **6**, eabj8825 (2021).
258. Principe, N. *et al.* Tumor Infiltrating Effector Memory Antigen-Specific CD8(+) T Cells Predict Response to Immune Checkpoint Therapy. *Front. Immunol.* **11**, 584423 (2020).
259. Ribas, A. *et al.* Enhanced Tumor Responses to Dendritic Cells in the Absence of CD8-Positive Cells. *J. Immunol.* **172**, 4762–4769 (2004).
260. Hung, K. *et al.* The central role of CD4(+) T cells in the antitumor immune response. *J. Exp. Med.* **188**, 2357–2368 (1998).
261. Skoberne, M. & Geginat, G. Efficient in vivo presentation of Listeria monocytogenes-derived CD4 and CD8 T cell epitopes in the absence of IFN-gamma. *J. Immunol.* **168**, 1854–1860 (2002).
262. Whitmire, J. K., Tan, J. T. & Whitton, J. L. Interferon-gamma acts directly on CD8+ T cells to increase their abundance during virus infection. *J. Exp. Med.* **201**, 1053–1059 (2005).
263. Stoycheva, D. *et al.* IFN-γ regulates CD8+ memory T cell differentiation and survival in response to weak, but not strong, TCR signals. *J. Immunol.* **194**, 553–559 (2015).
264. Bhat, P., Leggatt, G., Waterhouse, N. & Frazer, I. H. Interferon-γ derived from cytotoxic lymphocytes directly enhances their motility and cytotoxicity. *Cell Death Dis.* **8**, e2836 (2017).
265. Wang, Z. E., Reiner, S. L., Zheng, S., Dalton, D. K. & Locksley, R. M. CD4+ effector cells default to the Th2 pathway in interferon gamma-deficient mice infected with Leishmania major. *J. Exp. Med.* **179**, 1367–1371 (1994).
266. Wang, S., Fan, Y., Brunham, R. C. & Yang, X. IFN-gamma knockout mice show Th2-associated delayed-type hypersensitivity and the inflammatory cells fail to localize and control chlamydial infection. *Eur. J. Immunol.* **29**, 3782–3792 (1999).
267. Böhm, W. *et al.* T cell-mediated, IFN-gamma-facilitated rejection of murine B16 melanomas. *J. Immunol.* **161**, 897–908 (1998).
268. Larson, R. C. *et al.* CAR T cell killing requires the IFNγR pathway in solid but not liquid tumours. *Nature* **604**, 563–570 (2022).
269. Kantari-Mimoun, C. *et al.* CAR T-cell Entry into Tumor Islets Is a Two-Step Process Dependent on IFNg and ICAM-1. *Cancer Immunol. Res.* **9**, 1425–1438 (2021).
270. Nakayama, J., Guan, X. C., Nakashima, M., Mashino, T. & Hori, Y. In vitro comparison between mouse B16 and human melanoma cell lines of the expression of ICAM-1 induced by cytokines and/or hyperthermia. *J. Dermatol.* **24**, 351–360 (1997).
271. Nobumoto, A. *et al.* Galectin-9 suppresses tumor metastasis by blocking adhesion to endothelium and extracellular matrices. *Glycobiology* **18**, 735–744 (2008).
272. Ellison, M. A., Gearheart, C. M., Porter, C. C. & Ambruso, D. R. IFN-γ alters the expression of diverse immunity related genes in a cell culture model designed to represent maturing neutrophils. *PLoS One* **12**, e0185956 (2017).
273. Salzano, M. *et al.* Interferon-γ inhibits integrin-mediated adhesion to fibronectin and survival signaling in thyroid cells. *J. Endocrinol.* **215**, 439–444 (2012).
274. Almagro, J., Messal, H. A., Zaw Thin, M., van Rheenen, J. & Behrens, A. Tissue clearing to examine tumour complexity in three dimensions. *Nat. Rev. Cancer* **21**, 718–730 (2021).
275. Tanaka, N. *et al.* Mapping of the three-dimensional lymphatic microvasculature in bladder tumours using light-sheet microscopy. *Br. J. Cancer* **118**, 995–999 (2018).
276. Tanaka, N. *et al.* Whole-tissue biopsy phenotyping of three-dimensional tumours reveals patterns of cancer heterogeneity. *Nat. Biomed. Eng.* **1**, 796–806 (2017).

277. Ji, S., Lee, J., Lee, E. S., Kim, D. H. & Sin, J.-I. I. B16 melanoma control by anti-PD-L1 requires CD8+ T cells and NK cells: application of anti-PD-L1 Abs and Trp2 peptide vaccines. *Hum. Vaccines Immunother.* **17**, 1910–1922 (2021).
278. van Elsas, A., Hurwitz, A. A. & Allison, J. P. Combination immunotherapy of B16 melanoma using anti-cytotoxic T lymphocyte-associated antigen 4 (CTLA-4) and granulocyte/macrophage colony-stimulating factor (GM-CSF)-producing vaccines induces rejection of subcutaneous and metastatic tumors accompanied. *J. Exp. Med.* **190**, 355–366 (1999).
279. Wang, B. *et al.* Transition of tumor-associated macrophages from MHC class II(hi) to MHC class II(low) mediates tumor progression in mice. *BMC Immunol.* **12**, 43 (2011).
280. Lowe, R., Shirley, N., Bleackley, M., Dolan, S. & Shafee, T. Transcriptomics technologies. *PLoS Comput. Biol.* **13**, e1005457 (2017).
281. Reimand, J. *et al.* Pathway enrichment analysis and visualization of omics data using g:Profiler, GSEA, Cytoscape and EnrichmentMap. *Nat. Protoc.* **14**, 482–517 (2019).
282. Ogbeide, S., Giannese, F., Mincarelli, L. & Macaulay, I. C. Into the multiverse: advances in single-cell multiomic profiling. *Trends Genet.* **38**, 831–843 (2022).
283. Yamawaki, T. M. *et al.* Systematic comparison of high-throughput single-cell RNA-seq methods for immune cell profiling. *BMC Genomics* **22**, 66 (2021).
284. See, P., Lum, J., Chen, J. & Ginhoux, F. A Single-Cell Sequencing Guide for Immunologists. *Front. Immunol.* **9**, 2425 (2018).
285. Ginhoux, F., Guilliams, M. & Merad, M. Expanding dendritic cell nomenclature in the single-cell era. *Nat. Rev. Immunol.* **22**, 67–68 (2022).
286. Sidhom, J.-W., Larman, H. B., Pardoll, D. M. & Baras, A. S. DeepTCR is a deep learning framework for revealing sequence concepts within T-cell repertoires. *Nat. Commun.* **12**, 1605 (2021).
287. Single-cell transcriptomics of 20 mouse organs creates a Tabula Muris. *Nature* **562**, 367–372 (2018).
288. Gohil, S. H., Iorgulescu, J. B., Braun, D. A., Keskin, D. B. & Livak, K. J. Applying high-dimensional single-cell technologies to the analysis of cancer immunotherapy. *Nat. Rev. Clin. Oncol.* **18**, 244–256 (2021).
289. Lawson, K. A. *et al.* Functional genomic landscape of cancer-intrinsic evasion of killing by T cells. *Nature* **586**, 120–126 (2020).
290. Kearney, C. J. *et al.* Tumor immune evasion arises through loss of TNF sensitivity. *Sci. Immunol.* **3**, 1–15 (2018).
291. Armingol, E., Officer, A., Harismendy, O. & Lewis, N. E. Deciphering cell–cell interactions and communication from gene expression. *Nat. Rev. Genet.* **22**, 71–88 (2021).
292. Ramilowski, J. A. *et al.* A draft network of ligand-receptor-mediated multicellular signalling in human. *Nat. Commun.* **6**, 7866 (2015).
293. Efremova, M., Vento-Tormo, M., Teichmann, S. A. & Vento-Tormo, R. CellPhoneDB: inferring cell-cell communication from combined expression of multi-subunit ligand-receptor complexes. *Nat. Protoc.* **15**, 1484–1506 (2020).
294. Browaeys, R., Saelens, W. & Saeys, Y. NicheNet: modeling intercellular communication by linking ligands to target genes. *Nat. Methods* **17**, 159–162 (2020).
295. Kumar, M. P. *et al.* Analysis of Single-Cell RNA-Seq Identifies Cell-Cell Communication Associated with Tumor Characteristics. *Cell Rep.* **25**, 1458-1468.e4 (2018).
296. Mills, C. D., Kincaid, K., Alt, J. M., Heilman, M. J. & Hill, A. M. M-1/M-2 macrophages and the Th1/Th2 paradigm. *J. Immunol.* **164**, 6166–6173 (2000).
297. Mosser, D. M. & Edwards, J. P. Exploring the full spectrum of macrophage activation. *Nat. Rev. Immunol.* **8**, 958–969 (2008).
298. Ma, R.-Y. Y., Black, A. & Qian, B.-Z. Z. Macrophage diversity in cancer revisited in the era of single-cell omics. *Trends Immunol.* **43**, 546–563 (2022).
299. Adams, R. *et al.* Influencing tumor-associated macrophages in malignant melanoma with monoclonal antibodies. *Oncoimmunology* **11**, (2022).

300. Petrova, P. S. *et al.* TTI-621 (SIRPαFc): A CD47-blocking innate immune checkpoint inhibitor with broad antitumor activity and minimal erythrocyte binding. *Clin. Cancer Res.* **23**, 1068–1079 (2017).
301. Kaczanowska, S., Joseph, A. M. & Davila, E. TLR agonists: our best frenemy in cancer immunotherapy. *J. Leukoc. Biol.* **93**, 847–863 (2013).
302. Khalil, M. & Vonderheide, R. H. Anti-CD40 agonist antibodies: preclinical and clinical experience. *Update Cancer Ther.* **2**, 61–65 (2007).
303. Hoves, S. *et al.* Rapid activation of tumor-associated macrophages boosts preexisting tumor immunity. *J. Exp. Med.* **215**, 859–876 (2018).
304. Mirlekar, B. Tumor promoting roles of IL-10, TGF-β, IL-4, and IL-35: Its implications in cancer immunotherapy. *SAGE open Med.* **10**, 20503121211069012 (2022).
305. Jonsson, A. H. *et al.* Granzyme K(+) CD8 T cells form a core population in inflamed human tissue. *Sci. Transl. Med.* **14**, eabo0686 (2022).
306. Hay, Z. L. Z. & Slansky, J. E. Granzymes: The Molecular Executors of Immune-Mediated Cytotoxicity. *Int. J. Mol. Sci.* **23**, (2022).
307. Shifrin, N., Raulet, D. H. & Ardolino, M. NK cell self tolerance, responsiveness and missing self recognition. *Semin. Immunol.* **26**, 138–144 (2014).
308. Das, K. *et al.* Generation of murine tumor cell lines deficient in MHC molecule surface expression using the CRISPR/Cas9 system. *PLoS One* **13**, e0209719 (2018).
309. Loyher, P.-L. *et al.* CCR2 Influences T Regulatory Cell Migration to Tumors and Serves as a Biomarker of Cyclophosphamide Sensitivity. *Cancer Res.* **76**, 6483–6494 (2016).
310. de Oliveira, C. E. *et al.* CCR5-Dependent Homing of T Regulatory Cells to the Tumor Microenvironment Contributes to Skin Squamous Cell Carcinoma Development. *Mol. Cancer Ther.* **16**, 2871–2880 (2017).
311. Khantakova, D., Brioschi, S. & Molgora, M. Exploring the Impact of TREM2 in Tumor-Associated Macrophages. *Vaccines* **10**, (2022).
312. Briesemeister, D. *et al.* Tumor rejection by local interferon gamma induction in established tumors is associated with blood vessel destruction and necrosis. *Int. J. cancer* **128**, 371–378 (2011).
313. Lu, Y. *et al.* Responsiveness of stromal fibroblasts to IFN-gamma blocks tumor growth via angiostasis. *J. Immunol.* **183**, 6413–6421 (2009).
314. Braumüller, H. *et al.* T-helper-1-cell cytokines drive cancer into senescence. *Nature* **494**, 361–365 (2013).
315. Hammerl, D. *et al.* Spatial immunophenotypes predict response to anti-PD1 treatment and capture distinct paths of T cell evasion in triple negative breast cancer. *Nat. Commun.* **12**, 5668 (2021).
316. Peranzoni, E., Ingangi, V., Masetto, E., Pinton, L. & Marigo, I. Myeloid Cells as Clinical Biomarkers for Immune Checkpoint Blockade. *Front. Immunol.* **11**, 1–24 (2020).
317. Müller, E. *et al.* Both Type I and Type II Interferons Can Activate Antitumor M1 Macrophages When Combined With TLR Stimulation. *Front. Immunol.* **9**, 2520 (2018).
318. Müller, E. *et al.* Toll-Like Receptor Ligands and Interferon-γ Synergize for Induction of Antitumor M1 Macrophages. *Front. Immunol.* **8**, 1383 (2017).
319. Kersten, K. *et al.* Spatiotemporal co-dependency between macrophages and exhausted CD8(+) T cells in cancer. *Cancer Cell* **40**, 624-638.e9 (2022).
320. Zheng, X. *et al.* Spatial Density and Distribution of Tumor-Associated Macrophages Predict Survival in Non-Small Cell Lung Carcinoma. *Cancer Res.* **80**, 4414–4425 (2020).
321. Viganò, S. *et al.* Functional avidity: A measure to predict the efficacy of effector T cells? *Clin. Dev. Immunol.* **2012**, (2012).
322. Engels, B. *et al.* Relapse or eradication of cancer is predicted by peptide-major histocompatibility complex affinity. *Cancer Cell* **23**, 516–526 (2013).
323. Alexander-Miller, M. A., Leggatt, G. R. & Berzofsky, J. A. Selective expansion of high-

or low-avidity cytotoxic T lymphocytes and efficacy for adoptive immunotherapy. *Proc. Natl. Acad. Sci. U. S. A.* **93**, 4102–4107 (1996).
324. Wooldridge, L. *et al.* Tricks with tetramers: how to get the most from multimeric peptide-MHC. *Immunology* **126**, 147–164 (2009).
325. Hoon, D. S., Korn, E. L. & Cochran, A. J. Variations in functional immunocompetence of individual tumor-draining lymph nodes in humans. *Cancer Res.* **47**, 1740–1744 (1987).
326. Reticker-Flynn, N. E. *et al.* Lymph node colonization induces tumor-immune tolerance to promote distant metastasis. *Cell* **185**, 1924-1942.e23 (2022).
327. Slaney, C. Y., Kershaw, M. H. & Darcy, P. K. Trafficking of T cells into tumors. *Cancer Res.* **74**, 7168–7174 (2014).
328. White, L. G., Goy, H. E., Rose, A. J. & McLellan, A. D. Controlling Cell Trafficking: Addressing Failures in CAR T and NK Cell Therapy of Solid Tumours. *Cancers (Basel).* **14**, (2022).
329. Scheper, W. *et al.* Low and variable tumor-reactivity of the intratumoral TCR repertoire in human cancers. *Nat. Med.* **25**, doi: 10.1038/s41591-018-0266-5 (2019).
330. Simoni, Y. *et al.* Bystander CD8+ T cells are abundant and phenotypically distinct in human tumour infiltrates. *Nature* **557**, 575–579 (2018).
331. Meier, S. L., Satpathy, A. T. & Wells, D. K. Bystander T cells in cancer immunology and therapy. *Nat. Cancer* **3**, 143–155 (2022).
332. Mognol, G. P. *et al.* Exhaustion-associated regulatory regions in CD8+ tumor-infiltrating T cells. *Proc. Natl. Acad. Sci. U. S. A.* **114**, E2776–E2785 (2017).
333. Song, E. & Chow, R. D. Mutations in IFN-γ signaling genes sensitize tumors to immune checkpoint blockade. *Cancer Cell* (2023) doi:10.1016/j.ccell.2023.02.013.
334. Fowlkes, N. *et al.* Factors Affecting Growth Kinetics and Spontaneous Metastasis in the B16F10 Syngeneic Murine Melanoma Model. *Comp. Med.* **69**, 48–54 (2019).
335. Simon, A. K. *et al.* Generation of tumour-rejecting anti-carbohydrate monoclonal antibodies using melanoma modified with Fas ligand. *Int. Immunol.* **20**, 525–534 (2008).
336. Di Gregorio, A., Bowling, S. & Rodriguez, T. A. Cell Competition and Its Role in the Regulation of Cell Fitness from Development to Cancer. *Dev. Cell* **38**, 621–634 (2016).
337. Opperman, K. S. *et al.* Clodronate-Liposome Mediated Macrophage Depletion Abrogates Multiple Myeloma Tumor Establishment In Vivo. *Neoplasia (United States)* **21**, 777–787 (2019).
338. Zeisberger, S. M. *et al.* Clodronate-liposome-mediated depletion of tumour-associated macrophages: A new and highly effective antiangiogenic therapy approach. *Br. J. Cancer* **95**, 272–281 (2006).